IN TWO SECTIONS—SECTION ONE

Transactions of the ASME

Design of Chimneys to Control Down-Wash of Gases . . . . . *R. H. Sherlock and E. J. Lesher* 1

A Magnetic-Impulse Rapper System for Electrical Precipitators . . . . . *H. J. Hall and T. A. Pierson, 3rd* 11

Performance of the Periphery Pump . . . . . *H. W. Iversen* 19

Observations on Some Factors Affecting Timken Data for EP Lubricants . . . . . *A. J. DeArdo and E. M. Kipp* 29

On the Solution of the Reynolds Equation for Slider-Bearing Lubrication—VIII . . . . . *A. Charnes, F. Osterle, and E. Saibel* 33

Studies in Cold-Drawing—Part I, Effect of Cold-Drawing on Steel . . *H. Majors, Jr.* 37

Studies in Cold-Drawing—Part 2, Cold-Working 2S-O Aluminum . . *H. Majors, Jr.* 49

The Effect of Dispersions on Creep Properties of Aluminum-Copper Alloys . . . . . *W. H. Giedt, O. D. Sherby, and J. E. Dorn* 57

Machinability Research With J&L Tool Dynamometer on Titanium 150A . . . . . *Leif Fersing and D. N. Smith* 65

Testing Large Steam Turbines With Weighing Tanks . . . . . *W. A. Pollock* 79

Transient Gas-Flame Temperatures in a Spherical Bomb . . . . . *Y. M. Miao, T. W. Price, and J. H. Potter* 89

TRANSACTIONS OF THE AMERICAN SOCIETY OF MECHANICAL ENGINEERS

VOLUME 77 JANUARY 1955 NUMBER 1

Transactions

of The American Society of Mechanical Engineers

Published on the tenth of every month, except March, June, September, and December

OFFICERS OF THE SOCIETY:

DAVID W. R. MORGAN, *President*

JOSEPH L. KOPF, *Treasurer* — C. E. DAVIES, *Secretary*

EDGAR J. KATES, *Ass't Treasurer*

COMMITTEE ON PUBLICATIONS:

OTTO DE LORENZI, *Chairman*

COLIN CARMICHAEL — KERR ATKINSON

W. E. REASER — L. S. WELTSON

R. A. CEDERBERG, H. N. WEINBERG } *Junior Advisory Members*

GEORGE A. STETSON, *Editor* — K. W. CLENDINNING, *Managing Editor*

REGIONAL ADVISORY BOARD OF THE PUBLICATIONS COMMITTEE:

RICHARD L. ANTHONY—I
JOHN DE S. COUTINHO—II
WILLIAM N. RICHARDS—III
FRANCIS C. SMITH—IV
H. M. CATHER—V
J RUSSELL PARRISH—VI
J. KENNETH SALISBURY—VII
JOHN H. KEYES—VIII

Published monthly by The American Society of Mechanical Engineers. Publication office at 20th and Northampton Streets, Easton, Pa. The editorial department is located at the headquarters of the Society, 29 West Thirty-Ninth Street, New York 18, N. Y. Cable address, "Dynamic," New York. Price $1.50 a copy, $12.00 a year for Transactions and the *Journal of Applied Mechanics;* to members and affiliates, $1.00 a copy, $6.00 a year. Add $1.50 for postage to all countries outside the United States, Canada, and Pan-American Union. Changes of address must be received at Society headquarters seven weeks before they are to be effective on the mailing list. Please send old as well as new address.... By-Law: The Society shall not be responsible for statements or opinions advanced in papers or...printed in its publications (B13, Par. 4)....Entered as second-class matter March 2, 1928, at the Post Office at Easton, Pa., under the Act of August 24, 1912....

Copyrighted, 1955, by The American Society of Mechanical Engineers. Reprints from this publication may be made on condition that full credit be given the Transactions of the ASME and the author, and that date of publication be stated.

Design of Chimneys to Control Down-Wash of Gases

By R. H. SHERLOCK[1] and E. J. LESHER,[2] ANN ARBOR, MICH.

Studies to determine the laws of behavior of stack gases as they flow downwind, and to prevent down-wash of these gases, have been in progress at the University of Michigan since March, 1934, when a project (1, 2)[3] in this field was sponsored by the Commonwealth Edison Company of Chicago under the direction of Mr. William L. Abbott and Mr. Alex D. Bailey. That pioneer project was connected with the Crawford Avenue Station and was followed during the later years by other studies dealing with the extension of old plants and the design of stacks for new plants. The material presented in this paper was obtained almost entirely from recent studies sponsored by the Commonwealth Edison Company.

Introduction

UNDER favorable weather conditions the plume from a smokestack will rise gradually as it flows downwind and the gases will be dispersed until only a negligible concentration prevails in the atmosphere. Under such conditions the gases do not become a cause of annoyance to people on the ground. Unfortunately, however, there are several adverse natural influences which arise occasionally to disturb this orderly dispersion of the stack gases. For the purpose of this paper these influences will be classified as (1) aerodynamic influences, (2) unfavorable terrain, (3) meteorological and micrometeorological influences, (4) the settling of particulate matter.

This paper describes the results of an investigation which is intended to reduce the problem of controlling the down-wash of stack gases to a design basis, so that in the future it will be necessary to conduct additional research projects only in those cases where unusual conditions prevail. Only aerodynamic influences are considered here as a cause of down-wash, since it is one of the adverse influences which definitely can be brought under control and since practically all of the cases of persistent down-wash in the immediate neighborhood of most plants are from this cause. However, the other influences are discussed so as to establish their relation to the general problem.

A steam-electric power plant is used as a working example. The experiments described in this paper were of such scope as to enable the engineer to predict the pattern of stack-gas behavior at power plants having a size up to about 500,000 kw capacity and where the terrain is not so extraordinary as to constitute a special case.

Diagrams are given which show the dimensions of the hypothetical stations used in the test, together with diagrams of some of the supporting data and a summary sheet which shows the relation between the wind velocity, the stack-gas velocity, the height of stack, the height of the gas plume, and the height of the building.

Only a short description of the testing procedures and equipment is given here, since a more complete report of this work will soon appear elsewhere (3). The future bulletin likewise will contain additional cases for (*a*) a variable plant load and (*b*) for a situation where the gases must pass over a moderately high hill.

An illustrative example is given in the form of a case which may arise in plant design. It assumes a plant situated in flat country and operating under full load for the entire year.

Patterns of Gas Behavior

The patterns of flow which may be exhibited by a chimney plume are as varied as the weather and the topography of the nation. A plant may be located in a deep valley or it may be located on level ground. It may be in sparsely settled territory or in the midst of an urban community where there are many obstructions to smooth flow. In approaching a generalized solution of the problem of chimney design it is therefore necessary to have some standard of reference.

The Basic Plume. In this paper the standard of reference is a location in level open country and weather conditions which are most easily simulated in the wind tunnel, namely, a neutral or a stable atmosphere which is relatively free from vertical mixing. The flow patterns which are shown in the tunnel under these conditions are referred to as "the basic plume." It will be necessary for the designer to superimpose upon the basic flow patterns the effects of dispersion and diffusion, unfavorable terrain, and gas temperature.

(a) Light Wind, Neutral or Stable Atmosphere

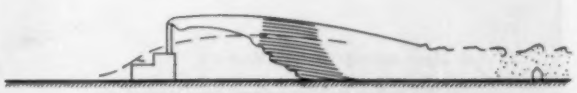

(b) Strong Wind, Neutral or Stable Atmosphere

FIG. 1 BASIC PATTERNS OF GAS FLOW

Fig. 1(*a*) shows the free-flowing plume which occurs with high stack-gas velocity in a light wind, and Fig. 1(*b*) shows the down-wash which may occur with low stack-gas velocity in a strong wind. It should be noted here that aerodynamic down-wash usually will occur in two steps, the first of which is caused by the eddies at the tip and in the wake of the stack (1). If this first step brings the gases low enough so that they penetrate the

[1] Professor of Civil Engineering, University of Michigan.

[2] Associate Professor of Aeronautical Engineering, University of Michigan.

[3] Numbers in parentheses refer to the Bibliography at the end of the paper.

Contributed by the Fuels Division and presented at the Annual Meeting, New York, N. Y., November 29–December 4, 1953, of THE AMERICAN SOCIETY OF MECHANICAL ENGINEERS.

NOTE: Statements and opinions advanced in papers are to be understood as individual expressions of their authors and not those of the Society. Manuscript received at ASME Headquarters, August 24, 1953. Paper No. 53—A-80.

vortex sheath over the building turbulence, the gases may be brought to the ground (2).

The wind-tunnel results must be supplemented by a decision as to the clearance which the bottom of the basic plume must have above the ground or other objects to be cleared by the gases. These clearances are shown as P and P', respectively, in Fig. 1(a). Usually the question which the designer must answer is, "How much clearance must be allowed between the basic plume and the ground or other obstructions, in order that diffusion may reduce the concentration of obnoxious constituents of the gases to within tolerable limits before they reach the ground?"

Dispersion and Diffusion of Stack Gases. Fig. 2 pictures the principal patterns of dispersion which need to be superimposed upon the basic plumes shown in Fig. 1. Fig. 2(a) simulates the idealized diffusion which is assumed in the equations of Sutton (4) and others (5). Isotropic turbulence is also usually assumed; that is, the same coefficients of diffusion ordinarily are used both vertically and horizontally.

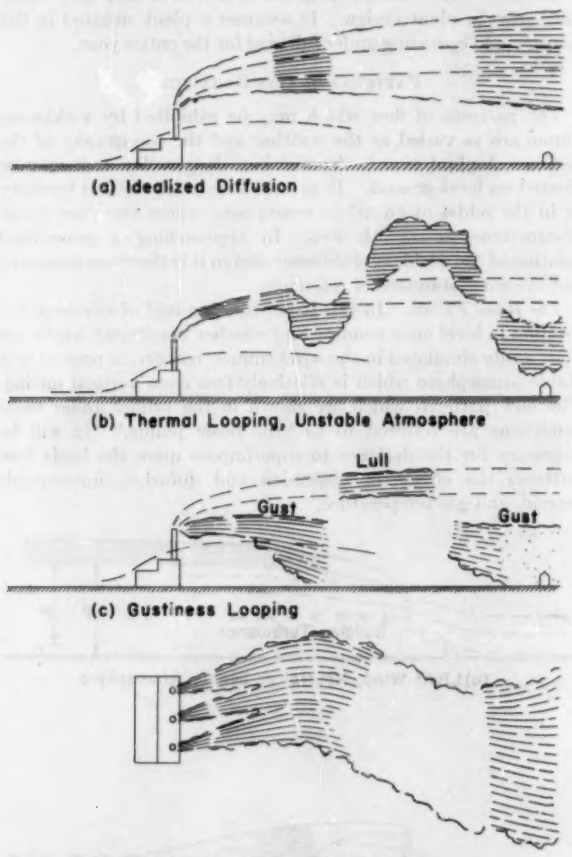

FIG. 2 SOME PATTERNS OF GAS DISPERSION

Obviously the foregoing assumptions are useful only if the coefficients can be made to approximate the actual conditions in nature reasonably well. There can be no doubt that isotropic turbulence rarely, if ever, occurs in nature except on a very small scale, and that major elements of wind structure occur frequently, as shown in Figs. 2 (b, c, d). This is especially true in an unstable atmosphere, that is, one in which the decrease of atmospheric temperature with height is greater than the adiabatic lapse rate. Vertical convection cells are common and the resulting shape of plume usually is referred to as thermal looping, shown in Fig. 2(b). These convection cells frequently extend to the ground and may extend upward hundreds or in some cases even thousands of feet. Their effect in dispersing the gases is very great, but unfortunately, they frequently bring the gases to the ground before the concentration of obnoxious constituents has been reduced within satisfactory limits.

Another form of looping is caused by rapid changes in the horizontal component of wind velocity, or in more common terms, due to gustiness. When the stack-gas velocity and the average wind velocity are such as to permit the basic plume to travel along a satisfactorily high path there may occur gusts of such intensity that the plume will be brought downward, even to the ground, as shown in Fig. 2(c).

In addition to the vertical components of wind structure there also are horizont l components, which cause meandering of the gas plumes as shown in Fig. 2(d). This component likewise produces dispersion which tends to reduce the concentration of obnoxious constituents of the stack gases, although in a temperature inversion it is possible to have meandering with very little diffusion.

Unfavorable Terrain. Because they require large amounts of water many power plants are placed close to the edge of a bay, a lake, or a river. Under such conditions the plant may be located on low land with a hill or bluff not far distant. When the wind is blowing toward the hill it will be deflected upward and the height to which this deflection extends may be two or more times the height of the hill. If the plume approaches the hill at a height sufficient to escape the turbulent boundary layer on the surface of the hill it actually may be deflected upward and escape contact with the hill. However, unless the surface of the hill is very smooth, a turbulent boundary layer will be built up which may extend to a considerable height, particularly if the face of the hill is covered with a growth of rugged trees. In that case the turbulent boundary layer may have a depth of 75 or 100 ft above the ground. On the other hand, if there is a dense growth of bushes or saplings on the face of the hill, a strong wind very well may have the effect of streamlining the direction of the small branches and leaves so that the over-all effect is one of smoothness rather than roughness.

Fig. 3 shows a very unfavorable situation with regard to the terrain. A basic plume has undergone a more or less idealized degree of diffusion as it approaches the hill. The bottom of the plume is not high enough to escape the turbulent boundary

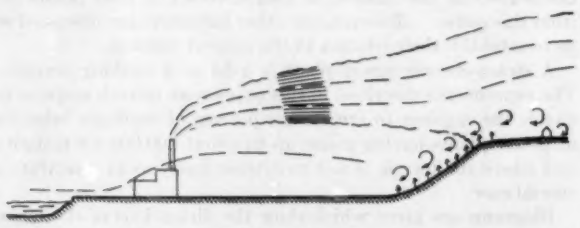

FIG. 3 UNFAVORABLE TERRAIN

layer with the result that the bottom of the plume performs the familar "diving" into the face of the hill.

Gas Temperature. In modern power plants the gases leave the stacks with temperatures from 250 to 375 F. The temperature of the plume decreases rapidly owing to diffusion in the ambient atmosphere. However, the flotational effect of the high temperature is not lost because, although the temperature of the gas plume decreases rapidly, the over-all heat content of the mixture of gas and air is not reduced. The theoretical rate of rise has been computed but, here again, as in the case of idealized dif-

fusion, the basic assumptions are only a rough approximation to nature.

In those cases where the plume has not escaped the adverse aerodynamic effects around the stack and in the wake of the building, or has not escaped the turbulent boundary layer at the face of a hill, the flotational effect of hot-gas temperatures offers very little in the way of a remedy(3).

Combined Effects. The basic plume in a neutral atmosphere serves as a satisfactory standard of reference to which other effects may be added. The most difficult of these effects to determine quantitatively are dispersion and diffusion. Extensive investigations are now in progress (6) in an attempt to evaluate these effects. Some of the results have been published (7) already and it is hoped that this aspect of the problem will be in better shape for the designer in the relatively near future. Complete information regarding the dispersion of stack gases requires that a statement of the concentration with which gases reach the ground be supplemented by a statement of both the probable frequency and duration of these events (8). High concentration for short periods or low concentration for long periods may be equally obnoxious.

The effects of unfavorable terrain can be anticipated on the basis of observations in the field and on the basis of well-controlled experiments in the wind tunnel. However, for a situation like the one shown in Fig. 3, it is well to resort to a special research program in the wind tunnel. For any given size of wind tunnel there is, of course, a limit to the height of hill which can be investigated without using a model which is so small that the results would be extremely questionable. A situation involving a hill will be published in a future bulletin (3). The experiments reported herein were performed with cold stack gases at a velocity which gives the same exit momentum per cubic foot as the hot gases at the plant. The flotational effect of hot gases is ignored, but this is of small effect close to the plant and it is on the safe side to ignore the effect.

Particulate Matter. This paper deals entirely with the behavior of stack gases and no attempt is made to include the behavior of particulate matter. This is a field in itself and one which is changing rapidly because of the changes which are now taking place in the practices of plant design and operations.

Wind Tunnel

The investigation was conducted at the University of Michigan in a wind tunnel which is 8 ft wide × 5 ft high, with a venturi working section approximately 14 ft long, as shown in Fig. 4(*a*). The velocity of the approaching undisturbed wind was always kept at 20 fps. The smoke consisted of a mixture of oil vapor and steam and was emitted from the stacks at a temperature of approximately 70 F. The desired changes in the ratio of the gas velocity to the wind velocity were obtained by varying the gas velocity. The smoke plume was photographed through a

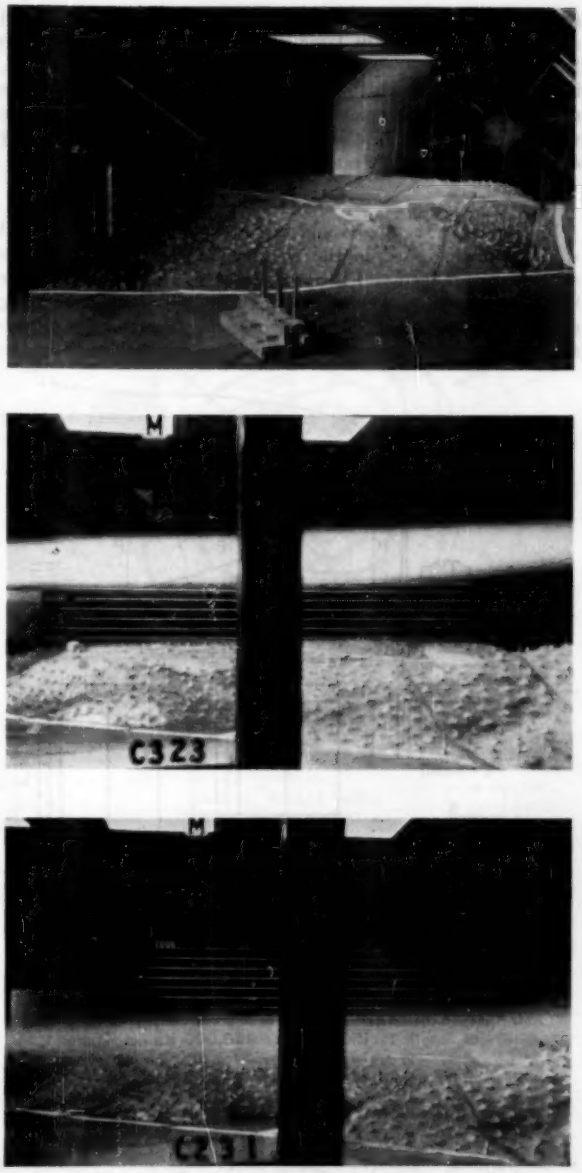

Fig. 4 Wind-Tunnel Setup, Unfavorable Terrain
[*a* (*top*) Looking downwind; *b* (*center*) free-flowing basic plume; *c* (*bottom*) down-wash.]

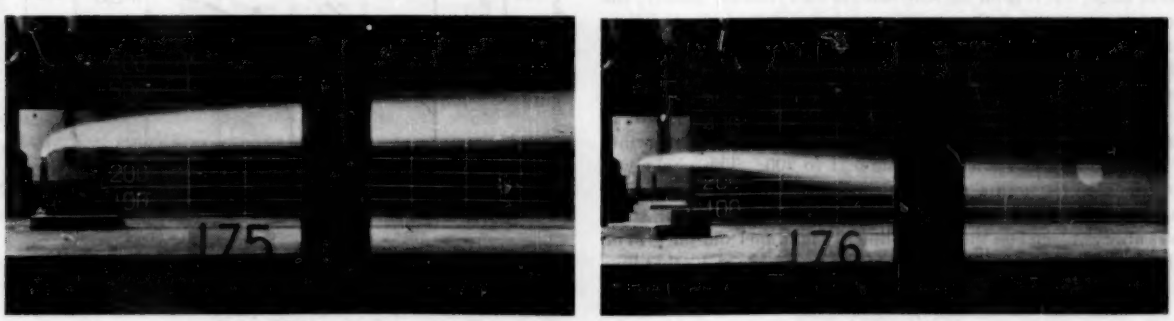

a, Free-flowing basic plume

b, Down-wash

Fig. 5 Wind-Tunnel Setup, Level Terrain

plate-glass window against a grid on the far side of the tunnel and with an exposure of 1 sec, (Figs. 4 and 5). This was too long an exposure to show the structure of the plume. Instead, it gave an integrated history of the plume for a period of 5 min at the plant site and made it possible to choose envelopes which were representative of the position of the basic plume under each particular velocity ratio.

The Model

Fig. 6 shows the shape and proportions of the hypothetical station building used in the wind-tunnel tests. Its profile is roughly streamlined and the stacks are set on one of the lower levels of the roof. This profile may be looked upon as being unusually well shaped for the purpose of minimizing down-wash from aerodynamic causes. It also will be noted that the length

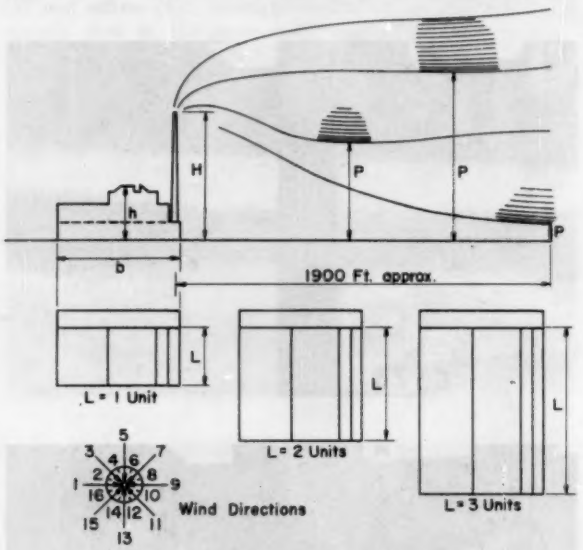
H
h
P
P
P
b
1900 Ft. approx.
L
L
L
L = 1 Unit
L = 2 Units
L = 3 Units
Wind Directions
H = height of stacks (250', 300', 350', or 400')
h = " " building = 125'
b = width " " = 290'
L = length " " = 1, 2, or 3 Units where each unit of length is 150 Feet for 150,000 Kw. of station capacity.
P = lowest height of smoke plume in 2000'±.

Fig. 6 Shape and Proportions of Hypothetical Plant

of the building is given in terms of units, each unit of length being 150 ft and corresponding to a hypothetical plant capacity of 150,000 kw. This length of 150 ft for a 150,000-kw plant may seem large, but it is on the safe side for two reasons, namely, the total momentum of the emerging gas per unit of the building, and the aerodynamic deflection of the passing wind. The greater the volume of building for a given rate of gas discharge the greater will be the deflective effect upon the plume. The position of the basic plume is identified by the minimum height to the bottom of the plume within approximately 2000 ft downwind.

The model was made to a scale of 1 to 300. The smoke was transmitted through a measuring orifice into a stilling chamber in the plant model and thence to the stacks. The center stack was always placed on the center line of the tunnel and the grid on the far wall measures the height of the gas plume along that line.

Test Results

Only sample test results from the supporting data can be given in the limited space of this paper.

Figs. 7, 8, and 9 are typical of the manner in which the original wind-tunnel data were plotted. In each diagram the height of the plume was plotted against the velocity ratio, that is, the velocity of the stack gases to the velocity of the wind, both being reduced to equivalent velocity at 70 F. This gives the ratio of the favorable momentum of the stack gases to the unfavorable momentum of the wind. It is important that these velocities be always referred to these standard conditions rather than to the operating temperatures. Since the building is never perfectly symmetrical with respect to the direction of the wind it is inevitable that there will be differences in the behavior of the stack plume for different wind directions. Also, there will be some experimental errors.

This means that in Fig. 7 the results for directions 1 and 9 will show some differences. Nevertheless, for the sake of simplicity these two directions were combined and a curve fitted to the

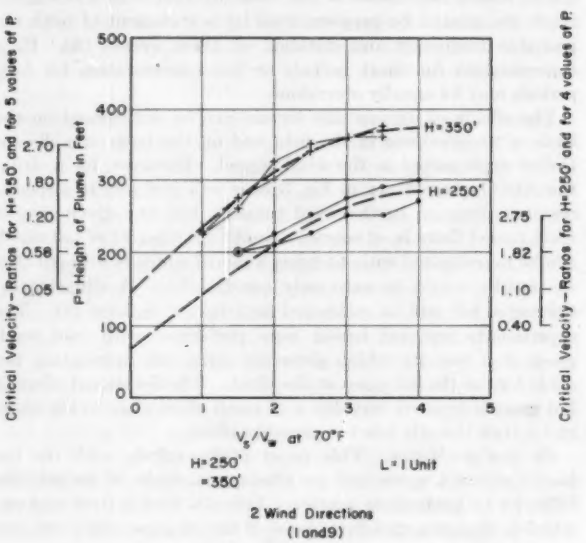

Fig. 7 Original Data

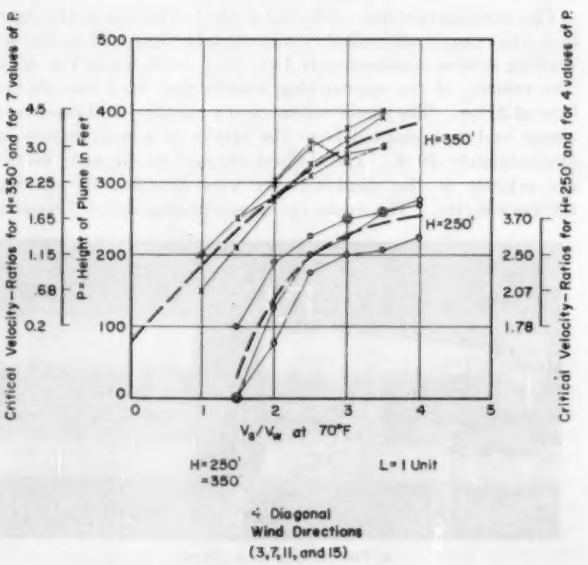

Fig. 8 Original Data

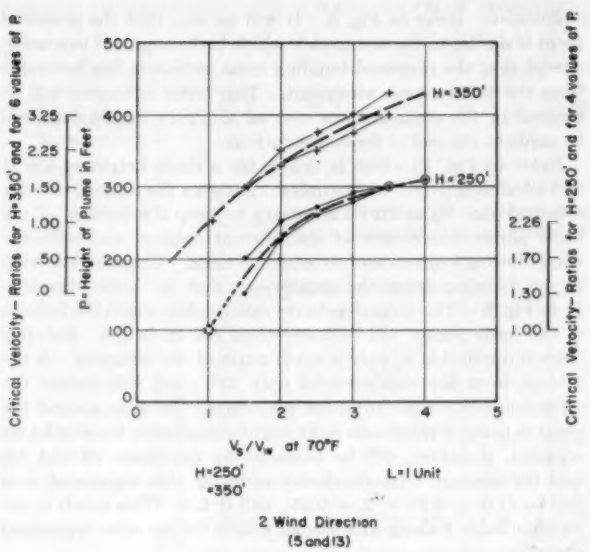
Critical Velocity – Ratios for H=350' and for 6 values of P
Critical Velocity – Ratios for H=250' and for 4 values of P
P = Height of Plume in Feet
H=350'
H=250'
V_s/V_w at 70°F
H=250'
=350'
L=1 Unit
2 Wind Direction
(5 and 13)

FIG. 9 ORIGINAL DATA

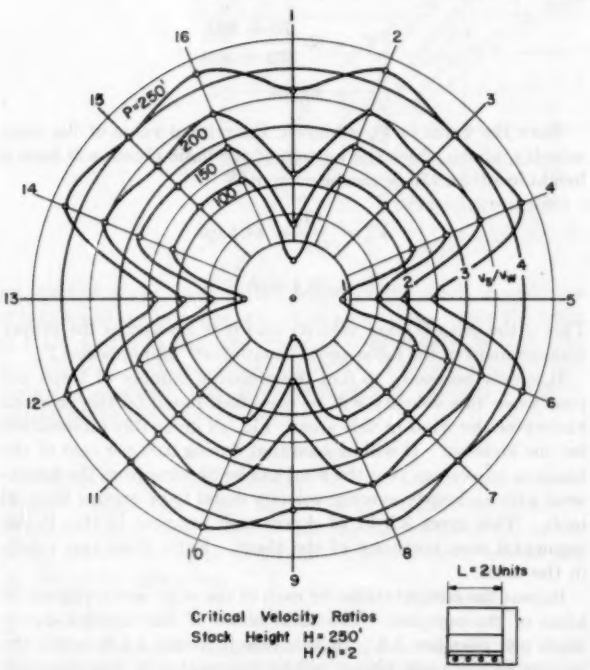

FIG. 10 CRITICAL-VELOCITY RATIOS V_s/V_w

average position of the experimental points. In some cases a mathematical curve was used but in others a curve was merely fitted by eye. An additional vertical scale is shown at either side of the diagram for convenience in transferring readings to the next set of diagrams.

Fig. 8 shows the experimental data for winds blowing diagonally across the plant where the departure from symmetry for each wind direction is much greater than in the previous case. The experimental data show a correspondingly greater degree of dispersion. Nevertheless, the data were combined into one diagram for each stack height and a curve fitted to the data. In like manner Fig. 9 shows the experimental data for the two wind directions along the axis of the line of stacks.

Figs. 10 to 13 give, for 16 wind directions, the relationship between critical-velocity ratios, height of stack, and height of plume, for a plant building 2 units (300 ft) long. Similar diagrams are available for buildings one unit (150 ft) and 3 units (450 ft)

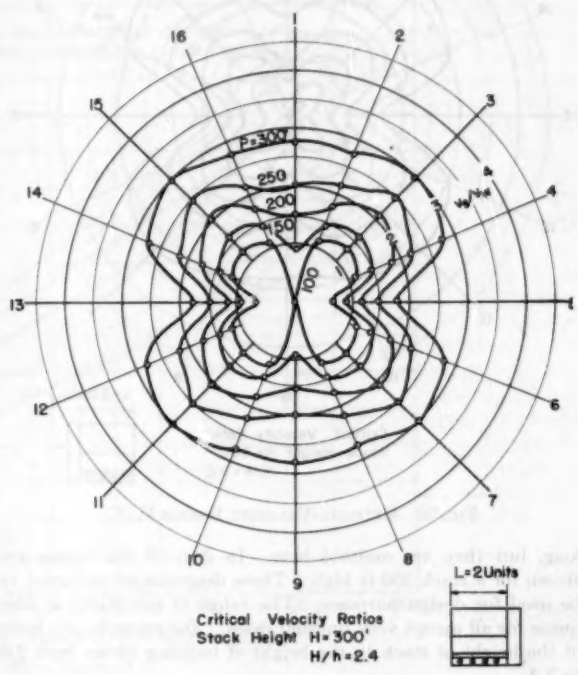

FIG. 11 CRITICAL-VELOCITY RATIOS V_s/V_w

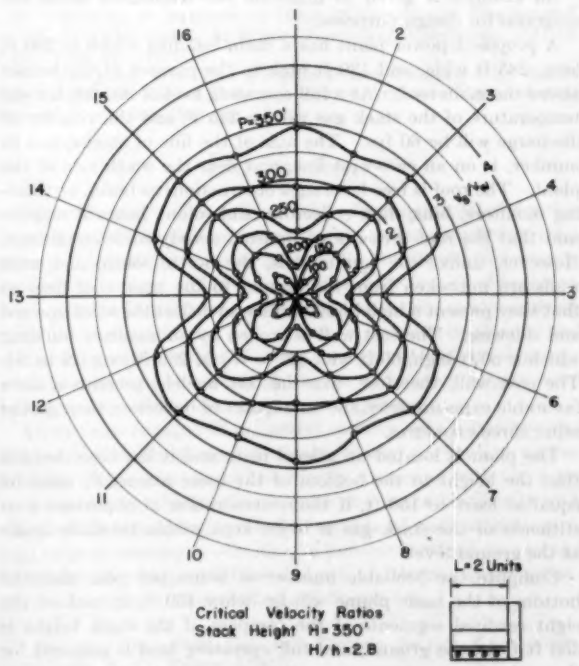

FIG. 12 CRITICAL-VELOCITY RATIOS V_s/V_w

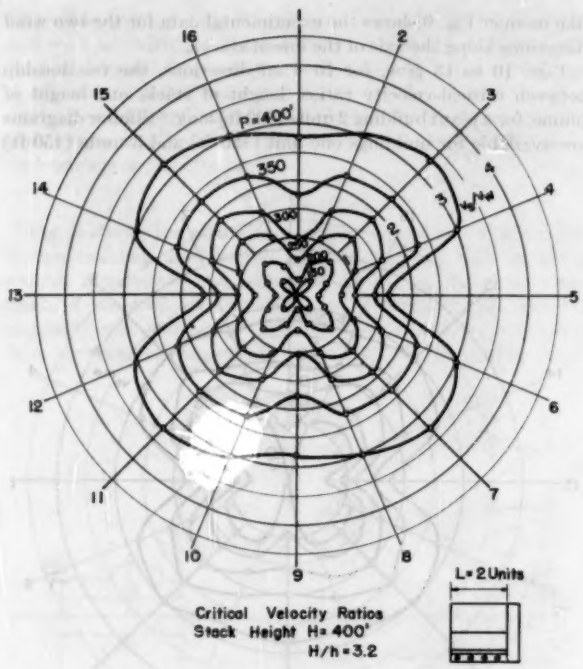

FIG. 13 CRITICAL-VELOCITY RATIOS V_s/V_w

long, but they are omitted here. In Fig. 12 the values are shown for a stack 350 ft high. These diagrams are intended to be used for design purposes. The range of conditions is adequate for all except very unusual cases. For example, the ratio of the height of stack to the height of building varies from 2.0 to 3.2.

ILLUSTRATIVE CASE

An example is given to illustrate the manner of using the diagrams for design purposes.

A proposed power plant has a main building which is 280 ft long, 285 ft wide, and 130 ft high to the parapet of the houses above the main roof. At a full operating load of 300,000 kw the temperature of the stack gas will be 335 F, and the velocity of discharge will be 60 fps. The axis of the line of stacks, two in number, is on an east-west line, and near the south side of the plant. The roof is free from such obstructions as tanks, ventilating monitors, bins, dust collectors, and so on; hence it may be said that the roof presents no unusual aerodynamic conditions. However, unlike the test models, the north, south, and west walls are unbroken from the ground to the main roof line, so that they present a high blunt surface to deflect the wind upward and sidewise. The east wall is broken by an auxiliary building which is 50 ft high, 60 ft wide (E to W) × 280 ft long (N to S). The east wall, therefore, like the test models, presents a more favorable exposure from the standpoint of deflection than do the other three exposures.

The plant is located on a level plain and it has been decided that the height to the bottom of the basic plume, P, must be equal at least to 150 ft, if the concentration of obnoxious constituents of the stack gas is to be kept within tolerable limits at the ground level.

Compute the probable number of hours per year that the bottom of the basic plume will be below 150 ft, in each of the eight cardinal segments of the compass, if the stack height is 350 ft from the ground, and full operating load is assumed for the entire year.

Solution. Refer to Fig. 6. It will be seen that the proposed plant is similar to the test models which had a length of two units, except that the proposed building cross section is less favorable from the aerodynamic viewpoint. This latter difference will be ignored in the computations and an arbitrary adjustment will be made at the end of the computations.

Refer to Fig. 12 which is drawn for a stack height of 350 ft and a building length of two units. It shows the critical-velocity ratios ($V_s \div V_w$ at 70 F) necessary to keep the bottom of the basic plume above each of six different heights, and with the wind blowing from each of sixteen directions. Consider the wind to be blowing from the southwest, that is, from direction 11 in Fig. 6. The critical-velocity ratio, below which the bottom of the basic plume will be lower than 150 ft, is 1.0. But this ratio is applicable to only a small angle of the compass. A deviation from the southwest of only $22\frac{1}{2}$ deg will reduce the critical-velocity ratio to about 0.7. Since the area around the plant is being divided into eight angular segments, the southwest segment, therefore, will be bounded by directions 10 and 12, and the average critical-velocity ratio for this segmental area will be $(1.0 + 0.7) \div 2 = 0.85$; call it 0.9. This result is entered in Table 1 along with similar results for the other segmental areas.

In order to complete the table the velocity of the gas must be reduced to equivalent velocity at 70 F, thus

$$V_s = 60 \frac{70 + 460}{335 + 460}$$

$$= 40 \text{ fps}$$

Since the value of V_s is known, the critical value of the wind velocity, above which the bottom of the basic plume will have a height less than 150 ft, can be computed

$$V_w = \frac{40}{0.9} = 44.4 \text{ fps}$$

$$= 30.4 \text{ mph}$$

This is the critical wind velocity and it is entered in the proper compartment of the table under "southwest" and opposite V_w.

It is now necessary to find the probable number of hours per year when this velocity will be exceeded, based on the previous history of the wind in this area. Fig. 14 gives this information for one location. It will be seen that during 0.04 per cent of the hours in an average year the wind will be blowing from the Southwest with an hourly average velocity equal to or greater than 30 mph. This gives 3.5 hr of down-wash per year in the 45-deg segmental area northeast of the plant. Enter these two values in the table.

Repeat the computations for each of the other seven segmental areas of the compass. The total hours of intermittent down-wash per year are 5.3. In this case it means 5.3 hr when the bottom of the basic plume will be intermittently less than 150 ft above the station yard. The word "intermittent" is used for clarity since, during most of these hours, the wind velocity will be sometimes above and sometimes below the critical velocity.

If the computations are repeated for other heights of stacks and other velocities of discharge of stack gas, diagrams can be drawn to show the relationship between down-wash and height of stacks, and also between down-wash and gas velocity.

The results in Table 1 are based upon a test model of a plant building having a most favorable profile from the aerodynamic viewpoint. As stated previously, the building for the illustrative case is somewhat less favorable because of the blunt exposure of the walls in three directions. Tunnel tests have shown that such adverse differences in the building shape may require an

TABLE 1 INTERMITTENT DOWN-WASH (150 FT) IN HOURS PER YEAR BASED ON WIND VELOCITIES 1943 TO 1948—FULL LOADING CONDITION

Wind direction	N	NE	E	SE	S	SW	W	NW	V_s' 335 F, fps	V_s 70 F, fps	$\frac{H}{h}$	H_s height, ft
$V_s \div V_w$	0.4	0.9	0.5	0.9	0.4	0.9	0.5	0.9	60	40	2.8	350
V_w (mph)	68.2	30.4	54.6	30.4	68.2	30.4	54.6	30.4	...	...	...	...
Per cent hours	...	...	...	...	...	0.04	...	0.02	...	...	...	...
Hours per year	...	...	...	...	...	3.5	...	1.8	...	...	...	...

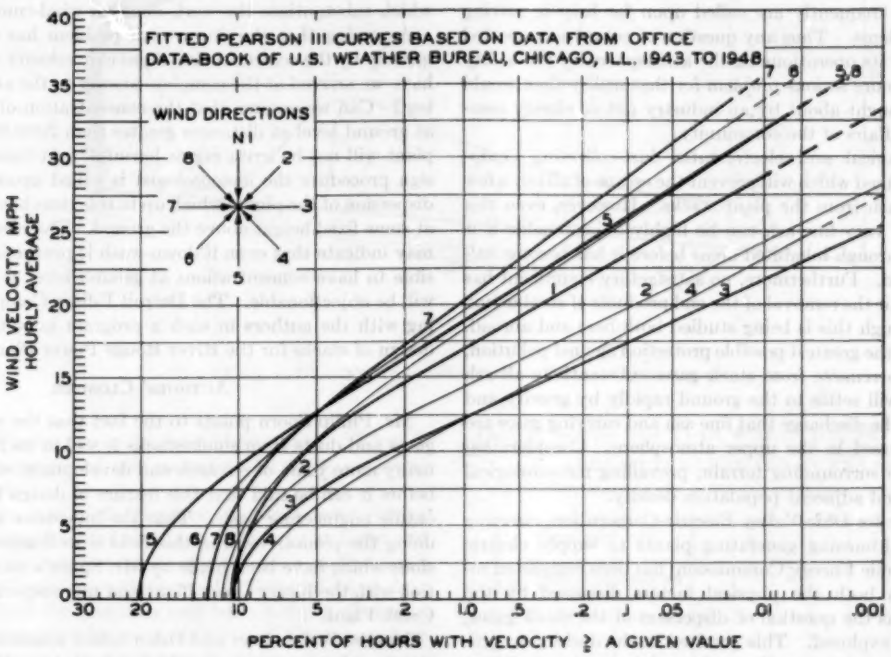

FIG. 14 SIX-YEAR WIND RECORDS

addition of about 25 ft to the height of the stack in order to obtain equal performance, except in those cases where the ratio of stack height to building height is large enough to eliminate the effect of building shape. There is also the slightly less favorable condition that the height of this building is 130 ft instead of the 125 ft used in the tests.

CONCLUSION

A method has been developed for the use of wind-tunnel testing of models by which the design of a station building and its stacks can be determined so that the down-wash of the smoke plume toward the earth as a result of aerodynamic effects can be practically eliminated.

BIBLIOGRAPHY

1 "The Control of Gases in the Wake of Smokestacks," by R. H. Sherlock and E. A. Stalker, *Mechanical Engineering*, vol. 62, 1940, pp. 455–458.

2 "A Study of Flow Phenomena in the Wake of Smokestacks," by R. H. Sherlock and E. A. Stalker, Engineering Research Bulletin No. 29, March, 1941.

3 "Design of Chimneys," by R. H. Sherlock, Engineering Research Bulletin No. 38, University of Michigan, Ann Arbor, Mich., 1954.

4 "The Theoretical Distribution of Airborne Pollution From Factory Chimneys," by O. G. Sutton, Royal Meteorological Society, *Quarterly Journal*, vol. 73, 1947, p. 426.

5 "The Spread of Smoke and Gases From Chimneys," by C. H. Bosanquet and J. L. Pearson, Trans. Faraday Society, vol. 32, 1936, p. 1249.

6 "Research on Turbulence and Diffusion of Particulate Matter in the Lower Layers of the Atmosphere," by E. Wendel Hewson, H. E. Cramer, G. C. Gill, and F. A. Record, Final Report Contract No. AF28(099)-7, Geophysical Research Directorate, Air Force Cambridge Research Center, 1951.

7 "Relation of Gustiness to Other Meteorological Parameters," by M. E. Smith and I. A. Singer, *Journal of Meteorology*, vol. 10, April, 1953, pp. 121–126.

8 "Analyzing Winds for Frequency and Duration," by R. H. Sherlock, Meteorological Monograph No. 4, American Meteorological Society, November, 1951, pp. 42–49.

Discussion

PHILIP SPORN.[4] The authors are to be congratulated for this important contribution to the relatively new but steadily growing library of technical papers on control of atmospheric discharges—gaseous and others. This comparatively new branch of engineering is now undergoing the painful and necessarily slow transition from an art to a science. As a science, it is still in its infancy and many man-years of study, research, experiment, and development work by scientists—chemists, physicists, and meteorologists—and by engineers, will be required to keep it growing.

All of those engaged in industrial activity, which involves the discharge of either gaseous or finely divided particulate matter into the atmosphere, should be vitally concerned with the associated problems. Failure to recognize and deal scientifically with the possible atmospheric-pollution aspects of such activity may lead to poor community relations, to possible legal action, and the future need for long equipment outages and large capital expenditures to correct unsatisfactory conditions.

[4] President, American Gas and Electric Service Corporation, New York, N. Y. Fellow ASME.

The electric utilities are especially sensitive to reactions from this source as they strive for and generally enjoy a high degree of respect and good will in the communities which they serve. And they cannot disregard the fact that practically every individual in the community is either individually, or as a member of a family group, a customer to be pleased. In many communities, and especially the smaller ones, local utility officials are quite active in civic affairs and frequently are called upon for help in solving community problems. Thus any question of actual or suspected adverse effect by its operations on the atmosphere by the utility creates an even more serious problem for that utility than would similar effect brought about by an industry not so closely associated with the affairs of the community.

Today, mechanical and electrostatic dust-collecting equipment can be obtained which will prevent the escape of all but a few per cent of the ash from the plant stacks. However, even this small amount of very fine ash can be highly objectionable if it passes directly through inhabited areas before it has become sufficiently dispersed. Furthermore, no satisfactory equipment has been developed for the removal of the end products of combustion of sulphur, although this is being studied both here and abroad. Thus, to provide the greatest possible protection against pollution, it is necessary to remove from stack gases substantially all ash particles which will settle to the ground rapidly by gravity and also to so direct the discharge that fine ash and carrying gases are thoroughly dispersed in the upper atmosphere. Consideration must be given to surrounding terrain, prevailing meteorological characteristics, and adjacent population density.

A design study for Ohio Valley Electric Corporation, covering its two new coal-burning generating plants to supply electric power to the Atomic Energy Commission, has been completed recently, in which both the physical factors discussed by the authors, as well as the question of dispersion of the stack gases, were thoroughly explored. This resulted in the decision to provide stacks higher than generally used to minimize the possibility of atmospheric pollution. The Kyger Creek Plant, 1000-mw capacity, will have three 535-ft reinforced-concrete stacks, two to serve two 200-mw units each and the third to serve a single 200-mw unit. The Clifty Creek Plant, 1200-mw capacity, will have three 680-ft reinforced-concrete stacks, each to serve two 200-mw units. The greater height decided upon for the Clifty Creek Plant stacks results from unusual local conditions, including hilly terrain. All six stacks are designed for 120 fps exit velocity.

C. M. Weinheimer[5] and M. S. Ozker.[6] The presentation of this paper is opportune since it is only of comparatively recent date that the designer of power plants has become conscious of his responsibility in diluting adequately the gases emitted from the stacks of power plants. For a number of years the chief concern of the designer of power plants was the dust-loading of the stack gases at the stack outlet. The installation of adequate dust-arresting equipment makes it possible to obtain any desired value of dust-loading in the stack gases. Also, the use of induced-draft fans minimizes the necessity for tall stacks for draft purposes. As a result of these factors, a tendency has developed to erect power plants with short stacks. With the advent of large power plants with very large steam generators and the use of high-sulphur coals, the power-plant designer was suddenly faced with the problem of diluting the stack gases adequately before they reached ground level. This problem has been accentuated by the publicity given to the whole question of air pollution.

The paper is the first step in developing a rational design procedure that will permit the designer of power plants to arrive at an adequate stack height for normal conditions—both atmospheric and neighboring terrain. The authors clearly point out that the phase of the dilution problem they are dealing with in this paper is down-wash within approximately 2000 ft of the point of emission of the gases. The difficulties of measuring plume height in the field are recognized. The writers would like to ask the authors if they know of any field investigations, the results of which substantiate the work done on wind-tunnel models.

Assuming that the down-wash problem has been solved adequately by the correct choice of gas exit velocity and stack height, have we arrived at the complete answer to the air-pollution problem? Can we assume that the concentration of obnoxious gases at ground level at distances greater than 2000 ft from the power plant will not be irritating or harmful? At this point in the design procedure the meteorologist is called upon to evaluate the dispersion of the plume which up to this time has been maintained at some fixed height above the ground. The results of his studies may indicate that even if down-wash is prevented, it may be possible to have concentrations at ground level at some point that will be objectionable. The Detroit Edison Company is co-operating with the authors in such a program in connection with the design of stacks for the River Rouge Power Plant.

Authors' Closure

Mr. Philip Sporn points to the fact that the art of controlling gases and dusts from smokestacks is still in its infancy, and that many more years of research and development remain to be done before it can be said that this feature of design is really on a scientific engineering basis. That the industries are not averse to doing the pioneer work in this field is well attested by the decisions which have been made by Mr. Sporn's company in connection with the Kyger Creek Plant and more especially at the Clifty Creek Plant.

Messrs. Weinheimer and Ozker asked whether any field investigations have been made which substantiate the work done on wind-tunnel models. It has been practicable to make quantitative comparisons of the actual behavior of the gas plume with the predicted behavior in the case of only one plant. These studies have not yet been published but it can be said that, based on the critical-velocity ratio, the predicted behavior and the actual behavior check very well. In other cases only qualitative observations were feasible but in all of these cases the predicted behavior and the actual behavior were substantially the same.

These discussers raised the further question whether the answers obtained from the wind tunnel constitute a complete solution to the problem. It must be answered that they do not, since it is then necessary to superimpose upon the predicted results in a neutral atmosphere, as shown by wind-tunnel investigations, the predicted atmospheric diffusion. The problem has not been completed until the probable ground concentrations have been computed for SO_2 or other constituents.

Fig. 15, herewith, is an idealized perspective drawing showing the relation between the basic plume and the ground concentrations downwind under the center line of the plume. It also shows the manner in which the concentrations occur on both sides of the plume as a result of lateral dispersion. The equations of Sutton and others may be used to compute the concentrations at different points on the ground provided the proper diffusion parameters are known for the particular situation that exists in any particular case. The best empirical information in regard to the proper value of these parameters is to be found in the work of E. Wendell Hewson, at Round Hill Observatory, and M. E. Smith, at Brookhaven, Long Island. However, the diffusion parameters will be largely affected by the turbulence behind the stacks and buildings, and neither of these investiga-

[5] Head, Mechanical Division Research Department, Detroit Edison Company, Detroit, Mich. Mem. ASME.

[6] Detroit Edison Company. Mem. ASME.

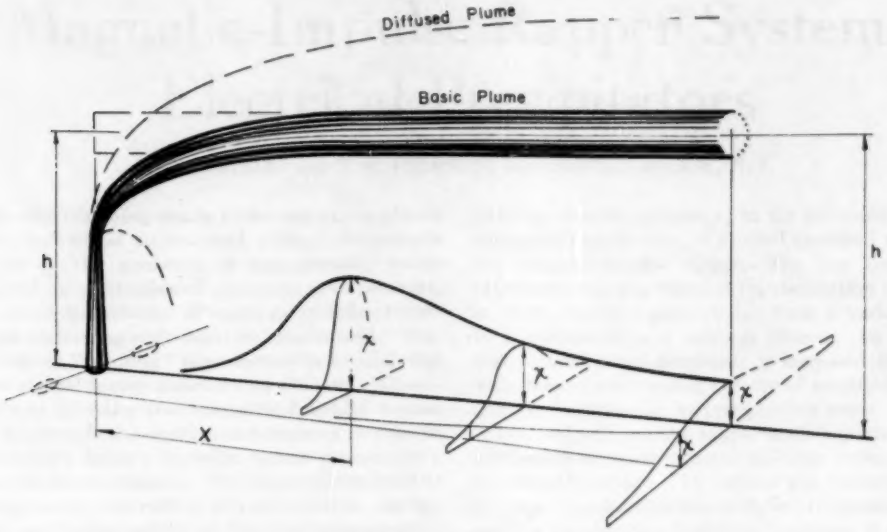

FIG. 15 χ = GROUND CONCENTRATION OF SO_2 AT DISTANCE x

tions includes such turbulence in their observations. There is a need for investigations of this nature to be made at actual plants in operation.

There is also the case of the fumigations which occur during the break-up of temperature inversions. During the night and early morning, temperature inversions may occur as the result of the radiation of heat from the ground. If the night is clear and the wind is light the inversion may have a depth of several hundred feet. Owing to the great stability of the atmosphere in an inversion there is very little vertical mixing and the plume will pass slowly downwind as a shallow ribbon which undergoes practically no vertical dispersion. Such plumes have been followed downwind for many miles. A certain amount of meandering may occur together with some slight lateral spreading. Under such conditions the concentration of the gases in the plume will remain very high.

After sunrise the ground is again heated and a layer of warm air is formed near the ground. The thickness of the layer of newly formed turbulent air increases until eventually it envelops the plume. The vertical mixing brings the gas to the ground in a high concentration. Very little experimental information is available regarding these concentrations and any computations must be based upon assumptions which may be plausible but whose validity is not well established. Nevertheless, it is sometimes necessary to make these plausible assumptions and to proceed with the computations of probable ground concentrations from this source.

Table 2 of this closure illustrates the manner in which information regarding ground concentrations may be tabulated. It shows the hours per year when the concentration of SO_2 lies within certain indicated limits for a particular segmental area to the leeward of the plant. The boxes near the left-hand side of the table contain the number of hours per year of a given concentration, obtained by applying Sutton's equation in the manner indicated in Fig. 15. The diffusion parameters were obtained from several sources, some of which are unpublished. The total number of hours per year that the wind will carry the plume into this particular segmental area is 785. Computations show that higher stacks have a tendency to place more of the hours of this particular wind direction in the lowest category of concentration. The items of four hours per year are due to the

TABLE 2 HOURS PER YEAR WHEN CONCENTRATION OF SO_2 LIES WITHIN LIMITS INDICATED FOR 22.5-DEG SEGMENTAL AREA TO THE LEEWARD OF THE PLANT

(Wind SW; stack height = 350 ft; stack-gas velocity = 60 fps.)

Distance Downwind, Miles	0	.5	1	1.5	2	4	6	8	10
2	405	380				4			
1	410	204	102	69			4		
0	279	200	180	126				4	

Parts per Million by Volume

fumigation which is coincident with the break-up of ground inversions in the morning.

Complete information regarding the dispersion of stack gases requires that a statement of the concentration with which gases reach the ground be supplemented by a statement of both the probable frequency and duration of these events. High concentration for short periods or low concentration for long periods may be equally deleterious.

In conclusion it may be said that a method has been developed for the use of wind-tunnel testing of models by which the design of a station building and its stacks can be determined so that the down-wash of the smoke plume toward the earth due to aerodynamic effects can be practically eliminated.

Knowledge gained in the wind tunnel concerning the behavior of the plume close to the plant can be used as a starting point for the computation of ground concentrations, and the results thus obtained will be more reliable than those based on the usual assumptions.

The techniques of bridging the gap between the tunnel observations and the tabulation of ground concentrations are too lengthy to be quoted here and must be left for further publications. The greatest need which now exists in the diffusion aspect of this problem is the determination of diffusion parameters on the leeward side of actual stacks and plants under various meteorological conditions so that the large-scale turbulence which is generated by the wind passing these obstructions may be represented in the parameters.

A Magnetic-Impulse Rapper System for Electrical Precipitators

By H. J. HALL[1] and T. A. PIERSON, 3rd,[2] BOUND BROOK, N. J.

Considerable effort is being made to reduce atmospheric pollution from industrial fumes and dusts. Attendant with this effort is the problem of transferring waste products, trapped on electrodes of electrical precipitators, to hoppers. Loss or disturbance of waste material or interference with the collecting unit must be minimized. Traditional methods of "rapping" the electrodes to dislodge the collected material leaves much to be desired. Therefore a new method utilizing the magnetic-impulse rapper was developed to provide the continuous rapping needed to convert precipitation from a variable batch process to a continuous and uniform process. This paper discusses the historical background, operating characteristics, design considerations, and application of the electromagnetic-rapper system.

Introduction

INTENSIFIED public and engineering interest in the reduction of atmospheric pollution from industrial fumes and dusts has resulted in increasing demands for higher and higher collection efficiencies from electrical precipitators. Considerable effort, therefore, is being spent to attain the practical and economic realization of the ultimate goal—visually clean stacks continuously maintained.

One of the most important problems in the path of progress toward this ideal has proved to be the efficient removal of the collected material from the precipitator electrodes. The problem, though simple in principle, nevertheless is complicated and difficult in practice. In the usual approach, mechanical vibrations, periodically induced in the electrodes by a process known as rapping, dislodge the accumulated deposits which then fall by gravity into suitable hoppers. The real difficulty arises in transferring the material successfully to the hoppers without causing significant losses as a result of re-entrainment, major disturbances of dust already in the hoppers, or interference with the electrical operation of the precipitator. Evidence of such losses caused by the intermittent rapping practices of the past appeared in substantial stack clouding and puffs during the rapping periods.

Experience has indicated that traditional-type mechanical and pneumatic rapping systems could not adequately meet the requirements for the reliable, uniform, and puff-free precipitator operation essential for gas cleaning in modern power stations. Therefore it was decided to develop a radically new type of rapping system based on electromagnetic operating principles and possessing the inherent characteristics necessary to meet the stringent operating requirements of modern precipitator installations.[3] This new approach to the precipitator-electrode cleaning problem culminated in the successful development and commercial application of a novel electrical rapping apparatus, the magnetic-impulse rapper. The new system provides the continuous rapping essential for elimination of stack puffs and, in effect, converts precipitation from a variable batch process to a continuous and uniform process. In addition, over-all collection efficiency frequently is increased above that possible with intermittent rapping because of continuous maintenance of uniform conditions in the precipitation zones.

The magnetic-impulse rapper is an important and interesting application of modern electronic-pulse techniques to a difficult mechanical problem. In view of the importance of electrode-cleaning operations in electrostatic precipitation and because of possible uses in other industrial processes, it seems worth while to consider, in the light of over three years' operating experience, the design and application factors involved in the new equipment.

First introduced on industrial precipitators in 1949, the magnetic-impulse rapper has proved a satisfactory solution to the difficult collecting-electrode cleaning problem. More recently, the equipment also has been applied to the cleaning of precipitator high-tension discharge electrodes (wires or rods).

After a brief historical background, this paper discusses the operating characteristics, the basic electric, magnetic, and mechanical design considerations, and the application of the electromagnetic-impulse rapper system.

Historical Background—The Rapping Problem

The electrode-cleaning problem began with the successful commercial application of electrostatic precipitation about 45 years ago. A number of different cleaning systems have been used, depending on the type of material being collected. In certain applications, for example, acid mists and tar, the material merely runs down the surfaces of the electrodes into appropriate receptacles, and no special cleaning is required. In other cases, particulate matter is often collected in a wetted state wherein the electrodes may be cleaned effectively by a water spray or flushing system. This method has been used successfully for many years in the electrostatic collection of blast-furnace dust.

On the other hand, there are many precipitators which collect dry materials, for example, fly ash, cement dust, and gypsum. In these cases, the dust gradually builds up into compacted layers on the extended surfaces of the collecting plates, and, although a certain amount continually breaks off by its own weight, additional cleaning is almost always required. Although generally to a lesser degree, the discharge electrodes (wires or rods) also frequently require rappers for cleaning, particularly for electrical precipitators treating dusts having a high percentage of very fine particles, i.e., less than 10 microns.

Many different rapping systems and devices have been tried over the years for cleaning precipitator electrodes. Traditional rapping methods have been based on mechanical or pneumatic operating principles, involving, for example, scraping, applying impulsive forces such as hammer-type blows, or applying forced vibrations at various frequencies. Common difficulties experienced with these earlier rapper systems include excessive complication—often involving cumbersome assemblies and complicated linkages or gears—fatigue failure of metal parts, in-

[1] Research Department, Research Corporation.

[2] Development Engineer, Research Corp. Assoc. Mem. ASME

[3] "Electrostatic Collection of Fly Ash," by H. J. White, L. M. Roberts, and C. W. Hedberg, *Mechanical Engineering*, vol. 72, 1950, pp. 873–880.

Contributed by the Fuels Division and presented at the Annual Meeting, New York, N. Y., November 29–December 4, 1953, of The American Society of Mechanical Engineers.

Note: Statements and opinions advanced in papers are to be understood as individual expressions of their authors and not those of the Society. Manuscript received at ASME Headquarters, April 20, 1953. Paper No. 53—A-131.

ability to perform consistently in the moist, dirty, and corrosive atmospheres often encountered, lack of rapping flexibility, and high initial as well as high maintenance costs.

In operation, general practice usually has been to rap the precipitator electrodes intermittently with fairly high intensities on a schedule varying from about once an hour to once a day. The large amounts of dust suddenly loosened from the collecting plates during such rapping periods gave ample opportunities for appreciable stack discharges caused by re-entrainment, hopper disturbances, and excessive sparking. Although the stack puffs or dust clouds emitted during such rapping periods may reduce average efficiency by no more than 2 or 3 per cent, the psychological effect of the puffs on the public is decidedly poor. Furthermore, with the present increasing trend toward high efficiencies of the order of 98 per cent or more, the continuous maintenance of optimum electrical conditions, the reduction of losses, and the elimination of stack puffs become increasingly important factors in achieving maximum performance. Various schemes, such as the use of pocket-type collecting electrodes or arrangements for closing dampers to shut off portions of the precipitator during rapping, are of limited application and have proved only partially effective in preventing extra dust loss during cleaning operations.

The effectiveness of the continuous-rapping method in eliminating objectionable stack puffs had been demonstrated in 1947.[4] However, subsequent field tests showed that the rapping intensity required for best operation usually is quite critical and in a range considerably below that for which rappers designed for intermittent operation are reliable and practical. Hence there was an urgent need for a new kind of rapping system to meet the basically different requirements imposed by the continuous-rapping principle.

The important requirements which must be met are as follows:

Reliability. Must operate continuously over long periods without service or adjustment in industrial atmospheres which frequently involve corrosive gases, moisture, and suspended dirt.

Wide Range of Intensity Control. Intensity must be easily and smoothly adjustable from zero to maximum. Although continuous rapping of banks of collecting electrodes in fly-ash precipitators generally requires very low impact intensities of the order of a few inch-pounds, much higher intensities also must be available to suit a variety of different applications and to effect thorough cleaning in a short time—for example, prior to precipitator inspections, and so on.

[4] Unpublished work of Research Corporation field engineers.

Uniform Operating Characteristics. Among individual rapper units, operating characteristics must be uniform.

Stable Performance. This must be possible over long periods of time without adjustment or maintenance. Rapper intensity at any given setting must remain constant.

General Description and Operation

The magnetic-impulse rapper system is based on electric and magnetic principles using pulse techniques developed for radar applications during the last war. Fig. 1 shows the basic elements employed. The rapping action is delivered by the armature of a solenoid electromagnet. The magnet coil is excited by the impulsive discharge of a capacitor which is timed and controlled by the thyratron and distributor switch. A large number of rapper units, up to 24 or more, which may include both plate and high-tension rappers, can be energized from one power unit. Both the intensity and the frequency of rapping are easily adjustable to meet varied requirements. Components of the new equipment, comprising rapper unit, pulse-generator power unit, and remote-control unit, are shown in Figs. 2, 3, and 4, respectively.

The rapper unit is a solenoid electromagnet consisting of a steel plunger held in normal position by a steel spring and surrounded by a concentric coil, all enclosed in a hermetically sealed steel case. The rapper case is welded to the end of a rapper bar protruding through the precipitator shell and connected to a group, or bank, of collecting-plate electrodes. When each magnet coil is consecutively energized by a short current pulse supplied from the pulse generator, the plunger is driven rapidly against the rapper bar, thereby producing the necessary shock vibrations to dislodge the dust accumulated on the plates.

Fig. 5 shows the basic electrical circuit of the pulse generator. Capacitor C is charged through resistance R from a d-c power supply consisting of a transformer and full-wave rectifier. Thyratron tube V acts as a controlled switch to discharge the condenser energy through the rapper coil. The distributor switch functions merely to connect consecutively each rapper coil into the circuit preparatory to each discharge of condenser C; it does not make or break any current. The construction of this switch is such that a closed-circuit path is continuously provided for the condenser-charging current. The thyratron is fired by a positive grid-voltage pulse controlled by switch S, which is automatically synchronized with the distributor switch. Both the rectifier tubes and the thyratron are Xenon-filled and, therefore, are unaffected by normal ambient-temperature variations. By means

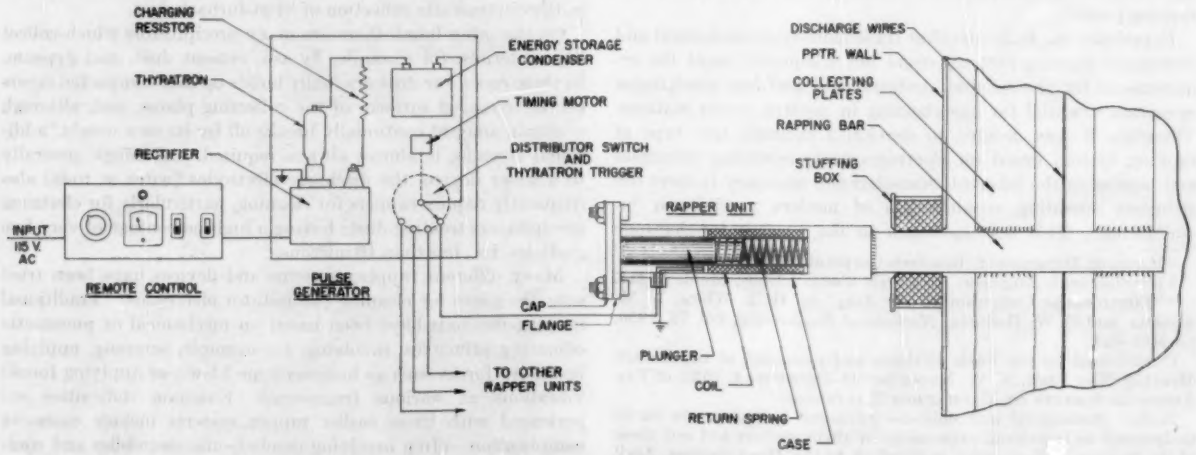

Fig. 1 Magnetic-Impulse Rapper System

FIG. 2(*a*) EXTERIOR VIEW OF HERMETICALLY SEALED MAGNETIC-IMPULSE RAPPER UNIT

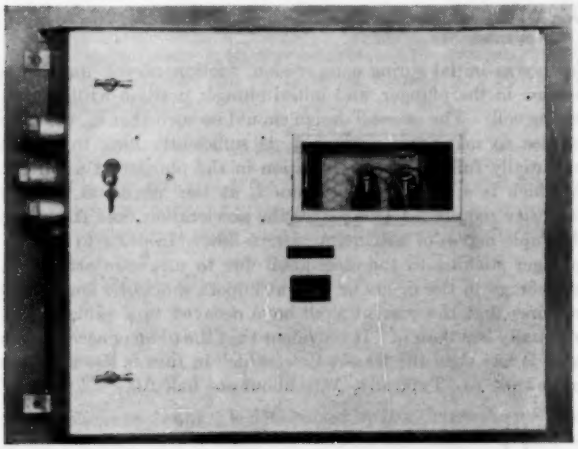

FIG. 3(*a*) EXTERIOR VIEW OF WEATHERPROOF, CABINET-TYPE PULSE GENERATOR

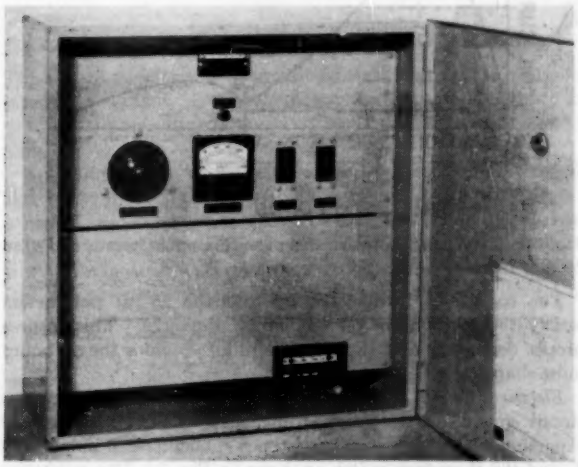

FIG. 4 MAGNETIC-IMPULSE-RAPPER REMOTE-CONTROL UNIT

of controlled-impulse energization, high-peak plunger energies may be obtained with low average power consumption.

General operating characteristics of the magnetic-impulse rapper system may be summarized as follows:

Power Input. 105–125 volts, single phase, 60 cps, maximum demand 0.5 kva. Also can be supplied with built-in distribution transformer for 230 or 460-volt input. Normal power consumption is approximately 300 watts per pulse generator.

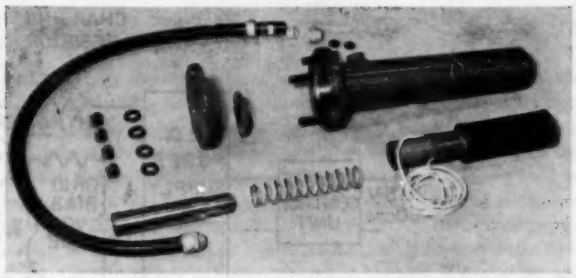

FIG. 2(*b*) COMPONENT PARTS OF MAGNETIC-IMPULSE RAPPER UNIT

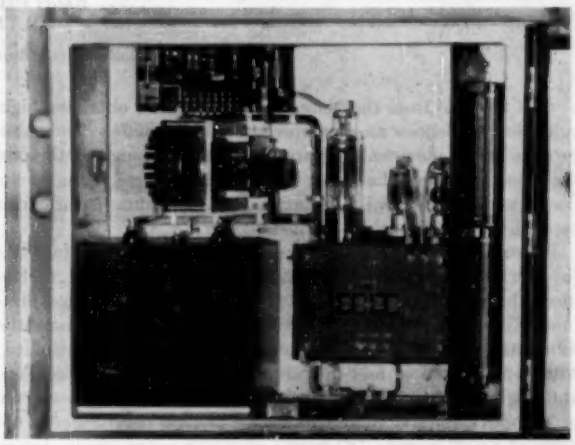

FIG. 3(*b*) INTERIOR VIEW OF PULSE GENERATOR

Number of Rapper Units. Any number up to 24 per power unit.

Rapping Intensity. Remotely controlled by variable autotransformer which regulates primary voltage to power transformer and hence the energy-storage-condenser voltage. Intensity is smoothly adjustable from zero to a maximum of about 20 ft-lb plunger energy at impact, corresponding to a condenser voltage of 2000 volts d-c.

Rapping Frequency. Controlled by the speed of distributor switch. Typically, a 1-rpm-switch motor is used to energize successive rappers at $2^1/_2$-sec intervals with a 24-point switch. Both the rapping frequency and the rapping sequence may be adjusted to suit the particular installation. Proper operation of the system is monitored by a flashing indicator light on the remote-control panel, thus eliminating frequent inspection trips to the rest of the equipment.

Starting Conditions. In order to overcome spring tension, friction, and the like, a minimum condenser voltage is required to cause the plunger to just strike the anvil. The average starting voltage is 630 volts, with a maximum variation of ±5 per cent measured on 500 production rapper units. Manufacturing tolerances on the rapper-coil inductance and d-c resistance are ±5 per cent.

Ambient Temperature. Rapper unit, 200 F maximum; power unit and remote-control unit, 122 F maximum.

With the new rapping method, the amount of dust buildup on the collecting plates is maintained continuously at the optimum thickness for maximum collection efficiency. With the rapping intensity properly adjusted for the conditions at hand, visual observation of the plates during operation reveals that the collected material becomes dislodged in random patches of limited size and tends to fall rather close to the plates in a region partially shielded from the main gas stream. These conditions

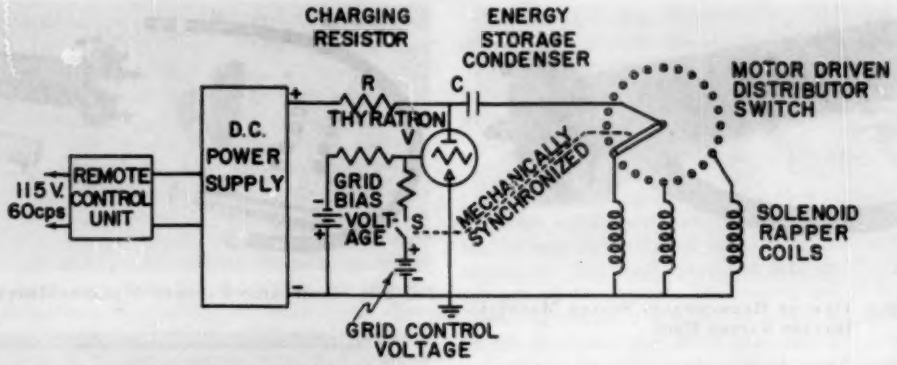

FIG. 5 BASIC ELECTRICAL CIRCUIT FOR MAGNETIC-IMPULSE RAPPER

of dust removal from the plates are favorable for obtaining high collection efficiencies and for preventing stack puffs. They also provide stable electrical operation and uniform and continuous dust removal from the precipitator. All of these factors help insure and are essential to obtaining the maximum performance capabilities of the precipitator installation.

Practical operating advantages of the new system include: (*a*) The use of only one major moving part in the rapper mechanism, the rapper plunger, which is hermetically sealed against dirt, moisture, and corrosive atmospheres, and which is permanently lubricated at the time of manufacture; (*b*) installation flexibility, with remote control and operation of both collecting-electrode and high-tension discharge-electrode rappers from a common power unit; (*c*) simple and reliable circuitry, requiring a minimum of maintenance; (*d*) very low power consumption, hence low operating costs and low-power capitalization penalties.

DESIGN CONSIDERATIONS

The electric, magnetic, and mechanical design factors involved in the magnetic-impulse rapper system are complex and interdependent. The basic electric and magnetic-circuit problem involves the production, distribution, and control of a current pulse of proper shape, duration, and amplitude to produce the plunger forces dictated by the rapping intensities required. Within the electric and magnetic-circuit requirements, the mechanical design must provide maximum reliability, at reasonable cost, with proper consideration for the basic requirements of:

1 Continuous operation.
2 Protection against dirty, moist, or corrosive atmospheres.
3 Rapper-unit ambient temperature up to 200 F; power unit and control-unit ambient temperatures up to 50 C (122 F) maximum.
4 Installation and operating flexibility.
5 Adequate accessibility.
6 Personnel safety.

Current-Pulse Requirements. The pulse generator produces a current pulse in the magnet coil shown in Fig. 6. The current rises in time Δt_0 to a value i_1 required for plunger motion to begin. The plunger is accelerated during time Δt_1 while the current is greater than the starting value. The current then falls to a low value i_2 by the time the plunger strikes the end of the rapper case. Thus the plunger transit time is Δt_2. The slight rise in the current after the plunger completes its stroke is due to the rebound effect which occurs only at relatively high intensities. The pulse length T is obtained by extending the current after i_2 to the time axis, as shown in Fig. 6.

The starting current i_1 and the time Δt_0 are determined by the physical system and the magnetic-circuit design, involving such factors as initial spring compression, friction effects, flux penetration in the plunger, and initial plunger position with respect to the coil. The over-all design should be such that t_m, the time of rise to maximum current i_p, is sufficiently long to permit essentially full magnetic saturation in the plunger at a current i_1 which is appreciably less than i_p at the maximum rapping intensity required. This places the acceleration time Δt_1 in the desirable region of maximum current flow. In order to prevent plunger sticking to the steel anvil due to magnetic attraction, the energy in the magnetic field at impact should be low. This requires that the current shall have decayed to a value i_2 substantially less than i_1. It is evident that the plunger acceleration time is less than the transit time, which in turn is less than the pulse time T. Typically, Δt_1 is about one half Δt_2.

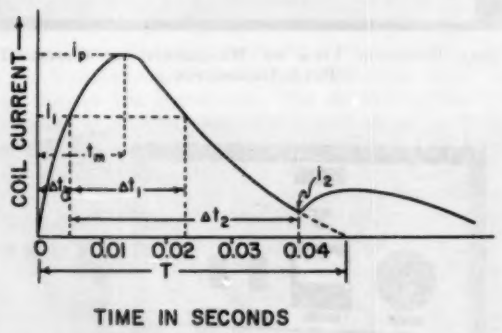

FIG. 6 TYPICAL MAGNETIC-IMPULSE-RAPPER CURRENT PULSE

The conditions further require that the circuit parameters satisfy the relationship for oscillatory discharge. This insures proper deionization of the thyratron and provides the optimum pulse shape.

Electrical Circuit Parameters. The equivalent pulse-discharge circuit consists of the series arrangement of the energy-storage capacitance C, effective coil resistance r, magnet-coil inductance L, and the thyratron switch as shown in Fig. 7. The resistance of the thyratron during conduction is negligible in comparison to r.

The equation for the current as a function of time for the oscillatory case, shown in Fig. 6, is well known and may be written as

$$i = \frac{E}{L\omega} \epsilon^{-\alpha t} \sin \omega t \quad \ldots\ldots\ldots\ldots\ldots [1]$$

where

E = voltage to which C is initially charged

$$\omega = \frac{1}{2L}\sqrt{\frac{4L}{C} - r^2}$$

$$\alpha = \frac{r}{2L}.$$

ϵ = base of natural logarithms

Also, $\omega^2 = \omega_0^2 - \alpha^2$, where $\omega_0^2 = 1/LC$

In practice, the current cannot reverse polarity because of the unidirectional properties of the thyratron; hence only the portion from $t = 0$ to $t = T$ is of interest. The equations for the various parameters follow.

Pulse Length

$$T = \pi/\omega \quad \ldots\ldots [2]$$

As a first approximation, we may assume that the average plunger velocity is about one half its terminal velocity and obtain an estimated transit time

$$\Delta t_2 \cong 2S\sqrt{m/2Q} \quad \ldots\ldots [3]$$

where S is the stroke, m is the mass of the plunger, and Q is the desired kinetic energy at plunger impact. The order of magnitude of the required pulse length T will then be slightly greater than Δt_2.

Time of Rise to Maximum Current

$$t_m = \frac{\tan^{-1}\dfrac{\omega}{\alpha}}{\omega} \quad \ldots\ldots [4]$$

The minimum value of t_m is determined by flux-penetration effects in the plunger. For a solid, cold-rolled steel plunger, slotted to reduce eddy currents, t_m should be of the order of 0.01 sec.

Peak Current

$$I_p = \frac{E}{L\omega}\epsilon^{-\alpha t_m}\sin \omega t_m \quad \ldots\ldots [5]$$

This is determined by the magnetic forces required for the rapping intensities desired, as discussed in the following section. In practice, the operating range of peak currents is between 3 and 8 amp.

These equations, with the exception of Equation [3], are all derived on the assumption that the magnet-coil inductance L is a constant, which of course is not strictly true after the plunger starts to move. However, the initial rise characteristic and the wave form in general are determined by the inductance of the coil with the plunger at its initial position. The peak current calculated from Equation [5], using $L = L_0$ and $\alpha = r/2L_0$, where r is the d-c resistance of the coil and L_0 is the inductance with the plunger at its initial position, is typically 10 to 20 per cent higher than that obtained in practice with plunger motion.

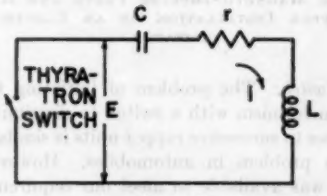

FIG. 7 EQUIVALENT PULSE-DISCHARGE CIRCUIT

Circuit Efficiency. The discharge circuit efficiency η_d is given by

$$\eta_d = \frac{W_m}{(1/2)CE^2} \quad \ldots\ldots [6]$$

where W_m is the mechanical work done by the motion of the plunger. With a solid-steel plunger, slotted to reduce eddy currents, η_d may be of the order of 15 to 20 per cent. Owing to the inherently low average power consumption with a pulse system of this type, discharge efficiencies of even 10 per cent or less can be tolerated. The greatest loss factor is the resistance of the rapper coil, wherein 70 to 75 per cent of the initial stored energy is dissipated. The hysteresis and eddy losses in the steel parts, the energy left in the condenser at the end of the pulse, and the loss in the thyratron are relatively small.

Magnetic Design. By equating to zero the algebraic sum of the forces acting on the plunger, we may write the dynamic equation of motion as

$$m\frac{dv}{dt} + k_1 v + kx = f - F_0 \quad \ldots\ldots [7]$$

where

m = mass of plunger
v = plunger velocity
x = plunger displacement from its initial position
k_1 = friction factor
k = spring constant
F_0 = static force due to initial spring compression
f = instantaneous magnetic force on plunger

Equation [7] is valid when $f \geqq F_0$. Referring to Fig. 6, this defines a time Δt_0 when motion begins, i.e., when $f = F_0$ and $i = i_1$.

The magnetic force on the plunger is given by

$$f = H\varphi_L \quad \ldots\ldots [8]$$

where H = magnetic intensity and φ_L = leakage flux.

The voltage equation from the electric circuit is

$$d\frac{(N\rho)}{dt} + ri + \frac{1}{C}\int i\,dt = 0 \quad \ldots\ldots [9]$$

The detailed solution of Equations [7] and [9] can be made by step procedures described in the literature[5] and the various parameters plotted as functions of time or distance x. However, by neglecting the last two terms in the left side of Equation [7], and assuming that plunger motion does not begin until the plunger flux has become practically constant as a result of saturation, we may obtain a direct solution adequate for general design purposes. The result, giving the approximate peak ampere-turns required for the desired plunger kinetic energy at impact, is, in practical units

$$NI_p = \frac{1.13 \times 10^4 h}{\eta B_p A}\left(\frac{\sqrt{2Qm}}{\Delta t_2} + F_0\right) \quad \ldots\ldots [10]$$

where

h = coil length, in.
Q = desired plunger kinetic energy at impact, ft-lb
B_p = saturation flux density for steel used in kilolines per sq in.
A = cross-section area of plunger, sq in.
Δt_2 = plunger transit time
η = efficiency factor including ratio of average current to peak current over interval Δt_2, flux-penetration effects, and factor relating leakage flux to plunger flux

[5] "Electromagnetic Devices," by H. C. Roters, John Wiley & Sons, Inc., New York, N. Y., 1945.

For a given type of steel and construction, the product ηB_p may be considered an empirical constant. The design procedure is, therefore, to make a reasonable assumption for ηB_p, calculate the required peak ampere-turns from Equation [10], and make a trial rapper unit with the various parameters selected to satisfy the electric-circuit design requirements. The design then is modified according to the test results until a satisfactory compromise among the various factors is obtained. Roters gives an excellent treatise on the details of magnetic-circuit design.[8]

Mechanical Design

The final mechanical design to meet the basic requirements previously stated was attained after considerable development, accelerated laboratory life tests, and field tests. The pertinent mechanical design features of the equipment are discussed in this section.

Rapper Unit. The rapper coil must withstand repetitive electrical stresses up to 2000 volts and very high mechanical stresses caused by the reaction to the magnetic forces on the plunger. Since the operation involves the conversion of electromagnetic energy to mechanical energy over a very short time interval, it is inherent that both electrical and mechanical stresses in the coil will be impulsive. The final coil evolved as one wound on a sturdy, preformed, phenolic form with rigid end plates for the winding space and of such diameter and extended length to fit snugly within the rapper case. The winding margins are filled in with insulation between wire and coil form to eliminate slippage or movement of the layers. The completed coil is vacuum impregnated with a suitable electrical varnish to form a solid, durable assembly. Careful internal splices from the No. 25 coil wire to heavier flexible-coil leads, plus adequate taping to the coil form, are required to provide connections impervious to shock operation.

The major requirement of the plunger is ability to withstand severe repetitive mechanical shocks. Tests on several selected magnetic materials, both laminated and solid construction, showed that a satisfactory compromise among magnetic properties, machining properties, shock resistance, and cost could be obtained with a solid plunger made of a low-carbon, cold-rolled steel. Diametrical, longitudinal slots are cut to reduce eddy currents and a slight end taper is used to prevent binding against the spring.

Compression-fatigue failures resulting in cross-sectional cracking of initial plunger models, occurring after about 50,000 blows, were traced by laboratory analysis to minute tool marks at the change in cross section. A ground fillet at this point eliminated the difficulty. Some peening of plunger ends occurred initially due to the presence of bits of foreign matter between contacting surfaces causing local bearing failures. With clean surfaces, however, no bearing failures are observed. Accelerated-life tests were conducted to investigate this and other features with test rappers operating at full voltage in a simulated mounting. While initial failures occurred after 75,000 blows, no failure had occurred with the final design after 1,500,000 blows, corresponding to a typical field-service operating period at very high rapping intensity of 1.4 years. The life tests also showed that the return spring diameter must be held to ±0.010 in. tolerance.

Since the rapper units may operate in dirty, corrosive, or moist atmospheres and must perform with an absolute minimum of maintenance, it was necessary to provide hermetic sealing with a permanent, dry-type lubrication. An eminently satisfactory solution to the lubrication problem was obtained with a press-fit, coil-form inner liner of graphite-impregnated phenolic material. This method has advantages of simplified assembly, few rejections, and low unit cost, combined with excellent performance.

The rapper case is made of standard seamless-steel tubing, welded to an anvil block at one end and a removable, bolted cap on the other end. The cap is gasketed with a special cork-neoprene material which absorbs the plunger-rebound shock as well as provides a gastight seal. A threaded end cap used on early models proved unsatisfactory because of a tendency for thread seizure caused by slight threading imperfections aggravated by repetitive shock conditions. The coil leads emerge from the case through a special washer, seal-tested at 15 psig, and pass through a short length of weatherproof flexible conduit to a nearby junction box. Thus the hermetic sealing of the complete assembly is achieved.

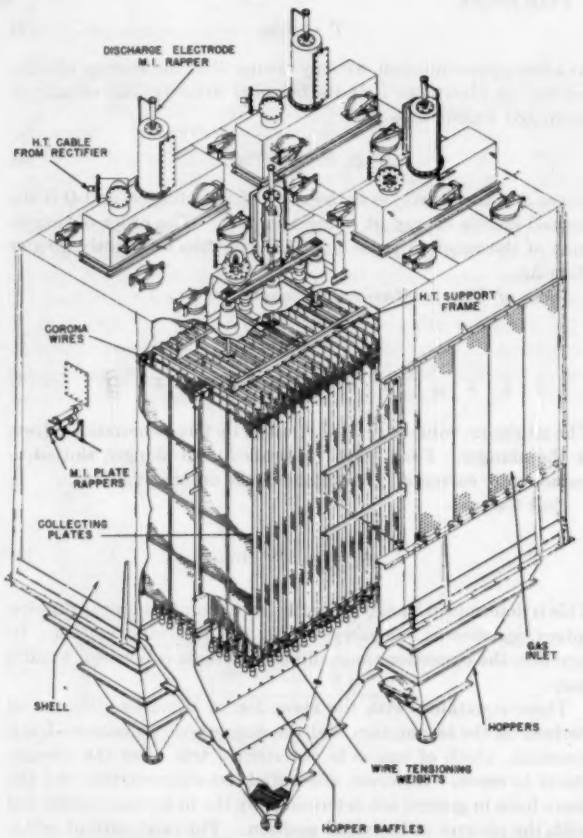

Fig. 8 Typical Magnetic-Impulse Plate and High-Tension-Electrode Rapper Installation on an Electrostatic Precipitator

Distributor Switch. The problem of initiating the capacitor discharge in synchronism with a switch to distribute the resulting current pulses to successive rapper units is similar to the well-known ignition problem in automobiles. However, no commercial switch was available to meet our requirements. After initial use of a special 12-contact piano-type switch, we recently adopted the 24-point rotary-switch design shown in Fig. 3(*b*). The components are mounted on a cast-aluminum base with machined mounting surfaces. A plate cam controlling the thyratron-grid circuit is mounted on the wiper-arm drive shaft, which is turned at the typical rate of 1 rpm by a small electric motor. The plate cam contains 24 small screws arranged in a circle and

adjusted to actuate a microswitch which fires the thyratron in automatic synchronization with the proper positions of the rapper distributor-switch arm. The microswitch roller bearing is made of a special hardened steel to minimize wear. The switch construction is such that one pair of contacts is always closed so that the circuit between the energy-storage condenser via the rapper coils to ground cannot be interrupted. In this way a closed circuit for the condenser-charging current is maintained. Connections from rapper units to the distributor switch are made at the back of the contact plate by means of special airplane-type, snap-on connectors for easy installation and maintenance. In addition, the over-all design combines rugged and compact construction with maximum operating reliability and flexibility.

Power Supply and Control Unit. The pulse-generator power unit, Fig. 3, comprises an accessible arrangement of the d-c filament and bias supplies, charging resistance, energy-storage condenser, distributor switch, thyratron, and trigger circuits. The three tubes are mounted integrally on the hermetically sealed transformer case. The charging resistance is contained in a separate ventilated compartment. The design provides a weatherproof cabinet of minimum size for field installation, located close to the rapper installation to reduce field wiring. Connections between the distributor switch and the rapper units are made via the three conduit outlets on the left side of the cabinet. The cabinet door has an observation window and is equipped with safety interlocks to shut off power and to discharge the condenser.

The control panel for this equipment was designed as a separate unit for convenient location, possibly some distance away from the rest of the installation. Only four wires in conduit to the power unit are required. Fig. 4 shows the control panel in a weatherproof cabinet. Smooth control of rapping intensity from zero to maximum is provided by a variable autotransformer with a panel voltmeter. The unit also is equipped with magnetic circuit breakers and a flashing pilot light indicating proper operation of the system. The particular control unit shown in Fig. 4 also contains a distribution transformer for operation from either 440, 220, or 110 volts, 60-cycle input.

Application

The magnetic-impulse rapper system described herein was first applied to the collecting-plate cleaning operation on fly-ash precipitators in the summer of 1949. At the present time, magnetic-impulse plate rappers are being specified on all new Research Corporation fly-ash precipitators. The method also has been used successfully on a number of other precipitator applications, including gypsum, cupola furnace dust, open-hearth gas cleaning, iron-ore sintering plants, and others.

Within the past two years the continuous rapping method and the magnetic-impulse rapper system also have been applied to high-tension electrode cleaning. For this purpose the standard plate-rapper solenoid unit is mounted vertically on a porcelain-post insulator through which the rapping energy is transmitted via a metal rod directly to the high-tension-electrode frame supporting the discharge wires or rods inside the precipitator. Fig. 8 shows a typical magnetic-impulse rapper installation for both plate and high-tension electrode cleaning on an electrostatic precipitator. Automatic operation of all the rappers from a single power unit provides an economical rapping system and greatly simplifies installation, operation, and maintenance.

Conclusions

Experience on over 700 operating rapper units has demonstrated the efficacy of impulse-type rapping and the value of sectionalized, continuous rapping of closely controlled intensity as an effective means for eliminating objectionable stack puffs and, equally important, for maintaining optimum electrical conditions. Under these conditions, electrostatic precipitators can be operated continuously at maximum collection efficiency.

Performance of the Periphery Pump

By H. W. IVERSEN,[1] BERKELEY, CALIF.

The periphery-pump performance is analyzed in terms of shear stresses imparted to the fluid by the impeller. The resulting expressions include two shear coefficients and an average impeller velocity, which are determined experimentally. The analysis predicts the shapes of the performance curves of head, power, and efficiency as functions of the flow rate. The shear coefficients, and hence the pump performance, are shown to be functions of the impeller roughness, and of the flow channel area.

Nomenclature

The following nomenclature is used in the paper:

a = shear area
A = flow area
C = shear-stress coefficient
D = diameter
e = efficiency
g = gravitational constant
H = head
m, n = flow-channel dimensions
N = rotational speed
p = pressure
Q = flow rate
U = impeller linear velocity
V = fluid linear velocity
w = fluid unit weight
ρ = fluid density = w/g
τ = shear stress

Subscripts:

c = casing
i = impeller
o = shutoff
1 = fluid inlet
2 = fluid outlet

Introduction

The periphery pump, also designated as the tangential, turbine-vane, regenerative, turbulence, or friction pump, produces pumping action by the motion of a rough surface in a channel containing fluid. The fluid is dragged along by the rough surface, and, with suitable restraints in the channel, the fluid head is increased in the direction of the flow.

The essential elements of the periphery pump are shown in Fig. 1. The impeller is a disk with vanes on the periphery. The casing contains the fluid passage, or raceway. Inlet and discharge ports connect the external-system piping to the raceway. Between the discharge and inlet, the casing clearance is reduced to block the high-pressure discharge from the low-pressure inlet. Clearances between the impeller disk and the casing are kept to a minimum to prevent leakage from the high-pressure side of the pump back to the low-pressure side.

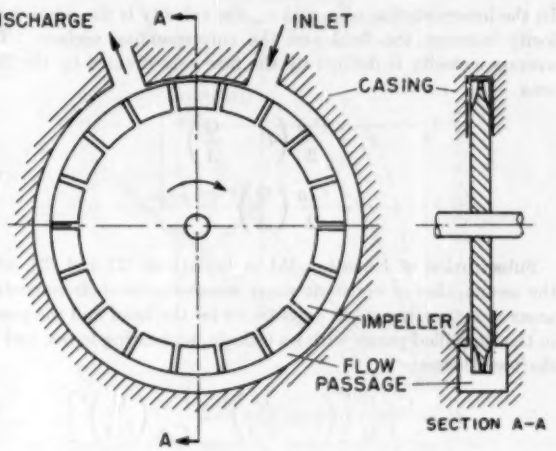

Fig. 1 Elements of Periphery Pump

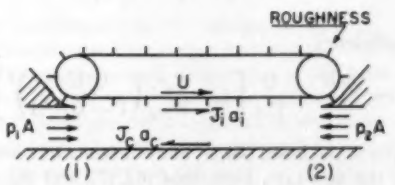

Fig. 2 Simplified Periphery Pump for Force Analysis

Analysis of Pumping Action

The pumping action is simply described from consideration of a linear system, Fig. 2, with a linear motion of the rough surface. A force balance on the fluid in the horizontal flow channel yields

$$p_1 A - p_2 A - \tau_c a_c + \tau_i a_i = 0 \quad \ldots\ldots [1]$$

where p_1 and p_2 are the inlet and discharge pressures, A is the constant net flow cross-section area, τ_c is the shear stress from the stationary wall of area a_c, and τ_i is the shear stress from the moving impeller of net area a_i. The fluid in the pockets between the vanes does not leave at section 2; hence the area A is the unobstructed flow area.

The pump head for an incompressible fluid, for the simple system with no leakage is, from Equation [1], and with the elevation $z_1 = z_2$ and the average velocity at inlet and outlet $V_1 = V_2$

$$H = \left(\frac{p_2}{w} + z_2 + \frac{V_2^2}{2g}\right) - \left(\frac{p_1}{w} + z_1 + \frac{V_1^2}{2g}\right) = \frac{\tau_i a_i - \tau_c a_c}{wA} \quad \ldots\ldots [2]$$

The same result would be shown if the unit were not horizontal.

In addition, the power input to the pumped fluid from the moving surface is

$$P = \tau_i a_i U \quad \ldots\ldots [3]$$

where U is the moving-surface velocity.

The shear stresses are expressed in the usual fashion in terms of

[1] Associate Professor of Mechanical Engineering, University of California. Assoc. Mem. ASME.

Contributed by the Hydraulic Division and presented at the Annual Meeting, New York, N. Y., November 29–December 4, 1953, of The American Society of Mechanical Engineers.

Note: Statements and opinions advanced in papers are to be understood as individual expressions of their authors and not those of the Society. Manuscript received at ASME Headquarters, July 14, 1953. Paper No. 53—A-102.

a shear coefficient and an average fluid velocity with the fluid density ρ

$$\tau = \frac{C\rho V^2}{2} \quad \ldots\ldots [4]$$

In the interpretation of τ_i and τ_e, the velocity is the relative velocity between the fluid and the corresponding surface. The average velocity is defined by the flow rate divided by the flow area

$$\left.\begin{aligned} \tau_i &= \frac{C_i\rho}{2}\left(U - \frac{Q}{A}\right)^2 \\ \tau_e &= \frac{C_e\rho}{2}\left(\frac{Q}{A}\right)^2 \end{aligned}\right\} \quad \ldots\ldots [5]$$

Substitution of Equation [5] in Equations [2] and [3], with the assumption of constant shear stresses over their respective areas of action, results in expressions for the head and the power in the simplified pump with no leakage, no bearing losses, and no shaft-seal losses

$$H = \frac{C_i a_i U^2}{A\,2g}\left[\left(1 - \frac{Q}{UA}\right)^2 - \frac{C_e a_e}{C_i a_i}\left(\frac{Q}{UA}\right)^2\right] \quad \ldots\ldots [6]$$

$$P = \frac{C_i a_i \rho U^3}{2}\left(1 - \frac{Q}{UA}\right)^2 \quad \ldots\ldots [7]$$

For the efficiency

$$e = \frac{QwH}{P} = \frac{Q}{UA}\left[1 - \frac{C_e a_e}{C_i a_i}\left(\frac{Q/UA}{1 - Q/UA}\right)^2\right] \quad \ldots\ldots [8]$$

The shapes of the head, power, and efficiency relationships as a function of the flow rate, Equations [6], [7], and [8], are shown in Fig. 3 for various values of the shear-coefficient ratio. Head and power are expressed as fractions of the zero flow, or shut-off, head and power. The flow rate is expressed as the fraction of the product UA, which corresponds to the condition of all the fluid in the flow channel moving with the surface velocity.

The assumption of constant shear-stress coefficients is reasonable in that the flow is highly turbulent from the action of the rough moving surface. The inertial effects in the flow pattern govern the flow. The fluid viscosity has negligible effect, similar to fluid flow in rough pipes at large Reynolds numbers.

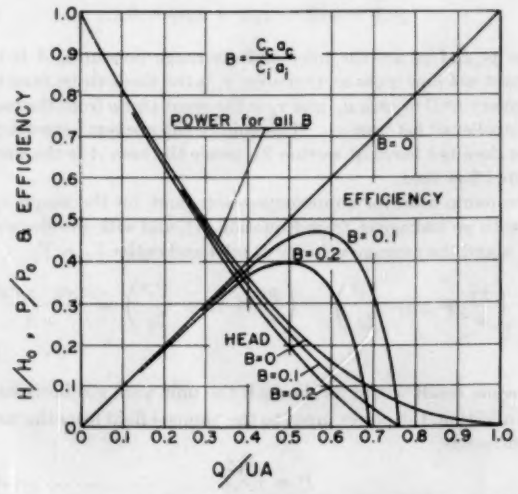

FIG. 3 PERFORMANCE CHARACTERISTICS AT CONSTANT SPEED, NEGLECTING LEAKAGE, BEARING, STUFFING-BOX, AND DISK-FRICTION LOSSES

The analysis is applicable to the actual pump of Fig. 1. Leakage, power losses in bearings, stuffing boxes, and disk friction, and interpretation of the moving-surface velocity must be considered.

Leakage between the high-pressure and low-pressure sides of the raceway through the clearance passages is a function of the pressure difference or head. Qualitatively, the leakage affects the predicted head-capacity relationship as shown in Fig. 4.

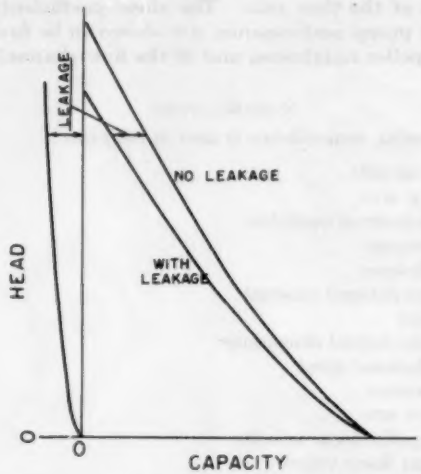

FIG. 4 EFFECT OF LEAKAGE ON HEAD-CAPACITY PERFORMANCE

Pump head is normally determined from inlet flange to discharge flange. Losses in the inlet and discharge passages reduce the net head delivered by the pump. Since the passage losses may be taken as proportional to the square of the flow rate, the passage-loss coefficient may be incorporated in the casing shear coefficient to increase the value of $C_e a_e$.

The power relationship of Equation [7] should have additional terms for bearing losses, stuffing-box losses, and disk-friction losses.

The analysis of the linear system was made with all portions of the vaned surface moving at the same velocity. In the actual pump, the linear velocity of the vanes varies from the vane root to the tip. An average effective velocity of the moving surface must be specified in Equations [6], [7], and [8] to retain the simple form of the equations.

Thus numerous particulars of the analysis are needed to establish numerical results. Exclusive of leakage, mechanical losses, and disk-friction losses, three variables, the two shear-stress coefficients, and the effective vane velocity, must be established numerically. No attempt will be made to obtain the three pumping-action variables by direct interpretation of the internal-flow mechanism. The variables will be obtained from test results of a periphery pump to show the correspondence of the predicted shapes of the performance curves of Equations [6], [7], and [8] with the shapes of the test curves.

TEST RESULTS

A periphery pump was tested with water at approximately 70 F at speeds of 900, 1200, and 1500 rpm, using standard laboratory procedures to determine capacity, head, and shaft power. Dimensions of the pump and test results are shown in Fig. 5. Bear-

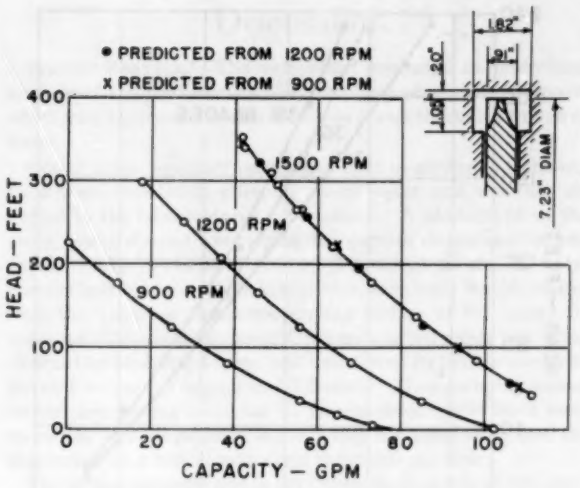

FIG. 5 TEST PERFORMANCE INCLUDING MODEL-LAW APPLICATION
(Pumped fluid is water at 70 F.)

ing and stuffing-box losses were eliminated from the power by deducting the power required to rotate the shaft without the impeller from the measured power input.

The end points of the head-capacity curve and the end point of the power curve at zero flow were used to obtain three equations to solve for the two shear coefficients and the effective impeller velocity. Leakage and disk friction were assumed small and negligible in order to apply Equations [6] and [7] directly. The assumption of small disk friction appears justified from the

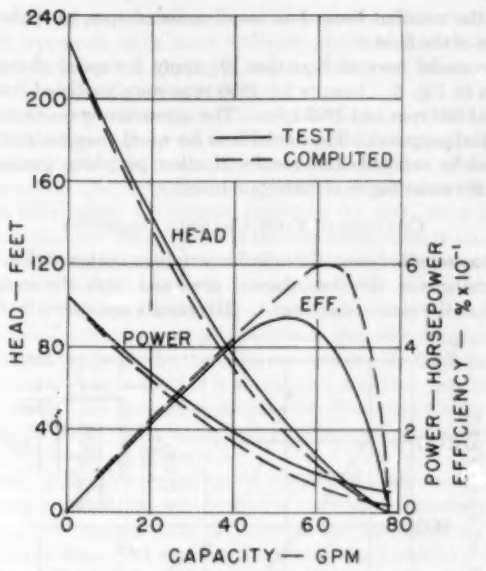

FIG. 6 COMPARISON OF 900-RPM PERFORMANCE OF FIG. 5 WITH COMPUTED PERFORMANCE
(Flow-channel area = 0.0084 sq in.; $C_{fs_f} = 0.206$; $C_{s_d s_c} = 0.0062$; $U = 24.3$ fps.)

low-power requirements at the maximum capacity. Minimum practical clearances in the pump minimized the leakage effects.

The predicted shapes and magnitudes of the head curve and power curve, Fig. 6, show reasonable agreement with the test curves. Of course the end points used to obtain the coefficients are the same for the test and predicted results. The shape of the predicted efficiency curve is the same as the test curve. The higher predicted maximum efficiency as compared to the test efficiency is expected due to the neglected disk-friction loss which becomes increasingly important at the low total-power input at high flows in the range of maximum efficiency.

The effective vane velocity of 24.3 fps is between the vane-tip velocity of 28.4 fps and the vane-root velocity of 20.2 fps. The effective vane velocity appears to be a weighted average which depends upon the geometry of the flow passage.

The preceding analysis, while not directly applicable to the prediction of performance of any selected pump geometry due to the unknown magnitudes of the shear coefficients and effective vane velocity, at least affords a simple representation of the performance of the periphery pump. Investigation of the performance of many different pumps may lead to methods of obtaining the magnitudes of necessary variables for complete performance prediction.

Senoo[2] gives an analysis of performance which results in much more complex expressions than Equations [6], [7], and [8]. This analysis also requires the determination of at least three coefficients from test results.

MODEL LAWS

The model laws for the periphery pump are derived from Equations [6] and [7] in terms of the rotational speed of the impeller and the diameter of the impeller. For geometrically similar pumps

$$\left.\begin{aligned} Q &\propto ND^3 \\ H &\propto N^2D^2 \\ P &\propto \omega N^2D^3 \end{aligned}\right\} \quad \ldots\ldots\ldots\ldots\ldots\ldots [9]$$

[2] "Theoretical Research on Friction Pump," by Y. Senoo, Reports of Research Institute for Fluid Engineering, Kyushu University, Japan, vol. 5, September, 1948, pp. 22–38.

N is the rotational speed in usual units of rpm, w is the unit weight of the fluid.

The model laws of Equation [9] apply for speed changes as shown in Fig. 5. Results for 1500 rpm were predicted from results at 900 rpm and 1200 rpm. The agreement is reasonable for practical purposes. The model laws for speed changes have been applied to available test results of other periphery pumps and show the same degree of correspondence.

Changes in Flow-Channel Geometry

Senoo reported shutoff heads for periphery pumps with systematic changes in the flow-channel area and with the same impeller at the same pump speed. His results are shown in Fig. 7.

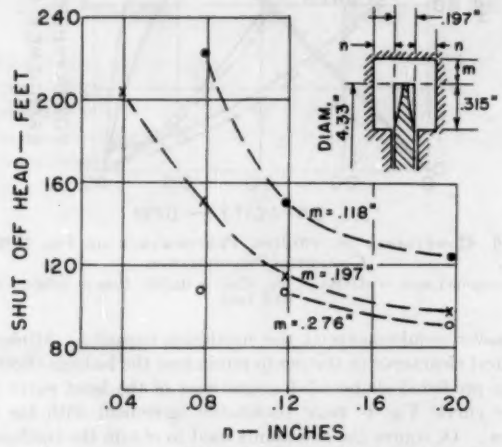

Fig. 7 Influence of Flow-Channel Geometry on Shutoff Head
(Pump speed = 1800 rpm.)

If the impeller shear coefficient is assumed to be a function of the impeller roughness alone, then, from Equation [6], the product of the shutoff head and the flow area should be constant with the assumption of constant effective vane velocity. The products are listed in Table 1. Considerable variation of the product is shown. The general trend shows higher products, hence higher shear coefficients, with an increase in flow area. Thus the effective roughness of the vane changes with a change in area.

TABLE 1 PERFORMANCE VARIATIONS WITH CHANGES IN FLOW-CHANNEL GEOMETRY

(Pump speed = 1800 rpm; impeller diameter = 4.33 in.)

Opening between impeller and flow channel				
Tip m, in.	Side n, in.	Flow area A, sq in.	Shutoff head H, ft	Product $HA/144$ cu, ft
0.118	0.079	0.091	223	0.141
0.118	0.118	0.130	151	0.136
0.118	0.197	0.217	125	0.189
0.197	0.039	0.079	204	0.112
0.197	0.079	0.119	151	0.125
0.197	0.118	0.167	115	0.133
0.197	0.197	0.279	99	0.192
0.276	0.079	0.147	108	0.111
0.276	0.118	0.204	108	0.153
0.276	0.197	0.341	92	0.218

Effect of Number of Impeller Vanes

For a particular impeller diameter and raceway area, an optimum number of impeller vanes would be expected to produce the greatest shear-stress coefficient. Results for impellers with different numbers of vanes are shown in Fig. 8. For a given

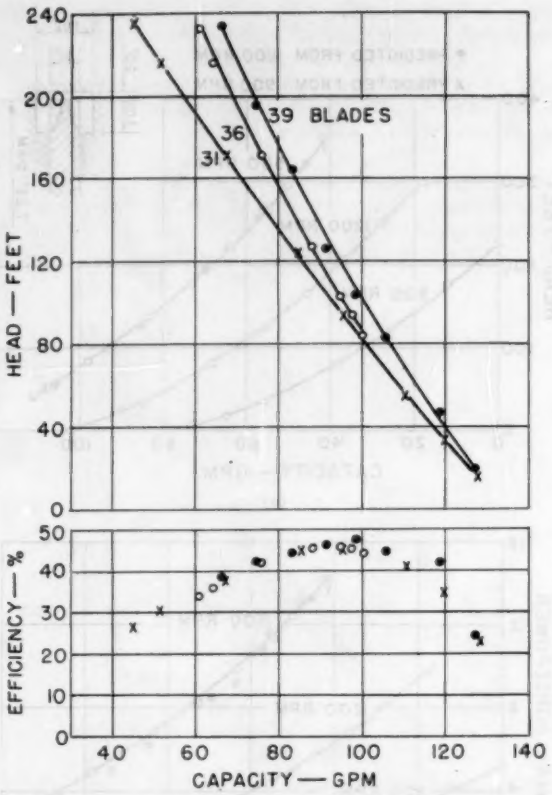

Fig. 8 Influence of Number of Impeller Vanes on Head and Efficiency
(Impeller diam = 7.23 in.; pump speed = 1500 rpm.)

capacity the head is increased with an increase in the number of vanes within the range tested. The trend shown cannot be carried to an infinite number of vanes since the roughness then decreases to zero as a plane disk. The optimum number of vanes for the greatest head at a given capacity was not reached. The tests were part of a series leading to the development of a pump for specified conditions which were reached within the reported range, and further changes were not made.

A noticeable increase in maximum efficiency is shown with the 39-blade impeller as contrasted to the 31-blade impeller. The increase in the impeller shear coefficient which produces the higher head also produces the increase in the maximum efficiency as expected from Equation [8].

Conclusion

The analysis of the periphery-pump performance shows reasonable prediction of the shapes of the performance relationships with three constants determined from selected points of the test results. Further investigation is needed to enable independent prediction of the magnitudes of the constants for a given pump.

Model laws of capacity proportional to speed, head proportional to speed squared, and power proportional to speed cubed apply to the periphery pump.

The impeller shear-drag coefficient, as used in the analysis, is a function of the impeller roughness or number of vanes, and of the flow-channel geometry.

Discussion

JEROME BARTELS.[3] The author has presented an interesting analysis of the performance of a periphery pump using a model which may be thought of as a metal file drawn through a trough of water.

One of these periphery pumps had been in service in Germany for 5 years, constantly pumping sandy water, and was then returned to the manufacturer for overhaul. A photograph of the pump casing showed a surprising flow pattern clearly marked out by the erosion of the sandy water. The doughnut-shaped water channel had two sets of helical scratches, each helix leading to and from the vanes on the corresponding surface of the rotor. It appeared that the water caught between radial vanes was slung outward by centrifugal force, and transferred its kinetic energy to the bulk stream by impact and diffusion. Thus pumping action, rather than having been due to viscous drag, might have been caused by centrifugal pumping in which the liquid re-entered the same rotor via a helical path along the pump channel.

The writer was presented in 1947 with the problem of establishing the pumping mechanism for this type of pump while doing graduate work at New York University. The first part of the laboratory work consisted of testing three rotors in the same pump casing. The first rotor was smooth, having no grooves or vanes; the second was grooved out to leave the radial vanes of conventional design; and the third had conventional radial vanes plus additional vanes normal to the radial ones. If the first rotor pumped, it would have to be due to the viscous drag of a smooth metal disk. If the second rotor pumped, it might be due either to the shearing stresses of viscous drag or to the mechanism of helically re-entrant centrifugal pumping. If the third rotor produced pumping, it would prove that viscous drag is the mechanism causing pumping, for the auxiliary sets of vanes normal to the first set prevented any possible radial flow through the impeller channels without disturbing the filelike action of the radial set of vanes. Conversely, if this third rotor did not pump, it would prove that the extra sets of vanes normal to the usual radial set had prevented radial flow through the impeller, and thereby had prevented centrifugal pumping which led to the cessation of pumping action even though viscous drag still occurred.

The results of this laboratory test were that the pump would work only when the rotor design permitted radial flow and centrifugal pumping.

The second part of the work was to obtain accurate data for the helix angle of the flow pattern within the doughnut-shaped pump channel while running the pump at one particular point on the head-capacity curve. A wax coating was applied to the pump-casing passage, pulverized coal and ground glass were added to the water to be pumped, and a photomicrographic technique was employed to measure the angle of the scratches. Finally, a mathematical analysis was made which produced a helix angle for re-entrant centrifugal pumping that agreed very closely with the angle measured in the laboratory. Thus the writer is inclined to forego the idea advanced by the author that the pumping mechanism in the periphery pump is caused by the shearing stresses created in the liquid by a rough impeller.

R. G. FOLSOM.[4] Most of the information in the technical literature with regard to the periphery pump has been descriptive in nature and has provided little information regarding design procedures and performance predictions. The author is to be congratulated on the development and presentation of a logical, simple approach to a most difficult problem. Although the methods are limited in scope, they represent an advance over presently available information.[5]

If all the internal motions of the fluids were known and the interrelationships understood, it would be possible to apply directly the principles of fluid mechanics to obtain a complete solution for the situation existing in the pump. Although considerable qualitative information is available regarding the flow, there are no quantitative data with respect to the flow phenomena in the pump rotor between the vanes. Owing to this lack of information, and the probability that none will be available in the near future, the author has developed a method of approach which is fundamentally sound, based on over-all conditions, and uses dimensionless coefficients to account for the unknown factors. The equations are dimensionally correct and it is anticipated that they may be used as a basis of determining conditions for dynamical similarity as applied to these pumps when built in different sizes and operated under different conditions.

There appears to be an infinite number of geometrical shapes and arrangements that may be used to construct periphery pumps. In an effort to understand the internal-flow mechanism, studies were made some time ago in a linear stationary unit to measure the hydraulic resistance of the simulated vane surface as a function of the geometry.[6] During these investigations it was shown that when the vanes were spaced closely together the fluid did not flow into the space between the vanes and, as a result, the exchange of momentum was much less than when the vanes were spaced farther apart. Data for optimum resistance configurations were obtained.

The next step in the development was to lock the rotor of a given periphery pump and measure the hydraulic resistance when forcing fluid through the unit. Comparison of the coefficients obtained by this process with those obtained by the author for the pump when operating, showed that the hydraulic-resistance coefficients varied by an order of magnitude. Thus the centrifugal effects produced by the impeller during the operation appeared to be a major factor in the momentum interchange taking place under pumping conditions. Wear on the inside of the case when erosive particles were present in the water has demonstrated that the flow was affected strongly by the centrifugal action occurring between the blades of the rotor. To date it has not been possible to solve in detail the problem of determining the additional momentum interchange produced by this centrifugal action.

Rewriting Equations [6], [7], and [8] of the paper in the following form indicates that conditions of dynamical similarity for geometrically similar pumps could be expressed in terms of the specific speed

$$\frac{H}{U^2} = f_1\left(\frac{Q}{UA}\right) \qquad \frac{P}{U^2} = f_2\left(\frac{Q}{UA}\right)$$

$$e = f_3\left(\frac{Q}{UA}\right)$$

and the specific speed is

$$N_{sq} = \frac{N\sqrt{Q}}{H^{3/4}}$$

[3] Associate Professor Mechanical Engineering, Polytechnic Institute of Brooklyn, Brooklyn, N. Y. Mem. ASME.

[4] Director, Engineering Research Institute, University of Michigan, Ann Arbor, Mich. Mem. ASME.

[5] "On the Characteristics of the Westco Type Pumps," by H. Takai, Transactions of the Society of Mechanical Engineers, Japan, vol. 2, 1936, pp. 223–229; "Theory of the Westco Rotary Pump," by A. Miyadzu, Transactions of the Society of Mechanical Engineers, Japan, vol. 5, 1939, pp. 109–115.

[6] "Frictional Resistance in Artificially Roughened Pipes," by V. L. Streeter, Proceeding of the ASCE, vol. 61, 1935, pp. 163–186; discussion by R. G. Folsom, Ibid., pp. 913–916.

Evaluation of the specific speed for the point of maximum efficiency shows that this type of pump has a characteristic low specific speed, meaning a low capacity-high head unit. The principal region of application of the pump would be at very low specific-speed conditions where the maximum efficiency for centrifugal pumps drops to extremely low values. It would be of interest to know if the author has any knowledge of tests on geometrically similar periphery pumps of different absolute size and of the relative performance attained by these units.

When predicting performance, it must be kept in mind that the operation of the pump is extremely sensitive to the axial clearance. Since the unit is a low-capacity pump, any variation in leakage quantity readily affects the performance, as demonstrated by the rapid drop in capacity of a periphery pump when erosive materials are carried in suspension.

The author presents test data to support the application of the affinity laws or speed changes for a given periphery pump. It should be noted that these relationships are valid as long as the suction conditions under which the pump operates are such that vapors or gases do not separate from the liquid in the spaces between the vanes in the area of the suction port of the pump. Owing to the circular flow processes occurring between the vanes, there is a region of local low pressure formed where vapors or gases can come out of solution. As a result, the area is not filled completely with a liquid and the capacity of the pump at a given head is reduced with respect to the capacity at the same head when a continuous liquid completely fills the pump case and impeller spaces. This drop in performance is similar to that experienced by a medium specific-speed centrifugal pump, because of cavitation.

J. R. Parker.[7] The author is to be congratulated on presenting an easily understood analysis of a typical periphery-pump design.

The writer has worked on this type of pump on several occasions and welcomes this information for his file of design data.

The author indicates the necessity for further study and to add to his list of investigations might be mentioned the following:

1 While it is known that a given periphery-pump-impeller diameter may be fixed and the channel size, vane length, and impeller width changed within certain limits, it would be interesting to develop just what these maxima and minima are. We know, for example, that as the channel width and height increase, along with the impeller width and vane length, the head flattens giving a higher-capacity pump with a correspondingly lower shut-off head to a point where efficiency drops rapidly. The correlation of various data on these changes would be helpful in determining the practical limits of any impeller diameter. Once these data are obtained, it would be simple to set up design data for various impeller diameters and cover a wide range of head and capacities for various applications.

2 In addition to the number of vanes in the impeller there are other points of design which might be considered, such as the radii used in the raceway, the clearances between the impeller and the raceway inner boundary, the radii of the cutter used to develop the peripheral impeller vanes, and the length of the high-pressure dam between the discharge and the inlet.

From a practical standpoint, we must remember that although the efficiency of the peripheral pump may be relatively low, the pump is very useful and excels in three ways over other types of pumps.

1 The pump develops relatively high heads at low speeds and gives industry a small-size, low-cost pump, well adapted to water or chemical service.

[7] Project Engineer, Peerless Pump Division, Food Machinery and Chemical Corp., Los Angeles, Calif.

2 Its ability to handle gases or a mixture of gas and liquid means it will self-prime readily.

3 It is particularly useful in handling water at a temperature near its boiling point or hydrocarbon fuels, which often give trouble with other type pumps.

W. A. Wilson.[8] The writer appreciates the lucid exposition of a well-defined theoretical model of the regenerative turbine pump given in this paper. The author's clarity of presentation is in marked contrast to previous published treatments of this much-neglected device.

The experimental results certainly bespeak the utility of the model presented by the author as the theoretical counterpart of the pump itself. Nevertheless, it leaves in some doubt what the detailed fluid-dynamic mechanism of this pump really is like.

At M.I.T., by virtue of a grant from the Worthington Corporation, we currently are developing a model with somewhat higher resolving power. It would be premature to make a formal presentation of our findings at this time, but borrowing a figure, Fig. 9,

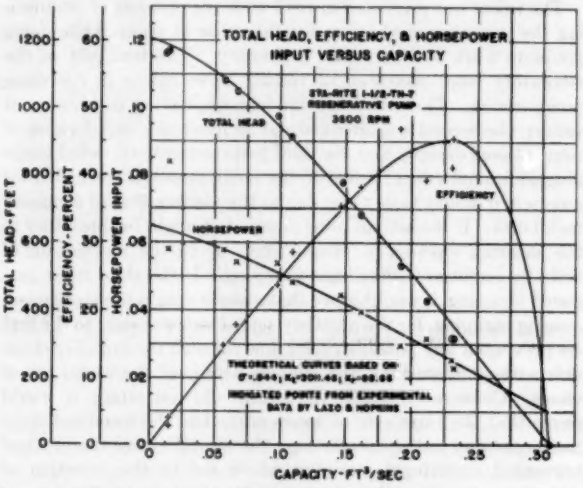

Fig. 9 Theoretical and Experimental Performance at 3600 Rpm of Regenerative Pump

from a recently completed thesis by Mr. John Oelrich, it is possible to show that a theory quite different from the author's accounts at least as well for observed performance of this class of pump.

As in the case of the author's work, agreement has been forced at three independent points between the theoretical and actual characteristics. It is quite remarkable that in both cases extremely good fits are thus obtained over the entire operating range.

The distinction between the two idealizations of the pump mechanism is much more fundamental than would seem possible in the light of the apparent success of each one. The author has chosen to neglect entirely centrifugal effects and treats the pump rotor as a super-rough surface. On the other hand, at M.I.T. we have focused our attention on the centrifugal character of the pump and have attributed to the rotor the essential qualities of a radial-flow runner. We believe that this approach sheds useful light upon the details of the internal mechanism of this pump.

We hope to present this theory and its consequences to the Society in the near future.

W. E. Wilson.[9] The author describes the mechanics of the operation of a periphery pump in a straightforward simple manner

[8] Associate Professor of Mechanical Engineering, Massachusetts Institute of Technology, Cambridge, Mass. Mem. ASME.

[9] Glen Lennox, Chapel Hill, N. C. Mem. ASME.

that is in contrast with older confused expositions. The writer engaged in a lengthy and interesting private correspondence several years ago in an effort to make the point that the operation of this type of pump does, as the author states, "produce pumping action by the motion of a rough surface in a channel containing fluid. The fluid is dragged along by the rough surface, and, with suitable restraints in the channel, the fluid head is increased in the direction of the flow."

There are indications that this description of the pumping action is not accepted by all engineers who are interested in pump design and operation. The writer presents herewith evidence in support of the author's position and suggests critical experiments that might prove significant in strengthening his points.

Critics of the transport theory of the pump action frequently advance the theory of a centrifugal action supposed to contribute to the building up of pressure in the flow channel. An effort is made here to show that such a concept is both unnecessary and erroneous.

In order to determine the relative merits of a theory based on the bodily transport of liquid by shearing action and one based upon centrifugal action it is desirable to select critical differences in performance characteristics for study. A difference of this type is found in the relationship between head and capacity. The transport theory predicts a head-capacity relationship in accordance with Equation [6] of the paper. A pump of the centrifugal type exhibits a head-capacity relationship that is vastly different.

Equation [6] predicts a nearly linear decrease of head with capacity for small values of Q at constant speed. A centrifugal pump shows little decrease in head with increasing Q and may show a significant increase in head with increasing Q up to large values of the capacity. Equation [6] predicts a continually decreasing head with increasing Q as shown in Fig. 5 of the paper.

A second significant and critical difference is the relationship of torque to discharge at constant speed. The theory advanced by the author predicts a decrease in torque with increasing discharge. A centrifugal pump requires greater input torque with increasing discharge at constant speed.

A sharp difference between the two theories appears in the case of a pump consisting of a smooth cylinder rotating inside of and concentric with a cylindrical housing. This might be described as a periphery pump that has an impeller without blades thus providing a rectangular flow channel. The transport theory accounts for the action of this pump in a wholly satisfactory manner, but it is difficult to visualize any action involving centrifugal effects that might explain the fact that such a pump could and would develop significant pressures with liquids of both high and low viscosities. The equation describing the performance of this pump with laminar flow is

$$Q = \frac{UA}{2} - \frac{wAd^2H}{12\pi\mu D} \quad \ldots\ldots [10]$$

where

D = diameter of impeller
d = radial dimension of flow passage
μ = coefficient of viscosity of liquid

Other terms are as defined in the paper.

The maximum head that can be developed by this pump is given by Equation [10], herewith, with a value of $Q = 0$; thus

$$H = \frac{6\pi\mu UD}{wd^2} \quad \ldots\ldots [11]$$

Extension of the experimental work to include pumps with no blades and liquids with high viscosities would provide data of value in determining the performance characteristics under extreme and critical conditions.

A. M. Wright.[10] It is a pleasure to read a paper on the "turbine" or peripheral-type pump (personally, the writer prefers the term "vortex pump," for reasons to be disclosed) that does not attempt to explain its action by viscosity effects. Having designed a successful vortex pump in which special pains were taken to minimize the effect of viscosity, the writer can state with assurance that viscosity variations over a reasonable range are of small importance. A vortex pump will pump gasoline just as well as lubricating oil.

The author therefore is to be congratulated for having recognized that the peripheral or vortex pump is a "dynamic" type, and it is in the same general class of rotating machinery as fluid couplings and torque converters. In fact, the family relationship between vortex pumps and fluid couplings is very close.

However, the writer disagrees with the author's explanation of the pumping action. The writer believes that, if an "in-line" pump, as shown in Fig. 1 of the paper, were constructed, the test results would be very disappointing; reasons for this will be given. The particular difference with the author is that he takes no account of the shape of the blading, which is of great importance, as the following simple theory will show: This theory is at variance with the author's treatment.

In Fig. 10 of this discussion is shown an enlarged view of the channel of the pump of Fig. 1 of the paper. To illustrate the method of analysis, the blades are assumed to be radial in the following discussion.

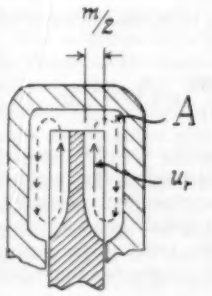

Fig. 10 Diagram of Pump Channel

Owing to rotation of the impeller, the fluid contained in the space between the blades certainly is subject to centrifugal force, exactly as in a conventional centrifugal pump.

Therefore the fluid between the blades is being continually thrown out radially at the pump periphery, and is replenished by fluid flowing in at the root of the impeller.

Hence the fluid in the impeller and casing has a kind of vortex motion, and for this reason we have named this type of pump a vortex pump.

The behavior of the pump can be analyzed by assigning a radial velocity u_r to the fluid in the space between the blades. Then neglecting blade thickness, the mass of fluid flowing radially outward per second is

$$\rho(2\pi r\alpha)mu_r \quad \ldots\ldots [12]$$

where α is the fraction of the periphery that is active in pumping (excluding the cutwater and the space taken by the inlet and discharge passages), and r is the mean radius of the channel and the blades. A more refined theory would consider the actual root and tip radii involved, but the use of a single average radius is near enough for most purposes, and makes the calculations simpler.

If A is the cross-section area of the cutwater or dam, and Q the discharge of the pump, then the average forward velocity (from inlet to discharge) of the fluid in the channel is Q/A, and its angular velocity is Q/Ar.

At the tip of the impeller, the forward velocity of the fluid being discharged from the impeller into the channel is equal to the blade velocity u, and its angular velocity is $\omega = u/r$.

[10] Chandler-Evans Division, Niles-Bement-Pond Company, West Hartford, Conn.

We thus see that the action of the impeller is to increase the angular velocity of $[\rho(2\pi r\alpha)mu_r]$ slugs of fluid per second from $Q/(Ar)$ to ω.

The torque on the impeller is the rate of change of angular momentum, viz.

$$T = [\rho(2\pi r\alpha)mu_r]r^2\left(\omega - \frac{Q}{Ar}\right) \quad [13]$$

The torque on the impeller must be balanced by the torque on the housing, which is created by the pressure difference across the cutwater plus the frictional loss in the housing as a result of the forward flow of fluid through the channel

$$T = [(p_2 - p_1)A + CQ^2]r \quad [14]$$

where C is a coefficient that can be estimated or determined experimentally.

Eliminating T from Equations [12] and [13], we get

$$(p_2 - p_1) = \frac{2\pi\alpha m}{A}\rho r^2 u_r\left(\omega - \frac{Q}{Ar}\right) - \frac{C}{A}Q^2 \quad [15]$$

The unknown in this equation is u_r, and the writer has assumed, as is done in analyzing torque converters, that this is proportional to u, say $u_r = ku = k\omega r$. Then Equation [15] becomes

$$(p_2 - p_1) = \frac{2\pi\alpha m\rho r^3 k}{A}\left(\omega^2 - \frac{\omega Q}{Ar}\right) - \frac{C}{A}Q^2 \quad [16]$$

Since $\omega = 2\pi N/60$, Equation [16] can be written in terms of the pump dimensions and the rpm

$$(p_2 - p_1) = \frac{2\pi\alpha m\rho r^3}{A}k\left(0.11N^2 - \frac{0.105}{Ar}QN\right) - \frac{C}{A}Q^2 \quad [17]$$

We are still left with the unknown quantity k, and it must be admitted that attempts to evaluate the magnitude of this constant have resulted in only very gross approximations. Actually, the velocity of circulation u_r is such that frictional losses due to this velocity are equal, at shutoff, to the power input to the pump. From the dimensions alone, it is practically impossible to predict what this velocity will be.

The power input to the pump is obtained from Equation [13], herewith

$$T\omega = [\rho(2\pi r\alpha)mr^4]k\left(\omega^2 - \frac{Q\omega}{Ar}\right) \quad [18]$$

The power output is $(p_2 - p_1)Q$ ft-lb per sec, and the hydraulic efficiency is thus easily obtained.

Despite the limitations of this theory, it has been put to practical use with good results.

We had made some tests with a conventional Worthington turbine pump, and examining the test results in light of the foregoing theory, we were sure that the approach was sound in principle. In particular, it is to be noted from Equation [17] that $(p_2 - p_1)/N^2$ is a unique function of Q/N; this plotted out very well.

The occasion arose to build a quantity of aircraft pumps to run at 3400 rpm to deliver 50 gpm at a medium pressure. In the light of the theory, it was obvious that for moderate pressures the channel area should be fairly large, and this was made equal to 1 sq. in., with a wheel diameter of about 4 in. The test results confirmed our expectations fairly well.

Confirmation of the correctness of the basis of the foregoing analysis came when a requirement arose to build another group of pumps to give the same pressure rise as those just mentioned, but to run at 6300 rpm instead of 3400. An examination of Equation [15] of this discussion gave the clue to the solution of meeting the high-speed requirement with only a minor design change. The angular speed ω here is of course the angular velocity of the fluid in the blades; it is only accidental that in the case of radial blades this is the same as the impeller velocity.

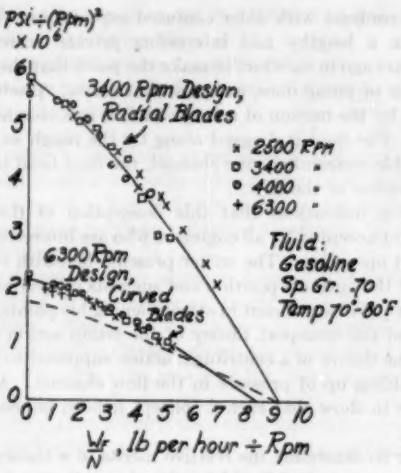
PSI ÷ (Rpm)²
× 10⁶
3400 Rpm Design, Radial Blades
× 2500 Rpm
○ 3400 "
○ 4000 "
+ 6300 "
6300 Rpm Design, Curved Blades
Fluid: Gasoline Sp Gr .70 Temp 70°-80°F
0 1 2 3 4 5 6 7 8 9 10
Wr/N, lb per hour ÷ Rpm

FIG. 11 VORTEX-PUMP PERFORMANCE

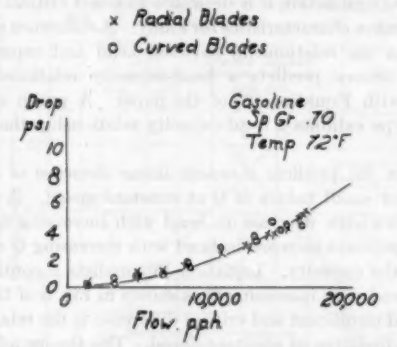

FIG. 12 VORTEX-PUMP PERFORMANCE; STANDSTILL HYDRAULIC-FRICTION LOSS

Obviously, if the foregoing theory is correct, we should be able to increase the pump rpm without increasing the shutoff pressure rise if the blades are given a suitable backward curvature. An estimate was made of the blade curvature that would be needed, and these curved-blade rotors were installed and tested.

The results are shown in Fig. 11 of this discussion. It was expected that the lower dotted line would be met with the curved-blade pumps. Actually, the pressure ran rather high over the operating range, but the agreement with expectations is not too bad. According to the author's formula, the blade curvature should have had small effect, and both pumps should have tested to the upper curve.

Zero pressure rise is obtained when the forward velocity of the fluid in the channel is nearly equal to the impeller speed, and hence in pumps of the same channel section, we expect the same Q/N at zero pressure rise. This also was confirmed by Fig. 11.

To extend Equation [17] to take care of the case of curved blades it should of course contain a term involving the blade angle.

If the blade tips are slanted backward at an angle α to the tangent at the periphery, then the velocity, relative to the casing, of the fluid leaving the impeller tip is

$$u_f = u - \frac{u_r}{\tan\alpha} \quad [19]$$

where ω is the angular velocity of the impeller; the angular velocity of the fluid leaving the impeller tip is

$$\omega_f = \frac{\mu_f}{r} \quad [20]$$

The pressure generated by the pump can then be estimated by using ω_f, from Equation [20], for the ω in Equation [15].

The results of Fig. 11 seem impossible to explain on the author's theory of a shear coefficient.

A test was made, in which the two pumps just mentioned were held at standstill, and fluid was pumped through them, the pressure drop being measured. The results are shown in Fig. 12.

No difference between the backward-curved blade and the straight-blade pumps can be noted, so that the "shear coefficient" seems independent of blade shape or angle, provided the channel contours are similar.

On the author's theory, then (Equation [6] of the paper) the rated shutoff pressure rise of the pumps should have been proportional to the square of their rated speeds, which were 3400 rpm and 6300 rpm, respectively. Actually, the observed pressure rise for the two pumps, identical except for blade angle, was pretty near the same when run at their rated speeds, as shown in Fig. 11.

This is why the writer stated earlier that an in-line pump like the author's Fig. 2, would give disappointing results if it were built and tested. The rotor torque, the power input, and the pressure generated, it would seem, must be essentially dependent on a rate of change of angular momentum of fluid passing through the rotor, just as in other types of turbomachinery.

Author's Closure

All discussers elaborated on the mechanics of the pumping action with agreement or disagreement with the analysis proposed in the paper. The author will comment on other pertinent remarks of each discusser and conclude with a single discussion of the pumping action.

Mr. Bartels states that he tested three impellers in the same pump casing and that the smooth rotor and the vaned rotor with additional normal vanes gave no pumping action. The author agrees that these rotors did not produce as much head as the standard radial vaned rotor, but disagrees that they gave no pumping action as Mr. Bartels infers.

Shear will exist on the fluid when any shape or condition of surface moves relative to fluid in contact with the surface. This is a property of a fluid. With shear on the fluid, the force balance is applicable as described in the paper, regardless of how the shear coefficients are interpreted. Thus head is produced.

Pumping action is possible with a smooth moving surface as shown by Equations [10] and [11] in the discussion of Mr. W. E. Wilson. These relationships have been confirmed by test results.[11] Schmiedchen [12] presents test results of periphery pumps with numerous shapes of impellers and flow passages. He obtained appreciable heads with vaned impellers in passages in which there was no radial clearance between the impeller and casing. This configuration prevented radial flow in a manner similar to that reported by Mr. Bartels of the vaned rotor with additional normal vanes.

A complete report by Mr. Bartels on his results and analysis would be of interest.

Mr. Folsom's comments on the maximum efficiencies of periphery pumps correlated by the specific speed in comparison to efficiencies of centrifugal pumps in the same range of specific speeds shows the application range of the periphery pump. A further comparison of the two pump types may be made. A centrifugal pump of the same diameter impeller, 7.23 in. as the periphery pump for which test results are reported in the paper, operating at a speed of 1200 rpm and at a flow rate of 70 gpm, produces a head of approximately 25 ft in contrast to the reported periphery pump head of 75 ft, Fig. 5 of the paper. To obtain the same head, the centrifugal pump must be larger than the periphery pump, or must have more stages. In the specific-speed range where the efficiencies of the two types of pumps are comparable, the periphery pump has the added advantage of smaller size.

The question was asked by Mr. Folsom whether test results were available on geometrically similar pumps of different absolute size. The author does not know of any. Such results, and also results to show the influence of the fluid viscosity on the limits of application of the model laws, are needed.

The additional studies listed by Mr. Parker are essential for the pump designer, and for confirmation of any proposed analysis of the mechanics of the pumping action.

Mr. Parker states that the periphery pump handles a gas for good self-priming characteristics. This is doubtful since, for example, the pressure equivalent of a head of 1000 ft of air at atmospheric conditions is equivalent to a pressure of 1.2 ft of water. A suction lift of this magnitude is hardly enough to be considered a self-priming feature.

The author looks forward to the promised analysis by Mr. W. A. Wilson on the mechanism of the pumping action of the periphery pump. Mr. Wilson does not state, but it is presumed from the numerical values of Fig. 9 of his discussion, that his test results were obtained with a pump handling air. The shape of the head curve of Fig. 9 at low capacities does not appear the same as the shape of the head curve in the paper, Fig. 5(*a*), which may be due to temperature rise effects in the pump handling air. The air-temperature rise is appreciable at low flow rates owing to the inefficiency of the pump. For example, at an air head of 1100 ft and a pump efficiency of 10 per cent, the temperature rise of the air (assuming all inefficiency appears in the air stream) is approximately 70 deg F. Consideration must be given to the temperature effects, and also to compressibility effects in evaluating the head.

The laminar flow-head capacity relation, Equation [10], as stated by Mr. W. A. Wilson, has been checked by test of a pump consisting of a square thread screw rotating inside a cylindrical housing.[11] The author recently tested a screw pump of similar design as a phase of another investigation and found that Equation [10] is valid.

Mr. Wright shows test results of two periphery pumps with different blade curvatures. His correlation of results in Fig. 11 is further confirmation of the applicability of the model laws, Equation [9] of the paper, for speed changes. The fact that the two pumps differ in performance is to be expected, even though Mr. Wright reports the same standstill hydraulic-friction losses, Fig. 12, for the two pumps. No statement to the contrary was made in the paper. The shear coefficients of Equation [5] will depend on the geometrical shape of the vanes which governs the velocity patterns producing the shear.

Equations [17] and [18], as proposed by Mr. Wright, are not dimensionally correct. If corrected with the constants rearranged, these equations may be compared to Equations [6] and [7] of the paper. The two sets of equations are similar in form; the major difference is in the assumption by Mr. Wright that his velocity u_r is proportional to u. The discussion following on the pumping action will clarify that point.

---

[11] "Screw Viscosity Pumps," *Engineering*, November 17, 1922, pp. 606–607; also "Screw Viscosity Pumps," by H. S. Rowell and D. Finlayson, *Engineering*, August 31 and September 28, 1928, pp. 249–250, 385–387.

[12] "Untersuchunger über Kreiselpumpen mit seitlichem Ringkanal," by W. Schmiedchen, (dissertation) Universitatsverlag von Robert Noske in Borna-Leipzig, 1932.

A brief treatment on the pumping mechanism to justify the use of Equation [5] appears to be in order from the comments of the various discussers. The author will borrow the symbols of Mr. Wright's Fig. 10, with the further comment that the flow pattern is not so simple as he proposes, but that additional circulations occur in radial planes and in tangential planes in the flow channel.

The variations in radius and in the moment of momentum may be ignored for simplicity. Fluid leaves the pockets of the impeller with some average velocity u_r through some effective area a. ("Average" and "effective" are specified in view of the complex fluid circulations.) Then the mass rate of movement from the impeller into the channel is $\rho u_r a$. The shearing force on the fluid is the mass rate times the change in velocity, and the shearing stress is the force divided by the area. The average velocity change is the difference between the tangential component of the fluid as it leaves the impeller and the fluid velocity in the flow channel. Again with average values, the tangential fluid velocity leaving the impeller is related to the impeller velocity and the flow-channel velocity is related to the average net flow. Then the change in velocity is $K(u - Q/A)$, where K is a proportionality coefficient.

Thus the shear force may be written

$$\rho u_r a K(u - Q/A) \quad [21]$$

So far this development follows that of Mr. Wright, except for the qualifications of average and effective.

I differ with Mr. Wright on the interpretation of u_r. At zero head, the shear stress is small, and except for the retardation of the flow-channel walls, all the fluid would be expected to rotate tangentially at the impeller velocity with no circulation through the pockets of the impeller, and u_r is zero. At zero net flow (shut-off), the intensity of circulation must be a maximum. This conclusion is reached since the net relative motion between the fluid in the flow channel and that in the impeller is a maximum, and eddy intensity, or circulation, is a maximum. Then it is reasonable to state that the velocity of circulation u_r is proportional to the relative velocity between the impeller and the net tangential fluid velocity in the flow channel, or

$$u_r = K_1 \left(u - \frac{Q}{A} \right) \quad [22]$$

Combining Equations [21] and [22] with the proportionality constants grouped into a single coefficient gives Equation [5] for the impeller shear coefficient.

Observations on Some Factors Affecting Timken Data for EP Lubricants

By A. J. DeARDO[1] and E. M. KIPP,[1] NEW KENSINGTON, PA.

The paper reports results of an investigation of variations in rubbing speed and viscosity variables when using the Timken machine for evaluation of EP lubricants.

IN a recent paper,[2] some observations were reported on the effect of variations in viscosity upon Timken OK and PSI values of straight mineral oils. Data also were presented on the effects of rubbing speeds and the manner in which they, in turn, were affected by the viscosity variable. The variations in the OK and PSI data with rubbing speed were of such magnitude as to warrant further investigation of the extent to which similar effects might be present when using the Timken machine for evaluation of EP (extreme-pressure) lubricants. The pronounced though secondary effect of the viscosity variable upon OK and values for straight mineral oils suggested that this factor also should be considered.

These questions are of practical significance to the lubrication engineer because of the widespread use of Timken OK and PSI values in describing the lubricating properties of EP lubricants or of EP additives. Usually, it has been the practice to quote the OK value at a standard rubbing speed of 800 rpm. Comparison of OK values of different EP additives is frequently made without reference to the viscosities of the resulting lubricants. It was decided, therefore, that it would be of interest to carry out a preliminary investigation of the magnitudes of the effects of the rubbing speed and viscosity variables upon Timken data for selected EP additives and lubricants.

As will be noted later, the rubbing-speed variable was found to be the more critical of the two, and therefore was emphasized in the present investigation. The data obtained, however, indicated that, as in the case with straight mineral oils, the effect of the viscosity variable may be a factor to be considered when evaluating EP additives or lubricants with the Timken machine.

Experimental

The Timken test procedures employed in this investigation were described in detail in a previous paper.[2]

The EP additives for which data are presented in this paper are described briefly in Table 1. The investigation of the dependence of Timken data for EP additives and lubricants upon the rubbing-speed variable was simplified by a short series of preliminary exploratory tests to determine the relative magnitudes of the effects of the variables of viscosity, viscosity index, and rubbing speeds. As will be noted later, the results of this preliminary study permitted a reduction in the number of mineral oil-additive combinations subsequently investigated. The viscosity index was regarded as a rough means for selecting mineral oils which would represent substantial variations in chemical and physical properties resulting from variations in sources of crude and refining procedures.

TABLE 1 GENERAL DESCRIPTION OF EP ADDITIVES

Code designation	Per cent			
	Cl	P	Pb	S
A	23.0	0.56	None	8.5[a]
B	None	None	33.0	None
C	None	None	None	17.0
D	41.0	None	None	None
E	19.5	0.04	None	6.8[a]
F	17.7	1.17	None	7.6[a]
G	31	None	None	11[a]

[a] Products meeting Mil-L-2105 specification.

For the preliminary investigation, nine straight mineral oils ranging in viscosities from 1000 SSU/100 F to 6000 SSU/100 F, and representing viscosity index values of 0, 50, and 100 in each of three viscosity levels, were selected. Timken OK and PSI values for 5 per cent solutions of each of two widely different chemical types of extreme-pressure additives were then determined for each oil at rubbing speeds of 400, 800, and 1200 rpm. The experimental data obtained are listed in Table 2.

The OK load data of Table 2 were evaluated by the "analysis of variance" technique, as summarized in Table 3. The results show the speed variable is predominant. They also indicate that the viscosity variable does not affect critically the OK data for EP additives and lubricants. However, separation of the experimental data of Table 1 on the basis of the two EP additives employed, Table 4, shows an effect of the viscosity variable in the case of additive A, but not in the case of additive B. Accordingly, without a broader investigation of this point, general conclusions cannot be drawn relative to the influence of the viscosity variable in the evaluation of EP additives and lubricants. The limited data do suggest, however, that the magnitude of the viscosity-variable effect may depend upon the specific EP agent under study and should not be overlooked, pending additional information on this point. Certainly, however, the rubbing-speed variable is by far the predominant one.

Some discussion of the significance of the analysis of variance data of Table 2 with regard to the "contribution" of the two EP additives to the OK and PSI values is also in order. It must be understood that the analysis of variance data indicate the "variance" effects of the two EP additives upon the OK and PSI values, relative to one another only, and are therefore not a measure of the actually large effect of either additive upon the OK and PSI values of the straight mineral-oil vehicles.

On the basis of the results presented in Tables 1 and 2 showing the rubbing-speed variables to be by far the most significant in the measurement of Timken OK loads for EP additives, investigation proceeded to determine the variation in OK loads with rubbing speeds for a large number of commercially available EP additives, utilizing a single "standard" straight mineral oil for all additives. Accordingly, the effects of the rubbing-speed variable upon Timken OK loads for 36 EP agents were determined, utilizing as the standard reference-base mineral oil one of 1000 SSU/100 F and a viscosity index value of 50. The EP agents selected constitute a representative cross section of com-

[1] Aluminum Research Laboratories, Aluminum Co. of America.

[2] "Effect of Variations in Viscosity of Lubricants Upon Timken OK and PSI Values," by I. S. Kolarik, C. A. Zeiler, and E. M. Kipp, Trans. ASME, vol. 74, 1952, p. 875.

Contributed by the Research Committee on Lubrication under auspices of ASME Lubrication Activity and presented at a joint session with the Machine Design Division, American Society for Testing Materials, and American Society of Lubricating Engineers at the Annual Meeting, New York, N. Y., November 29–December 4, 1953, of The American Society of Mechanical Engineers.

Note: Statements and opinions advanced in papers are to be understood as individual expressions of their authors and not those of the Society. Manuscript received at ASME Headquarters, April 7, 1953. Paper No. 53—A-39.

TABLE 2 EFFECT OF VISCOSITY, VISCOSITY INDEX, AND RUBBING SPEED UPON TIMKEN OK AND PSI VALUES FOR SOLUTION OF TWO EP ADDITIVES IN SELECTED MINERAL OILS—PRELIMINARY INVESTIGATIONS

Vehicle mineral oil	Viscosity index	Additive (5 per cent concentration)	Timken Speed 400 rpm OK load, lb	400 rpm PSI	800 rpm OK load, lb	800 rpm PSI	1200 rpm OK load, lb	1200 rpm PSI
1000 SSU/100 F oil	0	B[a]	95	32200	6	5800	<1	...
	50	B	100	31100	6	6050	2	2800
	100	B	100	26200	7	5700	<1	...
	0	G[a]	40	15600	12	7850	10	6000
	50	G	60	24900	20	12500	10	6800
	100	G	70	25000	20	10600	12	9000
3000 SSU/100 F oil	0	B	75	28700	6	5030	4	4300
	50	B	90	26400	10	7930	6	5100
	100	B	100	27600	10	7430	6	5100
	0	G	55	22200	16	9600	8	6800
	50	G	65	24100	18	9200	12	10400
	100	G	55	29000	20	11600	12	9600
6000 SSU/100 F oil	0	B	75	27600	10	8500	6	5900
	50	B	65	21700	12	10000	8	7400
	100	B	65	24100	12	7330	10	7800
	0	G	50	20900	12	7870	10	6750
	50	G	50	20100	18	9900	8	6400
	100	G	60	26200	20	11500	12	9650

[a] See Table 1.

TABLE 3 ANALYSES OF VARIANCE FOR OK LOAD DATA OF TABLE 2

	Degree of freedom	Sum squares	Mean squares	F quotient	Significant
Viscosity	2	165	82.5	1.97	Borderline
Viscosity index	2	295	147.5	3.85	Yes
Additive	1	327	327.0	8.54	Yes
Speed	2	43741	21870.5	571.03	Yes
Viscosity × viscosity index	4	87	21.7	0.52	.....
Viscosity × additive	2	48	24.0	0.57	.....
Viscosity × speed	4	779	194.7	5.08	Yes
Viscosity index × additive	2	37	18.5	.44	.....
Viscosity index × speed	4	99	24.7	.59	.....
Additive × speed	2	3896	1948.0	50.86	Yes
Residual	28	1171	41.8	....	
Total	53	50645	.....		
Corrected residual	42	1607	38.3		

NOTE: $\sigma = \sqrt{38.3} = 6.19$.

TABLE 4 EFFECT OF MINERAL-BASE-OIL VISCOSITY (SSU/100 F) UPON TIMKEN OK VALUES AT RUBBING SPEEDS OF 800 RPM AND 1200 RPM—ADDITIVE B[a] VERSUS ADDITIVE G[a]

Additive B: Oil viscosity	Viscosity index	OK value at 800 rpm	OK value at 1200 rpm	Additive G: Oil viscosity	Viscosity index	OK value at 800 rpm	OK value at 1200 rpm
1000	0	6	<1	1000	0	12	10
3000	0	6	4	3000	0	16	8
6000	0	10	6	6000	0	12	10
1000	50	6	2	1000	50	20	10
3000	50	10	6	3000	50	18	12
6000	50	12	8	6000	50	18	8
1000	100	7	<1	1000	100	20	12
3000	100	10	6	3000	100	20	12
6000	100	12	10	6000	100	20	12

[a] See Table 1.

mercially available materials and were investigated in concentrations of 10 per cent by weight in the mineral-oil base. This concentration was selected as the most representative on the basis of much preliminary research. From the large amount of data obtained, typical results have been selected, as shown in Fig. 1. Fig. 1 clearly illustrates the extreme sensitivity of the OK values to variations in Timken rubbing speeds. The rapid drop in the OK values with increasing rubbing speed is also strikingly demonstrated.

Discussion of Results

The results of this investigation demonstrate the importance of specifying and controlling within close limits the rubbing-speed variable in the determination of Timken data. They also suggest that the rubbing-speed variable may be an important contributing factor to the common difficulties in duplication of

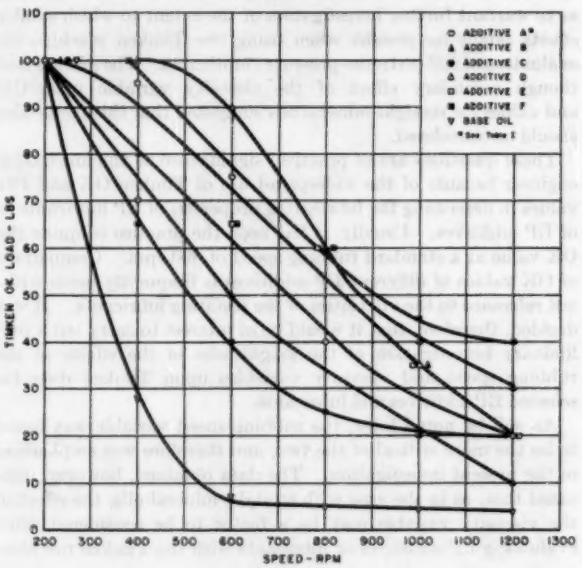

FIG. 1 EFFECT OF RUBBING SPEED UPON TIMKEN OK LOAD DATA FOR SELECTED EP MATERIALS

Timken data among different laboratories and operators, where the usual procedure is to check the nominal rubbing speeds only occasionally and then prior to the actual OK load determinations. It has been found that when the machine is running under load, it is not safe to assume that the speeds are those measured when the machine is not running under load. The results shown in Fig. 1 also suggest that evaluation of an extreme-pressure additive, or of an extreme-pressure lubricant, would be more informative if Timken data for the lubricant were to be obtained over the entire range of rubbing speeds of the commercial machine.

As indicated previously, it would appear that performance of a given EP agent as a boundary lubricant also may be a function of the viscosity of the mineral oil in which the additive has been incorporated. Therefore, if Timken data are to be used in evaluating the relative merits of different EP agents or lubricants, these data should be related to the particular viscosities and other properties of the specific mineral-oil vehicles in which they have been blended, if misleading conclusions as to the merits of the EP additives are to be avoided.

It is suggested that the foregoing can be accomplished, and

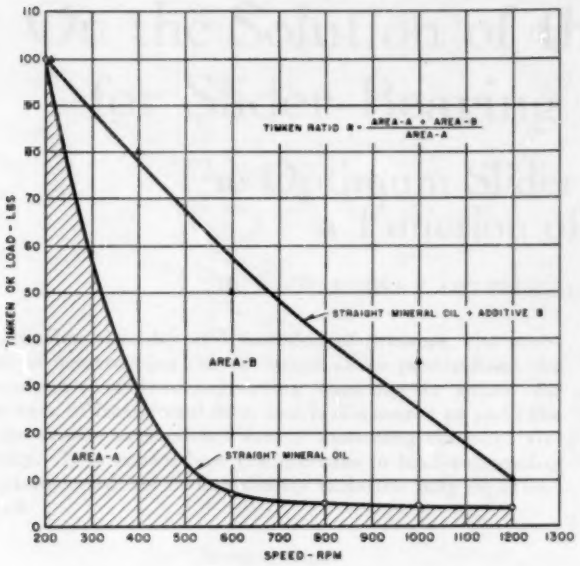

FIG. 2 PROPOSED TIMKEN EP FACTOR

the Timken data made more informative and of greater value to the research man and to the lubrication engineer, if one or both of the following procedures were to be adopted.

1 Determination of the Timken data over the entire speed range of the machine. These data should be related to similar data for the specific mineral-oil vehicle employed in the evaluation of the EP agent or in the blending of the finished lubricant. This could be done, for example, by calculating a ratio R of the two related areas: One, the area under the curve obtained by plotting the OK load over the entire speed range for the EP lubricant; and the other, a corresponding area under the control curve for the straight mineral-oil vehicle, Fig. 2.

2 Determination of a Timken EP factor, which is proposed as the ratio of the area under the curve for the particular oil under investigation, to an "ideal" area that would be the area under an imaginary curve represented by Timken OK-load values of 100 over the entire rubbing-speed range. In this case, a Timken OK load of 100 arbitrarily is considered as a perfect value, inasmuch as this is the maximum OK load at which the Timken machine is normally operated.

Discussion

W. H. MILLETT.[3] The authors point out that the viscosity variable does not affect the OK load data for EP additives and lubricants critically, although apparently there are secondary differences between different EP additives. Whereas this generalization appears to be a valid one for hydrocarbon oils, it is of interest that certain nonhydrocarbon fluids have been found to be characterized by a significant increase in OK load with increasing viscosity. The following data are cited for representative polyglycol fluids, using the standard Timken test procedure in which speed is set at 800 rpm:

Viscosity, SUS/100 F	Timken OK load
260	11
660	17
2000	28
3520	40
5100	50

Have the authors observed this phenomenon and, if so, do they have any theoretical explanation for it?

[3] Special Products Department, Carbide and Carbon Chemicals Company, New York, N. Y.

AUTHORS' CLOSURE

Dr. Millett reports in his discussion that whereas the authors did not find a significant viscosity effect in the OK load data for solutions of extreme-pressure additives in mineral oils, he has found that certain nonhydrocarbon fluids are characterized by a significant increase in OK load with increase in viscosity. Dr. Millett has asked whether the authors have observed this phenomenon and, if so, if we have any theoretical explanation for it.

In reply, we wish to point out that we also have observed the effect to which Dr. Millett refers. This is indicated by the data in Table 5, herewith, which are typical of work done by the authors utilizing the Shell four-ball extreme-pressure lubricant tester.

TABLE 5 FILM STRENGTH CHARACTERISTICS OF SYNTHETIC LUBRICANTS EVALUATED ON THE SHELL FOUR-BALL AND TIMKEN MACHINES

	Shell Four-Ball Tester				Timken	
Viscosity SSU/100 F	EP	2½ SD	Weld	Per cent ideal	OK load	PSI
55	18.6	43	100	51.7	8	2630
170	29.3	91	126	63.4	..	...
260	33.0	105	126	71.0	..	...
400	33.2	116	126	71.4	15	11000
660	39.5	...[a]	126	87.0	..	...
2000	44.5	...[b]	126	85.4	..	...
3520	45.9	...[b]	126	98.7	..	...
5100	50.3	...[b]	141	96.5	45	29700

[a] Welded before 2½ SD was reached.
[b] Welded at first load at which seizure occurred.

The significant correlation between viscosity and the extreme-pressure lubricating properties is apparent. While we have no theoretical explanation for these observations, we do wish to point out that the observed relationship between viscosity and extreme-pressure properties of certain synthetic lubricants is not necessarily contradictory to the results observed with mineral-oil lubricants of various viscosities containing added extreme-pressure agents. In the latter case we are dealing with nonpolar vehicles to which have been added varying amounts of chemically active extreme-pressure agents. In this case it does not seem surprising that the physical viscosity properties of the nonpolar and relatively chemically nonreactive (with respect to extreme-pressure effects) vehicle would play a secondary role in determining the resultant OK load values.

On the other hand, in the case of the synthetic fluids referred to by Dr. Millett, we are dealing with fluids whose extreme-pressure characteristics are related to the chemical properties of the fluid itself and are not dependent upon the further addition of extreme-pressure additives. Inasmuch as the varying viscosities of the synthetic fluids are controlled by the chemical structure and physical properties of the material itself, it is not surprising that there should be found a direct relationship between the viscosities of the synthetic fluids in question and their extreme-pressure properties.

On the Solution of the Reynolds Equation for Slider-Bearing Lubrication—VIII[1]

The Optimum Slider Profile for Viscosity a Function of the Pressure

By A. CHARNES,[2] F. OSTERLE,[3] and E. SAIBEL,[4] PITTSBURGH, PA.

Treating viscosity as a function of pressure, the problem of determining the optimum slider profile from the standpoint of load-supporting capacity is solved for the case of isothermal flow, and is discovered to yield the same profile as Rayleigh found[5] assuming constant viscosity. It is shown how the increase in load-supporting capacity resulting from viscosity variation may be calculated.

Introduction

In his classical paper[5] Rayleigh proposed and solved the following problem in hydrodynamical lubrication: For isothermal flow of the lubricant what slider profile $h(x)$ will make the load-supporting capacity P of a slider bearing a maximum, subject to the conditions of a given slider length B and a given minimum film thickness h_1, Fig. 1? In his solution Rayleigh did not permit variation of the lubricant viscosity with pressure.

H. Blok pointed out the engineering importance of this optimum problem, especially in the design of heavily loaded rubbing surfaces of machine elements, and suggested that the solution be sought which would take into account the variation of viscosity brought about by the high pressures associated with these heavy loads.

It is the purpose of this paper to present such a solution.

Theory

For an oil film which shows no side leakage the Reynolds equation of hydrodynamical lubrication theory reduces to

$$\frac{d}{dx}\left(\frac{Uh}{2} + \frac{h^3}{12\mu}\frac{dp}{dx}\right) = 0 \qquad [1]$$

with $p = 0$ on $x = 0$ and $x = B$; where p is the lubricant pressure which will be measured above the common pressure at inlet and outlet, μ is the lubricant viscosity and the other quantities

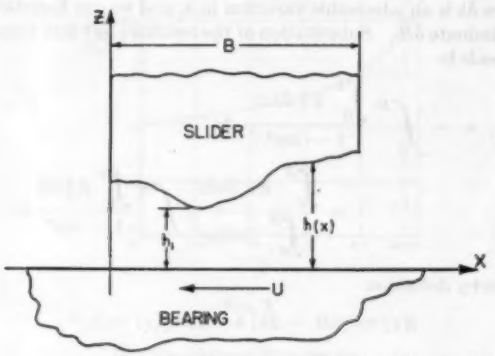

Fig. 1

are as defined in Fig. 1. If we let the zero-pressure viscosity be given by μ_0, then the well-known transformation

$$p^* = \mu_0 \int_0^p \frac{dp}{\mu} \qquad [2]$$

see Charnes and Saibel,[6] reduces Equation [1] to

$$\frac{d}{dx}\left(\frac{Uh}{2} + \frac{h^3}{12\mu_0}\frac{dp^*}{dx}\right) = 0 \qquad [3]$$

which is precisely the Reynolds equation which would apply if the viscosity did not vary (Rayleigh's case). Therefore p^* is the pressure distribution for this situation. In general, the superscript star on a variable will indicate its value under constant viscosity conditions (i.e., $\mu = \mu_0$).

If we introduce the following viscosity-pressure relationship

$$\mu = \mu_0 e^{\alpha p} \qquad [4]$$

where α is a constant, it follows from Equation [2] that

$$p = -\frac{1}{\alpha}\ln(1 - \alpha p^*) \qquad [5]$$

which relates the actual pressure in the film to the pressure which would occur if the viscosity did not vary (i.e., $\alpha = 0$).

The load-supporting capacity defined by

$$P \equiv \int_0^B p\,dx \qquad [6]$$

is given by

$$P = -\frac{1}{\alpha}\int_0^B \ln(1 - \alpha p^*)\,dx \qquad [7]$$

---

[1] This paper was supported in part by funds from a U. S. Air Force Contract with Carnegie Institute of Technology.

[2] Associate Professor, Department of Mathematics, Carnegie Institute of Technology.

[3] Assistant Professor, Department of Mechanical Engineering, Carnegie Institute of Technology. Assoc. Mem. ASME.

[4] Professor of Mechanics, Department of Mathematics, Carnegie Institute of Technology. Mem. ASME.

[5] "Notes on the Theory of Lubrication," by Lord Rayleigh, *Philosophical Magazine*, vol. 35, January, 1918, p. 1.

Contributed by the Research Committee on Lubrication under auspices of ASME Lubrication Activity, Machine Design Division, American Society for Testing Materials, and American Society of Lubricating Engineers and presented at the Annual Meeting, New York, N. Y., November 29–December 4, 1953, of The American Society of Mechanical Engineers.

Note: Statements and opinions advanced in papers are to be understood as individual expressions of their authors and not those of the Society. Manuscript received at ASME Headquarters, April 27, 1953. Paper No. 53—A-38.

[6] "On the Solution of the Reynolds Equation for Slider-Bearing Lubrication—II. The Viscosity a Function of the Pressure," by A Charnes and E. Saibel, Trans. ASME, vol. 75, 1953, p. 269.

from Equation [5]. The pressure p^* is obtained from the integration of Equation [3] which yields

$$p^* = 6\mu_0 U \left[H \int_0^x h^{-3} d\xi - \int_0^x h^{-2} d\xi \right] \quad [8]$$

where H is the film thickness at the point in the film where p^* is a maximum. H is given by

$$0 = H \int_0^B h^{-3} dx - \int_0^B h^{-2} dx \quad [9]$$

This follows from Equation [8] observing that p^* vanishes at both $x = 0$ and $x = B$.

Following Rayleigh, we let h in Equation [8] become $h + \delta h$ where δh is an admissible variation in h, and we use Equation [9] to eliminate δH. Substitution of the resulting δp^* into Equation [7] leads to

$$\frac{\delta P}{6\mu_0 U} = -\int_0^B \frac{\int_0^x i(\xi)\delta h d\xi}{1 - \alpha p^*} dx + \frac{\int_0^B i(x)\delta h dx}{\int_0^B j(x)dx} \int_0^B \frac{\int_0^x j(\xi)d\xi}{1 - \alpha p^*} dx \quad [10]$$

where by definition

$$i(x) \equiv (3H - 2h)\, h^{-4} \text{ and } j(x) \equiv h^{-3}$$

Integrating by parts, Equation [10] reduces to

$$\delta P = 6\mu_0 U \int_0^B i(x) \left\{ g(x) - \frac{\int_0^B g(\xi) j(\xi) d\xi}{\int_0^B j(\xi) d\xi} \right\} \delta h dx \quad [11]$$

where for convenience we define

$$g(x) \equiv \int_0^x \frac{d\xi}{1 - \alpha p^*}$$

Thus, for a prescribed infinitesimal variation in the slider profile along the film, Equation [11] gives the corresponding variation in load-supporting capacity. An optimum profile is one such that P does not increase for any admissible δh.

Equation [11] reduces immediately to Rayleigh's result if we let $\alpha = 0$, for then $g(x) = x$ and we have

$$\delta P = 6\mu_0 U \int_0^B i(x) \left[x - \frac{\int_0^B \xi\, j(\xi) d\xi}{\int_0^B j(\xi) d\xi} \right] \delta h dx \quad [12]$$

which is identical with Equation [32] in Rayleigh's paper.[5]

From this equation Rayleigh noted the possibility of satisfying the optimum condition by means of a profile of stepped form, Fig. 2. For if $h = h_1$ (the minimum film thickness) for $0 \leqslant x < B_1$ and $i(x)$ is taken equal to zero, i.e., $h = 3/2\, H$ for $B_1 < x \leqslant B$ where B_1 is limited by the inequality

$$B_1 \leqslant \frac{\int_0^B x\, j(x) dx}{\int_0^B j(x) dx} \quad [13]$$

every admissible δh from this stepped form diminishes P.

No matter how δh varies in $B_1 < x \leqslant B$ there is no contribution to δP since $i(x) = 0$ in this region. On the other hand, note that an admissible δh can only be non-negative for $0 \leqslant x < B_1$ since h must be greater than or equal to h_1 and this gives a non-positive contribution to δP. Therefore the optimum profile

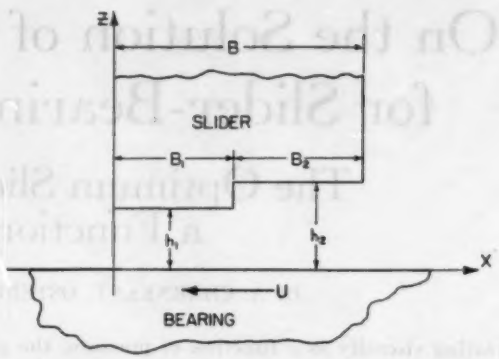

FIG. 2

must be of the "stepped" form just described. See Fig. 2.

Exactly the same conclusion can be drawn for the variable viscosity case characterized by Equation [11] except that the inequality [13] must be replaced by

$$g(B_1) \leqslant \frac{\int_0^B g(x)\, j(x) dx}{\int_0^B j(x) dx} \quad [14]$$

Therefore, in the variable viscosity case also, the optimum profile must be of the stepped form.

The form of the stepped profile is not precisely fixed until the proportions B_2/B_1 and h_2/h_1, Fig. 2, are determined. For h to equal $^3/_2\, H$ over a certain portion of the slider profile it is found from Equation [9] that

$$\frac{B_2}{B_1} = \left(\frac{h_2}{h_1}\right)^2 \left(2\frac{h_2}{h_1} - 3\right) \quad [15]$$

so that it is necessary only to determine h_2/h_1 in order to fix the slider profile. The load-supporting capacity is therefore a function of r where

$$r \equiv \frac{h_2}{h_1} \quad [16]$$

and we proceed to determine r so as to maximize load-carrying capacity.

Maximum Load-Carrying Capacity

From Equations [8] and [16] it can be shown that

$$\left.\begin{aligned} p^* &= \frac{2\mu_0 U}{h_1^2}(2r - 3)x,\ 0 \leqslant x < B_1 \\ p^* &= \frac{2\,\mu_0 U}{h_1^2} \frac{B - x}{r^2},\ B_1 < x \leqslant B \end{aligned}\right\} \quad [17]$$

The load-supporting capacity is then given by Equation [7].

From Equations [17] and [7] it can be shown that

$$P = \frac{\mu_0 U B^2}{h_1^2} f \frac{1 + \frac{1 - 2\beta f}{2\beta f} \ln(1 - 2\beta f)}{\beta f} \quad [18]$$

where

$$f \equiv \frac{2r - 3}{1 + 2r^2 - 3r^2} \quad [19]$$

and

$$\beta \equiv \frac{\alpha \mu_0 U B}{h_1^2} \quad [20]$$

It can be verified that P is actually a maximum (P_m) with respect to r when

$$\frac{df}{dr} = 0 \quad \ldots\ldots\ldots\ldots\ldots\ldots [21]$$

If we let R be the value of r at which Equation [21] is satisfied and F be the value of f at this point, it follows from Equation [19] that

$$R = 1 + \frac{\sqrt{3}}{2} = 1.866$$

and

$$F = \frac{4}{9}(2\sqrt{3} - 3) = 0.206$$

The profile dimensions are now determined as

$$\frac{h_2}{h_1} = 1.866$$

and, from Equation [15]

$$\frac{B_2}{B_1} = 2.55$$

Equation [18] can be written

$$P = \frac{\mu_0 U B^2}{h_1^2} f\left[1 + \frac{2}{3}\beta f + \ldots + \frac{2^n}{n(n+1)}(\beta f)^{n-1} + \ldots\right] \quad \ldots [22]$$

For the constant-viscosity case, $\beta = 0$ so that

$$P^* = \frac{\mu_0 U B^2}{h_1^2} f \quad \ldots\ldots\ldots\ldots\ldots [23]$$

This is precisely the relationship obtained by Rayleigh.[5] As before, P^* is a maximum (P_m^*) under exactly the same condition that made P a maximum (P_m), namely, when Equation [21] is satisfied. It follows then that $R^* = R$ so that the optimum profile for variable viscosity is identical with the optimum profile for constant viscosity.

The maximum load-supporting capacity P_m is now given by

$$P_m = \frac{\mu_0 U B^2}{h_1^2} F \frac{1 + \dfrac{1 - 2\beta F}{2\beta F}\ln(1 - 2\beta F)}{\beta F} \quad \ldots\ldots [24]$$

which for the constant viscosity case ($\beta = 0$) reduces to

$$P_m^* = \frac{\mu_0 U B^2}{h_1^2} F \quad \ldots\ldots\ldots\ldots\ldots [25]$$

Dividing Equation [24] by Equation [25] we obtain

$$\frac{P_m}{P_m^*} = \frac{1 + \dfrac{1 - 2\beta F}{2\beta F}\ln(1 - 2\beta F)}{\beta F} \quad \ldots\ldots\ldots [26]$$

This can be written

$$\frac{P_m}{P_m^*} = 1 + \frac{2}{3}\beta F + \ldots + \frac{2^n}{n(n+1)}(\beta F)^{n-1} + \ldots\ldots [27]$$

It is evident from this expression that P_m is greater than P_m^*, i.e., the maximum load-supporting capacity is increased by taking the viscosity variation into account.

From Equation [5], p becomes infinite when $\alpha p^* = 1$. From Equation [17] together with Equations [19] and [15], αp^* can be shown to have a maximum value of $2\beta F$. Therefore, as p approaches infinity, $2\beta F$ approaches 21, i.e., β approaches 2.43 since $F = 0.206$. Now, from Equation [27] we see that P_m/P_m^* is a strictly increasing function of βF, and from Equation [26] we see that $2\beta F$ must be less than 1 for Equation [26] to be meaningful. Thus, letting $2\beta F$ approach unity in Equation [26], an upper limit on P_m/P_m^* is established, namely, $P_m/P_m^* = 2$. This upper limit is fictitious of course since as p becomes greater and greater the assumed viscosity-pressure relationship, Equation [4], upon which Equation [26] is based becomes invalid, as has been pointed out by Charnes and Saibel.[6] Fig. 3 is a plot of Equation [26] up to this fictitious limit.

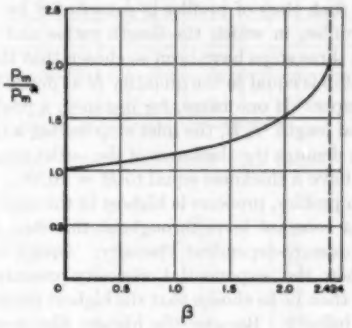

FIG. 3

NUMERICAL EXAMPLE

Consider a slider bearing operating under the following conditions:

Bearing length, $B = 2$ in.
Bearing velocity, $U = 400$ ips
Minimum film thickness, $h_1 = 0.001$ in.

Consider the lubricant to have a zero-pressure viscosity μ_0, of 5×10^{-6} lb sec per sq in. and a pressure coefficient of viscosity α, of 15×10^{-3} sq in. per lb. Then, if the viscosity is assumed constant, Equation [25] yields a value of 1648 lb for the maximum load capacity. If the viscosity variation with pressure is taken into account, Equation [24] yields a value of 1800 lb for the maximum load capacity, an increase of about 9 per cent over the constant-viscosity value.

Discussion

H. BLOK.[7] Although the writer so far has not been able to detect any significant error or any hidden restrictive condition in the authors' analysis, their ultimate result that Rayleigh's double-stepped film profile should be the optimum profile sought seems to be incorrect.

Let us first investigate the limiting cases where highest film pressure approaches infinity. In the authors' analysis these cases are characterized by the feature that $2\beta F$ approaches unity. Then, according to Equations [26] and [25] of the paper, load-supporting capacity approaches

$$P_m = 0.4125\ \mu_0 U B^2/h_1^2 \quad \ldots\ldots\ldots\ldots [28]$$

Now take, for instance, among the class of "straight-wedge" profiles (such as used in Kingsbury thrust bearings) those profiles where the ratio r between film thicknesses h_2 at the inlet and h_1 at the outlet amounts to any value between 1.59 and 2.99.

[7] Professor of Mechanical Engineering, University of Technology, Delft, Holland.

By referring to Muskat and Evinger's theory,[8] it can be shown that, when operating conditions are such that highest film pressure approaches infinity, the profiles considered will yield load-supporting capacities greater than that given by Equation [28].

In fact, if one takes, for instance, the optimum among these profiles ($r = 2.0935$), a formula similar to Equation [28] holds good; the only difference is that the "load-supporting capacity factor" 0.4125 is replaced by the distinctly greater factor 0.4632.

It is not difficult to construct other classes of profiles that, with the viscosity-pressure relationship under consideration, surpass even the optimum straight-wedge profile, and this to the extent that their load-supporting capacity factor is made infinitely great. One such class of profiles is constituted by those "triple-stepped" profiles, in which the length ratios and the thickness ratios of the three steps have been so chosen that the thickness of the middle step is equal to the quantity H as defined by Equation [9] of the paper. If one takes, for instance, a profile with three steps of equal length $^1/_3 B$, the inlet step having a thickness $h_2 = 2h_1$ (when h_1 denotes the thickness of the outlet step), the middle step should have a thickness equal to $H = 10/9h_1$.

With such profiles, pressure is highest in the middle step and it remains at a constant level throughout this step, both for constant and pressure-dependent viscosity. Operating conditions, at least when the exponential viscosity-pressure relationship applies, can then be so chosen that the highest pressure concerned approaches infinity. Because the highest film pressure (in contradistinction to, for instance, straight-wedge profiles) here extends over a "finite" portion of the available film length, load-supporting capacity factor (compare Equation [28]) will then tend also toward infinity.

Thus it would appear that as long as highest film pressure is permitted to approach infinity, there is no sense even in searching for the optimum film profile.

Let us now investigate the cases where highest film pressure is bound by some specified upper limit. It would appear that these, in contradistinction to the foregoing cases, actually occur in the practice of lubrication. In fact, whenever the elastic deformations that the profiles of mating gear teeth undergo under high loads become really pronounced, highest "film" pressure cannot but approach Hertz's pressure or exceed it only comparatively slightly. Hertz's pressure is here defined as the (finite) maximum "contact" pressure that would occur at the tooth load contemplated, if there were no oil at all.

If one neglects the possibility of an error or of a hidden restrictive condition in the authors' analysis, this analysis, up to and including Equation [27] would still apply to the new cases. This would mean that Rayleigh's profile would still constitute the optimum. However, any of the straight-wedge or triple-stepped profiles specified in the foregoing (and many other profiles as well) can yet be shown to be able to yield load-supporting capacities in excess of that of Rayleigh's profile.

Despite his doubts about the correctness of the authors' solution, the writer feels that their work provides a stimulating starting point for continued attempts to arrive at the ultimate solution sought for the cases where highest film pressure is bound by a specified upper limit. A correct solution could contribute very much to judging the potentialities of hydrodynamic lubrication, especially those of the severe "elastohydrodynamic" lubrication encountered on highly loaded gear teeth.[9]

F. S. Chaplin.[10] The method provided in this paper for calculating the increase in load-carrying capacity of stepped bearings due to the pressure-dependence of viscosity offers a method for verifying in machine elements the findings of Bridgeman and others on the variation in bulk viscosity with change in pressure. Experimentally, this would require applying known loads and the measurement of the film thickness. This will be extremely difficult to do, due to the accuracy required to show up the effect of the viscosity variation.

It is suggested that means are more readily available for measuring the friction force. Therefore it would be helpful if the expression for the friction force on a stepped bearing were available in a form to take into account the variation of viscosity with pressure as defined by the expression

$$\mu = \mu_0 e^{\alpha p}$$

For this it would not be necessary to develop the profile for minimizing the friction force. Rather, the expression for the friction force for the optimum load-carrying stepped slider developed in the paper would be sufficient.

Authors' Closure

The authors have deliberately restricted themselves to the case where the highest film pressure is finite, not infinite, since [as Charnes and Saibel have emphasized in footnote (6)] there is grave doubt that the current mathematical formulas adequately or correctly reflect the physical situation at extremely high film pressures.

Where the mathematical formulas do not adequately describe a physical situation, meaningless results may be inferred by employing such formulas, e.g., such conclusions that profiles exist which can support *any* load, *however great*.

The examples which the authors have seen of the type described by Professor Blok have all involved the illegitimate infinite film pressure. A legitimate analysis must take into account other considerations such as the validity of the Reynolds Equation and the proper viscosity-pressure relationship at high pressures. Certainly, as Professor Blok points out, the "elastohydrodynamic effect" will play an important role.

Mr. Chaplin suggests that this work on the stepped-slider would have an application in the experimental determination of pressure dependence of viscosity, if, in addition to the expression for load capacity developed in this paper, an expression for the friction force could be developed from the same basic equations. It is possible to do this quite readily.

The friction force per unit area exerted on the bearing by the lubricant is given by

$$S_x = \frac{\mu U}{h} - \frac{h}{2}\frac{dp}{dx} \quad \ldots\ldots [29]$$

Substituting from Equations [4] and [5] we obtain

$$S_x = \left(\frac{\mu_0 U}{h} - \frac{h}{2}\frac{dp^*}{dx}\right)\frac{1}{1-\alpha p^*} \quad \ldots\ldots [30]$$

Then from Equations [17], S_x could be obtained as a function of r and the friction force per unit slider width determined from the equation

$$F = \int_0^B S_x dx \quad \ldots\ldots [31]$$

---

[8] "The Effect of Pressure Variation of Viscosity on the Lubrication of Plane Sliders," by M. Muskat and H. Evinger, *Journal of Applied Physics*, vol. 11, 1940, pp. 739–748.

[9] See the paper by A. Cameron, "Hydrodynamic Theory in Gear Lubrication," *Journal of the Institute of Petroleum*, vol. 38, August and September, 1952, pp. 614–622. See also the present writer's discussion on pp. 673–677.

[10] Associate Director, Mechanical Engineering Department, The Franklin Institute Laboratories for Research and Development, Philadelphia, Pa. Mem. ASME.

Studies in Cold-Drawing

Part 1 Effect of Cold-Drawing on Steel[1]

By H. MAJORS, JR.,[2] UNIVERSITY, ALA.

In the study of cold-drawing SAE 1020 steel rod various amounts up to a true reduction in area of 0.76, several properties were obtained such as hardness, torsion, and tension. Residual stresses were measured and the microstructure was examined. The effect of the amount of reduction and the direction of drawing per pass (defined as sequence in drawing) on the various properties was determined. Some exploratory work was conducted on the influence of prior cold work and fatigue-stressing on the brittle transition temperature. Effects of size, machining, and time after cold work upon the tension and torsion properties were observed. Cold-drawing is compared with cold-rolling. Part 2[3] consists of studies in cold-drawing 2S-O aluminum, while Part 3[4] discusses some measurements on the coefficient of friction.

Introduction

COLD work in controlled amounts may be imparted to steel by stressing beyond the proportional limit in tension, by direct compressing, drawing, rolling, swaging, and twisting. There is general agreement that all of these operations of deforming metal need not yield the same effect. For example, rolling produces a greater change than rod-drawing for the same amount of reduction. Different operations in cold-working can produce degrees of embrittlement. Favorable residual stresses are produced in cold-drawing rod by a reduction of 1 per cent followed by a light draft of, say, 0.3 per cent reduction.

This is a study in cold-drawing where successive true reductions of rod area between dies are 7 per cent or larger. Several sequences were used, as defined in Table 1, with conical hardened-steel dies of dimensions as noted in Tables 2 and 3. Speed of drawing for all sequences was 2 ipm. The following properties were ascertained: (*a*) True stress-strain tension diagrams; (*b*) hardness; (*c*) torsional stress-strain diagrams; (*d*) residual stresses; (*e*) brittle transition temperature; (*f*) microstructure.

TABLE 1 EXPLANATION OF SEQUENCES IN DRAWING RODS

NOMINAL DIE SIZE, INCHES	1	63/64	31/32	30/32	29/32	28/32	27/32	26/32	25/32	24/32	23/32	22/32	
NOT REVERSED, NOT BY-PASSED	A	A	A	A	A	A	A	A	A	A	A	A	A
REVERSED, NOT BY-PASSED	A	B	A	B	A	B	A	B	A	B	A	B	B A
NOT REVERSED, BY-PASSED	A			A		A		A		A		A	A
REVERSED, BY-PASSED	A			B		A		B		A		B	B A

LETTERS INDICATE THE ROD END ENTERING THE DIE
BLANK SPACES INDICATE THE ROD DID NOT PASS THROUGH THAT DIE

TABLE 2 DIMENSIONS OF THE DIES[a]

Nominal size of die, in.	D_2	T	E	R	X	Y
1	0.996	1.2	1.27	2.20	2.9	1.3
63/64	0.978	1.0	1.20	2.37	2.9	1.4
31/32	0.966	0.87	1.10	1.20	2.8	1.1
15/16	0.930	1.12	1.18	1.90	2.9	1.4
29/32	0.898	1.09	1.14	1.08	2.9	1.4
7/8	0.872	1.07	1.03	2.13	2.9	1.3
27/32	0.842	1.10	1.13	1.20	2.8	1.3
13/16	0.808	0.96	1.01	1.09	2.9	1.3
25/32	0.775	0.98	1.09	0.50	2.8	1.3
3/4	0.747	1.06	1.00	0.68	2.9	1.3
23/32	0.719	1.14	0.95	0.83	2.9	1.3
11/16	0.685	0.98	0.99	0.52	2.9	1.3

[a] See Fig. 1 for coding. All quantities in inches.

TABLE 3 DIMENSIONS[a] A, D_1, D_2, AND θ FOR VARIOUS SEQUENCES

Nominal die size, in.	Sequence in drawing: Not reversed, not by-passed and Reversed, not by-passed				Not reversed, by-passed and Reversed, by-passed			
	A	D_1	D_2	θ	A	D_1	D_2	θ
1	0.76	1.000	0.996	0°10′	0.76	1.000	0.996	0°10′
63/64	0.67	0.997	0.978	0°49′				
31/32	0.41	0.978	0.966	0°50′				
30/32	0.76	0.966	0.930	1°21′	0.96	0.996	0.930	1°57′
29/32	0.83	0.930	0.898	1°00′				
28/32	0.62	0.898	0.872	1°11′	0.96	0.930	0.872	1°49′
27/32	0.73	0.872	0.842	1°12′				
26/32	0.74	0.842	0.808	1°19′	0.85	0.872	0.808	2°11′
25/32	0.88	0.808	0.775	1°40′				
24/32	0.57	0.775	0.747	1°30′	0.74	0.808	0.747	2°20′
23/32	0.67	0.747	0.719	1°12′				
22/32	0.54	0.719	0.685	1°48′	0.74	0.747	0.685	2°23′

[a] See Fig. 1 for coding. All quantities in inches unless noted otherwise.

Conditions of Test

Long, 1-in-diam rods of low-carbon steel, SAE 1020, were used as the starting material in order to minimize the possibilities of inequalities in chemical and physical properties that could occur and the imperfections in the shape and surface of the dies used. The rods were pulled in a 60,000-lb Baldwin universal testing

---

[1] This investigation was conceived in discussions with F. J. Mehringer, who outlined a general program. R. K. Newman, Plant Manager and F. S. Costelloe, Plant Metallurgist, both of Republic Steel Corporation, provided a series of dies and annealed SAE 1020 steel in the summer of 1949. Work was started in December, 1949, under a grant provided by the Research Corporation, 405 Lexington Avenue, New York 17, N. Y., to the University of Alabama.

[2] California Research and Development Company, Livermore, Calif.; now Research Professor, Bureau of Engineering Research, University of Alabama. Mem. ASME.

[3] "Studies in Cold-Drawing—Part 2 Cold-Working 2S-O Aluminum," by H. Majors, Jr., published in this issue, pp. 49–56.

[4] Studies in Cold-Drawing—Part 3 Effect of Sequence on the Coefficient of Friction in Cold-Drawing Low-Carbon Steel and 2S-O Aluminum Rods," by H. Majors, Jr., presented at the Annual Meeting, New York, N. Y., November 28–December 3, 1954, of THE AMERICAN SOCIETY OF MECHANICAL ENGINEERS, Paper No. 54—A-114.

Contributed by the Metals Engineering Division and presented at the Annual Meeting, New York, N. Y., November 29–December 4, 1953, of THE AMERICAN SOCIETY OF MECHANICAL ENGINEERS.

NOTE: Statements and opinions advanced in papers are to be understood as individual expressions of their authors and not those of the Society. Manuscript received at ASME Headquarters, April 29, 1953. Paper No. 53—A-73.

machine at a drawing speed of 2 ipm at room temperature. Drawing force was observed every 30 sec throughout the drawing operation. All rods were coated with a solution of Banox No. 5 (see Appendix) which formed a smooth, continuous film of an amorphous phosphate. Lubrication was prepared by making a paste of SAE 20 machine oil and type M Molykote (see Appendix).

The SAE 1020 steel was $1^1/_8$-in-diam bar stock, hot-rolled, pickled, and limed, which was annealed in a large electric oven at 1550 F for about 5 hr to a Vickers hardness of 114. Eighteen bars, 30 in. long, were machined to 1.000 in. diam and the ends were prepared for passing through the dies according to the particular sequence chosen in Table 1. An explanation of the sequences used follows.

"Not reversed, not by-passed" means that only one end was tapered for starting through each die, and if a rod finally passed through the 22/32-in-diam die, it was cold-worked by passing through 12 dies without any intermediate heating. To determine the effect of passing through the intermediate dies, sections of rod were removed after passing through a particular die and machined into suitable specimens. Then the drawing operation was continued. Several rods were used to determine the progressive effect of cold-working. Approximately, there was a 7 per cent reduction per pass, except through the 1-in., 63/64-in., and 22/32-in. dies.

"Reversed, not by-passed" indicates that both ends were tapered for starting each end (A and B) through alternate dies, respectively. By starting each end alternately, a reversed effect was produced. For example, end A was started through the 1-in. die, end B through the 63/64-in. die, end A through the 31/32-in. die, and so on. Approximately, there was a 7 per cent reduction per pass with reversed drawing, except through the 1-in., 63/64-in., and 22/32-in. dies.

"Not reversed, by-passed" means that the reduction per pass was approximately 15 per cent, except through the 1-in. die. Only one end was tapered and the rod passed through the 1-in., 30/32-in., 28/32-in. dies and so on, as indicated in Table 1. Properties were determined after passing each die.

In the "reversed, by-passed" sequence, both ends were tapered for starting each end A and B alternately. End A passed through the 1-in. die, B through the 30/32-in. die, A through the 28/32-in. die, B through the 26/32-in. die, A through the 24/32-in. die and the end B through the 22/32-in. die, giving approximately a 15 per cent reduction per pass and reversed drawing. This is illustrated in Table 1.

The material of rod No. 1 had the following chemical composition:

	Per cent
Carbon	0.20
Manganese	0.77
Phosphorus	0.022
Sulphur	0.034
Silicon	0.040

Tables 2 and 3 indicate the physical dimensions of the hardened-steel dies used to cold-work the cylindrical steel rods, while the coding appears in Fig. 1.

Tension Tests

Very little information is available in the literature of the effects of cold-working on the true stress-strain properties. Mehringer and MacGregor (1)[1] give an excellent account of the cold-rolling effect on the true stress-strain properties of a low-carbon steel. Godfrey (2) studied the effect of variation in wire-drawing on the physical properties of steel wire. Because of the small diameter of wire used, the only true quantity he could use was the true reduction of wire diameter. No reversed sequence was used but reductions of 10, 20, 30, and 40 per cent per pass were investigated which correspond to the not reversed, not by-passed and not reversed, by-passed sequence used in this work.

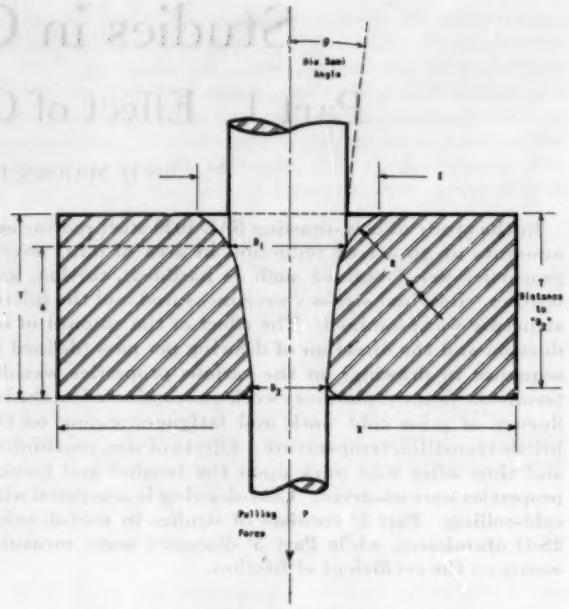

Fig. 1 Coding for Tables 2 and 3

Prior to the determination of the effect of drawing upon the true stress-strain properties at room temperature, tests were conducted to ascertain the influence of machining, size, and time after drawing on these properties, and the uniformity of hardness across the section. These effects were small and are discussed in the Appendix.

Fig. 2 shows the tension results in the elastic region and the influence of cold-drawing on the yield strength at 0.1 per cent offset (dotted line); and Fig. 3 indicates the progressive change in the true stress-strain properties up to rupture. Both curves are for rods passed through the dies in the not reversed, not by-passed sequence. The short arrows in Fig. 3 indicate the true stresses at maximum load which are increased by increasing amounts of cold-drawing. But no appreciable increase in the true fracture stress occurs up to a true rod reduction of 0.76. The true strain at maximum load or the true uniform strain is affected by cold-drawing to a true reduction in drawing of about 0.15; additional cold-working in drawing has hardly any influence up to a true rod reduction in area of 0.76; but the local necking-strain part of the total strain at fracture is decreased. Of course increasing amounts of cold work permit less and less total true tension-fracture strain.

Three variations of sequences are presented in Fig. 4 and two in Fig. 5. Direction and amount of drawing per pass has some effect on the yield strength of low-carbon steel but for true strains exceeding 0.01 in. per in. up to fracture, there was no effect on the true stress-strain diagram. An examination of the fractured surfaces in tension specimens revealed a predominance of perfect cup-cones for rods "reversed," whereas for rods not subjected to reversed drawing, the fractures were jagged but still ductile. Fujiwara (3) observed the same fracture appearances in his work on aluminum wires. Although he does not report any true tension values, he remarks that the wire drawn in the same direction was more hardened and brittle than that drawn in the reverse

[1] Numbers in parentheses refer to the Bibliography at the end of the paper.

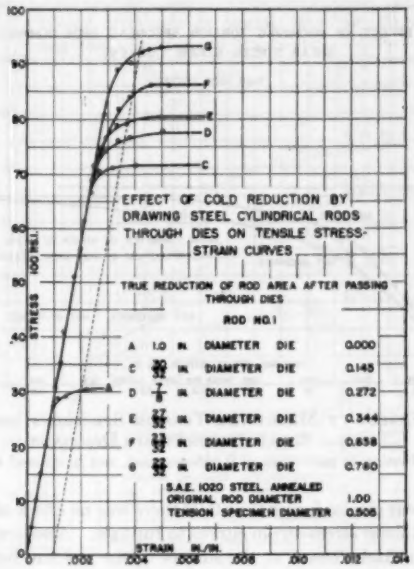
EFFECT OF COLD REDUCTION BY DRAWING STEEL CYLINDRICAL RODS THROUGH DIES ON TENSILE STRESS-STRAIN CURVES
TRUE REDUCTION OF ROD AREA AFTER PASSING THROUGH DIES
ROD NO.1
A 1.0 IN. DIAMETER DIE 0.000
C 20/32 IN. DIAMETER DIE 0.145
D 7/8 IN. DIAMETER DIE 0.272
E 27/32 IN. DIAMETER DIE 0.344
F 23/32 IN. DIAMETER DIE 0.638
G 22/32 IN. DIAMETER DIE 0.760
S.A.E. 1020 STEEL ANNEALED
ORIGINAL ROD DIAMETER 1.00
TENSION SPECIMEN DIAMETER 0.505
STRESS 100 PSI.
STRAIN IN./IN.

FIG. 2 EFFECT OF COLD-REDUCTION BY DRAWING STEEL CYLINDRICAL RODS THROUGH DIES UPON ELASTIC PART OF STRESS-STRAIN DIAGRAM
(Yield strength at 0.1 per cent offset indicated by dotted line.)

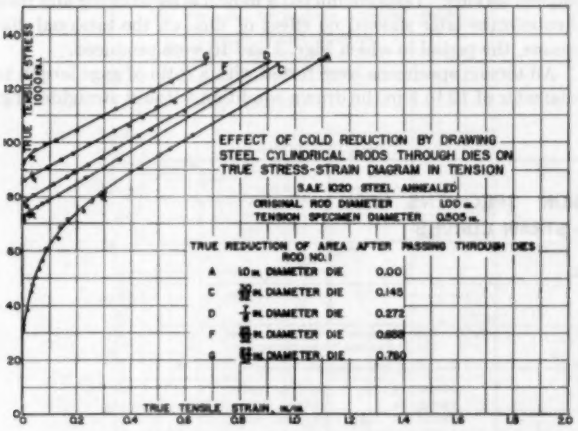
EFFECT OF COLD REDUCTION BY DRAWING STEEL CYLINDRICAL RODS THROUGH DIES ON TRUE STRESS-STRAIN DIAGRAM IN TENSION
S.A.E. 1020 STEEL ANNEALED
ORIGINAL ROD DIAMETER 1.00 in.
TENSION SPECIMEN DIAMETER 0.505 in.
TRUE REDUCTION OF AREA AFTER PASSING THROUGH DIES
ROD NO.1
A 1.0 in. DIAMETER DIE 0.00
C 20/32 in. DIAMETER DIE 0.145
D 7/8 in. DIAMETER DIE 0.272
F 23/32 in. DIAMETER DIE 0.638
G 22/32 in. DIAMETER DIE 0.760
TRUE TENSILE STRESS, 1000 PSI.
TRUE TENSILE STRAIN, in./in.

FIG. 3 EFFECT OF COLD-WORKING BY ROD-DRAWING ON TRUE STRESS-STRAIN DIAGRAMS IN TENSION UP TO FRACTURE

direction alternately. Also, there was a small difference in the conventional tensile strength for both cases. Table 4 shows that the manner of drawing had no influence on the hardness measurements.

TABLE 4 EFFECT OF SEQUENCE IN DRAWING STEEL RODS UPON AVERAGE VICKERS HARDNESS NUMBER—ROD NO. 1

Nominal size of die, in.	Sequence of drawing: Not reversed, not by-passed	Reversed, not by-passed	Not reversed, by-passed
1	120	120	120
63/64	141	...	...
31/32	150	...	...
30/32	171	...	175
29/32	187	...	192
28/32	187	...	...
27/32	194	...	197
26/32	201	...	...
25/32	207	...	...
24/32	208	...	...
23/32	209	212	...
22/32	222	221	...

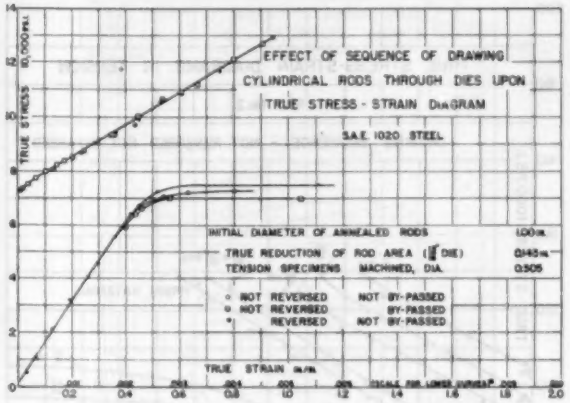
EFFECT OF SEQUENCE OF DRAWING CYLINDRICAL RODS THROUGH DIES UPON TRUE STRESS - STRAIN DIAGRAM
S.A.E. 1020 STEEL
INITIAL DIAMETER OF ANNEALED RODS 1.00 in.
TRUE REDUCTION OF ROD AREA (7/8 DIE) 0.145 in.
TENSION SPECIMENS MACHINED, DIA. 0.505
NOT REVERSED NOT BY-PASSED
NOT REVERSED BY-PASSED
REVERSED NOT BY-PASSED
TRUE STRESS 10,000 PSI.
TRUE STRAIN in./in.

FIG. 4 EFFECT OF SEQUENCE IN COLD-DRAWING UPON ELASTIC REGION IN TENSION AND TRUE STRESS-STRAIN DIAGRAM
(True reduction in rod area of 0.145.)

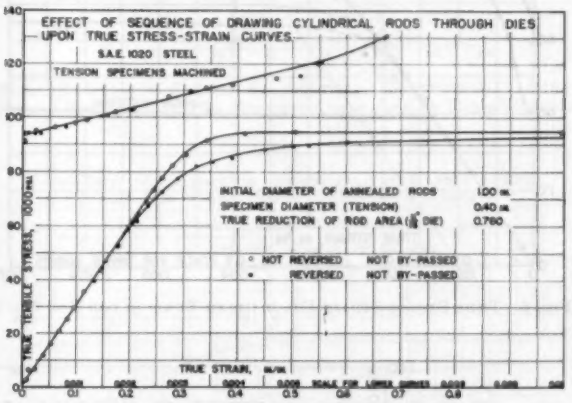
EFFECT OF SEQUENCE OF DRAWING CYLINDRICAL RODS THROUGH DIES UPON TRUE STRESS-STRAIN CURVES
S.A.E. 1020 STEEL
TENSION SPECIMENS MACHINED
INITIAL DIAMETER OF ANNEALED RODS 1.00 in.
SPECIMEN DIAMETER (TENSION) 0.40 in.
TRUE REDUCTION OF ROD AREA (7/8 DIE) 0.760
NOT REVERSED NOT BY-PASSED
REVERSED NOT BY-PASSED
TRUE TENSILE STRESS, 1000 PSI.
TRUE STRAIN, in./in.

FIG. 5 COMPARISON OF SEQUENCE EFFECT ON ELASTIC REGION AND ON TRUE STRESS-STRAIN DIAGRAMS TO FRACTURE
(True reduction in rod area of 0.760.)

In order to have more extensive data for the determination of the coefficient of friction and to determine the degree of reproducing test data, a second series of bars was cold-drawn of the following chemical composition and designated as rod No. 2:

	Per cent
Carbon	0.18
Manganese	1.03
Phosphorus	0.015
Sulphur	0.038
Silicon	0.047

This material was annealed in a large electric furnace at 1650 F and slow-cooled, resulting in a Vickers hardness of 120. The effect of cold-drawing on the true stress-strain diagrams are noted in Fig. 6. The parallel dotted line to the initial slope of the curves is for determining the yield strength at 0.1 per cent offset. Drawing loads are listed in the Appendix (see Tables 7, 8, and 9) for both rods Nos. 1 and 2, which can be used in conjunction with the tension curves for applying theories of wire-drawing.

TORSION EXPERIMENTS

Certain influences not observed in tension test specimens were noticed in the torsion test. Figs. 7 and 8 indicate that unmachined torsion specimens have lower yield strengths than those machined (much greater effect in torsion than in tension);

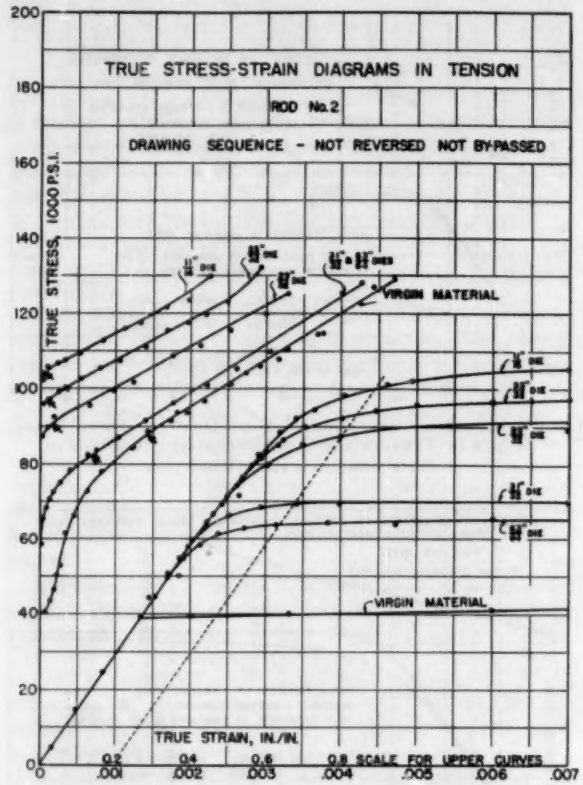
TRUE STRESS-STRAIN DIAGRAMS IN TENSION
ROD No. 2
DRAWING SEQUENCE - NOT REVERSED NOT BY-PASSED
TRUE STRESS, 1000 P.S.I.
VIRGIN MATERIAL
VIRGIN MATERIAL
TRUE STRAIN, IN./IN.
0.2 0.4 0.6 0.8 SCALE FOR UPPER CURVES
.001 .002 .003 .004 .005 .006 .007

FIG. 6 TRUE STRESS-STRAIN DIAGRAMS IN TENSION FOR ROD NO. 2

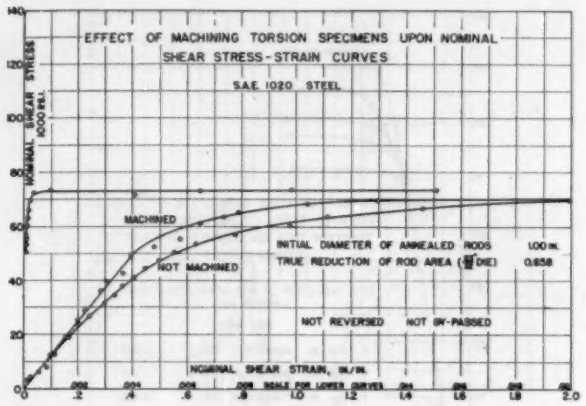
EFFECT OF MACHINING TORSION SPECIMENS UPON NOMINAL SHEAR STRESS-STRAIN CURVES
S.A.E. 1020 STEEL
NOMINAL SHEAR STRESS, 1000 P.S.I.
MACHINED
NOT MACHINED
INITIAL DIAMETER OF ANNEALED RODS 1.00 IN.
TRUE REDUCTION OF ROD AREA (DIE) 0.658
NOT REVERSED NOT BY-PASSED
NOMINAL SHEAR STRAIN, IN./IN.
SCALE FOR LOWER CURVES

FIG. 7 EFFECT OF MACHINING TORSION SPECIMENS ON CONVENTIONAL SHEAR STRESS-STRAIN DIAGRAMS
(True reduction in cold-work of 0.658 reversed, not by-passed sequence.)

yet for shear strains larger than 0.03 there was no effect on the conventional shear stress-strain curves to rupture. Also, owing to the residual biaxial stresses at the surface of the rod and because the maximum applied torsional stress is at the surface, it was decided to present torsion data from unmachined specimens. Size effects can occur in torsion specimens as shown by Morrison (4) and the maximum-shear theory, including size effect by Shaw (5). For the diameters used, 0.685 to 0.960 in., this effect was not considered serious. Tests conducted a month after drawing and then five months later showed no effect of time on the torsional diagrams, the period in which Figs. 9 and 10 were produced.

All torsion specimens were tested with a ratio of gage length to diameter of 10 to 1 in the drawn condition without straightening.

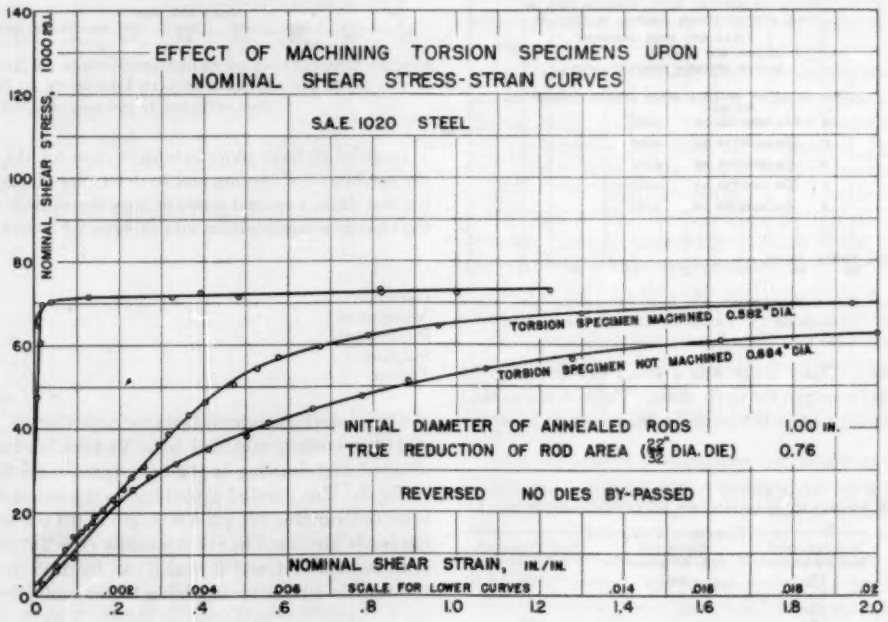
EFFECT OF MACHINING TORSION SPECIMENS UPON NOMINAL SHEAR STRESS-STRAIN CURVES
S.A.E. 1020 STEEL
NOMINAL SHEAR STRESS, 1000 P.S.I.
TORSION SPECIMEN MACHINED 0.592" DIA.
TORSION SPECIMEN NOT MACHINED 0.884" DIA.
INITIAL DIAMETER OF ANNEALED RODS 1.00 IN.
TRUE REDUCTION OF ROD AREA (DIA. DIE) 0.76
REVERSED NO DIES BY-PASSED
NOMINAL SHEAR STRAIN, IN./IN.
SCALE FOR LOWER CURVES

FIG. 8 INFLUENCE OF MACHINING OPERATION ON CONVENTIONAL SHEAR STRESS-STRAIN DIAGRAM IN ELASTIC REGION
(No effect on plastic curve to rupture.)

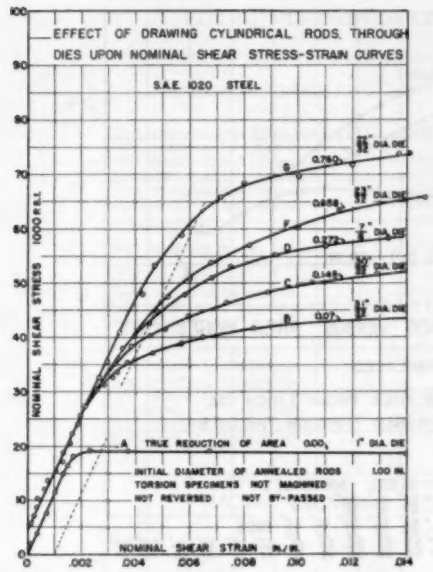
EFFECT OF DRAWING CYLINDRICAL RODS THROUGH DIES UPON NOMINAL SHEAR STRESS-STRAIN CURVES
S.A.E. 1020 STEEL
NOMINAL SHEAR STRESS 1000 P.S.I.
NOMINAL SHEAR STRAIN IN./IN.
INITIAL DIAMETER OF ANNEALED RODS 1.00 IN.
TORSION SPECIMENS NOT MACHINED
NOT REVERSED NOT BY-PASSED

FIG. 9 CONVENTIONAL SHEAR STRESS-STRAIN DIAGRAMS, SHOWING INFLUENCE OF COLD WORK UPON YIELD STRENGTH AT 0.1 PER CENT OFFSET—DOTTED LINE

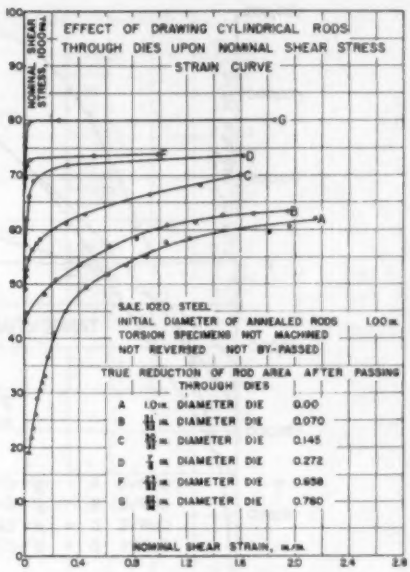
EFFECT OF DRAWING CYLINDRICAL RODS THROUGH DIES UPON NOMINAL SHEAR STRESS STRAIN CURVE
NOMINAL SHEAR STRESS, 1000 P.S.I.
S.A.E. 1020 STEEL
INITIAL DIAMETER OF ANNEALED RODS 1.00 IN.
TORSION SPECIMENS NOT MACHINED
NOT REVERSED NOT BY-PASSED
TRUE REDUCTION OF ROD AREA AFTER PASSING THROUGH DIES
NOMINAL SHEAR STRAIN, IN./IN.

FIG. 10 PLASTIC REGION TO RUPTURE, CONVENTIONAL SHEAR STRESS-STRAIN DIAGRAMS, SHOWING INFLUENCE OF COLD-WORKING

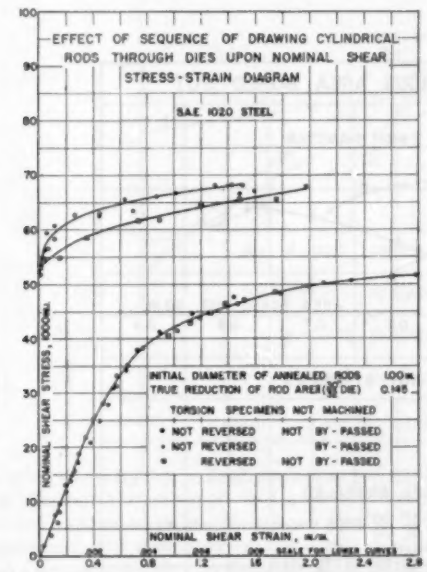
EFFECT OF SEQUENCE OF DRAWING CYLINDRICAL RODS THROUGH DIES UPON NOMINAL SHEAR STRESS-STRAIN DIAGRAM
S.A.E. 1020 STEEL
NOMINAL SHEAR STRESS, 1000 P.S.I.
INITIAL DIAMETER OF ANNEALED RODS 1.00 IN.
TRUE REDUCTION OF ROD AREA (.375" DIE) 0.145
TORSION SPECIMENS NOT MACHINED
NOMINAL SHEAR STRAIN, IN./IN.

FIG. 11 EFFECT OF SEQUENCE IN DRAWING ON CONVENTIONAL SHEAR STRESS-STRAIN DIAGRAM FOR TRUE REDUCTION IN ROD AREA OF 0.145

(Lower curve is elastic region; upper curves are plastic region.)

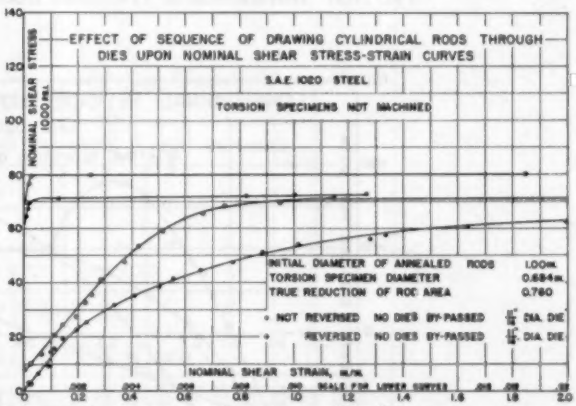
EFFECT OF SEQUENCE OF DRAWING CYLINDRICAL RODS THROUGH DIES UPON NOMINAL SHEAR STRESS-STRAIN CURVES
S.A.E. 1020 STEEL
TORSION SPECIMENS NOT MACHINED
NOMINAL SHEAR STRESS 1000 P.S.I.
INITIAL DIAMETER OF ANNEALED RODS 1.00 IN.
TORSION SPECIMEN DIAMETER 0.684 IN.
TRUE REDUCTION OF ROD AREA 0.760
NOT REVERSED NO DIES BY-PASSED
REVERSED NO DIES BY-PASSED
NOMINAL SHEAR STRAIN, IN./IN.

FIG. 12 COMPARISON OF MANNER OF ROD-DRAWING ON CONVENTIONAL SHEAR STRESS-STRAIN DIAGRAMS FOR TRUE ROD REDUCTION IN AREA OF 0.760.

(Lower curves, elastic region; upper curves plastic region to rupture.)

When the rods were about 33 in. long, there was a slight bowing but for lengths of 10 to 12 in., the specimens were quite straight. Tests were performed on a 60,000-in-lb Olsen torsion machine by increment loading in the elastic region and constant twisting-head speed in the plastic region to rupture.

The variation of the conventional shear stress-strain curves with increasing cold work (not reversed, not by-passed sequence) appears in Fig. 9, for the elastic region where the dotted line is the construction for determining the yield strength at 0.1 per cent offset in shear; and in Fig. 10 for the plastic region to rupture.

Because of premature failure of the unmachined specimens in the jaws of the torsion machine, strains at fracture are not quite the same. This is quite a contrast to the tension test for low-carbon steel where cold-working has no effect on the true tensile stress at rupture up to a true reduction of rod area of 0.76 and the true strain at fracture decreases as the cold work increases. For the amounts of cold work investigated, the shear stress at rupture increased with increased cold work.

An examination of Figs. 11 and 12 indicates that there is some sequence effect on the shear stress-strain diagram, especially at the true rod reduction of 0.76, but more tests are needed to establish its magnitude. Not enough material was available (of the same chemical composition) to explore torsion properties fully at this time.

A determination of the ratios of yield strengths (0.1 per cent offset) in torsion to tension revealed that it was approximately 0.62 in the annealed condition and with increasing cold work, it approached quickly an average of 0.57 (see Appendix). However,

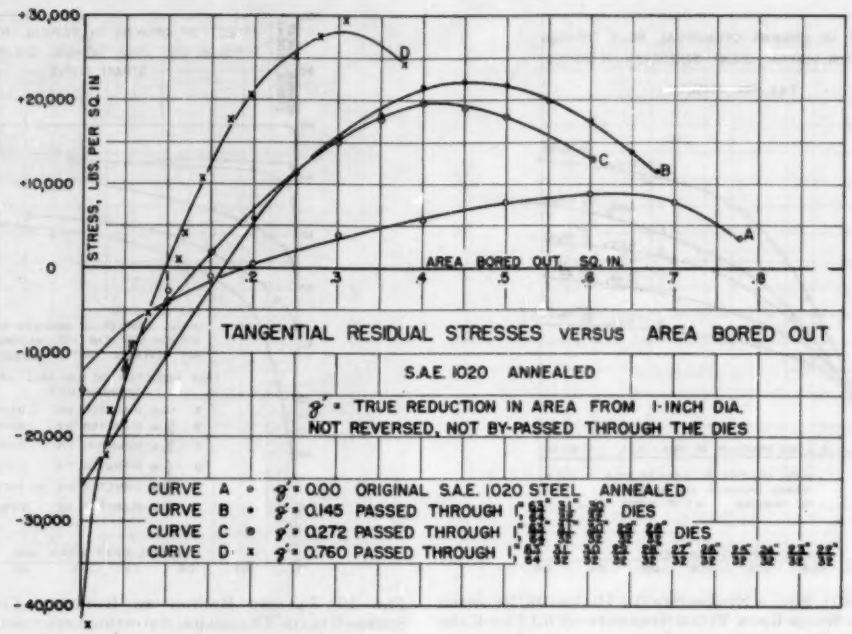
+30,000
+20,000
+10,000
0
-10,000
-20,000
-30,000
-40,000
STRESS, LBS. PER SQ. IN.
AREA BORED OUT, SQ. IN.
.2
.3
.4
.5
.6
.7
.8
TANGENTIAL RESIDUAL STRESSES VERSUS AREA BORED OUT
S.A.E. 1020 ANNEALED
g' = TRUE REDUCTION IN AREA FROM 1-INCH DIA.
NOT REVERSED, NOT BY-PASSED THROUGH THE DIES
CURVE A • g' = 0.00 ORIGINAL S.A.E. 1020 STEEL ANNEALED
CURVE B • g' = 0.145 PASSED THROUGH 1", 63/64", 31/32", 30/32" DIES
CURVE C • g' = 0.272 PASSED THROUGH 1", 63/64", 31/32", 30/32", 29/32", 28/32" DIES
CURVE D x g' = 0.760 PASSED THROUGH 1", 63/64", 31/32", 30/32", 29/32", 28/32", 27/32", 26/32", 25/32", 24/32", 23/32", 22/32" DIES
A
B
C
D

FIG. 13(a) DISTRIBUTION OF TANGENTIAL RESIDUAL STRESSES FOR VARIOUS AMOUNTS OF COLD WORK

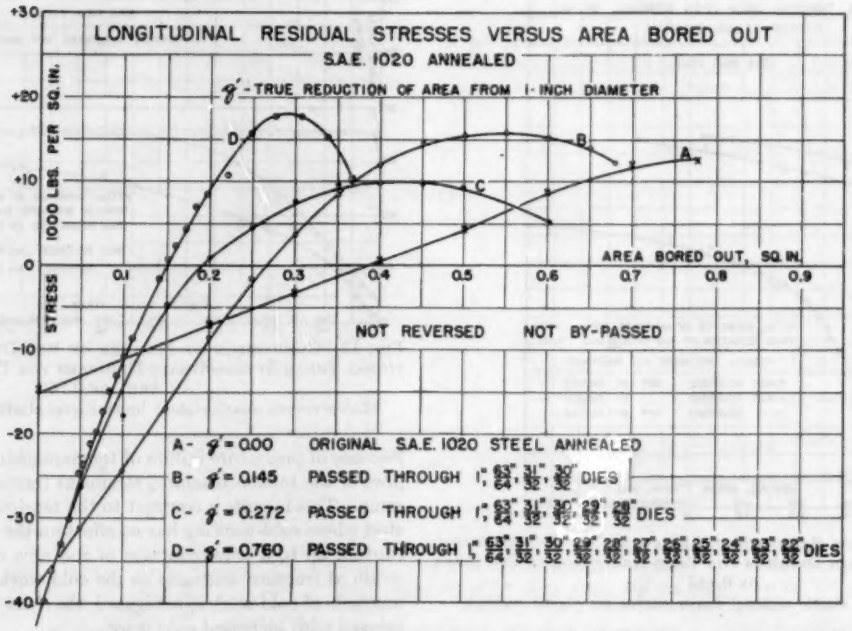

FIG. 13(b) DISTRIBUTION OF LONGITUDINAL RESIDUAL STRESSES FOR VARIOUS AMOUNTS OF COLD WORK

for a true reduction of rod area of 0.76, the ratio was found to be 0.68. More torsion data are needed to evaluate fully the effect of sequence, size of torsion specimen, amount of cold work, and residual stresses upon the yield-strength ratio of torsion to tension. Torsion specimens were not machined (except in the annealed condition); thus the diameters ranged from 0.685 to 0.960 in. Machined specimens showed higher yield strengths than those not machined, probably as a result of the influence of the residual stresses which are relieved somewhat by machining.

RESIDUAL STRESSES

A series of residual-stress measurements was made on several cylindrical rods whose length-to-diameter ratio was three to avoid end effects. Two resistance wire SR-4 gages were mounted on each cylinder, one in the tangential and the other in the longitudinal direction. All measurements were made using an SR-4 strain indicator type L, while the active sample and dummy circuits were kept in an oven at 100 F, where the temperature variation was plus or minus 0.5 deg F. Each cylinder was bored

TABLE 5 SUMMARY OF RESIDUAL-STRESS MEASUREMENTS—ROD NO. 1

Sequence of drawing	Center stress, psi	Maximum tensile stress, psi	Surface stress, psi	True reduction of rod area
		Tangential Stresses		
Not reversed, not by-passed.....	—26000	+22000	+11500	0.145
Not reversed, by-passed.....	0	+10000	−5000	0.145
Not reversed, not by-passed.....	—45000	+27500	+27500	0.658
Reversed, not by-passed.....	—29000	+27000	+24000	0.658
Not reversed, not by-passed.....	—45000	+24000	+18000	0.720
Reversed, not by-passed.....	—36000	+38000	+2000	0.720
		Longitudinal Stresses		
Not reversed, not by-passed.....	—30000	+26000	+13500	0.145
Not reversed, by-passed.....	0	+8500	+4000	0.145
Not reversed, not by-passed.....	—44000	+20000	+20000	0.658
Reversed, not by-passed.....	—27000	+25000	+25000	0.658
Not reversed, not by-passed.....	—43000	+19000	+10500	0.720
Reversed, not by-passed.....	—52000	+28000	+3500	0.720
		Radial Stresses		
Not reversed, not by-passed.....	—22000		0	0.145
Not reversed, by-passed.....	0		0	0.145
Not reversed, not by-passed.....	—33000		0	0.658
Reversed, not by-passed.....	—42500		0	0.658
Not reversed, not by-passed.....	—22000		0	0.720
Reversed, not by-passed.....	—37000		0	0.720

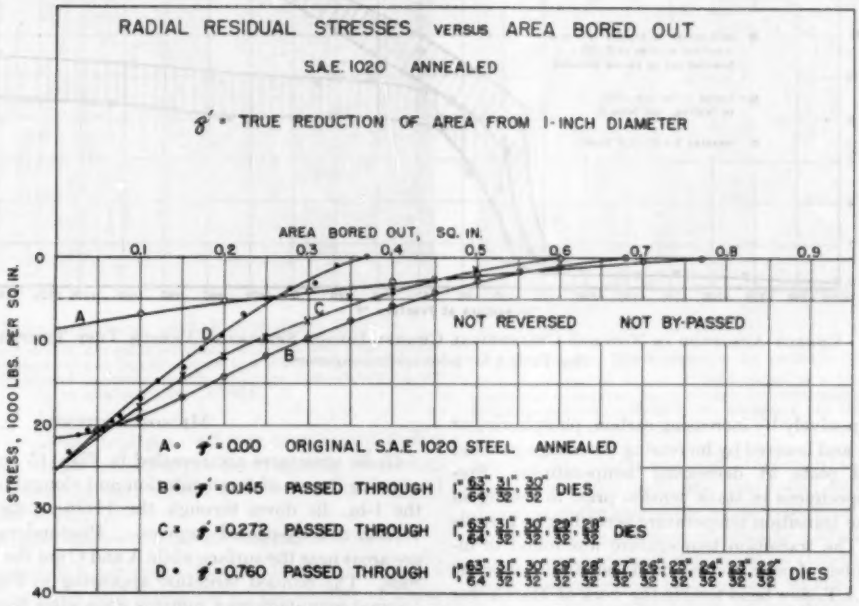

FIG. 13(*c*) DISTRIBUTION OF RADIAL RESIDUAL STRESSES FOR VARIOUS AMOUNTS OF COLD WORK

carefully, using an air stream to keep the boring tool cool. Three strain-gage readings were made on each gage after every boring which covered a period of 24 hr. Before and after each residual-stress experiment, the constancy of the strain indicator was checked on a separate circuit. On the same material two separate stress determinations were made in which the degree of reproducing the test data was good.

Sachs (6) method for computing the residual stresses was used where the results were plotted versus area bored out in square inches as indicated in Figs. 13 (*a*, *b*, and *c*) for the not reversed, not by-passed sequence in cold-drawing. It is interesting to note that curve A is for the annealed condition. The entire work on residual stresses is summarized in Table 5. Cold-working influences the tangential stresses more than either the longitudinal or radial stresses as indicated in Figs. 13 (*a*, *b*, and *c*). Sequence in cold-drawing has an effect on the surface stresses. The lowest surface stresses are obtained with the not reversed, by-passed and reversed, not by-passed sequences. The rods were not straightened after cold-drawing.

Thus residual stresses may be reduced by mechanical means upon the introduction of a sequence in drawing. A redistribution of stress with a lowering of peak values by annealing often involves temperatures at which there is some risk of losing surface quality or reducing tensile properties. The type, amount, and distribution of fesidual stress in a cold-drawn bar are dependent upon the reduction of rod area. With reductions of more than 0.8 per cent, there is compression in the center of the bar and usually tension at the surface, such as indicated in Figs. 13 (*a*, *b*, and *c*). But, if the reduction is under 0.6 per cent, the surface usually is under compression and there is tension at the center of the bar. Mechanical methods of reducing residual stresses on the basis of economy, improvements of surface, or retaining mechanical properties of low-carbon steel apply to the tensile and fatigue properties.

IMPACT TESTS

Although this phase of the work is limited because of the lack of time, nevertheless it gives some indication of the change in impact value resulting from prior cold work and fatigue cycling. The brittle behavior of steels at very low temperature compared with their room-temperature ductility is of general interest. Banta and Lorig (7) report that the brittle transition temperature (in im-

TABLE 6[a] CYCLING CYLINDRICAL NOTCHED IMPACT SPECIMENS IN FATIGUE PRIOR TO CHARPY IMPACT TEST—ROD NO. 1

True reduction of rod area in cold-drawing	Stress rotating cantilever, psi	Cycles of stress reversal	Cycles to fracture line	Energy absorbed in impact, ft-lb	Temperature of impact test, deg F
0.760	30000	100000	600000	0.75	—109
0.760	27500	20000000	Endurance limit	4.68	—99
0.760	20000	20000000	Below endurance limit	7.60	—72
0.760	15000	12000000	Below endurance limit	6.50	—101

[a] See Fig. 14.

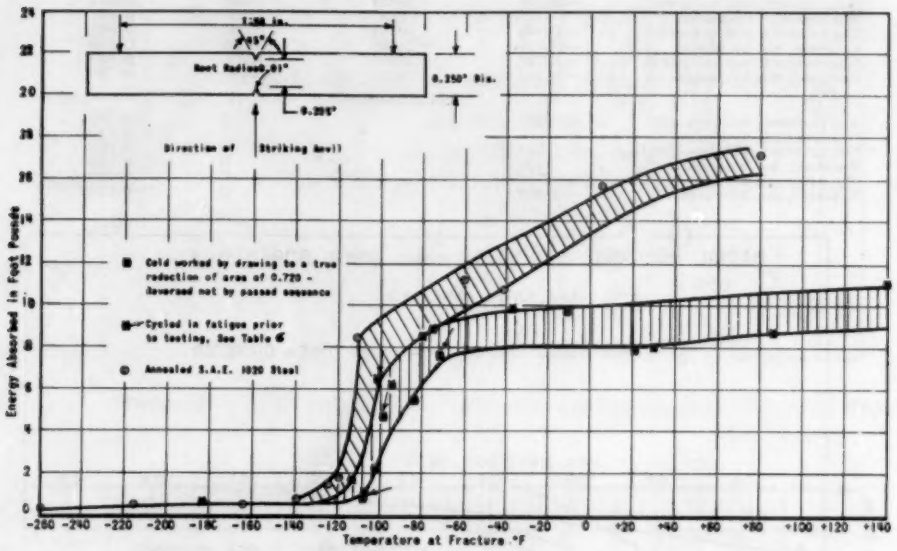
Energy Absorbed in Foot Pounds
Temperature at Fracture °F
Direction of Striking Anvil
0.250" Dia.
Cold worked by drawing to a true reduction of area of 0.720 - Reversed not by passed sequence
Cycled in fatigue prior to testing, See Table 6
Annealed S.A.E. 1020 Steel

FIG. 14 ENERGY ABSORBED IN NOTCHED CYLINDRICAL CHARPY IMPACT SPECIMENS VERSUS TEST TEMPERATURE
(See Table 6 for prior cycling sequence.)

pact) is raised progressively by increasing carbon, phosphorus, or vanadium content; and lowered by increasing the manganese and finishing hot-rolled plate at decreasing temperatures. Prestraining notched specimens in static tension prior to testing in impact increased the transition temperature according to Lessells and Jacques (8). The transition temperature was found to increase with the number of prior cycles—both above and below the endurance limit (M.I.T. slow bend test) in the work of MacGregor and Grossman (9).

Cylindrical V-notch specimens were fabricated as indicated in Fig. 14, so that they could be tested in the Krouse 200-in-lb fatigue machine as well as in the Sonntag universal impact machine using the 25-ft-lb energy range. Even though the notch surface was not polished after careful machining, an examination of each specimen in the optical comparator revealed that all notch radii were 0.01 in. After the test temperature had been reached in each specimen, less than 8 sec were consumed during the time that the sample was removed from the cooling medium until it was ruptured.

Fig. 14 is a plot of the results in which the brittle transition temperature is increased when rods were cold-worked to a true reduction of 0.76 and the reversed sequence was used. No tests were made of other sequences owing to limited material. Nevertheless, it is not certain that the use of the fast impact method would segregate the various influences of sequence in drawing. The slow bend test as used at M.I.T. should prove superior to the Charpy impact test. Prior cycling in fatigue and then testing under a fast impact blow did not show remarkable differences from those impact specimens having no prior fatigue cycling (cold-worked condition).

MICROSTRUCTURE

Grain structures are revealed in Figs. 15 and 16, with an increasing degree of fragmentation and elongation in passage from the 1-in. die down through the 11/16-in. die for the not reversed, not by-passed sequence. Photomicrographs B and D are areas near the surface while A and C are the center areas of the rods. The banded structure appearing in Fig. 15 A, due to the original manufacturing remains even after the annealing operation. Although the hardness traverse with the diamond pyramid does not reveal a significant change, a comparison of the microstructures of Fig. 16 D with Fig. 16 C shows that the material near the die wall is subjected to a more severe distortion than the center.

Four methods of drawing were used in Fig. 17 to determine how the structure at the rod center was modified by reducing 1-in. rods down through 15/16-in. dies. For this reduction the sequences produce no radical differences in microstructure. Figs. 18 C and 18 D are to be compared with Figs. 16 C and 16 D, respectively, for the effect of sequence on microstructure. Photomicrographs, Figs. 16 D and 18 D, are the outer surfaces. A reversed, not by-passed sequence has a microstructure similar to the not reversed, not by-passed sequence. Thus no marked differences were observed in the microstructure.

CONCLUSION

This is a study in the cold-working of SAE 1020 steel by-passing the rods through a series of hardened, conical steel dies where the half angles were about 1 deg as noted in Table 3. The speed of cold-drawing was 2 ipm. Successive true reductions per pass

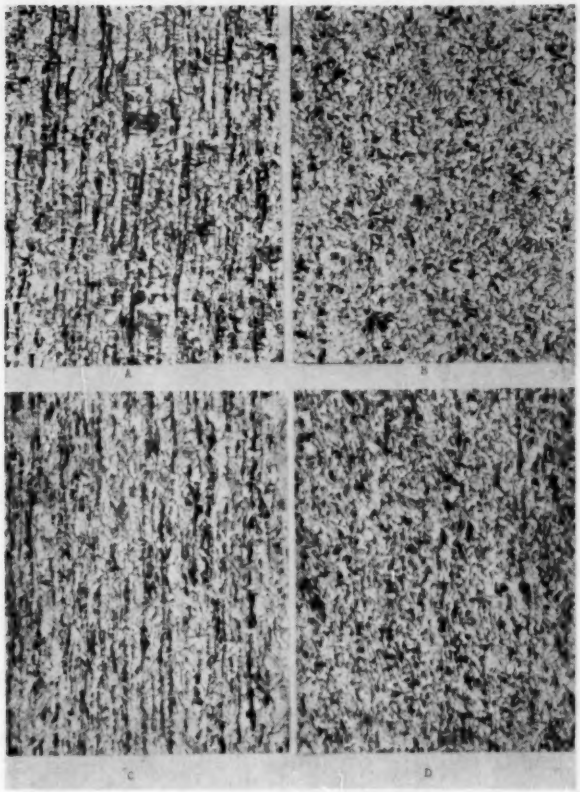

FIG. 15 MICROSTRUCTURE OF SAE 1020 STEEL RODS

(Photomicrographs A and B, annealed condition, at center and edge, respectively. Photomicrographs C and D, cold-drawn to a true reduction of 0.344, not reversed, not by-passed sequence, center and edge, respectively; 2 per cent nital solution; ×100.)

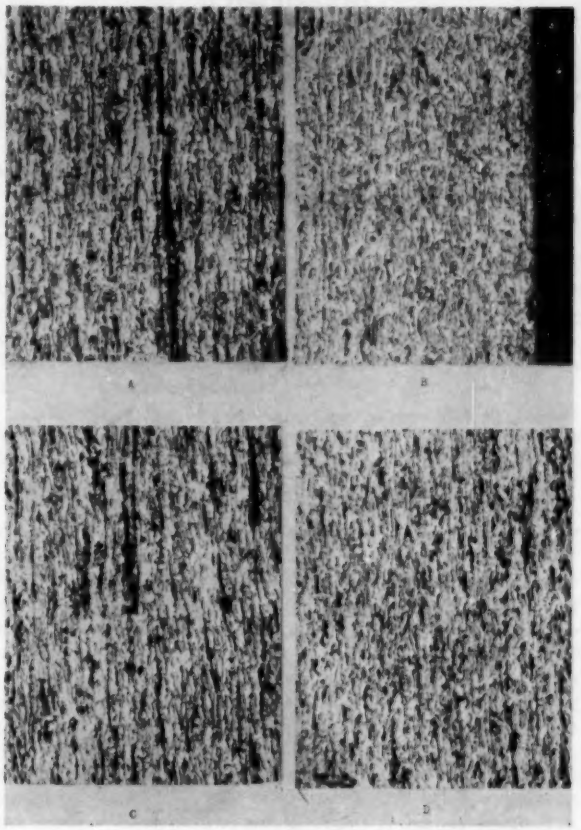

FIG. 16 MICROSTRUCTURE OF SAE 1020 STEEL RODS

(Photomicrographs A and B, cold-drawn to a true rod reduction of 0.510 center and edge areas, respectively. Photomicrographs C and D, cold-drawn to a true rod reduction of 0.760, center; 2 per cent nital solution; ×100.)

were about 0.07 in per in. or larger. All rods were coated with a solution of Calgon which formed a powdered coating on drying. This surface was lubricated with a paste made from SAE 40 oil and type M Molykote powder.

The results of these studies in cold-drawing are as follows:

1 Yield strength (0.1 per cent offset) in tension is varied a maximum of about 5 per cent depending on the manner of drawing.

2 Sequence in drawing had no effect upon the true stress-strain diagrams in tension.

3 Sequence had no effect upon the average Vickers hardness number.

4 More tests are needed to determine the effect of manner of drawing on the torsion properties. Tests conducted so far indicate some effect.

5 Sequence influences the magnitude of the surface residual stress. The not reversed, by-passed, and reversed, by-passed sequences produce lower surface stresses than the not reversed, not by-passed sequence.

6 An examination of the grain structures across the rod section did not reveal a significant change for the various sequences. No examination was made of the rod surface.

7 As the amount of cold-working increases up to a true reduction of 0.76 in rod area, the average true tensile stress at fracture remains approximately the same, but the true strain at fracture decreases. The true uniform strain or true strain at maximum load decreases up to a true cold reduction in area of 0.15; additional working has little influence, this value being about 0.03 (see Fig. 6). Mehringer and MacGregor (1) found similar results when low-carbon steel was cold-rolled and also found that the direction of the axis of the tension specimen to that of rolling had no appreciable influence on the true uniform strain.

8 A comparison of cold work by cold-rolling (1) with that by cold-drawing reveals that the true tensile strains at fracture for the same of reduction in area are less in cold-rolled specimens. It is concluded that the cold-rolling is a more drastic operation.

9 More torsion data are needed for an evaluation of the influence of several variables on the yield-strength ratio of torsion to tension such as sequence, size, amount of cold work, and residual stresses (also amount of machining as related to the residual stresses).

ACKNOWLEDGMENT

Funds for this investigation were provided in a grant from the Research Corporation for which the author expresses his appreciation especially to Charles H. Schauer, Director of Grants. F. J. Mehringer provided the original suggestion of this project and outlined a general scheme of tests. Prof. E. C. Wright solved the problem of lubrication for which the author is grateful. R. K. Newman and F. S. Costelloe of Republic Steel Corporation, provided a series of dies and the steel rods. Space and technical services were provided by the Engineering Experiment Station, University of Alabama. The work of Charles Hoffman is acknowledged for careful preparation of drawings. Thanks are due to Charles Adams and Charles Allinder for excellent machine

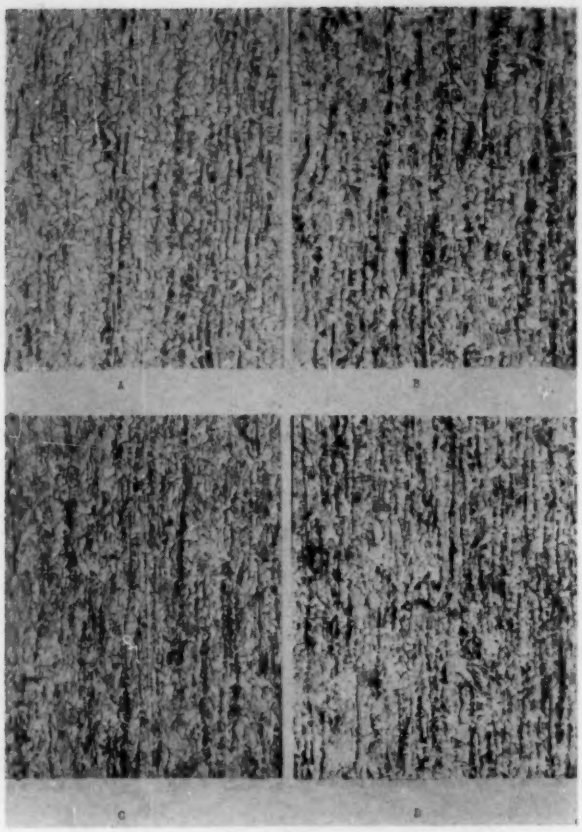

FIG. 17 COMPARISON OF MICROSTRUCTURES FOR DIFFERENT SEQUENCES, FOR A TRUE REDUCTION OF 0.145 IN ROD AREA

(A, not reversed, not by-passed sequence. B, reversed, not by-passed sequence. C, by-passed, not reversed sequence. 2 per cent nital solution; ×100.)

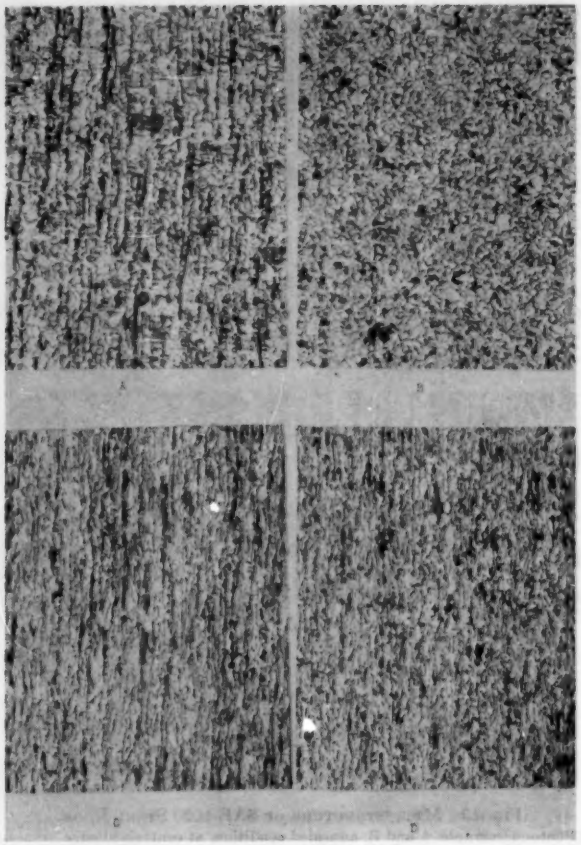

FIG. 18 MICROSTRUCTURE OF STEEL RODS

(A, center area, annealed condition. B, edge area, annealed condition. C, center area, true rod reduction of 0.760, not by-passed, reversed sequence. D, edge area, true reduction of 0.760, not by-passed, reversed sequence; 2 per cent nital solution; ×100.)

work. Chas. T. Roland was instrumental in furnishing Banox No. 5, manufactured by Calgon, Inc.

BIBLIOGRAPHY

1 "Effects of Cold-Rolling on the True Stress-Strain Properties of a Low-Carbon Steel," by F. J. Mehringer and C. W. MacGregor, Tech. Pub. No. 1849, *Metals Technology*, September, 1945, AIME.

2 "Effect of Variation in Wire Drawing on Physical Properties of Steel Wire," by Howard Godfrey, ASTM Trans., vol. 42, 1942, pp. 513–531.

3 "Effects of the Direction of Drawing on the Arrangement of the Micro-Crystals in Aluminum Wire and on Its Tensile Strength and Broken Fracture," by Takeo Fujiwara, Kyoto University, College of Science Memoirs, series A, vol. 15, 1932, pp. 35–42.

4 "The Yield of Mild Steel With Particular Reference to the Effect of Size of Specimen," by J. L. M. Morrison, Proceedings of The Institution of Mechanical Engineers, vol. 142, 1939, p. 193.

5 "A Yield Criterion for Ductile Metals Based Upon Atomic Structure," by M. C. Shaw, *Journal of The Franklin Institute*, vol. 254, August, 1952, pp. 109–126.

6 "Der Nachweiss inveres Spannungen im Stangen und Rohren," by B. Sachs, *Zeitschrift fiir Metallkunde*, vol. 19, 1927, p. 352.

7 "Some Metallurgical Aspects of Ship Steel Quality," by H. M. Banta and C. H. Lorig, *Welding Journal*, vol. 30, February, 1951, pp. 89-S.

8 "Effect of Fatigue on Transition Temperature of Steel," by J. L. Leasells and H. E. Jacques, *Welding Journal*, vol. 29, February, 1950, pp. 74-S.

9 "Some New Aspects of the Fatigue of Metals Brought Out by Brittle Transition Temperature Tests," by C. W. MacGregor and N. Grossman, *Welding Journal*, vol. 27, March, 1948, pp. 132-S.

Appendix

A solution is prepared by mixing 2 oz. of Banox No. 5[6] to 1 gal of water. The smooth, continuous film of an amorphous phosphate is deposited spontaneously from an unheated solution by dipping the rods for 4 hr and drying for 4 hr, alternately three times.

Tension specimens could be tested in either the machined or unmachined condition. Testing unmachined specimens resulted in premature fracture at the grips which prevented computing and plotting the true stress and strain at rupture. Machining affected only the elastic region of the stress-strain diagram a small amount. No effect was observed in the plastic region to rupture. Size of test specimen from 0.400 in. diam to 0.850 in. diam had no effect on the tension results. This was important because it was not necessary to use tension specimens of different diameters to have the same relative dimensions. A hardness transverse across the diameter was essentially constant, even within 0.02 in. from the edge of the rod. All tension tests were conducted in a period of three weeks to three months. No time effect was found which influenced the hardness readings or tensile curves. Some hardness readings were obtained three years later which showed hardly any changes.

[6] Banox No. 5 is manufactured by Calgon, Inc., Pittsburgh, Pa. Type M Molykote is manufactured by the Alpha Corporation, Greenwich, Conn.

TABLE 7 SUMMARY OF LOADS REQUIRED TO COLD-DRAW SAE 1020 STEEL CYLINDRICAL RODS—ROD NO. 1

(Calgon coating—lubricant, paste of SAE 40 machine oil and Molykote powder)

True reduction of rod area	Nominal die size, in.	Average drawing load, lb — Not reversed, not by-passed	Reversed, not by-passed
0.007	1	2150	2150
0.044	63/64	8100	7920
0.070	31/32	9010	7630
0.145	15/16	13740	12420
0.212	29/32	14145	13510
0.272	7/8	15570	10680
0.344	27/32	14750	11770
0.427	13/16	15100	13820
0.510	25/32	13360	9830
0.580	3/4	13390	10330
0.658	23/32	14160	12320
0.760	11/16	12680	11920

TABLE 8 SUMMARY OF LOADS REQUIRED TO COLD-DRAW SAE 1020 STEEL CYLINDRICAL RODS—ROD NO. 1

(Calgon coating—lubricant, paste of SAE 40 machine oil and Molykote powder)

True reduction of rod area	Nominal die size, in.	Average drawing load, lb — Not reversed, by-passed sequence —			
0.007	1	..	..	2240	2240
0.044	63/64	..	..	..	..
0.070	31/32	9980	..	..	..
0.145	15/16	..	18700	15500	
0.212	29/32	..	...	...	22050
0.272	7/8	..	...	...	...
0.344	27/32	..	...	20900	...
0.427	13/16	..	...	...	20300
0.510	25/32	..	...	...	...
0.584	3/4	..	...	...	16120
0.658	23/32	..	...	...	...
0.760					

TABLE 9 SUMMARY OF LOADS REQUIRED TO COLD-DRAW SAE 1020 STEEL CYLINDRICAL RODS—ROD NO. 2

(Calgon coating—lubricant, paste of SAE 40 machine oil and Molykote powder)

True reduction of rod area	Average drawing load, lb — Not reversed, not by-passed	Reversed, not by-passed	Not reversed, by-passed	Reversed, by-passed
0.007	2240	2240	2240	2240
0.044	8470	6570	...	...
0.070	8840	8520	8570	8570
0.145	13850	14890	...	...
0.212	15610	13410	20190	19400
0.272	15020	12830	...	...
0.344	16680	12810	16850	17710
0.427	14580	14230	...	...
0.510	14940	13210	18200	16950
0.584	14945	13630	...	10520
0.658	14290	12970	16270	12380
0.760	13650	11710	10860	12280

In order to obtain the ratios of yield strength in torsion to that in tension at 0.1 per cent offset, the torsion and tension values were plotted versus the true reduction in rod diameter and smooth curves produced for the not reversed, not by-passed sequence. The torsion specimens were not machined. This ratio is needed in wire-drawing theory and is of some importance. This ratio is affected by the residual stress state at the time of the torsion test, by the sequence used in cold-drawing and amount of material removed in machining specimens.

Tables 7, 8, and 9 summarize the average pulling loads when various sequences in cold-working are used. Even though rod No. 1 is of different chemical composition from rod No. 2, there is only a small difference in the average drawing force. Table 8 presents procedures in by-passing intervening dies to note the effect of prior cold-working on the pulling load.

True reduction of rod area is defined as follows

$$q_x = \ln_e \frac{Ao}{Ax}$$

where

q_x = true reduction of rod area
Ao = 0.7854 sq in. (1-in-diam rod)
Ax = area of rod after passage through xth die

Discussion

E. S. NACHTMAN.[7] This paper should be of interest to those concerned with the development of fundamental theories of metal deformation. It is a pleasure to discuss this work which, we hope, will encourage further academic study in this field.

The measurement of true stress-strain curves for various sequences in drawing gives necessary information for any theoretical evaluation of the drawing process. The author is to be complimented for initiating this work. Further contributions in this field would be of considerable interest.

The results of the torsion and impact tests are not conclusive but certainly arouse one's curiosity about possible effects. General experience would indicate that cold deformation during a drawing process tends to raise the transition temperature. Whether peculiar or different effects result from variations in drawing sequences is not clear.

In discussing the results obtained by the author during his investigation of the distribution and intensity of residual stresses in rods drawn through dies in various sequences, consideration of some previous experimental work might be helpful.

In Germany, in the late 1920's and early 1930's, the cold-deformation process was investigated in many laboratories. Early references of this period recall the pioneer work of G. Sachs,[8] E. Heyn,[9] H. Bühler,[10] E. Siebel,[11] and H. Buchholtz (reference 10, first item) who experimentally and theoretically explored the effects of various cold-drawing operations on the properties of cold-drawn rods.

In the early 1930's H. Bühler and Associates published the results of experimental investigations on the effects of varying per cent reductions of area as they influenced the residual-stress distribution in cold-drawn rods. Generally, it was shown that reductions in area under $1^1/_2$ per cent resulted in rods having surface stresses which were compressive with tensile stresses in the center. Reductions in area of over $1^1/_2$ per cent resulted in surface tensile stresses with compressive stresses concentrated in the center of the rod.

The intensity of stress was shown by Bühler to increase as the per cent reduction increases from $1^1/_2$ per cent to approximately 5 per cent and then to level off. In this connection there is work reported by G. Sachs in 1927, which indicates that residual stres-

[7] Manager, Product Engineering Laboratory, La Salle Steel Company, Chicago, Ill. Assoc. Mem. ASME.

[8] "Innere Spannungen in Metallen," by G. Sachs, *Zeitschrift des Vereins deutscher Ingenieure*, vol. 71, 1927, pp. 1511–1516.

"Über das Aufreissen von kaltgezogenem Rundeisen," by W. Fahrenhorst and G. Sachs, *Metallwirtschaft*, vol. 10, 1931, pp. 783–788.

"Versuche über die Eigenschaften gezogener Drähte und den Kraftbedarf beim Drahtziehen," by W. Linicus and G. Sachs, *Mitteilungen der Deutschen Materialprüfungsanstalten*, Sonderheft 16, 1931, pp. 38–67.

"Effect of Spacing Between Dies in the Tandem Drawing of Tubular Parts," by G. Sachs and G. Espey, Trans. ASME, vol. 69, 1947, pp. 139–143.

[9] "Einige weitere Mitteilungen über Eigenspannungen und damit zusammenhängende Fragen," by E. Heyn, *Stahl und Eisen*, vol. 37, 1937, pp. 442–448, 474–479, 497–500.

[10] "Einfluss der Querschnittsverminderung beim Kaltziehen auf die Spannungen in Rundstangen," by H. Bühler and H. Buchholtz, *Archiv für das Eisenhüttenwesen*, vol. 7, 1933–1934, pp. 427–430.

"Einfluss des Ziehgrades sowie des Anlassens auf die Eigenspannungen in Stahldrähten," by H. Bühler and W. Püngel, *Archiv für das Eisenhüttenwesen*, vol. 8, 1934–1935, pp. 165–168.

"Eigenspannungen in prägepolierten Stahlstangen," by H. Bühler, *Archiv für das Eisenhüttenwesen*, vol. 8, 1934–1935, pp. 515–516.

[11] Die Formgebung im bildsamen Zustande (Shaping in Plastic Condition), by E. Siebel, Düsseldorf, Verlag Stahleisen m.b.H., 1932.

ses may again decrease in intensity for reductions beyond 55 per cent.

In later work by Bühler and coworkers various sequences of drawing are investigated and discussed. They indicate that rods given reductions in excess of $1^1/_2$ per cent may have the attendant high level of surface stresses lowered by subsequent reductions of less than $1^1/_2$ per cent.

In 1947 Sachs and Espey discussed an investigation of multiple dies related in this case to a deep-drawing operation. The work showed that it was possible to achieve a greater over-all deformation by appropriate pressing sequences.

Thus the findings in this paper with respect to creation of lower surface stresses in cold-drawn rods by appropriate drawing sequences agrees in broad outline with earlier work. We are honored in being asked to discuss this latest contribution by the author and shall look forward with anticipation to further work on cold-deformation sequences as they affect the true stress-strain measurements. Such information would shed further light on the cold-drawing process.

Author's Closure

The author wishes to acknowledge with thanks Mr. Nachtman's revealing discussion.

WAV
PAG

Studies in Cold-Drawing

Part 2 Cold-Working 2S-O Aluminum[1]

By H. MAJORS, JR.,[2] UNIVERSITY, ALA.

This is a study in the cold-working of 2S-O aluminum up to a true reduction in rod area of 0.76 by drawing through conical dies of 1 deg half-angle. Various properties were obtained such as true stress-strain diagrams in tension, hardness, conventional shear stress-strain diagrams, and the distribution of the residual stresses. The effect of the amount of reduction and the direction of drawing per pass (defined as sequence in drawing) on the properties were determined. Some fatigue data are re- rengths in sses some

VY

GES

metal when
. In deep-
ws could be
ep-drawing
steel strip is
ection is re-
ng in Part 1[4]
(Table 1) in-
eld strengths
or direction
nger[5] effect.
diam, the
easurements
dness effects

m sheet that
rolled in one
ned to work-
ction. Also,
rinks[3] to con-
sses through

nce of cold-

rant provided
New York 17.
rial was made
Company of

Available through the publishing ... America.

[2] California Research and Development Company, Livermore, Calif.; now Research Professor, Bureau of Engineering Research, University of Alabama. Mem. ASME.

[3] "Softening of Metals During Cold Working," by N. H. Polakowski, *Journal of Iron and Steel Institute*, vol. 169, December, 1951, pp. 337–346.

[4] "Studies in Cold-Drawing—Part 1 Effect of Cold-Drawing on Steel," by Harry Majors, Jr., published in this issue of Transactions, pp. 37–48.

[5] "Structure of Metals," by C. S. Barrett, McGraw-Hill Book Company, Inc., New York, N. Y., 1943, p. 329.

Contributed by the Metals Engineering Division and presented at the Annual Meeting, New York, N. Y., November 29–December 4, 1953, of THE AMERICAN SOCIETY OF MECHANICAL ENGINEERS.

NOTE: Statements and opinions advanced in papers are to be understood as individual expressions of their authors and not those of the Society. Manuscript received at ASME Headquarters, April 29, 1953. Paper No. 53—A-74.

TABLE 1 EXPLANATION OF SEQUENCES IN DRAWING RODS

NOMINAL DIE SIZE INCHES	1	63/64	31/32	30/32	29/32	28/32	27/32	26/32	25/32	24/32	23/32	22/32	
NOT REVERSED NOT BY-PASSED	A	A	A	A	A	A	A	A	A	A	A	A	A
REVERSED NOT BY-PASSED	A	B	A	B	A	B	A	B	A	B	A	B	A B
NOT REVERSED BY-PASSED	A			A		A		A		A		A	A
REVERSED BY-PASSED	A			B		A		B		A		B	B A

LETTERS INDICATE THE ROD END ENTERING THE DIE
BLANK SPACES INDICATE THE ROD DID NOT PASS THROUGH THAT DIE

drawing aluminum rod through dies was investigated according to the procedure of Table 1, but Fujiwara[6] compared the crystalline structure of small aluminum wires drawn in one direction with those reversed drawn. No true stress-strain data was presented to show the effect of cold wire-drawing. Black[7] shows the effect of tension and compression tests on cold-drawn welded steel tubing, in which compression stress-strain curves begin to deviate appreciably from a straight line at lower stresses than curves obtained in tension for most of the series tested.

METHOD OF TESTING

Sixty feet of 1-in-diam 2S-O aluminum rod was received in lengths of 10 ft per rod, manufactured from the same melt. The rods were pulled in a 60,000-lb Baldwin universal testing machine, Fig. 3, at a speed of about 2 ipm according to the sequences outlined in Table 1, and through hardened steel dies of dimensions listed in Tables 2 and 3. Fig. 1 contains the headings for Tables 2 and 3. These dies were worn considerably from another use, having different degrees of surface finish; but in spite of this smooth rod finishes were obtained.

A trial-and-error procedure was followed before a satisfactory lubricant was found (see acknowledgments). A paste made of Molykote (see Appendix) powder and kerosene served best. Prior to drawing, all rods were coated with a solution of Banox No. 5 (see Appendix) which formed a smooth, continuous film of an amorphous phosphate. By using the lubricant paste in conjunction with the Banox coating, good finishes were obtained.

Fig. 2 shows how the bars appeared for the various sequences with tapered ends for starting through the dies. These "sequences" or manner of drawing are explained in Part 1,[4] since the same dies were used for aluminum and steel. In Fig. 2, bar A was reduced by using the "reversed, not by-passed" sequence (see Table 1). This means that end A was started through the 1-in. die, end B was started through the $^{63}/_{64}$-in. die, end A through the $^{31}/_{32}$-in. die, and so on down, through the $^{11}/_{16}$-in. die. (See Table 1 for meaning of A and B as distinct from A, B, C, and D of Fig. 2.) Bar B is prepared for the "reversed, by-passed" sequence which means that end A (see Table 1) was started through the 1-in. die, end B was started through the $^{30}/_{32}$-in. die, end A through the $^{29}/_{32}$-in. die, end B through the $^{28}/_{32}$-in. die, end A through the

[6] "Effects of the Direction of Drawing on the Arrangement of the Micro-Crystals in Aluminum Wire and on Its Tensile Strength and Broken Fracture," by Takeo Fujiwara, Kyoto University, College of Science Memoirs, series A, vol. 15, 1932, pp. 35–42.

[7] "Effect of Cold-Drawing on Mechanical Properties of Welded Steel Tubing," University of Illinois Bulletin, vol. 40, No. 27, February 23, 1943, Engineering Experiment Station Bulletin, series No. 341.

ses may again decrease in intensity for reductions beyond 55 per cent.

In later work by Bühler and coworkers various sequences of drawing are investigated and discussed. They indicate that rods given reductions in excess of $1^1/_2$ per cent may have the attendant high level of surface stresses lowered by subsequent reductions of less than $1^1/_2$ per cent.

In 1947 Sachs and Espey discussed an investigation of multiple dies related in this case to a deep-drawing operation. The work showed that it was possible to achieve a greater over-all deformation by appropriate pressing sequences.

Thus the findings in this paper with respect to creation of lower surface stresses in cold-drawn rods by appropriate drawing sequences agrees in broad outline with earlier work. We are honored in being asked to discuss this latest contribution by the author and shall look forward with anticipation to further work on cold-deformation sequences as they affect the true stress-strain measurements. Such information would shed further light on the cold-drawing process.

Author's Closure

The author wishes to acknowledge with thanks Mr. Nachtman's revealing discussion.

Studies in Cold-Drawing

Part 2 Cold-Working 2S-O Aluminum[1]

By H. MAJORS, JR.,[2] UNIVERSITY, ALA.

This is a study in the cold-working of 2S-O aluminum up to a true reduction in rod area of 0.76 by drawing through conical dies of 1 deg half-angle. Various properties were obtained such as true stress-strain diagrams in tension, hardness, conventional shear stress-strain diagrams, and the distribution of the residual stresses. The effect of the amount of reduction and the direction of drawing per pass (defined as sequence in drawing) on the properties were determined. Some fatigue data are reported. Drawing loads and ratios of yield strengths in torsion to tension are reported. Part 3 discusses some measurements on the coefficient of friction.

Introduction

CHANGES can occur in the physical properties of metal when they are plastically deformed in various ways. In deep-drawing operations it was found that deeper draws could be reached in strip steels that are drawn in reversed deep-drawing than in deep-drawing only in one direction.[3] When steel strip is rolled in one direction, it is harder than when the direction is reversed after each pass. In the studies of cold-working in Part 1[4] it is found that the reversal in drawing direction (see Table 1) influenced the distribution of residual stresses and the yield strengths in torsion (SAE 1020 steel). The "sequence" effect or direction of cold-working in rod-drawing may be a Bauschinger[5] effect. Because the rods of Part 1 originally were 1 in. diam, the Bauschinger effect did not appear in the hardness measurements on the cross section owing to the size, whereas hardness effects have been observed in thin sheets.[3]

It has been found in the cold-rolling of aluminum sheet that recrystallization occurs at a lower temperature when rolled in one direction than when cross-rolled. Cross-rolling seemed to work-harden the material less than rolling in one direction. Also, straight-rolled aluminum sheets were reported by Trinks[3] to contain more residual stresses than when the alternate passes through the mill are reversed in direction.

No reference has been found in which the sequence of cold-drawing aluminum rod through dies was investigated according to the procedure of Table 1, but Fujiwara[6] compared the crystalline structure of small aluminum wires drawn in one direction with those reversed drawn. No true stress-strain data was presented to show the effect of cold wire-drawing. Black[7] shows the effect of tension and compression tests on cold-drawn welded steel tubing, in which compression stress-strain curves begin to deviate appreciably from a straight line at lower stresses than curves obtained in tension for most of the series tested.

TABLE 1 EXPLANATION OF SEQUENCES IN DRAWING RODS

NOMINAL DIE SIZE INCHES	1	63/64	31/32	30/32	29/32	28/32	27/32	26/32	25/32	24/32	23/32	22/32	
NOT REVERSED NOT BY-PASSED	A	A	A	A	A	A	A	A	A	A	A	A	A
REVERSED NOT BY-PASSED	A	B	A	B	A	B	A	B	A	B	A	B	B A
NOT REVERSED BY-PASSED	A			A		A		A		A		A	A
REVERSED BY-PASSED	A			B		A		B		A		B	B A

LETTERS INDICATE THE ROD END ENTERING THE DIE
BLANK SPACES INDICATE THE ROD DID NOT PASS THROUGH THAT DIE

Method of Testing

Sixty feet of 1-in-diam 2S-O aluminum rod was received in lengths of 10 ft per rod, manufactured from the same melt. The rods were pulled in a 60,000-lb Baldwin universal testing machine, Fig. 3, at a speed of about 2 ipm according to the sequences outlined in Table 1, and through hardened steel dies of dimensions listed in Tables 2 and 3. Fig. 1 contains the headings for Tables 2 and 3. These dies were worn considerably from another use, having different degrees of surface finish; but in spite of this smooth rod finishes were obtained.

A trial-and-error procedure was followed before a satisfactory lubricant was found (see acknowledgments). A paste made of Molykote (see Appendix) powder and kerosene served best. Prior to drawing, all rods were coated with a solution of Banox No. 5 (see Appendix) which formed a smooth, continuous film of an amorphous phosphate. By using the lubricant paste in conjunction with the Banox coating, good finishes were obtained.

Fig. 2 shows how the bars appeared for the various sequences with tapered ends for starting through the dies. These "sequences" or manner of drawing are explained in Part 1,[4] since the same dies were used for aluminum and steel. In Fig. 2, bar A was reduced by using the "reversed, not by-passed" sequence (see Table 1). This means that end A was started through the 1-in. die, end B was started through the $^{63}/_{64}$-in. die, end A through the $^{31}/_{32}$-in. die, and so on down, through the $^{11}/_{16}$-in. die. (See Table 1 for meaning of A and B as distinct from A, B, C, and D of Fig. 2.) Bar B is prepared for the "reversed, by-passed" sequence which means that end A (see Table 1) was started through the 1-in. die, end B was started through the $^{30}/_{32}$-in. die, end A through the $^{29}/_{32}$-in. die, end B through the $^{28}/_{32}$-in. die, end A through the

---

[1] This work was started December, 1949, under a grant provided by the Research Corporation, 405 Lexington Avenue, New York 17, N. Y., at the University of Alabama. The 2S-O material was made available through the generosity of the Aluminum Company of America.

[2] California Research and Development Company, Livermore, Calif.; now Research Professor, Bureau of Engineering Research, University of Alabama. Mem. ASME.

[3] "Softening of Metals During Cold Working," by N. H. Polakowski, *Journal of Iron and Steel Institute*, vol. 169, December, 1951, pp. 337–346.

[4] "Studies in Cold-Drawing—Part 1 Effect of Cold-Drawing on Steel," by Harry Majors, Jr., published in this issue of Transactions, pp. 37–48.

[5] "Structure of Metals," by C. S. Barrett, McGraw-Hill Book Company, Inc., New York, N. Y., 1943, p. 329.

Contributed by the Metals Engineering Division and presented at the Annual Meeting, New York, N. Y., November 29–December 4, 1953, of The American Society of Mechanical Engineers.

Note: Statements and opinions advanced in papers are to be understood as individual expressions of their authors and not those of the Society. Manuscript received at ASME Headquarters, April 29, 1953. Paper No. 53—A-74.

[6] "Effects of the Direction of Drawing on the Arrangement of the Micro-Crystals in Aluminum Wire and on Its Tensile Strength and Broken Fracture," by Takeo Fujiwara, Kyoto University, College of Science Memoirs, series A, vol. 15, 1932, pp. 35–42.

[7] "Effect of Cold-Drawing on Mechanical Properties of Welded Steel Tubing," University of Illinois Bulletin, vol. 40, No. 27, February 23, 1943, Engineering Experiment Station Bulletin, series No. 341.

24/32-in. die, and end B through the 23/32-in. die. Bar C is prepared for the "not reversed, not by-passed" sequence which means that only one end A was prepared for starting through each die. Bar D was prepared for starting only one end A through the 1-in. die, 30/32-in. die, 28/32-in. die, 26/32-in. die, 24/32-in. die, and 22/32-in die; the reduction per pass was about 15 per cent whereas for bar C the reduction was about 7 per cent.

TABLE 2 DIMENSIONS OF DIES[a]

Nominal size of die, in.	D_2	T	E	R	X	Y
1	0.996	1.2	1.27	2.20	2.9	1.3
63/64	0.978	1.0	1.20	2.37	2.9	1.4
31/32	0.966	0.87	1.10	1.20	2.8	1.1
15/16	0.930	1.12	1.18	1.90	2.9	1.4
29/32	0.898	1.09	1.14	1.08	2.9	1.4
7/8	0.872	1.07	1.03	2.13	2.9	1.3
27/32	0.842	1.10	1.13	1.20	2.8	1.3
13/16	0.808	0.96	1.01	1.09	2.9	1.3
25/32	0.775	0.98	1.09	0.50	2.8	1.3
3/4	0.747	1.06	1.00	0.68	2.9	1.3
23/32	0.719	1.14	0.95	0.83	2.9	1.3
11/16	0.685	0.98	0.99	0.52	2.9	1.3

[a] See Fig. 1 for coding. All quantities in inches.

Tension Tests

The tensile properties of the various sequences were determined on specimens machined to 0.400 in. diam with a 1.6-in. gage length. Tests were conducted on a 120,000-lb Baldwin universal testing machine in which Huggenberger extensometers were used for the elastic region and a lateral dial gage in the plastic region for measuring the diameter as the specimen was stretched to rupture. All tension tests were conducted at room temperature, and the observation of data in the plastic region for each tension test was made in about 12 min.

Tensile diagrams for strains up to 0.006 in. per in. appear in Fig. 4 for all sequences at several true reductions in rod area. True rod reduction is defined as the natural logarithm of the ratio of original area to the final rod area after passing through a die (see Appendix). The dotted line is the yield-strength determina-

TABLE 3 DIMENSIONS[a] A, D_1, D_2, AND θ FOR VARIOUS SEQUENCES

	Sequence in drawing							
	Not reversed, not by-passed		and	Reversed, not by-passed		Not reversed, by-passed		and	Reversed, by-passed	
Nominal die size, in.	A	D_1		D_2	θ	A	D_1		D_2	θ
1	0.76	1.000		0.996	0° 10′	0.76	1.000		0.996	0° 10′
63/64	0.67	0.997		0.978	0° 49′	...	...		...	...
31/32	0.41	0.978		0.966	0° 50′	...	...		...	...
30/32	0.76	0.966		0.930	1° 21′	0.96	0.996		0.930	1° 57′
29/32	0.83	0.930		0.898	1° 00′	...	...		...	...
28/32	0.62	0.898		0.872	1° 11′	0.96	0.930		0.872	1° 49′
27/32	0.73	0.872		0.842	1° 12′	...	...		...	...
26/32	0.74	0.842		0.808	1° 19′	0.85	0.872		0.808	2° 11′
25/32	0.88	0.808		0.775	1° 40′	...	...		...	...
24/32	0.57	0.775		0.747	1° 30′	0.74	0.808		0.747	2° 20′
23/32	0.67	0.747		0.719	1° 12′	...	...		...	...
22/32	0.54	0.719		0.685	1° 48′	0.74	0.747		0.685	2° 23′

[a] See Fig. 1 for coding. All quantities in inches unless noted otherwise.

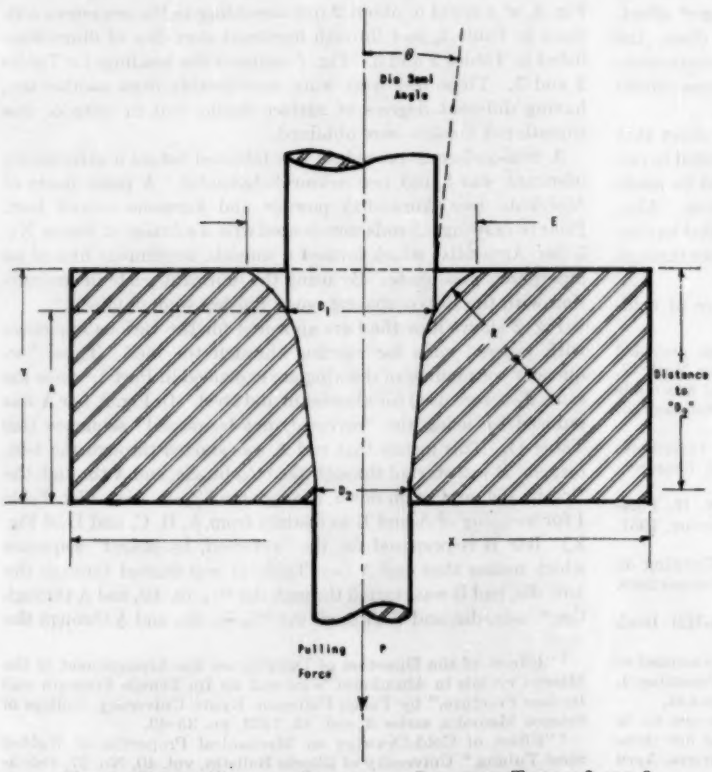

Fig. 1 Coding Used for Dimensions Listed in Tables 2 and 3

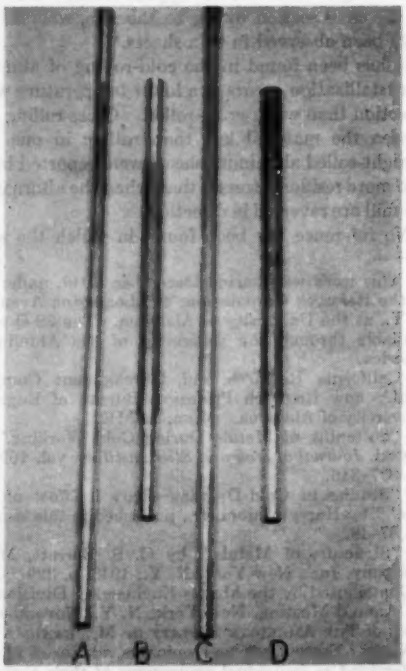

Fig. 2 Appearance of Rods for Cold-Drawing in Sequences Outlined in Table 1

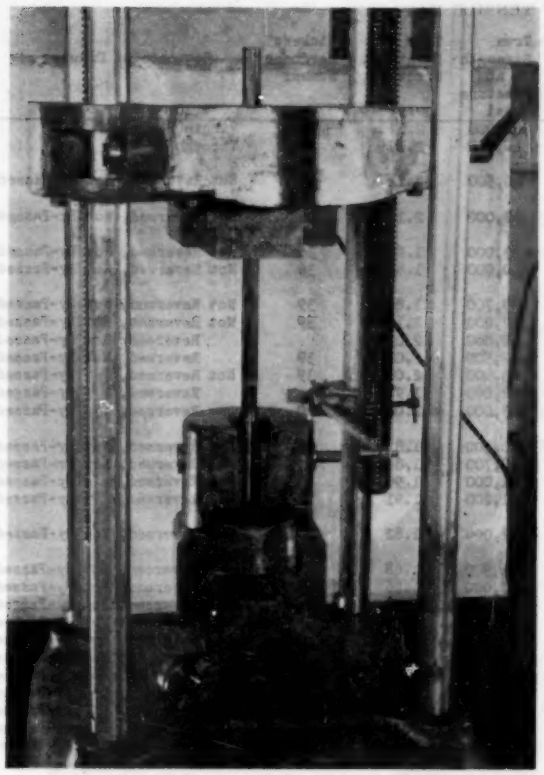

FIG. 3 USE OF 60,000-IN-LB BALDWIN TESTING MACHINE AS DRAW BENCH

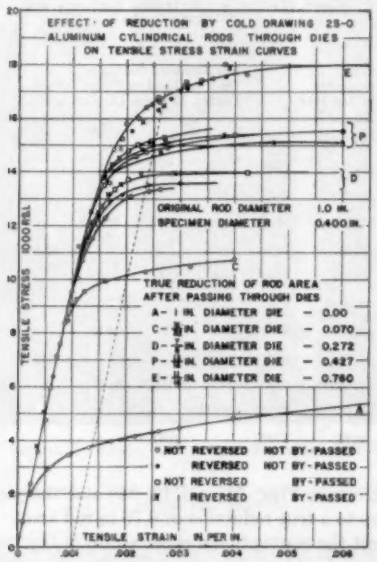
EFFECT OF REDUCTION BY COLD DRAWING 2S-O ALUMINUM CYLINDRICAL RODS THROUGH DIES ON TENSILE STRESS STRAIN CURVES
TENSILE STRESS 1000 PSI
ORIGINAL ROD DIAMETER 1.0 IN.
SPECIMEN DIAMETER 0.400 IN.
TRUE REDUCTION OF ROD AREA AFTER PASSING THROUGH DIES
A - 1 IN. DIAMETER DIE - 0.00
C - 7/8 IN. DIAMETER DIE - 0.070
D - 3/4 IN. DIAMETER DIE - 0.272
P - 5/8 IN. DIAMETER DIE - 0.427
E - 1/2 IN. DIAMETER DIE - 0.760
NOT REVERSED NOT BY-PASSED
REVERSED NOT BY-PASSED
NOT REVERSED BY-PASSED
REVERSED BY-PASSED
TENSILE STRAIN IN PER IN.
.001 .002 .003 .004 .005 .006

FIG. 4 STRESS-STRAIN DIAGRAMS IN ELASTIC REGION SHOWING INFLUENCE OF SEQUENCE AND AMOUNT OF COLD-DRAWING ON YIELD STRENGTH AT 0.1 PER CENT AS DETERMINED BY THE DOTTED LINE; 2S-O ALUMINUM

tion at 0.1 per cent offset. Curve A represents a condition of no cold work. For true rod reductions of 0.272 and 0.427 there is a small effect on the yield strength but for rods subjected to a true

TABLE 4 EFFECT OF SEQUENCE IN COLD-WORKING 2S-O ALUMINUM ON VICKERS HARDNESS NUMBER

Sequence in cold-drawing	True rod reduction of area from 1.00 in. diam 0.272	0.760
Not reversed, not by-passed	38.6	45.5
Reversed, not by-passed	39.3	45.8
Not reversed, by-passed	39.3	45.8
Reversed, by-passed	39.9	45.5

NOTE: Original hardness, 29.3 Vhn.

TABLE 5 SUMMARY OF RESIDUAL-STRESS MEASUREMENTS; 2S-O ALUMINUM

(True reduction of rod area 0.760)

Sequence of drawing	Center stress, psi	Maximum tensile stress, psi	Surface stress, psi
Tangential Stresses			
Not reversed, not by-passed	—6500	+2700	+2800
Not reversed, by-passed	—6200	+5800	+3800
Reversed, not by-passed	—6200	+ 800	+ 100
Reversed, by-passed	—3600	+5000	+ 400
Longitudinal Stresses			
Not reversed, not by-passed	—22500	+2000	+2000
Not reversed, by-passed	—10000	+2400	+1300
Reversed, not by-passed	—11000	+3400	—1000
Reversed, by-passed	— 5600	+4000	—1200
Radial Stresses			
Not reversed, not by-passed	—7800		0
Not reversed, by-passed	—6900		0
Reversed, not by-passed	—4900		0
Reversed, by-passed	—3800		0

reduction of 0.760 in area, no difference could be detected in the stress-strain diagrams. Regardless of sequence, the yield strength is increased by cold-working. All of the tensile data are summarized in the Appendix, Table 6, while the drawing loads are tabulated in Tables 7 and 8.

Figs. 5, 6, and 7 show the true stress-strain tension diagrams to fracture. For the amount of cold reductions investigated, sequence (the reduction per pass and direction of drawing) as noted in Table 1, had no effect on the true stress-strain diagrams for the same amount of cold reduction. A similar conclusion was reached for SAE 1020 steel. Also, cold work had hardly any influence on the true stress at fracture, see Figs. 5, 6, and 7. But the true strain at fracture decreased with increased cold work. The true stress at maximum load is indicated by the arrows in Figs. 5, 6, and 7, which increases with cold work. This is not so for the true strain at maximum load or true uniform strain. For reductions in rod area of 0.15 or larger, the true uniform strain remains constant at about 0.05 in. per in. A similar observation was noted in Part 1[4] for either cold-drawn or cold-rolled steel.

The hardness test results recorded in Table 4 revealed that the sequence in cold-drawing had no effect upon the Vickers hardness number.

TORSION TESTS

Conventional shear stress-strain diagrams were obtained by conducting torsion tests on a Tinius-Olsen 60,000-in-lb balanced-beam torsion machine. The angle of twist was measured by placing graduated sectors at sections on a torsion bar, about a distance equal to ten times the diameter. All torsion bars were machined such that the ratio of the reduced section to rod diameter was 0.9, in order to prevent ruptures at the gripping chucks of the machine. Because the drawn aluminum rod had a large anisotropy, the torsion bars elongated during the test, Fig. 8, necessitating continual longitudinal movement of one chuck to prevent buckling. In the elastic region, the rate of twist was 0.1 deg per ipm; during the remainder of the test to rupture, the rate was 36 deg per ipm.

The progressive change in the yield strength at 0.1 per cent offset with cold-working is determined by means of the dotted line in Fig. 9. An examination of Figs. 10 and 12 shows the

TABLE 6 SUMMARY OF TENSILE DATA

Tension Specimen Number	True Reduction of Rod area	Diameter Inches	Prop. Limit psi	Yield Strength 0.2% offset psi	Tensile Strength psi	% Elong. in 2.00 in.	True Strength at Fracture psi	True Strain at Fracture	Vickers Hardness Number	Sequence of Drawing
1	0.00	0.507	1,500	4,250	12,100	44.0	42,000	2.12	29	Virgin
29	0.007	0.501	4,000	6,200	9,930	50.0	40,500	2.15	29	Through 1" Die
30	0.044	0.506	7,200	9,500	12,000	34.5	40,500	2.14	31	Not Reversed, Not By-Passed
24	0.070	0.397	8,250	10,500	12,700	30.0	42,000	2.12	34	Not Reversed, Not By-Passed
31	0.212	0.506	9,600	13,800	15,150	28.0	43,000	1.95	36	Not Reversed, Not By-Passed
2	0.212	0.506	10,000	13,800	14,450	27.5	40,000	1.82	36	Not Reversed, Not By-Passed
9	0.272	0.401	9,500	14,000	14,750	25.0	39,700	1.89	39	Not Reversed, Not By-Passed
16	0.272	0.401	10,000	13,500	14,750	20.5	42,200	2.10	39	Not Reversed, Not By-Passed
11	0.272	0.502	9,500	14,000	15,700	27.5	42,000	2.02		Reversed, Not By-Passed
20	0.272	0.400	10,000	13,500	14,750	19.5	42,500	2.02	39	Reversed, Not By-Passed
18	0.272	0.400	10,000	13,950	15,150	19.5	43,400	2.06	39	Not Reversed, By-Passed
15	0.272	0.504	10,000	14,000	15,650	24.0	42,000	1.94		Reversed, By-Passed
22	0.272	0.399	10,200	14,000	15,050	20.5	43,000	2.06	40	Reversed, By-Passed
27	0.427	0.504	11,500	15,200	15,910	23.5	40,800	1.87	41	Not Reversed, Not By-Passed
28	0.427	0.501	11,500	15,000	15,700	24.0	40,700	1.89		Reversed, Not By-Passed
25	0.427	0.505	11,500	15,700	16,150	23.0	41,000	1.90		Not Reversed, By-Passed
26	0.427	0.505	11,500	15,300	16,100	22.5	41,200	1.91		Reversed, By-Passed
3	0.658	0.401	11,200	16,400	17,900	21.9	42,000	1.82		Not Reversed, Not By-Passed
4	0.760	0.401	11,600	18,200	18,450	23.1	41,500	1.68		Not Reversed, Not By-Passed
6	0.760	0.400	12,000	18,550	17,700	21.8	42,000	1.86		Not Reversed, Not By-Passed
8	0.760	0.250	12,000	17,700	18,820	21.0	42,400	1.79		Not Reversed, Not By-Passed
5	0.760	0.250	12,300	17,800	19,000	20.0	42,000	1.66		Not Reversed, Not By-Passed
17	0.760	0.398	11,000	17,600	18,700	17.5	42,300	1.76	46	Not Reversed, Not By-Passed
10	0.760	0.400	12,000	18,400	19,450	19.3	42,500	1.78		Reversed, Not By-Passed
21	0.760	0.400	11,000	17,700	18,600	17.0	42,700	1.81	46	Reversed, Not By-Passed
12	0.760	0.398	11,800	18,200	19,650	21.2	42,000	1.73		Not Reversed, By-Passed
19	0.760	0.400	11,700	17,600	18,730	16.0	42,800	1.84	46	Not Reversed, By-Passed
14	0.760	0.402	12,300	18,500	19,700	20.8	40,500	1.57		Reversed, By-Passed
23	0.760	0.401	11,700	17,600	18,350	17.0	42,600	1.79	46	Reversed, By-Passed

TABLE 7 SUMMARY OF DRAWING LOADS REQUIRED TO COLD-DRAW 2S-O ALUMINUM CYLINDRICAL RODS

Calgon Coating - Lubricant, Kerosene and Molykote Paste

Nominal Die Size Inches	True Reduction of Rod Area	Average Drawing Load in Pounds			
		Not Reversed Not By-Passed	Reversed Not By-Passed	Not Reversed By-Passed	Reversed By-Passed
1"	0.007	686	686	686	686
63/64"	0.044	1840	1680		
31/32"	0.070	1603	1590		
15/16"	0.145	2452	2650	3140	3037
29/32"	0.212	2132	2535		
7/8"	0.272	2124	2384	3700	3262
27/32"	0.344	2330	2353		
13/16"	0.427	2723	2752	3525	3645
25/32"	0.510	1910	2053		
3/4"	0.584	2370	1697	2955	2850
23/32"	0.658	2380	2168		
11/16"	0.760	1760	1990	2187	2765

TABLE 8 SUMMARY OF DRAWING LOADS REQUIRED TO COLD-DRAW 2S-O ALUMINUM CYLINDRICAL RODS

Calgon Coating - Lubricant, Kerosene and Molykote Paste

Nominal Die Size Inches	True Reduction of Rod Area	Not Reversed Sequence Drawing Load in Pounds When Passing Through Die Indicated					
1"	0.007	686		686		686	686
63/64"	0.044	1840	2110				
31/32"	0.070	1603	1328				
15/16"	0.145	2452	2650	3140	2650		
29/32"	0.212	2132	2510			4500	
7/8"	0.272	2124	2090	3700	3150		5036
27/32"	0.344	2330	2120				
13/16"	0.427	2723	2630	3525	3630		
25/32"	0.510	1910					
3/4"	0.584	2370		2955			
23/32"	0.658	2380					
11/16"	0.760	1760		2187			

effect of sequence in drawing upon the yield strengths. Apparently there is no effect on the proportional limit in shear. If one were to compute the ratio of yield strength in shear to that in tension, this would vary somewhat depending on the manner of drawing. For the not reversed, not by-passed sequence, the average ratios of yield strength in shear to tension at 0.1 per cent offset was 0.65 when the true reduction in rod area varied from 0.07 to 0.76.

Figs. 11 and 13 are the conventional shear stress-strain diagrams to rupture, whereas Figs. 9, 10, and 12 are in the elastic region. There is no effect of the manner of drawing upon the torque-twist curve, Figs. 11 and 13, beyond the yield strength to rupture up to a true reduction of 0.76 in rod area. Cold-working does affect the conventional shear strain at fracture in which, as the amount of cold-working increases, the shear strain at fracture decreases. It is to be noted that the fracture shear strains are very large and the torsion specimens distorted very much by elongating and reducing in diameter.

Residual Stresses

Residual-stress measurements were made on cylindrical rods where the length-to-diameter ratio was 3. Two wire-resistance

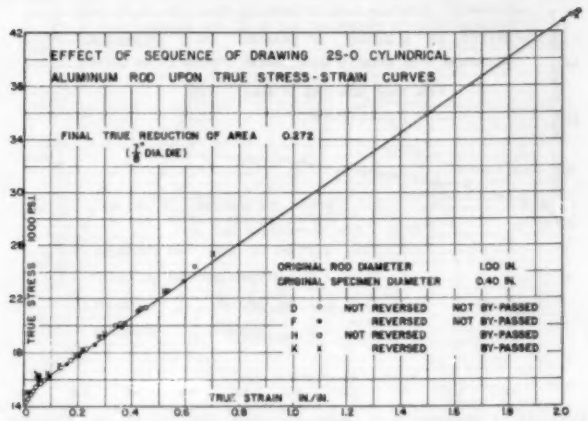
EFFECT OF SEQUENCE OF DRAWING 2S-O CYLINDRICAL ALUMINUM ROD UPON TRUE STRESS-STRAIN CURVES
FINAL TRUE REDUCTION OF AREA 0.272
TRUE STRESS 1000 PSI
TRUE STRAIN IN./IN.
ORIGINAL ROD DIAMETER 1.00 IN.
ORIGINAL SPECIMEN DIAMETER 0.40 IN.
D NOT REVERSED NOT BY-PASSED
F REVERSED NOT BY-PASSED
H NOT REVERSED BY-PASSED
K REVERSED BY-PASSED

FIG. 5 TRUE STRESS-STRAIN DIAGRAM TO RUPTURE FOR TRUE REDUCTION OF 0.272 IN ROD AREA, SHOWING THAT SEQUENCE HAS NO INFLUENCE

(Arrow indicates true stress at maximum load.)

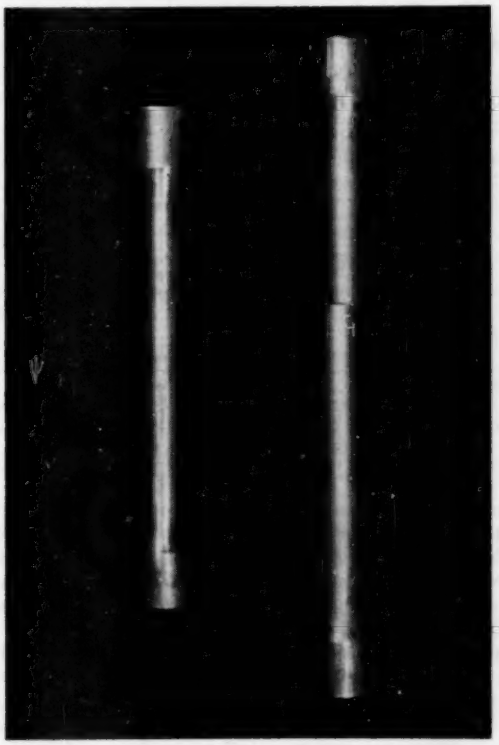

FIG. 8 TYPICAL TORSION SPECIMENS BEFORE AND AFTER TORSION TEST

(Owing to anisotropy, there was a large extension longitudinally, and a lateral contraction.)

bonded SR-4 strain gages were mounted on each cylinder, one in the tangential, and the other in the longitudinal direction. All strain measurements were made using a Baldwin type L strain indicator while the active sample and dummy circuits were kept in an oven at 100 F where the temperature variation was plus or minus 0.5 deg F. The cylinders were bored carefully, using a stream of air to keep the boring tool cool. Three readings were made on each gage, after a boring operation, over a 24-hr period. A complete boring operation usually lasted 4 weeks. Throughout

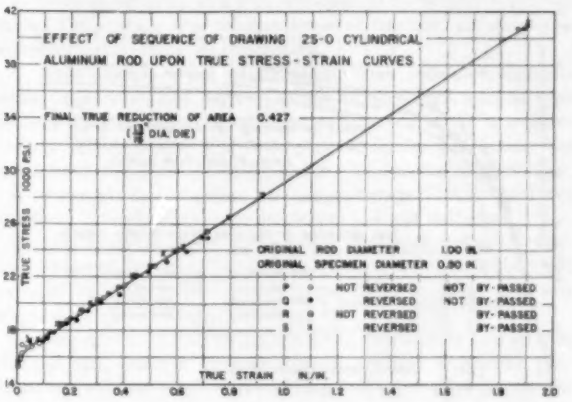
EFFECT OF SEQUENCE OF DRAWING 2S-O CYLINDRICAL ALUMINUM ROD UPON TRUE STRESS-STRAIN CURVES
FINAL TRUE REDUCTION OF AREA 0.427
TRUE STRESS 1000 PSI
TRUE STRAIN IN./IN.
ORIGINAL ROD DIAMETER 1.00 IN.
ORIGINAL SPECIMEN DIAMETER 0.30 IN.
P NOT REVERSED NOT BY-PASSED
Q REVERSED NOT BY-PASSED
R NOT REVERSED BY-PASSED
S REVERSED BY-PASSED

FIG. 6 TRUE STRESS-STRAIN DIAGRAM TO RUPTURE FOR TRUE REDUCTION OF 0.427 IN ROD AREA, SHOWING THAT SEQUENCE HAS NO INFLUENCE

(Arrow indicates true stress at maximum load.)

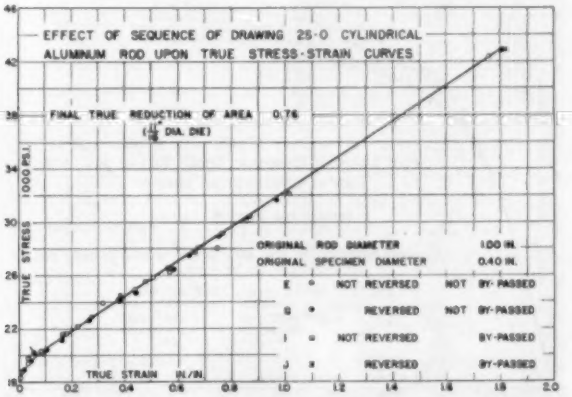
EFFECT OF SEQUENCE OF DRAWING 2S-O CYLINDRICAL ALUMINUM ROD UPON TRUE STRESS-STRAIN CURVES
FINAL TRUE REDUCTION OF AREA 0.76
TRUE STRESS 1000 PSI
TRUE STRAIN IN./IN.
ORIGINAL ROD DIAMETER 1.00 IN.
ORIGINAL SPECIMEN DIAMETER 0.40 IN.
E NOT REVERSED NOT BY-PASSED
G REVERSED NOT BY-PASSED
I NOT REVERSED BY-PASSED
J REVERSED BY-PASSED

FIG. 7 TRUE STRESS-STRAIN DIAGRAM TO RUPTURE FOR TRUE ROD REDUCTION OF 0.760 IN ROD AREA, SHOWING THAT SEQUENCE HAS NO INFLUENCE IN PLASTIC REGION

(Arrow indicates true stress at maximum load.)

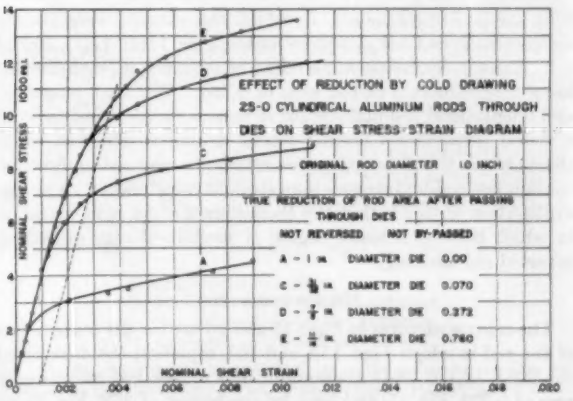
EFFECT OF REDUCTION BY COLD DRAWING 2S-O CYLINDRICAL ALUMINUM RODS THROUGH DIES ON SHEAR STRESS-STRAIN DIAGRAM
NOMINAL SHEAR STRESS 1000 PSI
NOMINAL SHEAR STRAIN
ORIGINAL ROD DIAMETER 1.0 INCH
TRUE REDUCTION OF ROD AREA AFTER PASSING THROUGH DIES
NOT REVERSED NOT BY-PASSED
A - 1 IN. DIAMETER DIE 0.00
C - 1/2 IN. DIAMETER DIE 0.070
D - 7/16 IN. DIAMETER DIE 0.272
E - 5/16 IN. DIAMETER DIE 0.760

FIG. 9 CONVENTIONAL SHEAR-STRESS DIAGRAMS, ILLUSTRATING INFLUENCE OF AMOUNT OF COLD WORK UPON YIELD STRENGTH AT 0.1 PER CENT OFFSET AS DETERMINED BY DOTTED LINE

the testing period the constancy of the strain indicator was checked.

Sachs' method was used for computing the residual stresses

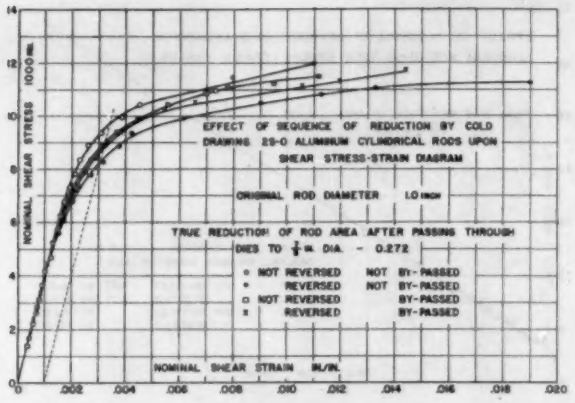
EFFECT OF SEQUENCE OF REDUCTION BY COLD DRAWING 2S-O ALUMINUM CYLINDRICAL RODS UPON SHEAR STRESS-STRAIN DIAGRAM
ORIGINAL ROD DIAMETER LO inch
TRUE REDUCTION OF ROD AREA AFTER PASSING THROUGH DIES TO 1/4 in. DIA. - 0.272
NOT REVERSED NOT BY-PASSED
REVERSED NOT BY-PASSED
NOT REVERSED BY-PASSED
REVERSED BY-PASSED
NOMINAL SHEAR STRAIN IN./IN.
NOMINAL SHEAR STRESS 1000 lb.

FIG. 10 CONVENTIONAL SHEAR STRESS-STRAIN DIAGRAMS IN ELASTIC REGION FOR A COLD REDUCTION OF 0.272, SHOWING INFLUENCE OF SEQUENCE

(Dotted line is yield-strength determination at 0.1 per cent offset.)

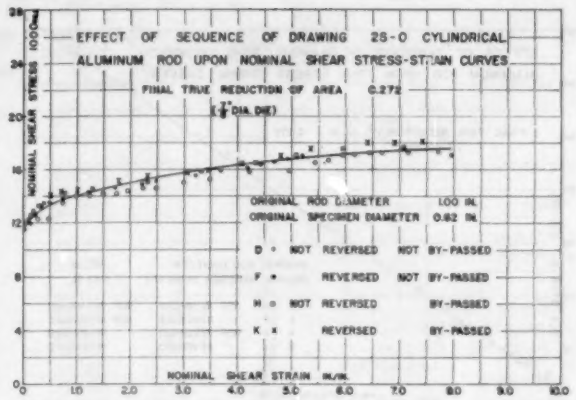
EFFECT OF SEQUENCE OF DRAWING 2S-O CYLINDRICAL ALUMINUM ROD UPON NOMINAL SHEAR STRESS-STRAIN CURVES
FINAL TRUE REDUCTION OF AREA 0.272
ORIGINAL ROD DIAMETER LOO IN.
ORIGINAL SPECIMEN DIAMETER 0.62 IN.
D NOT REVERSED NOT BY-PASSED
F REVERSED NOT BY-PASSED
H NOT REVERSED BY-PASSED
K REVERSED BY-PASSED
NOMINAL SHEAR STRAIN IN./IN.
NOMINAL SHEAR STRESS 1000 lb.

FIG. 11 CONVENTIONAL SHEAR-STRESS DIAGRAMS IN PLASTIC REGION TO RUPTURE FOR COLD REDUCTION OF 0.272, SHOWING THAT SEQUENCE HAS NO INFLUENCE

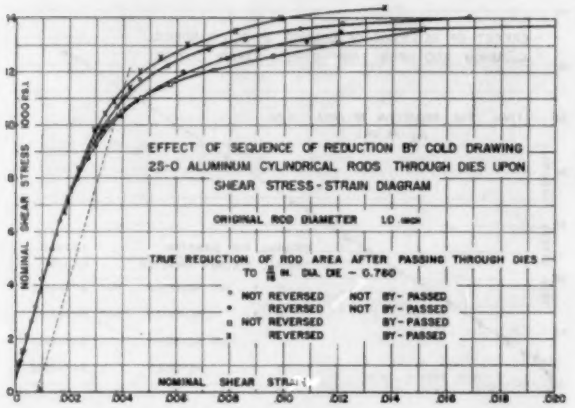
EFFECT OF SEQUENCE OF REDUCTION BY COLD DRAWING 2S-O ALUMINUM CYLINDRICAL RODS THROUGH DIES UPON SHEAR STRESS-STRAIN DIAGRAM
ORIGINAL ROD DIAMETER LO inch
TRUE REDUCTION OF ROD AREA AFTER PASSING THROUGH DIES TO 3/8 in. DIA. DIE - 0.760
NOT REVERSED NOT BY-PASSED
REVERSED NOT BY-PASSED
NOT REVERSED BY-PASSED
REVERSED BY-PASSED
NOMINAL SHEAR STRAIN
NOMINAL SHEAR STRESS 1000 lb.

FIG. 12 CONVENTIONAL SHEAR STRESS-STRAIN DIAGRAMS IN ELASTIC REGION FOR COLD REDUCTION OF 0.760, PORTRAYING INFLUENCE OF SEQUENCE

(Dotted line is yield-strength determination at 0.1 per cent offset.)

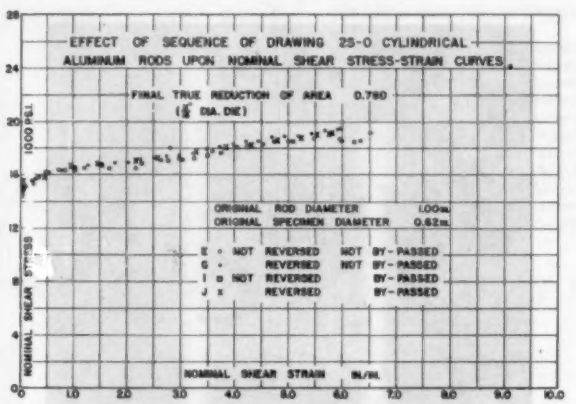
EFFECT OF SEQUENCE OF DRAWING 2S-O CYLINDRICAL ALUMINUM RODS UPON NOMINAL SHEAR STRESS-STRAIN CURVES
FINAL TRUE REDUCTION OF AREA 0.760
(3/8" DIA. DIE)
ORIGINAL ROD DIAMETER LOO in.
ORIGINAL SPECIMEN DIAMETER 0.62 in.
E NOT REVERSED NOT BY-PASSED
G REVERSED NOT BY-PASSED
I NOT REVERSED BY-PASSED
J REVERSED BY-PASSED
NOMINAL SHEAR STRAIN IN./IN.
NOMINAL SHEAR STRESS 1000 P.S.I.

FIG. 13 CONVENTIONAL SHEAR STRESS-STRAIN DIAGRAMS IN PLASTIC REGION TO RUPTURE FOR COLD REDUCTION OF 0.760

(Sequence had no effect.)

from strain measurements, in which the stresses were plotted versus area bored out in square inches, Figs. 14(*a*), 14(*b*), and 14 (*c*). Table 5 summarizes the effect of sequence in cold-drawing for a true reduction in rod area of 0.760. The least tangential and longitudinal residual surface stresses were produced by both reversed sequences. Trinks[3] found a similar effect in rolled sheets where the alternate passes which are reversed in direction contain less residual stresses than straight rolled sheets. A partial explanation of this is that the Bauschinger effect is in operation in which there is a lesser degree of work-hardening caused by reversed rod-drawing.

MICROSTRUCTURE

The microstructures in Figs. 15 and 16 are for the center areas of the rod in which Figs. 15A and 16A represent the as-received condition of the 2S-O aluminum. For a true rod reduction in area of 0.272, Fig. 15, and for a true reduction of 0.76, Fig. 16, no noticeable difference was observed because of sequence in drawing. Also, areas at the edge of the rod were compared with photomicrographs of areas at the center. There were no marked differences.

ENDURANCE CURVES

Room-temperature rotating cantilever-beam fatigue tests were conducted on a Krouse machine at 6000 rpm, using $^1/_2$-in-diam specimens. The purpose was to discover if the manner of cold-drawing influenced the S-N diagram. There is a tendency for the reversed, not by-passed, and reversed, by-passed sequence to show lower endurance limits than the other two sequences as plotted in Fig. 17. The normal scatter resulting from the test does not permit a definite conclusion except that there is no large effect on fatigue curves up to 40,000,000 cycles.

CONCLUSION

Studies in the cold-drawing of 2S-O aluminum rod were made by means of true stress-strain tension diagrams, hardness measurements, conventional torsion stress-strain curves, residual-stress measurements, and photographs of the microstructure. A series of hardened conical steel dies were used with half-angles of about 1 deg. Drawing speeds were about 2 ipm. True reductions in rod area per pass were 0.07 in. per in. or larger. All rods were coated with a Calgon solution and then lubricated with a paste made from Molykote type M-powder and kerosene. Several conclusions were reached as follows:

1 The manner of drawing (Table 1) had only a small effect on the yield strength. Maximum difference in values was about 4 per cent depending upon the sequence. For a true reduction of

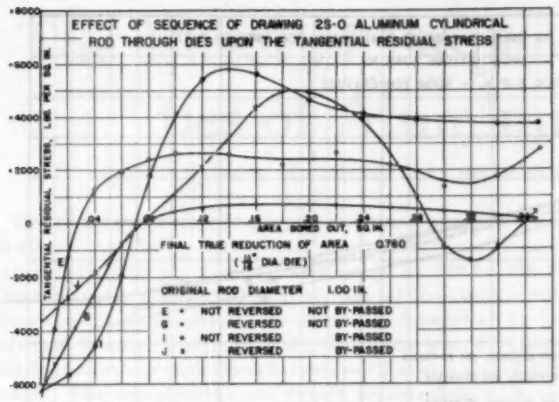
EFFECT OF SEQUENCE OF DRAWING 2S-O ALUMINUM CYLINDRICAL ROD THROUGH DIES UPON THE TANGENTIAL RESIDUAL STRESS
TANGENTIAL RESIDUAL STRESS, LBS. PER SQ. IN.
AREA BORED OUT, SQ. IN.
FINAL TRUE REDUCTION OF AREA 0.760
(11/16" DIA. DIE)
ORIGINAL ROD DIAMETER 1.00 IN.
E = NOT REVERSED NOT BY-PASSED
G = REVERSED NOT BY-PASSED
I = NOT REVERSED BY-PASSED
J = REVERSED BY-PASSED

FIG. 14(*a*) EFFECT OF SEQUENCE IN DRAWING 2S-O ALUMINUM THROUGH DIES UPON TANGENTIAL RESIDUAL STRESS; TRUE ROD REDUCTION IN AREA, 0.760

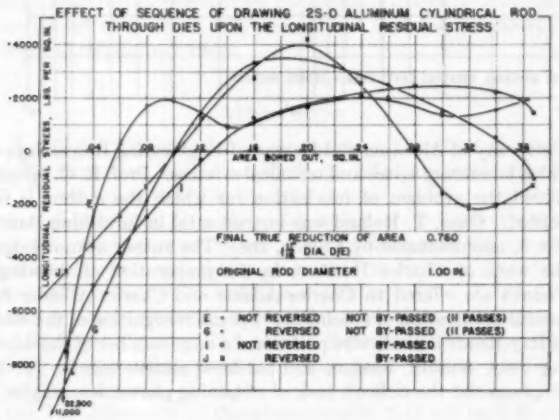
EFFECT OF SEQUENCE OF DRAWING 2S-O ALUMINUM CYLINDRICAL ROD THROUGH DIES UPON THE LONGITUDINAL RESIDUAL STRESS
LONGITUDINAL RESIDUAL STRESS, LBS. PER SQ. IN.
AREA BORED OUT, SQ. IN.
FINAL TRUE REDUCTION OF AREA 0.760
(11/16" DIA. DIE)
ORIGINAL ROD DIAMETER 1.00 IN.
E = NOT REVERSED NOT BY-PASSED (II PASSES)
G = REVERSED NOT BY-PASSED (II PASSES)
I = NOT REVERSED BY-PASSED
J = REVERSED BY-PASSED

FIG. 14(*b*) EFFECT OF SEQUENCE IN DRAWING 2S-O ALUMINUM THROUGH DIES UPON LONGITUDINAL RESIDUAL STRESS; TRUE ROD REDUCTION IN AREA, 0.760

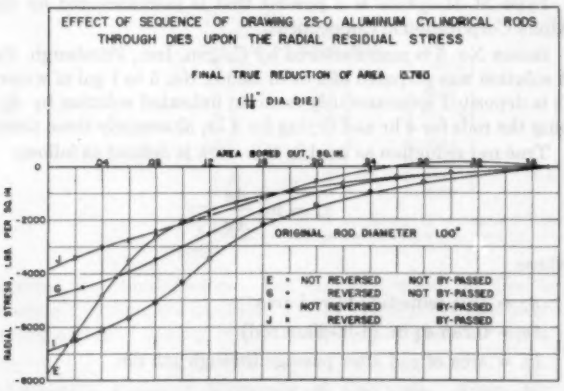
EFFECT OF SEQUENCE OF DRAWING 2S-O ALUMINUM CYLINDRICAL RODS THROUGH DIES UPON THE RADIAL RESIDUAL STRESS
FINAL TRUE REDUCTION OF AREA 0.760
(11/16" DIA. DIE)
AREA BORED OUT, SQ. IN.
RADIAL STRESS, LBS. PER SQ. IN.
ORIGINAL ROD DIAMETER 1.00"
E = NOT REVERSED NOT BY-PASSED
G = REVERSED NOT BY-PASSED
I = NOT REVERSED BY-PASSED
J = REVERSED BY-PASSED

FIG. 14(*c*) EFFECT OF SEQUENCE IN DRAWING 2S-O ALUMINUM THROUGH DIES UPON RADIAL RESIDUAL STRESS; TRUE ROD REDUCTION IN AREA, 0.760

0.760 in area, sequence had very little effect. The same order of difference was observed for SAE 1020 steel.

2 Sequence in drawing (Table 1) had no effect on the true stress-strain diagrams. A similar conclusion was reached for SAE 1020 steel.

3 Cold-working up to a true reduction of 0.760 in area did not change the average true tension stress at fracture, although the true strain at fracture was decreased.

4 True tension stress at maximum load increases with increased cold work but the true strain at maximum load or true uniform strain is constant at about 0.05 in. per in. for a true reduction in rod area of 0.15 or larger. A similar conclusion was found for steel when cold-worked either by drawing or by rolling.

5 Sequence had no effect upon the average Vickers hardness number. A hardness travers across the rod was uniform.

6 Conventional shear stress-strain diagrams indicated that the manner of drawing (Table 1) had some influence on the yield strength in shear. The proportional limit in shear was not changed by the manner of drawing.

7 Sequence in cold-drawing alters the distribution and magnitude of the residual stresses. Both reversed sequences produced the smallest tangential and longitudinal stresses on the rod surface.

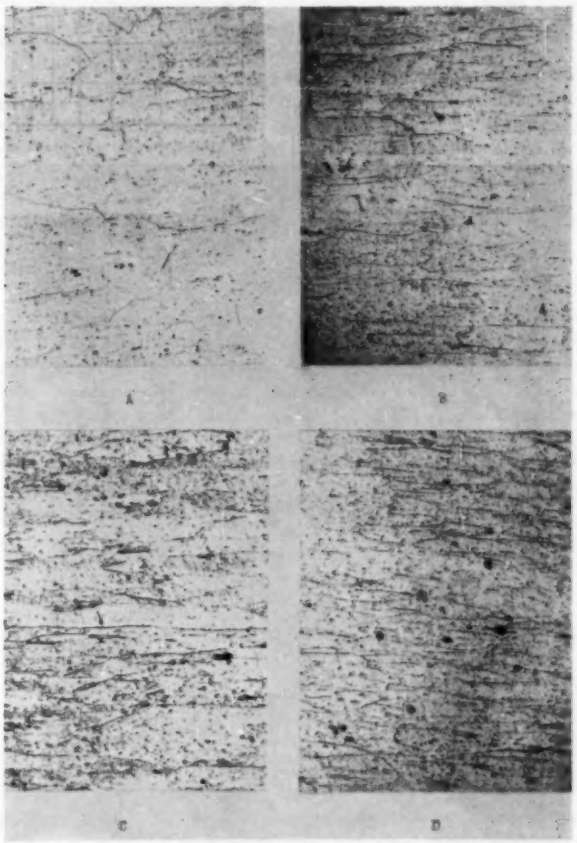

A, As-received condition
B, Reversed, not by-passed sequence
C, Not reversed, by-passed sequence
D, Reversed, by-passed sequence

FIG. 15 PHOTOMICROGRAPHS OF 2S-O ALUMINUM ROD COLD-DRAWN IN VARIOUS SEQUENCES TO A TRUE REDUCTION IN ROD AREA OF 0.272 (Center area of rod; etched 3 per cent HF; ×100. Bright field illumination.)

ACKNOWLEDGMENT

Funds for this investigation were obtained in a grant from the Research Corporation for which the author expresses his appreciation especially to Charles H. Schauer, Director of Grants. The

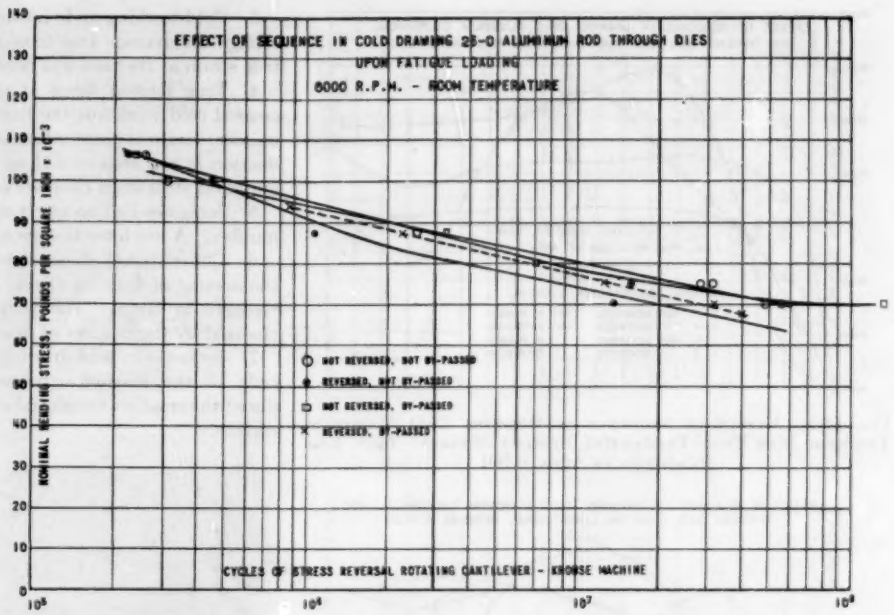
EFFECT OF SEQUENCE IN COLD DRAWING 2S-O ALUMINUM ROD THROUGH DIES
UPON FATIGUE LOADING
6000 R.P.M. - ROOM TEMPERATURE
NOMINAL BENDING STRESS, POUNDS PER SQUARE INCH x 10^-3
NOT REVERSED, NOT BY-PASSED
REVERSED, NOT BY-PASSED
NOT REVERSED, BY-PASSED
REVERSED, BY-PASSED
CYCLES OF STRESS REVERSAL ROTATING CANTILEVER - KROUSE MACHINE

FIG. 17 EFFECT OF SEQUENCE IN COLD-DRAWING UPON ENDURANCE CURVES OBTAINED AT ROOM TEMPERATURE AND 6000 RPM

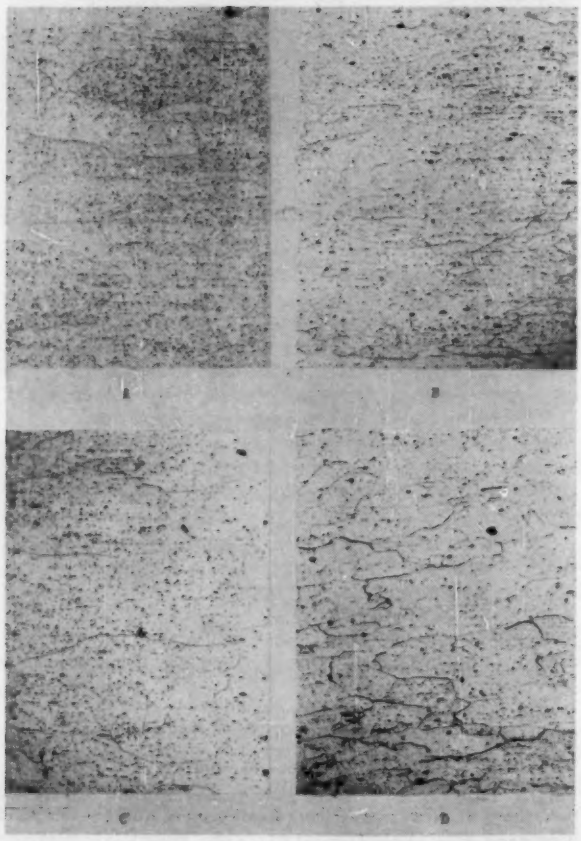

A, Not reversed, not by-passed sequence
B, Reversed, not by-passed sequence
C, Not reversed, by-passed sequence
D, Reversed, by-passed sequence

FIG. 16 PHOTOMICROGRAPHS OF 2S-O ALUMINUM ROD COLD-DRAWN IN VARIOUS SEQUENCES TO A TRUE ROD REDUCTION OF AREA OF 0.760 (Center area of rod; etched 3 per cent HF; ×100. Bright field illumination.)

University of Alabama and Bureau of Engineering Research provided laboratory space and technical services. Prof. E. C. Wright solved the problem of lubrication for which the author is indebted. Chas. T. Roland was instrumental in furnishing Banox No. 5, manufactured by Calgon, Inc. The author acknowledges the work of Charles Hoffman in the preparation of drawings. Thanks are offered to Charles Adams and Charles Allinder for careful preparation of specimens. Special recognition of the work of Ray Reade is made who performed a large number of the drawing tests, tension, torsion, and hardness measurements. T. E. Stephens did the difficult task of obtaining photomicrographs.

Appendix

Type M Molykote is a powder that is manufactured by the Alpha Corporation in Connecticut.

Banox No. 5 is manufactured by Calgon, Inc., Pittsburgh, Pa. A solution was prepared of 2 oz of Banox No. 5 to 1 gal of water.[8] It is deposited spontaneously from an unheated solution by dipping the rods for 4 hr and drying for 4 hr, alternately three times.

True rod reduction as used in this work is defined as follows

$$q_x = \ln_e \frac{Ao}{Ax}$$

where

q_x = true reduction in rod area
Ao = 0.785 sq in. (1-in-diam rod)
Ax = area of rod after passage through xth die

Table 6 is a complete summary of the tensile data and hardness measurements.

Table 7 shows a comparison of drawing loads through the various dies with the sequence in drawing.

Table 8 is another summary of drawing loads required to cold-draw 2S-O aluminum rod. This is for various severe reductions.

[8] This coating is discussed in an article, "Special Phosphate Coating," *Steel*, June 6, 1949.

The Effect of Dispersions on Creep Properties of Aluminum-Copper Alloys

By W. H. GIEDT,[1] O. D. SHERBY,[2] and J. E. DORN,[3] BERKELEY, CALIF.

The creep properties of a system of 3 to 5 per cent Cu in Al alloys containing hard particles of $CuAl_2$ were investigated throughout a temperature range of 350 to 578 K. The results supplemented with additional tensile-test data show that these properties are primarily dependent on the volumetric mean free path of the $CuAl_2$ particles and independent of minor variations in composition and heat-treatment. The creep stress was found to correlate with the creep rate-temperature parameter $Z = \dot{\epsilon}_s e^{\Delta H/RT}$. Above ln $Z = \ln(\dot{\epsilon}_s e^{\Delta H/RT}) = 46.0$ and below ln $Z = 27.5$ the finer dispersions are superior, whereas over the intervening range of Z-values the coarser dispersions are superior. The energy for activation ΔH, was found to be a constant of about 37,000 cal per mol.

Introduction

ALTHOUGH extensive investigations already have been conducted on biphase alloys, no definitive conclusion has yet been reached on how the fineness of dispersions of intermetallic compounds in the alpha matrix affects their creep resistance. Several investigators (1, 2)[4] found that the coarser dispersions exhibit superior creep resistance; and this prevailing conclusion is consistent with the widely postulated thesis that the most stable structure induces the greatest creep resistance. But the generalization that coarser dispersions always provide greater creep resistance should not be made without qualifications:

(*a*) The differences in the pretreatments that are used to develop the various dispersions also might alter other less readily detected structural factors. For example, when the fine and coarse dispersions are produced by the crude procedure of chill casting and sand casting, respectively, it cannot be clear whether the observed differences in creep behavior should be ascribed to the differences in the dispersion, differences in the grain sizes of the alpha solid-solution matrix, differences in residual stresses, or even differences in the strain-hardened state arising from plastic deformation resulting from thermal gradients that were introduced during cooling.

(*b*) The creep properties at low temperatures and high strain rates parallel somewhat the tensile properties. In this range, therefore, the finer dispersions would be expected to exhibit superior creep resistance.

(*c*) A few observations at relatively high temperatures have shown that the finer dispersions are superior in creep resistance to coarser dispersions.

It is possible that the present state of knowledge regarding the effect of dispersions on creep is due to the fact that thus far only few tests have been made on isolated examples; no systematic study has yet been reported on the effects of dispersions on the creep resistance of biphase alloys. Therefore it was the intent of this investigation to attempt a systematic study on the effects of dispersions of $CuAl_2$ on the creep behavior of high-purity Al-Cu alloys.

Materials and Techniques

Alloys containing dispersions of $CuAl_2$ in the alpha solid-solution matrix of Al were selected for this investigation because adequate heat-treating techniques for making a series of dispersions already had been developed during studies on the effect of dispersions on the tensile properties of biphase alloys (3). Since the heat-treatments were reasonably similar for each of the dispersions, it was thought that the small differences in time and temperature of annealing that were required to produce the various dispersions might not be too serious a factor per se in masking the desired relationship between dispersion and creep resistance. The good correlations that were obtained between the tensile properties and dispersions suggested that these minor differences in heat-treatment did not introduce significant auxiliary effects.

Since the details of the heat-treatments have been reported already they will not be reproduced here (3). The chemical composition, grain size, and dispersion of the heat-treated alloys are given in Table 1. As shown in the second column of Table 1, the grain size of the alpha solid-solution matrix was held to about the same value for all dispersions with the exception of the 3 per cent very coarse (3VC) alloy. The volumetric mean free path (VMFP), λ, between the $CuAl_2$ particles in the alpha solid-solu-

TABLE 1 CHEMICAL COMPOSITION, GRAIN SIZE, AND VOLUMETRIC MEAN FREE PATH

Dispersion designation per cent	Grain size, grains/mm	λ VMFP cm	Composition by weight, per cent[b]				
			Chemical analysis	Spectrochemical analyses			
			Cu	Si	Fe	Mn	Zn
3 M[a]	2.4	0.00096	3.05	0.002	0.002	trace	0.0004
3 C	2.3	0.00365					
3 VC	0.8	0.0097					
4 F	2.3	0.00078	4.03	0.002	0.002	0.001	0.0004
4 M	2.3	0.00155					
4 C	2.4	0.0064					
5 F	2.1	0.00062	5.05	0.003	0.002	0.002	0.0006
5 M	2.2	0.0047					
5 C	2.3	0.0069					

[a] F = fine; M = medium; C = coarse; VC = very coarse.
[b] Chemical analyses and alloys supplied by courtesy of Aluminum Company of America research laboratories.

[1] Assistant Professor, University of California. Assoc. Mem. ASME.
[2] Research Engineer, University of California.
[3] Professor of Metallurgy, University of California.
[4] Numbers in parentheses refer to Bibliography at end of paper.
Contributed by the Metals Engineering Division and presented at the Annual Meeting, New York, N. Y., November 29–December 4, 1953, of The American Society of Mechanical Engineers.
Note: Statements and opinions advanced in papers are to be understood as individual expressions of their authors and not those of the Society. Manuscript received at ASME Headquarters, February 10, 1953. Paper No. 53—A-78.

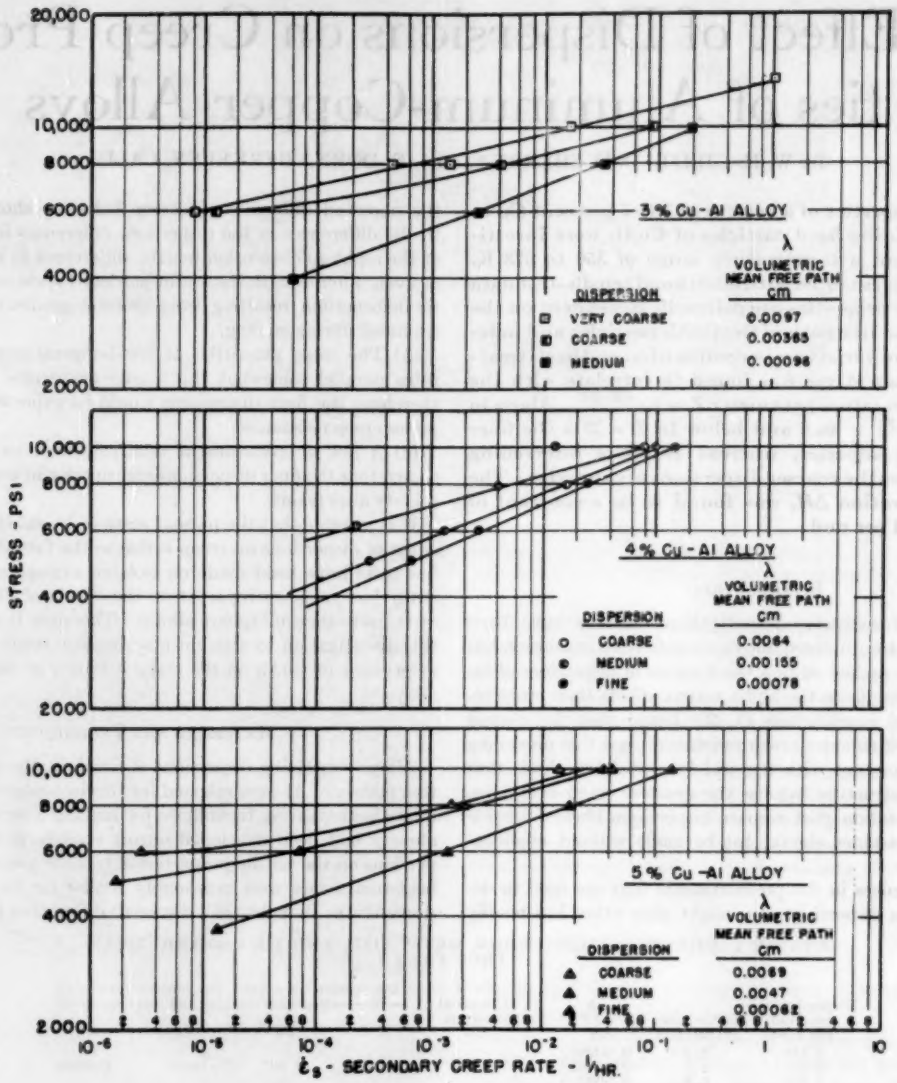

FIG. 1 CREEP PROPERTIES OF AL-CU ALLOYS AT 422 K

tion matrix, shown in the third column, varied over a factor of 15 times among the various dispersions.

Constant-load creep tests up to about 6 weeks' duration were conducted over a range of temperatures from 350 to 578 K (170 F to 580 F). The experimental details recounting the precision of stressing, temperature control, and strain measurement have been reported already (4).

RESULTS AND DISCUSSION

Effect of Dispersions on Creep Properties at 422 K. The stress versus the secondary creep-rate curves, shown in Fig. 1, were selected to provide a facile comparison of the effect of dispersions on the creep resistance of Al-Cu alloys at 422 K. In each alloy the coarse dispersion (large values of λ) exhibited the greatest creep resistance, whereas the fine dispersion (small values of λ) was least creep-resistant.

The data shown in Fig. 2 illustrate more clearly that the creep stress for a given secondary creep rate increases with the volumetric mean free path λ between the dispersed particles. This effect is most pronounced for the lowest secondary creep rate that is recorded. Some minor scatter was obtained in the data, suggesting that some unknown factor might yet be affecting the creep resistance. But the general consistency of the results implies strongly that the creep resistance of biphase alloys depends primarily on the mean free path between the dispersed particles and is independent of minor differences in the percentages of that phase and minor differences in heat-treatment that are required to produce the different dispersions.

Effect of Temperature. As shown in Fig. 3, the high-temperature tensile properties of these dispersion alloys, obtained from a previous report (5), exhibit two inversions. Below about 450 K and above about 600 K, the flow stress at a strain of 10 per cent is greater for the finer dispersion. Over the intermediate range from 450 K to 600 K, the coarser dispersion exhibits the highest flow strength in tension. These results have been attributed to the effects of recovery on the properties. At the low tempera-

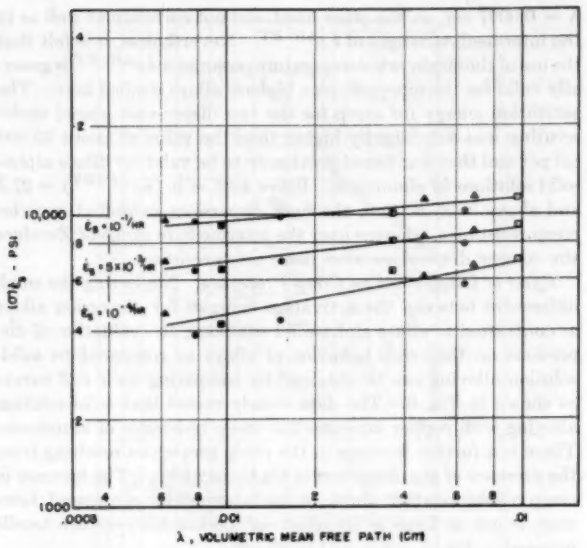

FIG. 2 EFFECT OF DISPERSIONS ON CREEP RESISTANCE OF AL-CU ALLOYS AT 422 K

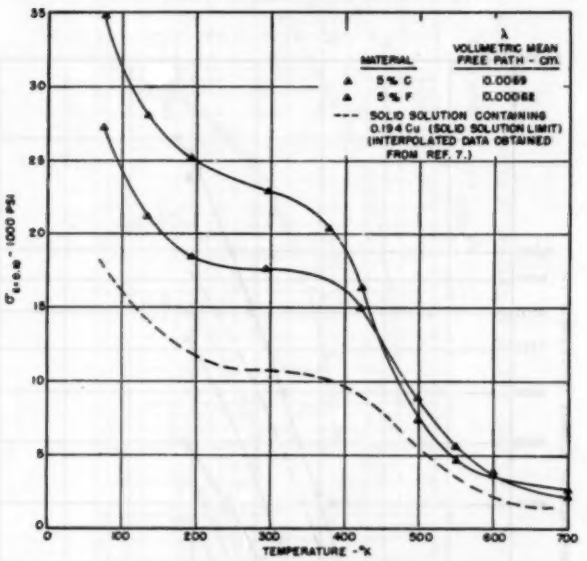
MATERIAL
λ VOLUMETRIC MEAN FREE PATH - CM.
5% C 0.0069
5% F 0.00062
SOLID SOLUTION CONTAINING 0.194 Cu (SOLID SOLUTION LIMIT) (INTERPOLATED DATA OBTAINED FROM REF. 7.)
TEMPERATURE - °K

FIG. 3 EFFECT OF TEMPERATURE ON DEFORMATION STRENGTH OF A FINE AND COARSE AL-CU DISPERSION ALLOY (5)

tures where recovery is absent, the finer dispersions have higher tensile properties, and at the higher temperatures, where recovery is practically complete, the finer dispersions again exhibit the higher tensile properties. But, as shown by the less precipitous decrease in tensile properties of the coarser dispersion with temperature, over the range of temperatures where only partial recovery occurs, the coarser dispersion alloys recover more slowly than the finer dispersions, causing the inversions. If creep properties are also dependent upon somewhat the same factors of strain-hardening and recovery that are operative in determining the tensile properties, the same inversions also might be applicable to creep. In view of the lower strain rates in a creep test, however, the inversions might be expected to occur at lower temperatures

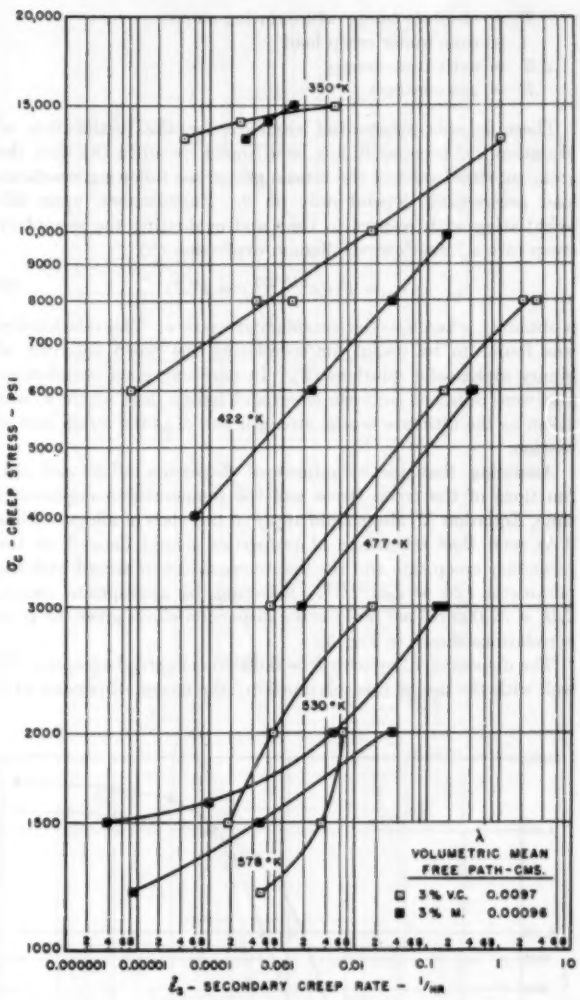

FIG. 4 EFFECT OF TEMPERATURE ON CREEP PROPERTIES OF A FINE AND COARSE AL-CU DISPERSION ALLOY

than those recorded for the tension data. Furthermore, for constant-temperature creep tests the inversions will appear as a function of the secondary creep rates.

The data recorded in Fig. 4 reveal that the suspected inversions in creep behavior do, in fact, occur. At 350 K and higher secondary rates, the finer dispersion alloy exhibits higher values of creep stress, whereas at lower secondary creep rates the coarser dispersions are more creep-resistant. At 530 K and $\dot{\epsilon}_s = 3 \times 10^{-4}$ and at 578 K and $\dot{\epsilon}_s = 3 \times 10^{-3}$, the second inversion occurs wherein the finer dispersion is again superior to the coarser dispersion for the lower secondary creep rates.

Creep Rate-Temperature Relationships. In previous investigations on the creep behavior of binary alpha-solid solutions (6), the creep strain for a constant-load test was found to be a simple function of a temperature-compensated time according to which

$$\epsilon = f(\theta, \sigma_o) \quad [1]$$

where

ϵ = total creep strain
σ_o = initial stress in a constant-load test
$\theta = te^{-\Delta H/RT}$ = temperature-compensated time

T = absolute temperature during creep
t = time under creep load
ΔH = activation energy
R = gas constant

There is now substantial credence for the justification of Equation [1] because it has been shown recently (8) that the grain substructure and the tensile properties following constant-load precreeping depend only on θ. Furthermore, upon differentiating with respect to time and evaluating the secondary creep rate $\dot{\epsilon}_s$, the Zener-Hollomon expression (9)

$$\sigma_c = F(\dot{\epsilon}_s e^{\Delta H/RT}) = F(Z) \quad [2]$$

is obtained, where $\dot{\epsilon}_s$ is the secondary creep rate. This relationship was found to be useful for correlating the creep behavior of binary alpha-solid solutions (6). In addition, good correlations also were obtained between creep and tensile data where σ_c was taken as the ultimate tensile strength and $\dot{\epsilon}_s$ as the strain rate in tension.

Assuming that the structures of dispersion alloys are also functions of the creep stress and the temperature-compensated time, Equation [2] also should apply to this class of alloys. Thus it is seen that inversions of properties should depend on the secondary creep rate and the test temperature in accord with the parameter $(Z) = \dot{\epsilon}_s e^{\Delta H/RT}$. Selecting, by appropriate means, $\Delta H = 37{,}000$ cal per mol for the dispersion alloys gives the good correlations shown in Fig. 5.

The dispersion alloy with $\lambda = 0.00096$ cm agreed exceptionally well with the use of this relationship; the coarse dispersion with $\lambda = 0.0097$ cm, on the other hand, did not correlate as well as in the intermediate ranges of $\dot{\epsilon}_s e^{\Delta H/RT}$. Nevertheless, it is felt that the use of the strain rate-temperature parameter $\dot{\epsilon}_s e^{\Delta H/RT}$ is generally valid for the more complex biphase alloys studied here. The activation energy for creep for the two dispersions placed under scrutiny was only slightly higher than the value of about 35,800 cal per mol that was found previously to be valid for dilute alpha-solid solutions in aluminum. Below $\ln Z = \ln(\dot{\epsilon}_s e^{\Delta H/RT}) = 27.5$ and above $\ln Z = 46.0$, the finer dispersions exhibited superior creep resistance, whereas over the intermediate range of Z-values the coarser dispersions were more creep-resistant.

Effect of Dispersions on Creep Properties. Neglecting the small differences between the activation energies for dispersion alloys as contrasted to dilute alpha-solid solutions, an evaluation of dispersions on the creep behavior of alloys as compared to solid-solution alloying can be obtained by comparing their σ-Z curves as shown in Fig. 6. The data clearly reveal that solid-solution alloying with copper increases the creep resistance of aluminum. There is a further increase in the creep properties resulting from the presence of the dispersion of $CuAl_2$ particles. The increase in creep resistance attributable to the intermetallic compound, however, is not as large as its effect on the low-temperature tensile properties, Fig. 3.

Creep Strain as a Function of Temperature-Compensated Time. The general validity of Equation [2] for the dispersion alloys implies that Equation [1] also should be valid. The correlations

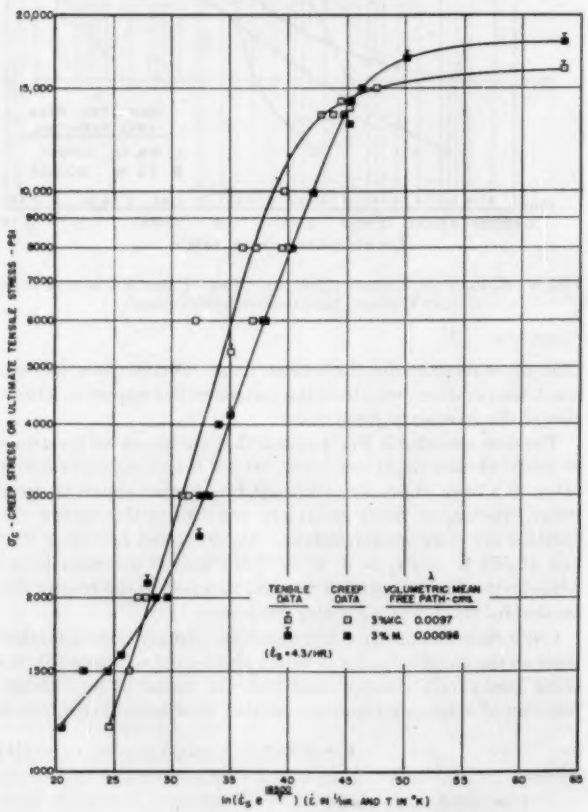
σ_c - CREEP STRESS OR ULTIMATE TENSILE STRESS - PSI
TENSILE DATA
CREEP DATA
λ VOLUMETRIC MEAN FREE PATH - CMS.
3%MG. 0.0097
3% M. 0.00096
($\dot{\epsilon}_s$ = 4.3/HR)
$\ln(\dot{\epsilon}_s e^{\frac{18500}{T}})$ ($\dot{\epsilon}$ IN 1/HR AND T IN °K)

FIG. 5 CORRELATION OF CREEP DATA IN FIG. 4 BY MEANS OF PARAMETER $Z = (\dot{\epsilon}_s e^{\Delta H/RT})$

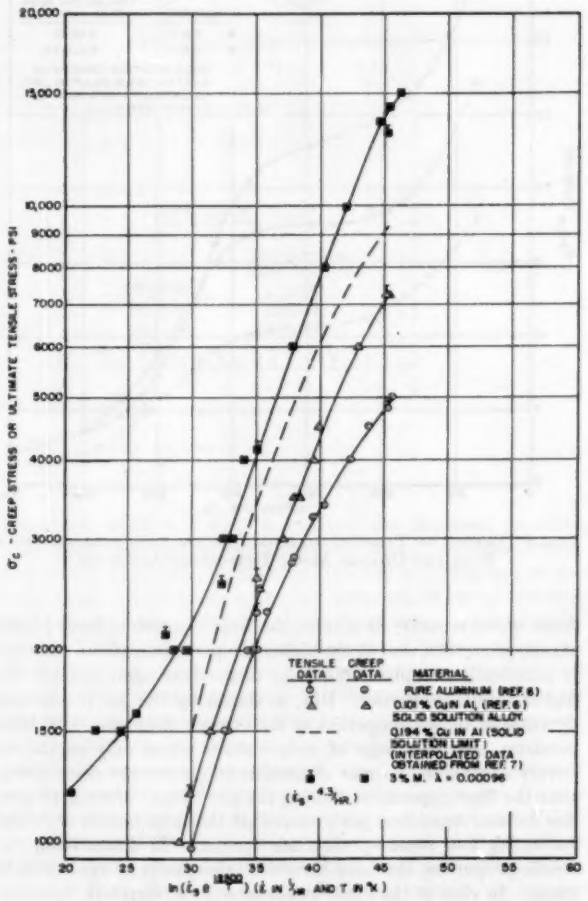
σ_c - CREEP STRESS OR ULTIMATE TENSILE STRESS - PSI
TENSILE DATA
CREEP DATA
MATERIAL
PURE ALUMINUM (REF. 6)
0.101 % Cu IN Al (REF. 6) SOLID SOLUTION ALLOY
0.194 % Cu IN Al (SOLID SOLUTION LIMIT) (INTERPOLATED DATA OBTAINED FROM REF. 7)
3 % M. λ = 0.00096
($\dot{\epsilon}_s$ = 4.3/HR)
$\ln(\dot{\epsilon}_s e^{\frac{18500}{T}})$ ($\dot{\epsilon}$ IN 1/HR AND T IN °K)

FIG. 6 EFFECT OF DISPERSIONS ON $(\sigma_c - \dot{\epsilon}_s e^{\Delta H/RT})$ CURVE

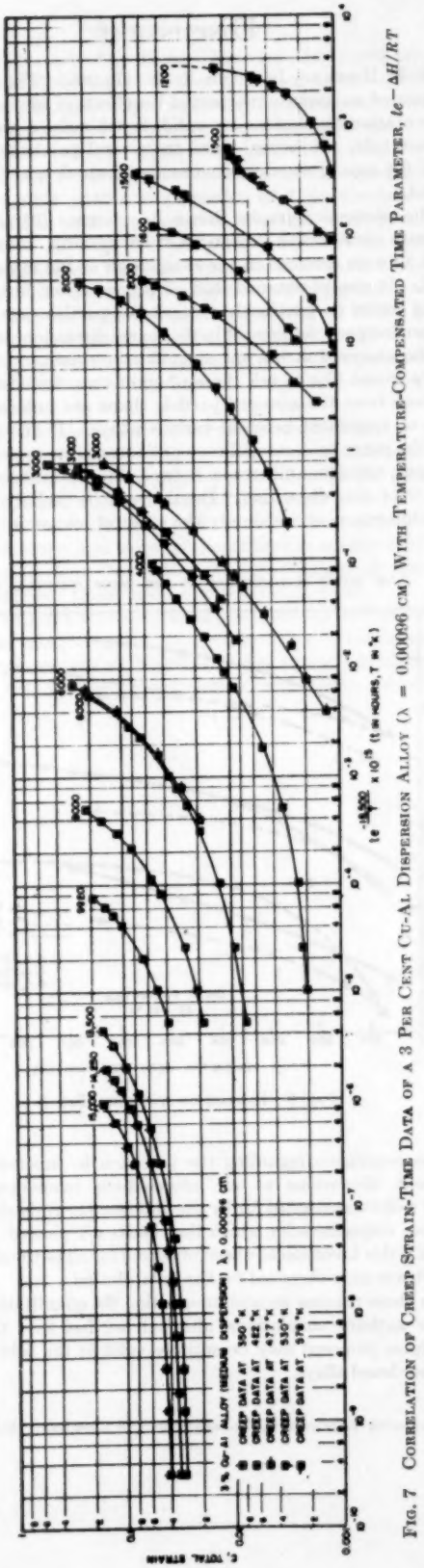

FIG. 7 CORRELATION OF CREEP STRAIN-TIME DATA OF A 3 PER CENT CU-AL DISPERSION ALLOY ($\lambda = 0.00086$ CM) WITH TEMPERATURE-COMPENSATED TIME PARAMETER, $te^{-\Delta H/RT}$

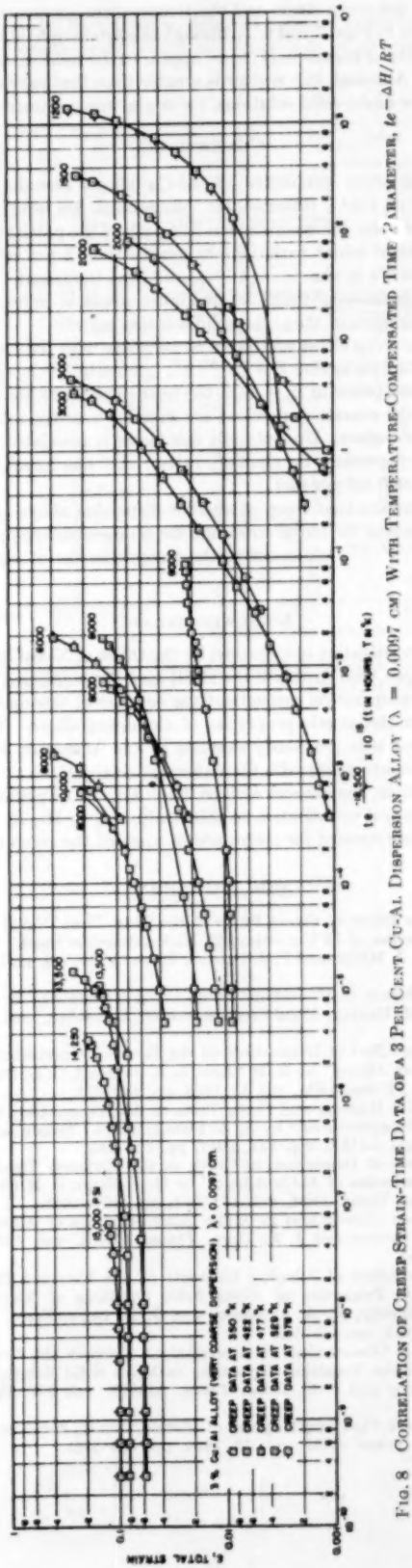

FIG. 8 CORRELATION OF CREEP STRAIN-TIME DATA OF A 3 PER CENT CU-AL DISPERSION ALLOY ($\lambda = 0.0097$ CM) WITH TEMPERATURE-COMPENSATED TIME PARAMETER, $te^{-\Delta H/RT}$

between the creep strain and the temperature-compensated time are shown in Figs. 7 and 8. Although these data uphold the nominal validity of Equation [1] there appears to be some scatter in the results. Although this scatter is greater than that previously obtained for alpha-solid solutions, its origin was not uncovered.

Conclusions

1 The creep properties of Al-Cu alloys containing hard particles of $CuAl_2$ intermetallic compounds are primarily dependent on the volumetric mean free path of the particles and independent of minor variations in composition (3 per cent Cu to 5 per cent Cu in aluminum alloys) and heat-treatment.

2 Dispersions of $CuAl_2$ in aluminum result in improving the creep resistance of the alpha solid-solution matrix.

3 The creep stress was found to correlate with the creep rate-temperature parameter $Z = \dot{\epsilon}_s e^{\Delta H/RT}$. Above $\ln Z = \ln(\dot{\epsilon}_s e^{\Delta H/RT}) = 46.0$ and below $\ln Z = 27.5$, the finer dispersions are superior, whereas the coarser dispersions are superior over the intervening range of Z-values. Undoubtedly this factor is associated with the effect of dispersions on recovery rates. ΔH was found equal to about 37,000 cal per mol.

4 Constant-load creep strains for dispersion alloys appear to be functions of the initial stress and the temperature-compensated time, $te^{-\Delta H/RT}$, analogous to the creep behavior of alpha-solid solutions.

Acknowledgments

This investigation is sponsored by the Office of Naval Research. The authors wish to thank the ONR staff for continued interest and full co-operation throughout the conduct of this and related studies on the plastic properties of aluminum alloys. The materials used were graciously supplied by the Aluminum Research Laboratories together with their chemical analyses.

In addition, the authors wish to thank Dr. C. Dean Starr for his interest in and contribution to this study, and to Mr. R. Frenkel thanks are extended for assistance in some of the creep tests.

BIBLIOGRAPHY

1 "The Effect of Sigma Phase on the Short-Time High-Temperature Properties of 25 Chromium-20 Nickel Stainless Steel," by G. J. Guarnieri, J. Miller, and F. J. Vawter, Trans. ASM, vol. 42, 1950, pp. 981–1007.

2 "Influence of Microstructure on Creep Resistance," by G. Delbart and M. Ravery, *Metal Progress*, vol. 60, December, 1951, pp. 62–68.

3 "The Effect of Dispersions on the Tensile Properties of Aluminum-Copper Alloys," by R. B. Shaw, L. A. Shepard, C. D. Starr, and J. E. Dorn, Trans. ASM, vol. 45, 1953, pp. 249–271.

4 "Stress Rupture and Creep Tests on Aluminum-Alloy Sheet at Elevated Temperatures," by A. E. Flanigan, L. F. Tedsen, and J. E. Dorn, Trans. AIME, vol. 171, 1947, pp. 213–245.

5 "Effect of Dispersions of $CuAl_2$ on the Elevated Temperature Tensile Properties of Al-Cu Alloys," by C. D. Starr, R. B. Shaw, and J. E. Dorn, Trans. ASM, vol. 46, 1954, pp. 1075–1088.

6 "Creep Correlations in Alpha Solid Solutions of Aluminum," by O. D. Sherby and J. E. Dorn, Trans. AIME, vol. 194, 1952, pp. 959–964.

7 "The Effect of Alloying Elements on the Elevated Temperature Plastic Properties of Alpha Solid Solutions of Aluminum," by O. D. Sherby, R. A. Anderson, and J. E. Dorn, Trans. AIME, vol. 191, 1951, pp. 643–652.

8 "Some Observations on Correlations Between the Creep Behavior and the Resulting Structures in Alpha Solid Solutions," by O. D. Sherby and J. E. Dorn, Trans. AIME), vol. 197, 1953, pp. 324–330.

9 "Plastic Flow and Rupture of Metals," by C. Zener and J. H. Hollomon, Trans. ASM, vol. 33, 1944, pp. 163–235.

Discussion

W. R. Hibbard, Jr.,[5] and R. W. Guard.[5] The authors investigated an important aspect of the effects of alloying. If their quantitative conclusions are valid, it will make a great advance in this field. However, there are several points in connection with the experimental procedure about which questions may be raised.

The photomicrographs shown in reference (3) of the paper indicate considerable deviations from uniform, round particles such as were assumed in the calculation of the mean free value used. It also is assumed that all precipitation during the final aging occurs on previously precipitated particles and that there are no fine particles present in the coarse dispersions which would not be observed at the low magnifications used.

We would like to ask the authors if they feel that these deviations from the assumed particle shape are sufficient to cause lack of agreement between various alloys. If one replots Fig. 2 of the paper on rectangular co-ordinates, there appear to be significant, consistent differences between the different compositions, Fig. 9 of this discussion. Do the authors feel that these are real differences or are simply the effect of scatter in the results?

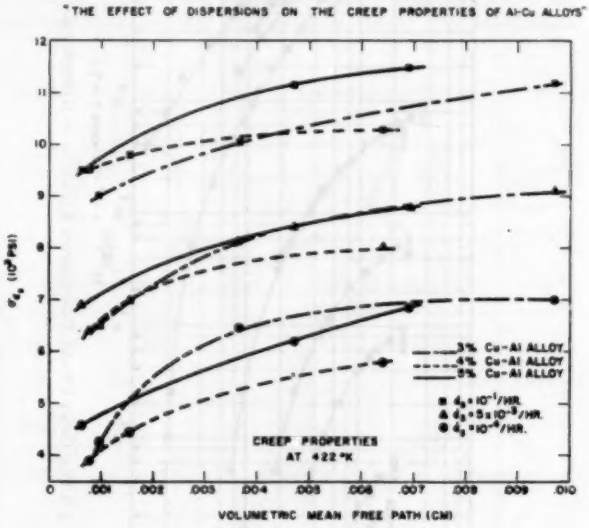

Fig. 9 Replot of Authors' Fig. 2

The conclusion regarding the inversion in superiority of the different dispersions at an intermediate temperature region could well be accounted for by the difference in grain size between the two dispersions for which the results are plotted. We wish to ask if this inversion has been observed for all of the dispersions, or if it was only observed for the data plotted.

For these reasons we wish to question the quantitative validity of the authors' conclusions, although we feel that the general principles proposed may be entirely valid in the field of dispersion-hardened alloys.

---

[5] Research Laboratory, General Electric Company, Schenectady, N. Y.

Authors' Closure

The questions raised by Messrs. Hibbard and Guard are well taken and are deserving of further attention. The superiority of the coarse dispersions in the intermediate-temperature range has been demonstrated for all the alloys during elevated temperature tensile tests (5). Since it has been shown (Fig. 5 of the paper) that the creep-stress or ultimate tensile-strength data superimpose when plotted as a function of Z, tensile data alone can be utilized to prove the points of inversion of the properties as a function of Z. Fig. 10 of the paper is a plot of the ultimate tensile strength versus the mean free path as a function of Z for all the alloys. It can be seen readily that a first inversion occurs at $\ln Z \cong 45.0$, and a second inversion at $\ln Z \cong 29.0$. These results are in good agreement with the inversion of the creep properties for the 3 per cent M and 3 per cent VC dispersions and suggest that the results of Fig. 5 are not to be attributed to grain-size differences.

With regard to the scatter of the data noted in Fig. 2 or as replotted in Fig. 9, attention is called to the statement recognizing that "some unknown factor might yet be affecting the creep resistance." During the study of the data other possible correlations in terms of variables such as alloy composition, heat-treating procedure, and shape of dispersions in conjunction with the volumetric mean free path were investigated. It was not possible, however, to establish any additional trend.

It is not believed that additional precipitation took place during the final aging treatment of the alloys: (*a*) Examination of the coarse dispersions at ×2000 did not reveal additional fine particles. (*b*) If such precipitation had taken place, the amounts would have been so different for each aging treatment, that the results likely would not have been so generally consistent.

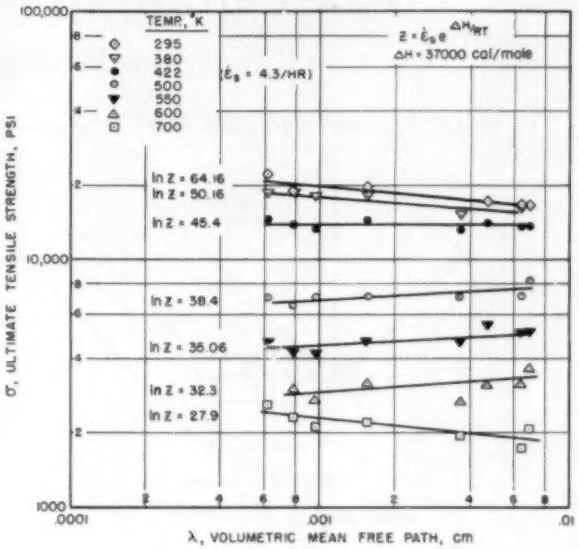

Fig. 10 Correlation Between Ultimate Tensile Strength and Volumetric Mean Free Path as a Function of $z = \dot{\epsilon}_s e^{\Delta H/RT}$

Machinability Research With J&L Tool Dynamometer on Titanium 150A

By LEIF FERSING[1] AND D. N. SMITH,[2] SPRINGFIELD, VT.

A broad definition of machinability would be the relative cost per square inch of machined surface when all cutting conditions are at an optimum for most economical production. For several years the J&L tool dynamometer (1, 2)[3] has been used successfully for evaluating a number of factors affecting machinability such as grades of carbides, types of coolants, methods of applying coolants, tool geometry, tool finish, cutting speeds, feeds, and materials. With knowledge of these factors, it is possible to approximate a most economical rate of production. In this paper the relation between changes in loads on tools and tool wear is shown through test results and how, in a short time, with the help of a tool dynamometer, reliable information for successfully machining titanium 150A was obtained.

Introduction

THE J&L tool dynamometer permits measuring the three component loads, the tangential, the feed, and the radial, Fig. 1, on a tool in cut. With recording instruments, the three components are recorded continuously and permanently as a tool progresses in the cut. The tangential load is predominantly determined by the cross section of a cut and changes only slightly as a tool wears. The tangential load may be termed the "horsepower component" because this load times the surface speed accounts for substantially all the power expended. The feed load and radial load are mainly penetrating and frictional loads and are very sensitive to wear and tool geometry. They often increase by several times during the useful life of a tool.

In Fig. 2 curves of the feed and the radial loads on a tool in cut are plotted against square inches of machined surface together with a curve showing the measured wear land. The characteristics of the radial and feed-load curves and the wear-land curves are generally similar. The loads increase more rapidly at the beginning of a cut, then level off, only to increase more rapidly again as a tool nears the end of its useful life (3). Obviously, the wear land is zero on a sharp tool whereas the three initial component loads depend upon the material, tool geometry, and cutting conditions.

This proportionality between load increase and wear-land increase makes it possible and valid to use the load increase as a control when running comparative tests of tool life. By running each test to the same percentage increase of feed load over its initial value, and measuring performance in terms of square inches of surface developed, valid comparisons can be made. This technique is more convenient than using the wear land itself as a control for two reasons; a visible record is produced concurrent with the running of the test, making interruption and inspection unnecessary; and the indicated load is the result of combined average dimensions of cratering and the wear land which is frequently of very irregular shape and therefore difficult to measure. It is not necessary to leave a tool in a cut until it is worn out. Reliable information can be obtained, whether 50, 100, or 150 per cent increase in feed load is used as the terminating point of the test.

In order to determine expected tool life for a production line, it is necessary to correlate maximum permissible wear land or cratering with the resultant increase in feed load. The permissible increase in a feed load varies greatly with material, tool geometry, and carbide. (Example; see Fig. 35 and tools shown in Fig. 36.)

When cutting-speed tests are run using preselected feed-load increase as the index of tool life, and the life (measured as area turned) is plotted against cutting speed as the variable, the curve is hyperbolic and on a log-log plot is a straight line. This is also

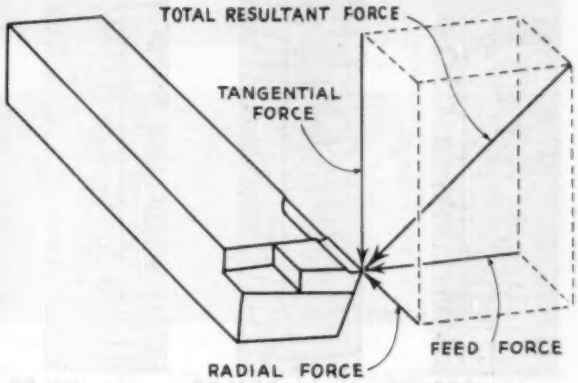

FIG. 1 COMPONENTS OF TOOL LOADS

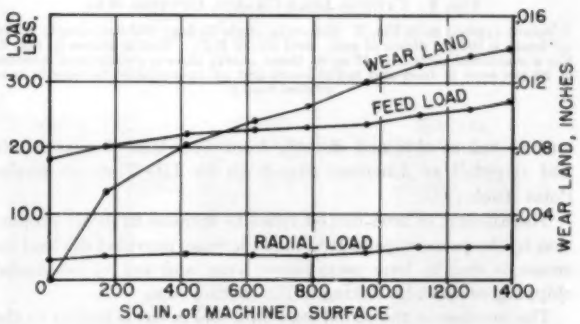

FIG. 2 TYPICAL RELATIONSHIP BETWEEN INCREASE IN FEED LOAD AND WEAR LAND

(Cutting speed 500 fpm; feed 0.015 ipr; depth of cut 0.100 in. Coolant: Dry. Tool, Fig. 11. Material: Steel 8647; hardness RC 12–14. Each segment represents a new pass.)

---

[1] Experimental Engineer, Jones & Lamson Machine Company. Mem. ASME.

[2] Jones & Lamson Machine Company.

[3] Numbers in parentheses refer to the Bibliography at the end of the paper.

Contributed by the Research Committee on Metal Processing and presented at the Annual Meeting, New York, N. Y., November 29–December 4, 1953, of THE AMERICAN SOCIETY OF MECHANICAL ENGINEERS.

NOTE: Statements and opinions advanced in papers are to be understood as individual expressions of their authors and not those of the Society. Manuscript received at ASME Headquarters, September 29, 1952. Paper No. 53—A-207.

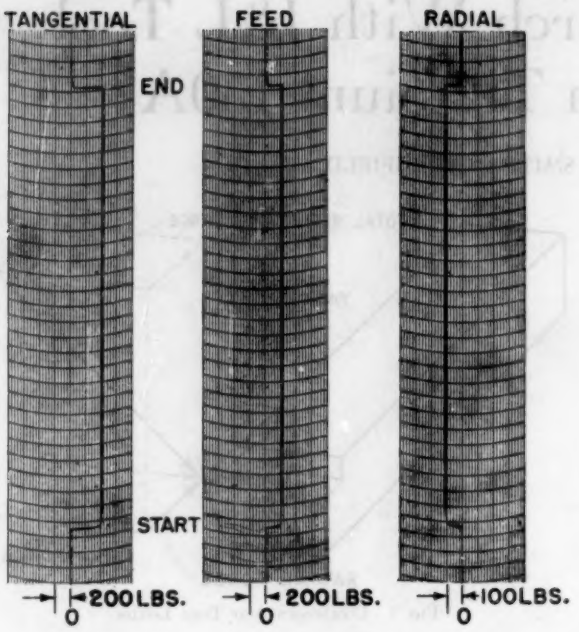

FIG. 3 TYPICAL LOAD CHARTS, CUTTING WET

(Coolant applied as in Fig. 5. Side-rake angle 10 deg; 600 fpm speed; 0.015 ipr feed; 0.100 in. depth of cut; steel 30–32 R.C. Tool is shown in Fig. 6. For a machined surface of 47 sq in. these charts show a steady load increase of 20 per cent in feed and radial loads and no appreciable increase in tangential load.)

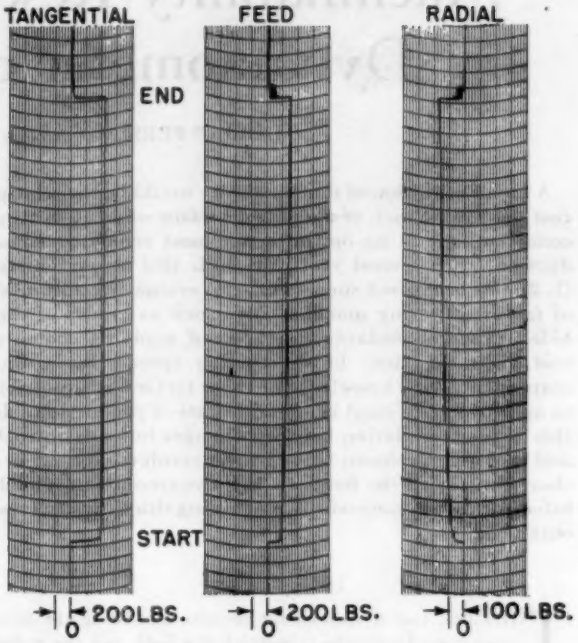

FIG. 4 TYPICAL LOAD CHARTS, CUTTING DRY

(Cutting data same as for Fig. 3. For same area of machined surface feed load has increased 80 per cent, radial load 180 per cent, and tangential load 10 per cent. Tool is shown in Fig. 6.)

true of values obtained directly from wear-land measurements and accepted as American Standards for Life Tests on Single-Point Tools (4).

The amount of area turned tends to increase in direct proportion to the percentage of feed-load increase, provided the load increase is due to true progressive wear and not to accidental chipping or sporadic flaking of the cutting edge.

The increase in the radial load on a tool in cut is similar to the increase in feed load. However, the radial load does not increase proportionally to square inches of machined surface when several passes are necessary for sufficient data because the steadily decreasing diameter of the work reduces the bearing of the work on the nose of the tool. (See Fig. 2 where every point represents a new pass, i.e., a smaller diameter on the work. Loads indicated are those at the end of each pass.) The feed load, on the other hand, for all practical purposes seems to be independent of work diameter. The rate of increase in the tangential load on a tool due to wear is too low to be used reliably as an index of tool life.

Two factors which determine tool life are rate of wear and chipping or flaking of the cutting edge. When a tool is taken out after a test cut and the wear land measured, it is almost impossible to differentiate between the two. A great advantage of a tool dynamometer with recording instruments is that wear and chipping can each be "observed" as a separate phenomenon as the tool progresses in a cut. Sudden or erratic increases in either the feed or the radial loads indicate chipping or flaking of the cutting edge. The test can be stopped without unnecessary loss of time and material; also, misleading test cuts can be discarded if the records show anything other than regular wear. Improved surface finish on a tool or retipping if a tool has been reground several times may overcome difficulties caused by chipping. Some carbides stand repeated regrinding better than others.

In Figs. 3 and 4 are shown charts of the three component loads on two tools, one from a dry cut and one from a wet cut, with two jets as shown in Fig. 5, all other factors such as cutting speed, diameter of work, and so on, being alike. Photographs of the two tools are shown in Fig. 6.

The tool used without coolant shows a common type of wear land, deep at the nose, encountered on most carbides when cutting either dry or with the standard method of cooling by a single source flooding the top of the tool. The tool used with two coolant jets (see also Fig. 36) shows a uniform, ideal type of wear along the cutting edge. The load charts indicate very clearly what has happened. The radial and the feed loads for the dry tool have increased considerably more than for the cooled tool. There is no doubt which condition would produce the better tool life.

Other variables can be introduced, such as tool grind, grade of carbide, and so on, and comparative test runs made with one variable changed at the time. With a minimum amount of effort it is thus possible to determine the best over-all cutting condition for a given material and cutting speed. The chip breakers for these two tools, Figs. 3 and 4, were provided with a 10-deg positive rake. In order to emphasize the importance of tool grind, tools with zero rake angle used under identical conditions are shown in Fig. 6, and the load charts in Figs. 7 and 8. The cutting edges of both tools are flaked or chipped. The flaking can be noticed both on the tool itself (Fig. 6, lower left to right) and on the feed-load chart which shows small abrupt increases in load. Severe cases show distinct steps on the chart. A comparison between the increase in feed load and radial load, both of which are mainly frictional loads, indicates that something erratic is happening to the feed load.

The use of high cutting speeds in tests has the advantage that tool life becomes short; thus both material and time are saved. For reliable data it is important to know that a tool has been subjected to wear only and not to both wear and chipping.

The results of accelerated tests for determining the influence of hardness of material on tool life are shown in Fig. 9. Two cuts

have been taken on several test bars of 8647 steel which were all of different hardness, ranging on the Rockwell C scale from 18–20 to 42–43. For each hardness it was necessary to choose a maximum speed at which a valid test cut could be taken and a slower speed for a second test cut in order to obtain two points on the curve and draw the life line for each hardness of steel. The increase in feed load was chosen at 50 per cent over the initial value for each test. This assumes that an equal amount of wear will produce the same percentage increase in feed load regardless of hardness of material, which is only approximate.

The relation between cratering and edge wear changes with hardness of a material, cratering occurring relatively more rapidly with harder materials, and edge wear relatively more rapidly with softer materials, Fig. 10. Both types of wear show up as an increase in feed load, provided the cut is permitted to last long enough. No attempt was made to modify tool geometry

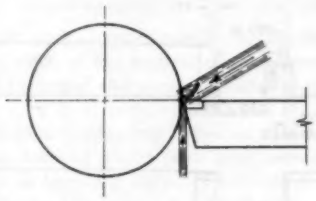

FIG. 5 METHOD OF APPLYING COOLANT

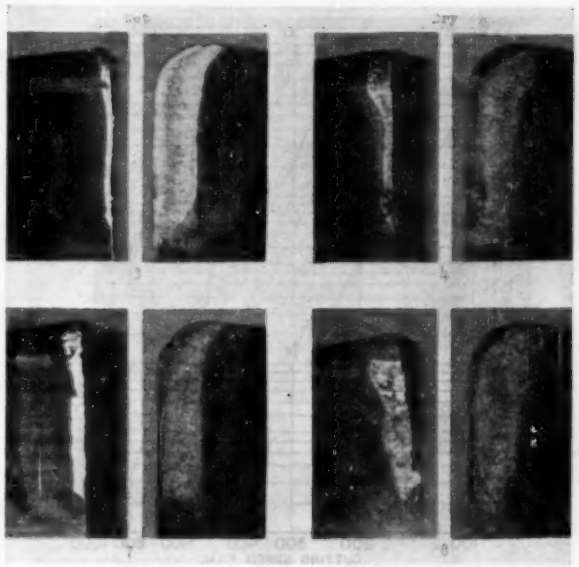

FIG. 6 PHOTOGRAPHS OF TOOLS FOR WHICH CHARTS ARE SHOWN IN FIG. 3, UPPER LEFT; FIG. 4, UPPER RIGHT; FIG. 7, LOWER LEFT; AND FIG. 8, LOWER RIGHT

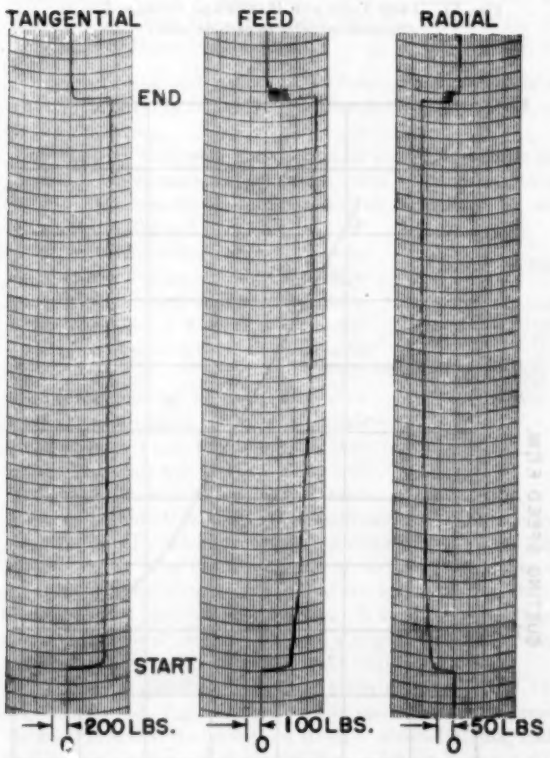

FIG. 7 TYPICAL LOAD CHARTS, CUTTING WET, WITH CUTTING EDGE CHIPPING

(Side-rake angle 0 deg; 600 fpm speed; 0.015 ipr feed; 0.100 in. depth of cut; steel 30–32 RC. Tool is shown in Fig. 6. Slightly irregular increase in feed load is indication of chipping or flaking on side-cutting edge. For a machined surface of 52 sq in. feed load has increased 70 per cent, radial load 70 per cent, and tangential abou t 11 per cent.)

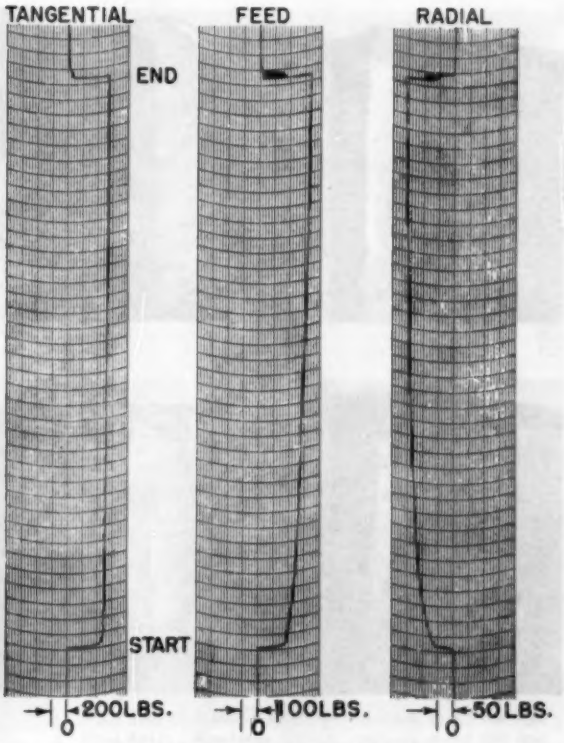

FIG. 8 TYPICAL LOAD CHARTS, CUTTING DRY, WITH CUTTING EDGE CHIPPING

(Cutting data same as for Fig. 7. For same machined area feed load has increased 90 per cent, radial load 200 per cent, and tangential about 11 per cent. Tool is shown in Fig. 6.)

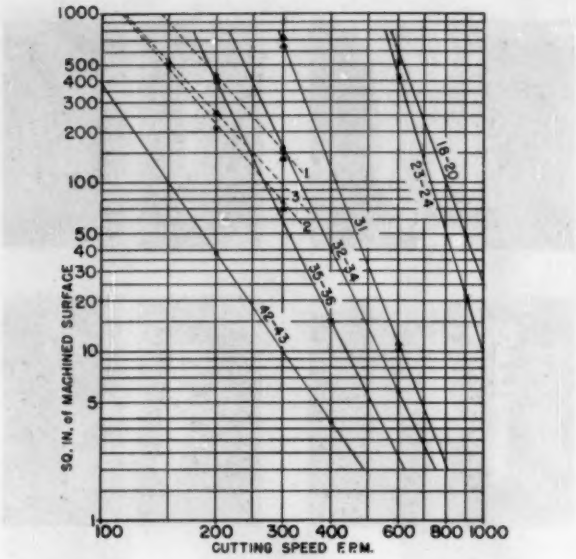

FIG. 9 CUTTING SPEED-TOOL LIFE LINES AT VARIOUS HARDNESSES OF 8647 STEEL—FULL LINES

(Tool shown in Fig. 11; 0.015 ipr feed; 0.100 in. depth of cut. Tests run to 50 per cent increase of feed load; dry. Also shown in comparison are some curves for titanium 150A, run at 0.050 in. depth of cut to 50 per cent increase of feed load, as follows: [1] 0.022 ipr feed, wet; [2] 0.022 ipr feed, dry; [3] 0.015 ipr feed, dry. These data also are shown in Fig. 31.)

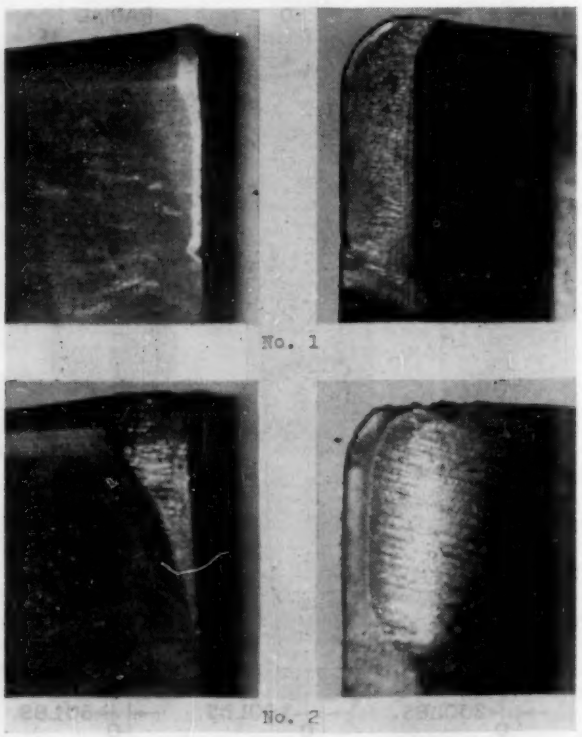

FIG. 10 PHOTOGRAPHS OF TOOL WEAR

(1, Material 8647; hardness RC 32-34; cutting speed 300 fpm; depth of cut 0.100 in.; feed 0.015 ipr. Cratering starts close to cutting edge. Compare with Fig. 36. 2, Material 8647; hardness RC 18-20; cutting speed 1000 fpm; depth of cut 0.100 in.; feed 0.015 ipr. Cratering starts away from cutting edge.)

to give maximum tool life for each hardness. The tool geometry is shown in Fig. 11.

The life-line chart, replotted as in Fig. 12, gives a conception as to how cutting speed should be changed with respect to hardness in order to maintain constant tool life when cutting dry and with all other factors held constant. The points represent an area of 100 sq in. and a feed-load increase of 50 per cent.

It is not always true that a feed load will increase as a tool progresses in a cut. Cratering many times has the effect of lowering the feed load for a short time before this load starts to increase. A factor which also may have considerable influence on the magnitude and behavior of a feed load is the design of a chip breaker. If a chip is crowded by the breaker, the pressure on the heel of the breaker influences not only the feed load, but all three components of the tool load, and results may lead to conflicting test data.

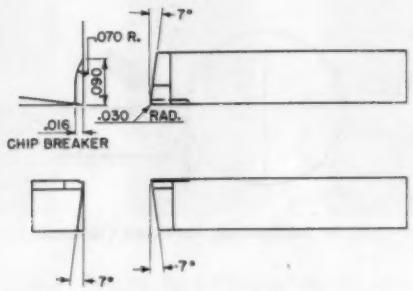

FIG. 11 TEST TOOL FOR HARDENED STEELS, FIG. 9

(Dimensions refer to carbide only.)

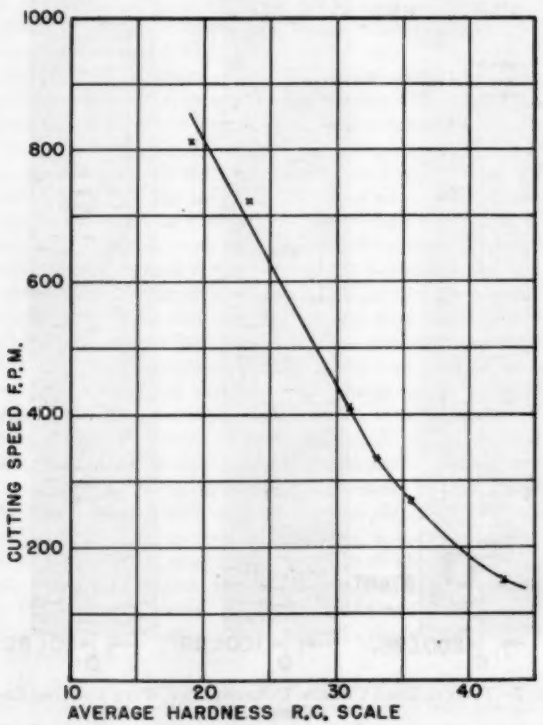

FIG. 12 EFFECT OF HARDNESS OF STEEL ON CUTTING SPEED FOR CONSTANT TOOL LIFE

(Machined areas 100 sq in.; increase in feed load 50 per cent. Plotted from Fig. 9.)

The chip breaker used on tools in Figs. 6 and 10 shows how a tool should wear with respect to a breaker in order to obtain negligible influence from the same. There is little load on the heel of the breaker (5). Another irregularity in this type of testing occurs when several passes are required for a test cut. In this case, loads are generally lower at the start of each new pass than they were at the end of the previous pass. Apparently the temperature at the cutting edge has a definite effect on the coefficient of friction between the chip and the tool..

Flaking of a cutting edge, which is actually an excessive type of wear, can be overcome by other means than changing tool grind. In many cases an increase in cutting speed will help, whereas in other cases a speed reduction is necessary. This inconsistency in behavior of carbide many times has led to wrong conclusions as tool-life lines are no longer straight when plotted on log-log paper.

Machinability of Titanium 150A

The research work on machinability of titanium 150A was done in February, 1952, at the request of the General Electric Company, which furnished the titanium metal and carboloy cutting tools.

A few preliminary tests had indicated definitely that the tool-dynamometer method would offer great advantages in making tool-life tests on titanium 150A. Three billets of titanium 150A were available for the tests. A typical microstructure of these billets is shown in Fig. 13. These billets had been rough-turned and were of the following dimensions and hardnesses:

Billet No. 1: Diam $5^{9}/_{32}$ in., length $16^{1}/_{2}$ in., hardness RC 39–40
Billet No. 2: Diam $3^{17}/_{64}$ in., length $16^{1}/_{8}$ in., hardness RC 37–40
Billet No. 3: Diam $5^{21}/_{32}$ in., length $10^{1}/_{2}$ in., hardness RC 37

Rough-turning of titanium 150A forgings for removing scale was not included in this project. Therefore results do not apply to this operation.

Preliminary tests were made to obtain some information about tool loads when machining titanium 150A as compared to steel X-1315, hardness 67–68 on the Rockwell B scale. The results are shown in Table 1.

Surface deformations due to machining, shown in Fig. 14, are a further indication that titanium is difficult to machine. When hardness of a steel is increased, surface deformations due to machining are reduced.

It is interesting to note that even though the titanium 150A was considerably harder than the steel, the tangential load (hp) was smaller. The feed load, however, was higher when a steel grade of carbide was used. The coefficient of friction between steel and steel grades of carbide, therefore, is less than for titanium 150A. The cast-iron grade of carbide, 883, shows more favorable friction characteristics and the loads indicate that this carbide should permit longer tool life. It was also noted that the cast-iron grades of carbide produced a bright silver chip, whereas the steel grades produced a discolored chip.

The effect of cutting speed on tool loads is shown in Figs. 15 and 16, and of feed in Fig. 17. The cutting-speed curves indicate that the friction is lowest at a cutting speed of about 150 fpm, and the feed curves indicate that the friction is lowest between 0.011–0.020 in. feed per revolution. They also show that the coefficient of friction when machining titanium is considerably higher than when machining both high and low-carbon steels (1). (Coefficient of friction = feed load/tangential load at 0 rake angle and with sharp tools.)

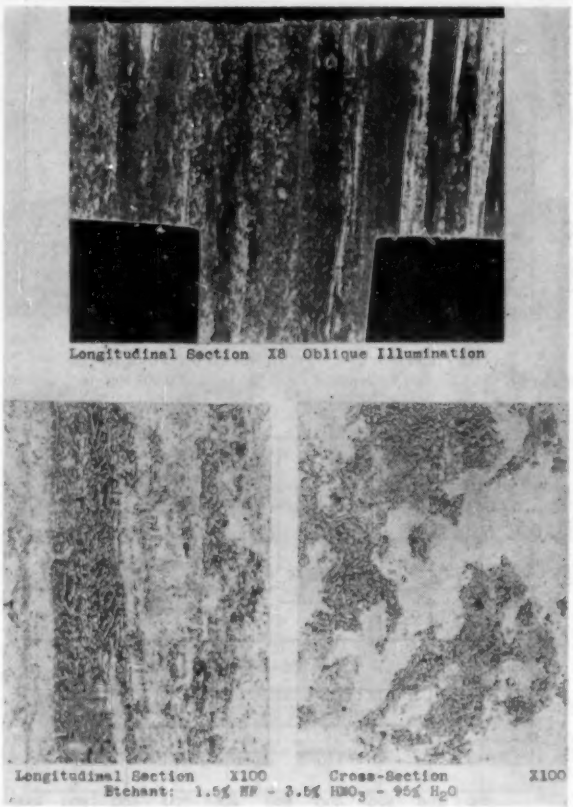
Longitudinal Section X8 Oblique Illumination
Longitudinal Section X100
Cross-Section X100
Etchant: 1.5% HF - 2.5% HNO3 - 96% H2O

Cr, 4.5 N, 0.10
Fe, 1.75 C, 0.04
O, 0.30 W, 0.01

Fig. 13 Macro and Microstructure of Titanium 150A; ×100
(Courtesy Thomson Laboratory, General Electric Company.)

TABLE 1 RESULTS OF TESTS COMPARING TITANIUM 150A AND STEEL X-1315

Material	Carbide	Rake angle, deg	Depth of cut, in.	Feed, ipr	Speed, fpm	Coolant	Feed load, lb	Tangential load, lb
X-1315	KM[a]	5°	0.125	0.022	120	dry	420	900
X-1315	KM	5°	0.125	0.022	120	wet	440	850
Ti 150A	KM	5°	0.125	0.022	118	dry	520	750
Ti 150A	KM	5°	0.125	0.022	118	wet	550	800
Ti 150A	883[b]	0°	0.125	0.022	118	dry	400	720

[a] Steel grade.
[b] Cast-iron grade.

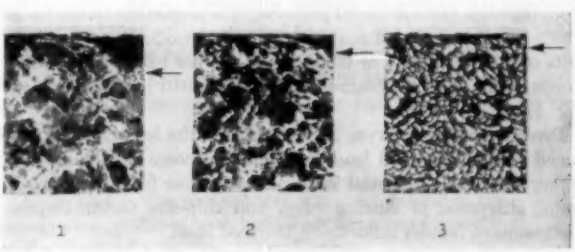

1 Steel 8647; Hardness RC 14; cutting speed 100 fpm
2 Steel 8647; Hardness RC 14; cutting speed 600 fpm
3 Titanium 150A; Hardness RC 40; cutting speed 150 fpm

Fig. 14 Microstructure of Surface Deformations Due to Cutting Speed at 0.015 Ipr Feed; ×200
(Arrows indicate depth of deformation.)

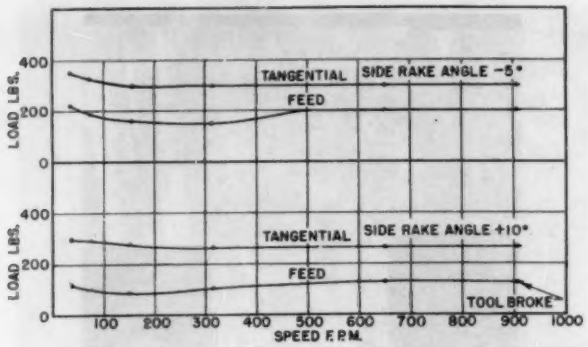

FIG. 15 EFFECT OF CUTTING SPEED ON TOOL LOADS
(Material, titanium 150A; depth of cut 0.125 in. feed 0.007 ipr, dry; carbide 883.)

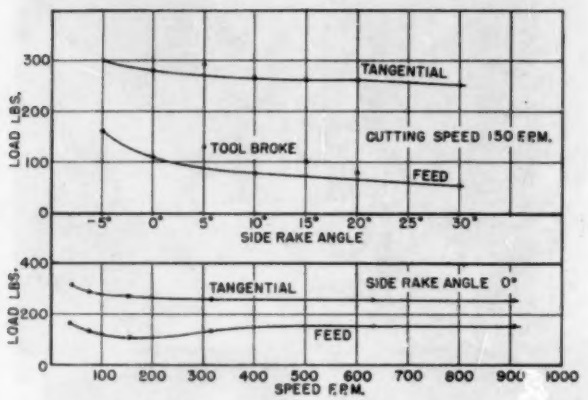

FIG. 16 EFFECT OF SIDE-RAKE ANGLES ON TOOL LOADS AND CUTTING SPEED ON TOOL LOADS
(Material, titanium 150A; depth of cut 0.125 in.; feed 0.007 ipr, dry; carbide 883.)

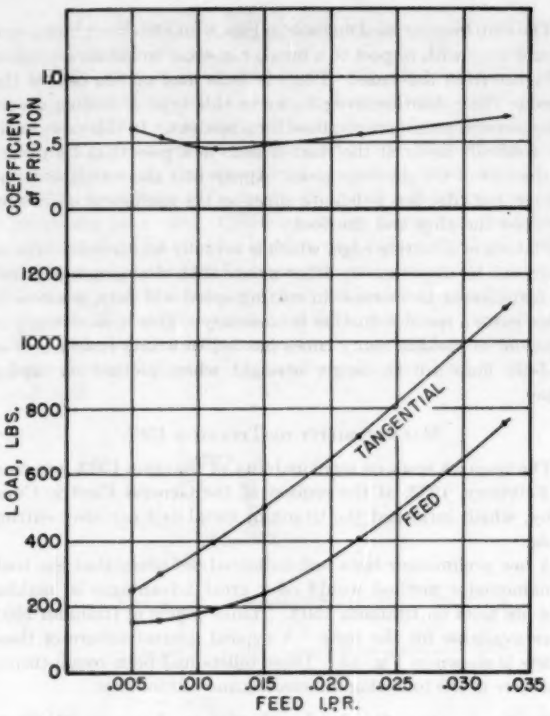

FIG. 17 EFFECT OF FEED ON TOOL LOADS AND ON COEFFICIENT OF FRICTION FOR SHARP TOOLS
(Material, titanium 150A; cutting speed, 118 fpm; side-rake angle 0 deg; depth of cut, 0.125 in.; carbide 883; one tool. Feed changed during cut.)

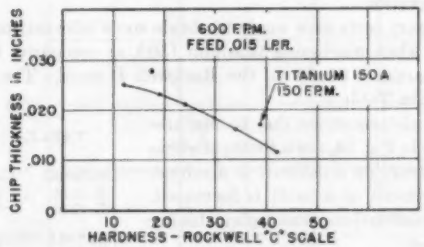

FIG. 18 EFFECT OF HARDNESS OF STEEL 8647 ON THICKNESS OF FRACTURE OF CHIP
(Included here for comparison is also shown the thickness of chip from titanium 150A at 0.015 ipr.)

Another comparison between steel and titanium 150A is shown in Fig. 18. Here the thickness of a steel chip is plotted against hardness of steel. The thickness of the fracture of broken chips was measured with a microscope. Tool life or machinability of steel has a definite relation to the ratio of chip thickness to feed. Tool life becomes shorter as this ratio decreases because the load per square inch on carbide goes up (compare Figs. 10 and 36). The thickness of a titanium chip at the same feed, but much lower cutting speed, indicates very definitely that machining of titanium is difficult because the chip thickness decreases with increasing speed. In this connection it may be pointed out that when studying high rates of metal removal, it is important to use feeds which are practical and economical on the production line. Results obtained at feeds of 0.005 in. or less per revolution are apt to contradict results obtained at feeds of 0.010 ipr and up (11), Fig. 17.

Directions of the curves indicate that if the feed had been reduced further, the feed load would have become as high or even higher than the tangential load. At very fine feeds work hardening, sharpness of cutting edge, and chip-size factor become predominant factors influencing the feed load.

TOOL LIFE

The amount of material available for this research work was very limited. In order to cover enough variables, it was necessary to limit each test to one cut, study trends, and draw conclusions without the benefit of statistical averages of a number of duplicate tests. Experience has shown, however, that the load-measurement technique of testing does give reliable results even without repeat tests. Reproducibility of results is indicated in Fig. 9 where points from a few duplicate runs are plotted, with obviously good agreement. Only when the feed-load chart definitely indicated that misleading results were probable was a test repeated. Any grade of carbide is in itself a variable. This fact had to be neglected. Great care was taken that the desired tool geometry was correct and that the finish along the cutting edge was good.

It was further necessary to assume that the titanium 150A was homogeneous and that no work hardening took place. These assumptions, of course, are not correct. However, as tests progressed, duplicate runs were made on several promising carbides to gain more reliable information with respect to carbides and to reduce possible errors. Furthermore, in order to save

material, test cuts were limited to 0.050 in. depth and to an increase in feed load to 50 per cent over initial values.

The project was divided into six steps which covered the following variables:

Test 1: Grades of carbides, without coolant.
Test 2: Types of coolants.
Test 3: Tool geometry, without coolant.
Test 4: Cutting speed with and without coolant.
Test 5: Feed without coolant.
Test 6: Tool-life tests with coolant.

Tests 1, 3, and 5 should have been made both with and without coolant. Lack of material prevented this.

Test 1 Cast-Iron Grades of Carbide

It had already been established during preliminary tests that the cast-iron grade of carbide, 883, was superior to the steel grades, KM and K5H. Reports in various periodicals on machining of titanium indicated that cast-iron grades of carbide consistently outperformed steel grades of carbide (7). Therefore it was decided to narrow the scope of this research work mainly to cast-iron grades of carbide made by different manufacturers in a search for the most suitable grades.

A number of different grades of carbides were supplied by the Carboloy Department of General Electric Company, for cutting tests in order to establish some kind of trend in carbide composition (8). It was found that if cobalt was above 6 per cent, tool life would go down. For example, carbides 77B, 78C, and 55B had a tool life of approximately zero. By zero tool life is meant a condition when the feed load shows no sign of leveling off. The result was always a completely broken-down cutting edge.

A high percentage of tantalum carbide had a rather damaging effect on tool life. No. 907 with 20 per cent TaC lasted only one eighth as long as 905 with 3.85 per cent TaC. Chromium carbide and titanium carbide both had a tool life of zero. Carbides 2A5, 883, 2A7, K6, 905 HE, HA, and HF have none, or a very small percentage of TiC, whereas steel grades of carbide generally contain 4 per cent or more titanium carbide. Of importance also may be the fact that the thermal conductivity of cast-iron grades of carbide is much higher than of steel grades of carbide (9).

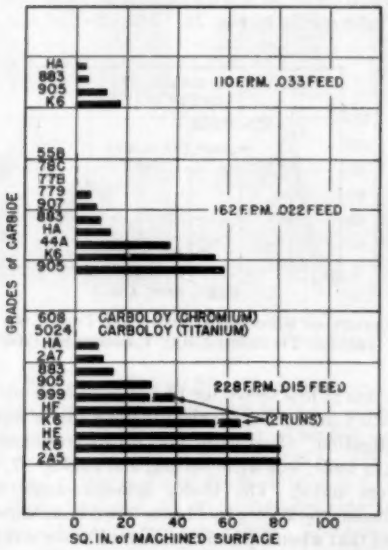

Fig. 19 Comparison of Carbides for Machining Titanium 150A, Dry, 0.050 In. Depth of Cut; 50 Per Cent Increase in Feed Load

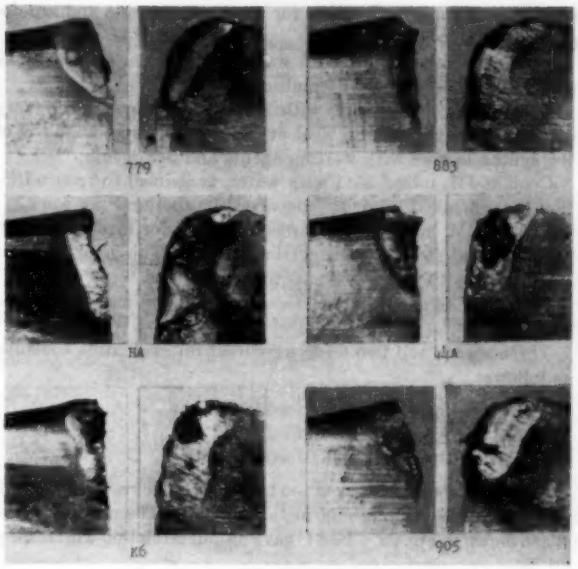

Fig. 20 Photographs of Tools Used in Test 1 at 162 Fpm Cutting Speed and 0.022 Ipr

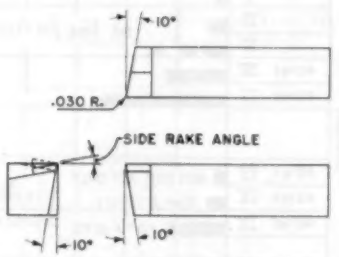

Fig. 21 Geometry of Test Tool; Angles Refer to Carbide Only; Side-Rake Angle Varied From —10 to 20 Deg in Test 3A

Three speeds and three feeds were used for evaluating grades of carbide. The speeds and feeds were so chosen that each combination resulted in approximately a constant rate of metal removal. The data (10) are shown in Fig. 19, photographs of various tools in Fig. 20, and tool grind in Fig. 21 (10-deg side rake angle). The affinity of titanium 150A for the various grades of carbide is noticeable, the breakdown of the cutting edge being caused by cratering and welding rather than edge wear. Only carbides HE, HF, and 779 show definite edge wear. It also was noticed that if a tool was allowed to dwell in a cut, titanium 150A would weld to the cutting edge and destroy it. A few irregularities occurred in this test with respect to depth of cut. It is not believed, however, that this error had much effect on the results.

Test 2 Coolants

As in Test 1, the coolant test was an accelerated one. High speeds were combined with high feeds to obtain a quick indication of the merit of a coolant. Furthermore, a carbide was picked which had shown only average performance in the previous test. Types of coolants were chosen without preference but with the hope that one of the various characteristics of the coolants would give a positve indication of advantage. The mixtures used were those recommended for steel. Five different coolants were

available at Jones & Lamson for comparative tests and are described as follows:[4]

Coolant I, mixed 40:1 with water, was chosen arbitrarily as representative of standard emulsions.

Coolant II, mixed 50:1 with water, has proved itself very effective when machining steel at high cutting speeds and is of the synthetic type with wetting agents and detergents.

Coolant III, mixed 25:1 with water, is claimed to reduce friction by "chemical lubricity" between the tool and the work.

Coolant IV, mixed 40:1, is recommended for machining both cast iron and steel at high cutting speeds. This is also a synthetic type with wetting agents and detergents.

Coolant V is a cutting oil recommended for machining titanium.

Three speeds and two feeds were used for evaluating coolants, as follows:

A, Cutting speed 440 fpm; feed 0.015 ipr
B, Cutting speed 315 fpm; feed 0.015 ipr
C, Cutting speed 218 fpm; feed 0.022 ipr

A speed of 440 fpm proved too fast for reliable results. Tests B and C give the same rate of metal removal. The results of Test B are shown in Fig. 22. Test C gave a similar relation with respect

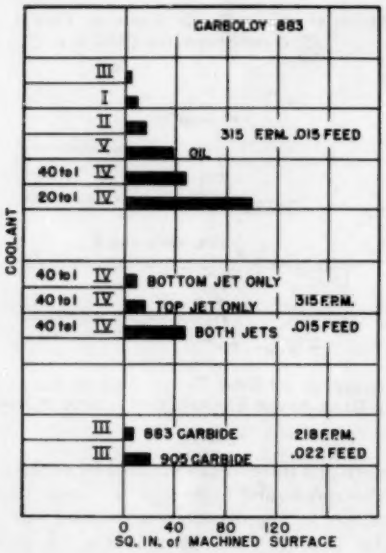

FIG. 22 EVALUATION OF COOLANTS FOR MACHINING TITANIUM 150A

(Method of applying coolant shown in Fig. 5; tool geometry in Fig. 21; 10-deg side-rake angle.)

to coolants. The coolant was applied as shown in Fig. 5, the bottom jet being 1/8 in. diam. The pressure in the system was about 1 1/2 psi. This pressure is definitely too low for best results. The relative value of each jet as against both jets also is shown in this figure as well as a re-evaluation of two grades of carbide, 883 and 905. The relative merits of these carbides were the same when cutting dry or wet.

Coolant IV gave the longest tool life. In order to gain some information regarding mixture, a second test run was made with Coolant IV mixed 20:1 with water. The gain in square inches of machined surface was considerable. Coolant IV 20:1 was used in all other wet tests.

A certain conception of machinability of titanium can be gained from Tests 1 and 2. A feed of 0.015 in. was consistently better

[4] Trade names withheld by request.

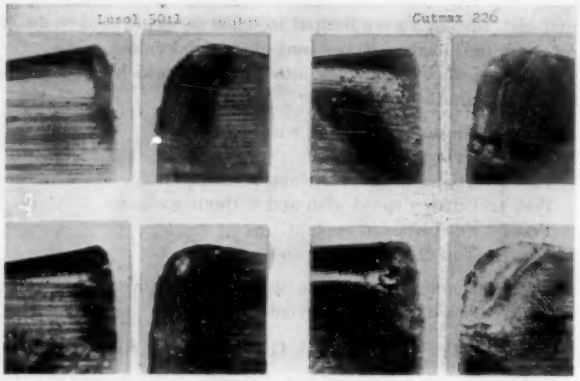

Upper row: 0.015 in. feed, 315 fpm cutting speed
Lower row: 0.022 in. feed, 218 fpm cutting speed

FIG. 23 PHOTOGRAPHS OF A FEW TOOLS USED ON TITANIUM 150A FOR EVALUATING COOLANTS. TEST 2, CARBIDE 883

than 0.022 in., and 0.022-in. feed was better than 0.033-in. feed when the rate of metal removal was kept constant. Photographs of tools are shown in Fig. 23.

The cutting oil, Coolant V, showed relatively good results. However, there is a definite fire hazard in using oil as a coolant when machining titanium because when a tool breaks down, the heat at the point becomes very high, producing a white-hot chip. At high cutting speeds the glare resembles that of arc welding. For this reason all further research with cutting oils was discontinued.

TEST 3 TOOL GEOMETRY

This test was subdivided into five tests, as follows:

3A, Side-rake angle.
3B, Side-cutting-edge angle (lead angle).
3C, Nose radius.
3D, Side-relief and end-relief angles.
3E, End-cutting-edge angle.

Test 3A. The tests of tool life versus side-rake angles were made at 281 fpm cutting speed and 0.015 ipr feed. The tool is shown in Fig. 21 and the results in Fig. 24. The effect of side-rake angles

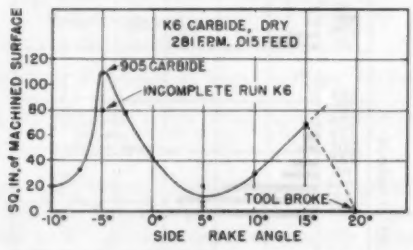

FIG. 24 EFFECT OF SIDE-RAKE ANGLE ON TOOL LIFE WHEN MACHINING TITANIUM 150A; CARBIDE K6 (905)

on tool life was at first tested for 10, 5, 0, —5, and —10 deg. The great variation in tool life for the different angles warranted further investigation. Two more test runs were made with 5-deg positive-rake tools; one with —5 deg, and angles —7, —3, 15, and 20 deg were added. The 15-deg side-rake-angle tool showed promise whereas the 20-deg tool broke down immediately. It also was noticed that when a positive-rake tool broke down, the damage to the carbide was much more severe than for negative-rake tools.

The second test with a —5-deg rake tool was not completed because the rate of increase in feed load indicated that the first test was valid. The 5-deg positive tools also supported the results obtained in the first test run. Because the aim was to find the highest practicable rate of metal removal, the possibilities of high positive rakes combined with slow speeds (100 fpm and lower) and/or feeds were not investigated further.

Tool-life lines of the type shown in Fig. 9 would have given a complete picture of side-rake angles versus cutting speed, especially if values had been obtained both with and without coolant and for several grades of carbide. The temperature of the chip and the tool increased noticeably with negative rakes. A dull red chip was produced during the entire cut when the —10-deg rake tool was tested. It was felt that the included angle of the cutting edge was of more importance with respect to strength of the cutting edge and the ability to dissipate heat than the value of rake angle itself. Even though loads are higher for negative rakes than for positive rakes, Fig. 16, the larger included angle is advantageous. For this reason it was decided to do all further testing with —5-deg rake tools, the rake angles to be measured at right angles to the cutting edge. Photographs of tools from Test 3A are shown in Fig. 25.

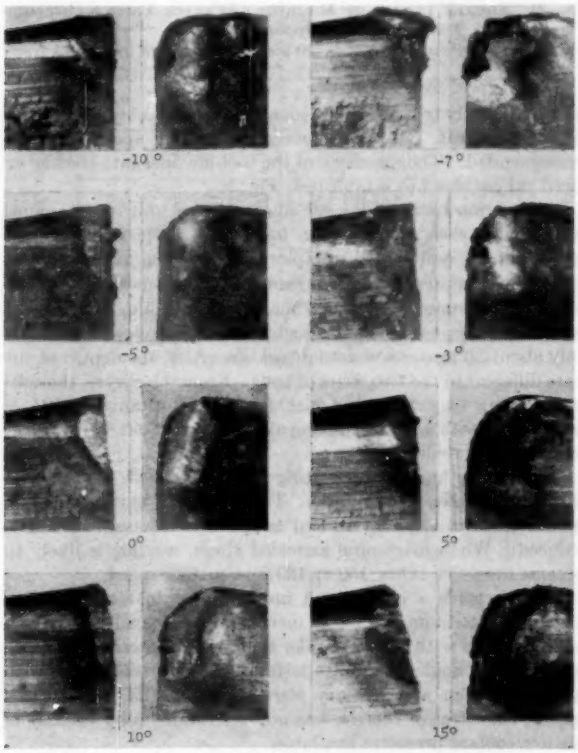

FIG. 25 PHOTOGRAPHS OF TOOLS USED IN TEST 3A; CARBIDE K6

Test 3B. (Tool shown in Fig. 27). Tool life improved with an increase in side cutting-edge angle, with 60 deg, the highest angle tested, giving longest life, Figs. 26 and 28. This test, as well as all further tests on tool geometry, was accelerated further by increasing cutting speed to 300 fpm with feeds of 0.015 to 0.022 ipr.

Test 3C. Tools having 0, 30, 45, and 60-deg side-cutting-edge angles were provided with zero nose radius. The side-relief angle and the end-relief angle were lapped so as to produce a sharp point. All tools showed a substantial increase in tool life when compared to tools with 0.030-in. nose radius, Fig. 27.

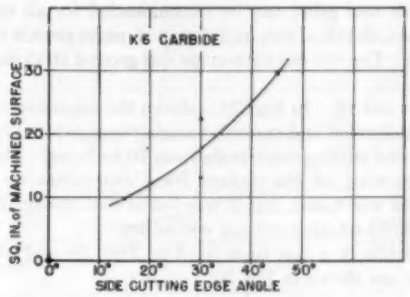

FIG. 26 EFFECT OF SIDE-CUTTING-EDGE ANGLE ON TOOL LIFE WHEN MACHINING TITANIUM 150A
(Cutting speed 300 fpm, feed 0.015 ipr, dry. Drawing of tool, Fig. 27.)

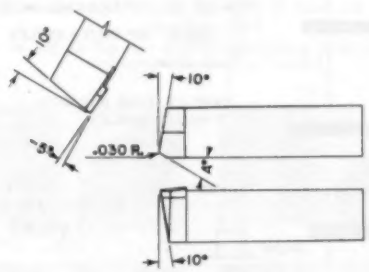

FIG. 27 GEOMETRY OF TEST TOOL FOR TEST 3B, FIG. 26
(Dimensions refer to carbide only.)

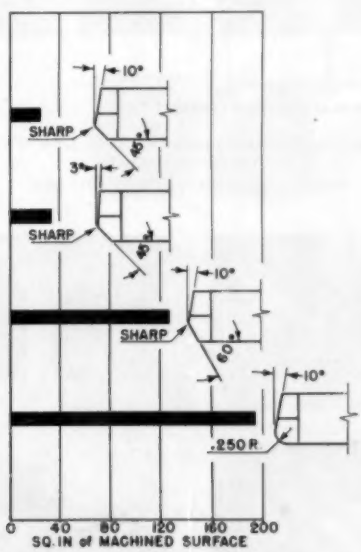

FIG. 28 EFFECT OF TOOL GEOMETRY ON TOOL LIFE WHEN MACHINING TITANIUM 150A, DRY
(Cutting speed 300 fpm; feed 0.022 ipr; side-relief and end-relief angles 10 deg; side-rake angles —5 deg at right angle to cutting edge.)

Another tool was ground as shown at the top in Fig. 30 to determine if reducing the contact along the end-cutting-edge angle would improve tool life. The results indicated that this was the case. The finish on the work obtained with sharp-pointed tools was very acceptable for roughing operations.

A tool with 1/4-in. nose radius, Fig. 28, was tested for comparison with tools having substantial side-cutting-edge angles. This tool gave the longest tool life and also the most easily handled

chips. This tool grind can be recommended for all cuts where tool pressure, depth of cut, and design of parts permit the use of such a tool. The —5-deg rake angle was ground at 45 deg relative to shank.

Tests 3D and 3E. In Fig. 29 is shown the improvement in tool life when side-relief and end-relief angles were reduced from 10 to 7 deg and end cutting-edge angle from 10 to 3 deg. The adverse effect of choking off the coolant from underneath by reducing these angles was tested, but it was found that the smaller angles were beneficial whether cutting wet or dry.

Photographs of a few tools used in Test 3B and of a $\frac{1}{4}$-in. radius tool are shown in Fig. 30.

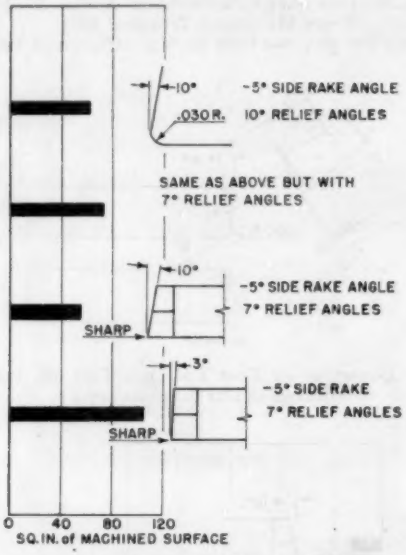

FIG. 29 EFFECT OF TOOL GEOMETRY ON TOOL LIFE WHEN MACHINING TITANIUM 150A, DRY
(Cutting speed 300 fpm; feed 0.015 ipr.)

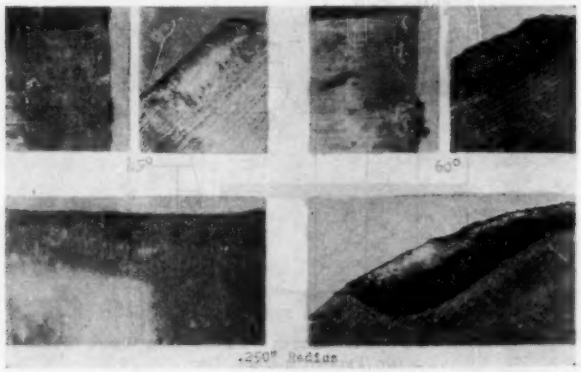

FIG. 30 PHOTOGRAPHS OF A FEW TOOLS USED IN TEST 3B; CARBIDE K6

TEST 4 CUTTING SPEED

The tool used in these tests was provided with —5-deg side-rake angle and is shown in Fig. 21.

Tool life goes up as speed is decreased, Fig. 31. At 300 fpm cutting speed, running dry, the chip comes off at a dull red heat. The edge of the chip, which is thinner as a result of the nose radius, comes off at a white heat. At very high speeds (600 fpm),

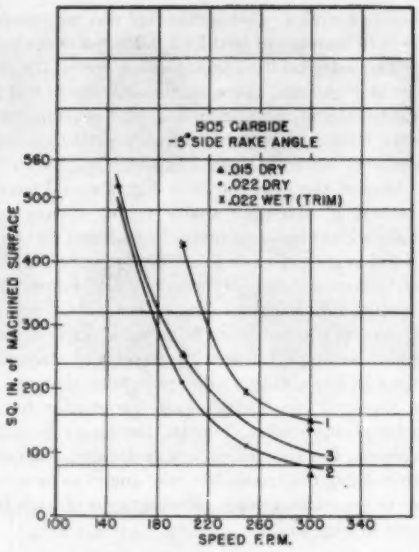

FIG. 31 SQUARE INCHES OF MACHINED SURFACE VERSUS CUTTING SPEED, TITANIUM 150A
(Life lines of curves in Fig. 9; 50 per cent increase in feed load.)

the chip is likely to catch fire as soon as the tool has been subjected to a slight wear. Therefore excessive cutting speeds are not recommended. The extension of the tool-life lines into the higher speed ranges was not established, Fig. 9.

The relation between the life lines for steel and for titanium, even though each represents an increase of 50 per cent in feed load, does not represent a true picture of relative machinability. The 50 per cent increase in feed load on the tools used for machining titanium represents almost maximum tool life, whereas the 50 per cent increase in feed load when machining steels represents only about 30 per cent of actual tool life. Also, the depths of cut were different in the two series of tests. From the curves, the conclusion may be drawn that machinability of titanium 150A is comparable with an oil-hardening alloy steel of about 42–43 Rockwell on the C scale.

On the other hand, when cutting speed is reduced, the behavior of titanium differs from steel. Titanium can be machined at speeds down to almost zero and as speed is reduced, welding is reduced. When machining annealed steels, welding is likely to become excessive below 150 or 180 fpm cutting speed.

Coolant gives a pronounced improvement in tool life when machining titanium. Rate of increase of feed load was halved for some cuts with negative-rake tools. A few tools with large positive-rake angles also were tested and improvements as high as 5:1 between wet and dry were recorded. At high cutting speeds, the effect of coolant was not determined fully because of the low coolant pressures available.

TEST 5 FEED

The same tool geometry and carbide were used as in Test 4. This permitted using some data from the previous test. Feeds 0.011, 0.015, 0.022, and 0.033 were tested at 150 fpm; feeds 0.007, 0.011, 0.015, and 0.022 at 200 fpm; and 0.011 and 0.022 at 250 fpm cutting speed. The results are shown in Fig. 33. The results at 200 fpm cutting speed are somewhat erratic when compared with 150 fpm cutting speed, probably because the billet (No. 3) for this and the following test had more blowholes and hard spots than the two previous billets. Photographs of tools are shown in Fig. 32.

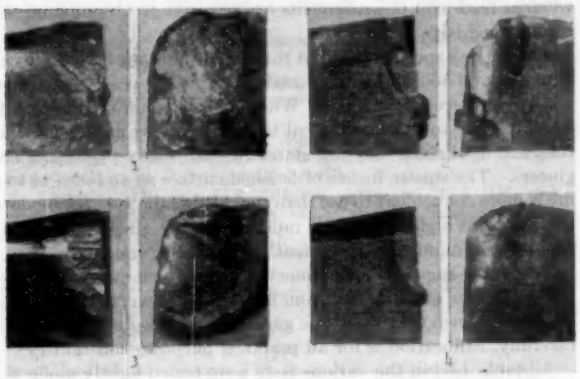

FIG. 32 PHOTOGRAPHS OF A FEW TOOLS USED FOR DETERMINING EFFECT OF SPEED AND FEED ON TITANIUM 150A

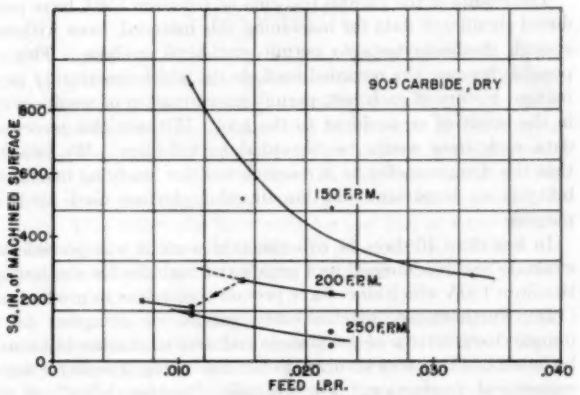

FIG. 33 EFFECT OF FEED AND SPEED ON TOOL LIFE; TITANIUM 150A
(Fifty per cent increase in feed load.)

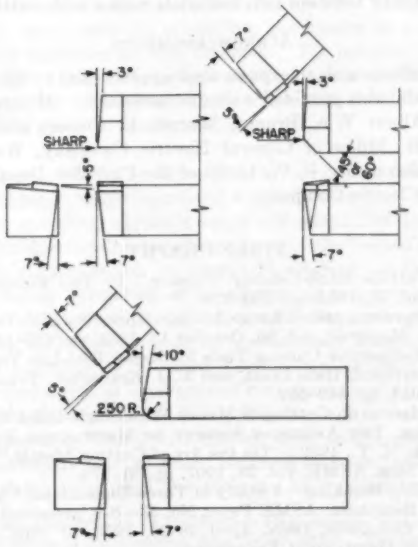

FIG. 34 TOOL GRINDS RECOMMENDED AS A RESULT OF TESTS 1 to 5
(0 deg side-cutting-edge angle tool for turning to shoulders only.)

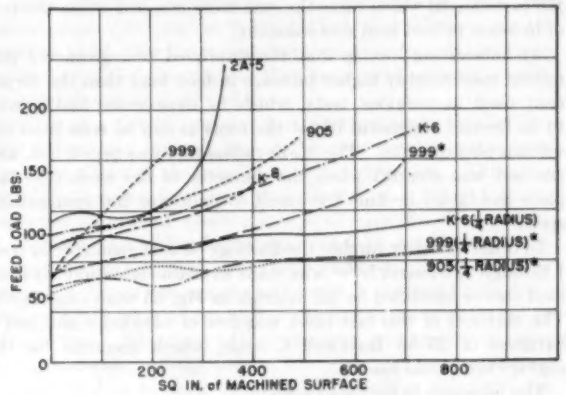

FIG. 35 FEED-LOAD CHANGES DURING TOOL-LIFE TESTS ON TITANIUM 150A
(Coolant: IV, 20:1, Fig. 5. Curves condensed from feed-load charts, approximately 35:1 in length.)

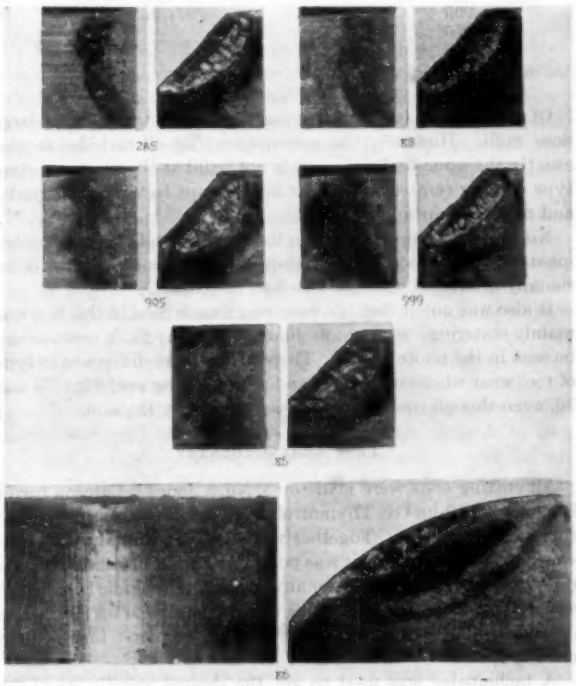

FIG. 36 PHOTOGRAPHS OF TOOLS USED IN TEST 6

TEST 6 TOOL LIFE

Three tools, designed as a result of Tests 1 to 5, are shown in Fig. 34. The 45-deg side-cutting-edge angle tool and the 0.250-radius tool were used in the life tests. Only carbides which had shown a definite promise with respect to tool life in Test 1 were tried. The results of these tests are shown in Fig. 35 and photographs of tools in Fig. 36. Indications were that cutting speeds 125 and 150 fpm and feeds of 0.011 or 0.015 ipr would permit reasonable tool life on the production line under optimum cutting conditions. However, to permit tests of several carbides, it was decided to run life tests at 200 fpm cutting speed and 0.015 ipr feed. None of the tools was permitted to stay in the cut until it broke down. As soon as the rate of increase in feed load started to climb more rapidly, the cut was stopped, except for the 905 and

K6 carbides, in which cases the cuts were stopped while the rate of increase in feed load was constant.

An interesting fact is that the improved tool geometry permitted considerably higher increase in feed load than the 50 per cent used in previous tests, which in most cases had proved to be beyond the useful life of the tools as can be seen from the various photographs. The 1/4-in-radius tool was tested last, and the test was stopped when the diameter of the work (the last piece available) became too small to maintain 200 fpm cutting speed.

In order to verify further the findings on tool geometry in tests 1 through 5, a fourth billet was made available later and the feed-load curves identified by an asterisk in Fig. 35 were established. The material of this last billet was free of blowholes and had a hardness of 35–36 Rockwell C scale, which accounts for the slightly lower tool loads.

The increases in feed load were:

Billet 3	per cent	Billet 4	per cent
2A5	100	999*	100
K8	100	1/4 in. rad 999*	45
905	95	1/4 in. rad 905*	60
K6	75		
999	175		
1/4 in. rad K6	25		

Of those tested, the tools giving the longest tool life had large nose radii. However, the assumption that all carbides require exactly the same tool geometry is not valid as the predominating type of wear (cratering or wear land) is apt to vary with grades and makes of carbide.

No chip breakers were used in the life tests and this had a detrimental effect on some of the results as long curling chips occasionally interfered with the free flow of coolant.

It also was noted that the wear on all tools used in this test was mainly cratering. Some tools did not show any flank wear, as can be seen in the photographs. There is a definite difference in type of tool wear when cutting dry and when cutting wet, Figs. 30 and 36, even though tool geometry was practically the same.

Test Arrangements

All cutting tests were made on a No. 5 Jones & Lamson turret lathe with a 10-hp GE Thymotrol drive, permitting infinite variation in motor speed. Together with the gear shifts in the headstock of the turret lathe, it was possible to utilize maximum horsepower capacity of the drive for any speed of the spindle between 30 and 1500 rpm. The Thymotrol was not available for Tests 1 to 3A, inclusive, on titanium 150A which accounts for the odd cutting speeds.

A tachometer was used to get the desired spindle speed for each cut. Tool loads caused a negligible speed drop when machining titanium 150A as the depth of cut was only 0.050 in. It was necessary, however, to make a preliminary cut and correct for speed drop in all test cuts on hardened steels (0.100 in. depth). The drop in spindle speeds varied between 3 and 5 per cent depending upon hardness of material and cutting speed.

Tool geometry was checked and tool wear measured with a J&L comparator, magnifications 31.25:1 and a toolmaker's microscope. Photographs of tools were taken on the comparator at a magnification of 20:1.

Only two load components—tangential and feed—were recorded in the research on titanium 150A. Later work has proved definitely the value of recording the radial load also. This load is the smallest, permitting the highest sensitivity, Figs. 3, 4, 7, and 8, within the range of the recording equipment and is therefore valuable for detecting chipping at the edge of the tool nose, whereas feed-load measurements are sensitive to chipping on the side-cutting edge of the tool.

The cutting speed is taken at the OD of the work before the cut is made, and tool life is measured in terms of area of generated surface produced by the cut. Where the diameter of the work is small relative to the depth of cut these indexes are not precise, but they are used since they are standard with many processing engineers. The square inches of finished surface as an index to tool life is more convenient to use than tool life in minutes. In modern machining at high speeds with multiple tooling, surprisingly short tool lives in minutes are frequently the most economical.

The strain-gage tool dynamometer, having no moving parts, has the advantage of being free from hysteresis. Several years of use also have shown that when the gages are attached and protected, carefully, calibration is for all practical purposes constant (1).

All tools used in the various tests were honed lightly along the cutting edge with a 400-grit diamond hone to remove any saw edge produced by grinding.

Conclusions

The results of the various test cuts on titanium 150A have produced significant data for machining this material, even without enough duplicate tests to permit statistical analysis. This is possible because the recorded load charts, which constitute a permanent history of each test, permit interpretation of results even in the event of an accident to the tool. Without this recorded data such tests would be discarded as valueless. We believe that the dynamometer as a research tool for studying machinability is an important addition to other devices used for this purpose.

In less than 10 days of experimental work it was possible to evaluate and recommend tool grinds and carbides for machining titanium 150A which since have proved themselves in production (12). Furthermore, machinability cannot be accepted as a unique characteristic of one material relative to another but must be based on all factors involved in the machining process for most economical production. For example, "machinability" of titanium 150A itself varies greatly with side rake angles, carbides, coolants, and so on, Figs. 19, 24, and 35. The difference in the slopes of the cutting-speed life lines between hardened steel and titanium 150A, Fig. 9, is a definite indication that relative machinability between two materials varies with cutting speed.

Acknowledgments

The authors wish to express their appreciation to the following individuals who provided valuable assistance: Messrs. Charles Sadon, Albert Wm. Brunot, Warren E. Fraser, and the late Wesley B. Millet of General Electric Company, West Lynn, Mass.; also to Mr. F. W. Lucht of the Carboloy Department of General Electric Company.

BIBLIOGRAPHY

1 "Carbide High-Velocity Turning," by Leif Fersing, Trans. ASME, vol. 73, 1951, pp. 359–374.

2 "Dynamometers Change Art to Science," by E. J. Tangerman, *American Machinist*, vol. 96, October 13, 1952, pp. 130–134.

3 "Radioactive Cutting Tools for Rapid Tool-Life Testing," by M. E. Merchant, Hans Ernst, and E. J. Krabacker, Trans. ASME, vol. 75, 1953, pp. 549–559.

4 "Manual on Cutting of Metals With Single-Point Tools," second edition, The American Society of Mechanical Engineers, New York, N. Y., 1952. "On the Art of Cutting Metals," by F. W. Taylor, Trans. ASME, vol. 28, 1907, pp. 31–279.

5 "Chip Breaking—A Study of Three-Dimensional Chip Flow," by E. K. Henriksen, ASME Paper No. 53—S-9, presented at Spring Meeting, Columbus, Ohio, April 28–30, 1953, of The American Society of Mechanical Engineers.

6 "Practical Approach to Optimum Machining I to IV," by A. B. Albrecht, *American Machinist*, vol. 97, May 25, 1953, pp. 121–125.

June 8, 1953, pp. 142–145; June 22, 1953, pp. 130–133; July 6, 1953, pp. 142–144.

7 "Increased Production, Reduced Costs," Curtiss-Wright Corporation, Wood-Ridge, N. J., vol. 2, 1951.

8 "Properties of Carboloy, Cemented Carbides," Carboloy Department of General Electric Company. Firthite Grade Selection, Technical Data 60-003.

9 "Supplementary Notes on Metal Cutting," "Metallurgical Considerations in Machining," Machine Tool Laboratory, Massachusetts Institute of Technology, Cambridge, Mass., 1951.

10 Carbides 55B, 78C, 77B, 779, 608, 5024, 907, 44A, 905, 883, 999 are manufactured by Carboloy Department of General Electric Company.

Carbides KM, K5H, K6, and K5 are manufactured by Kennametal, Inc.

Carbides HE, HA, and HF are manufactured by Firth Sterling Steel & Carbide Corporation.

Carbides 2A5 and 2A7 are manufactured by Vascoloy-Ramet Corporation.

11 "The Grinding Process," by D. R. Walker, Metal Cutting Research Laboratory, Massachusetts Institute of Technology Publication, Cambridge, Mass., February 26–27, 1952.

12 "How GE Works Titanium," by V. L. Coughlin, *American Machinist*, vol. 97, February 16, 1953, pp. 176–181.

Discussion

O. W. Boston.[5] The writer is very much interested in the work being done by the authors on the subject of machinability.

The method of determining machinability, based on flank wear determined by the longitudinal component of the cutting force, has been used by others, such as Mr. Boulger of Battelle Memorial Institute, with success. It has been more general to determine the flank wear as a function of the time of cutting. This makes the flank wear for tool life, or time of cutting for a given flank wear, a definite relationship. This is the procedure outlined in two of the American Standards on life tests of single-point tools.

The first of these Standards is for cutting-tool materials other than sintered carbide and is known as ASA B5.19-1946; reaffirmed, 1953. That for sintered-carbide tools is a present tentative standard. In the proposed method, the longitudinal cutting force measures the resultant effect of the flank wear and the cratering on the face. Usually the cratering will cause a longitudinal decrease in the cutting force because of an increase in rake angle, so that the method, as proposed, does indicate tool wear but is not associated directly with flank wear. This method is, however, satisfactory for comparing the results of a cutting test, as other variables are also involved. For instance, no two metals machine alike; different grades of carbide wear differently for a given metal. These are all factors which should be considered in any study of machinability.

C. J. Oxford, Jr.[6] The authors are to be commended for devising a technique which permitted a survey of a great number of tool and operating variables using a minimum of time and equipment and with minimum expenditure of the limited amount of titanium alloy available to them. Monitoring the feed load with a recording dynamometer during cutting can give reasonable assurance that the data in such a rapid test are representative and free of the influence of the occasionally defective tools which are encountered in most tool-testing programs. The writer has used a similar arrangement with good results in testing high-speed-steel end mills and it is gratifying to find that similar good test results are found with carbide tools on titanium alloy.

It is unfortunate that sufficient material was not available to permit at least three identical tools to be run on each test log under identical conditions. Until this can be done, the shape of some of the curves in the authors' Fig. 35 must remain suspect as to whether the curvature reversals are normal for these operating conditions or whether they are caused, at least in part, by normal "cascading" of tool wear.

The use of a flat 50 per cent (or other convenient value) increase in feed load for each tool as the wear criteria is also open to question although the possible error is not serious. There is a possibility that the final feed load should be a percentage increase over the average starting load of all tools of a given geometry. Thus a tool with a higher starting load would not be run to a higher final load than one with a lower starting load. The writer's hypothesis has been found correct in the previously mentioned end-mill tests where higher starting loads were found to be due to small differences in tool geometry and tools with lower starting loads showed the longest life when run to a prescribed final feed load or to total destruction. Whether this holds for carbide-tipped tools cutting titanium alloy can only be answered by further tests.

It is hoped that the authors will be able to continue this research sufficiently to verify the interesting trends established in this paper.

H. J. Siekmann.[7] The authors have reported on one of the more valuable and newest methods of determining tool life to evaluate the effect of the variables of metal cutting. They have increased the usefulness of laboratory test results in determining the optimum tool design, feeds, and speeds for shop operations by producing this information in a more reasonable length of time and with greater accuracy.

The development of reliable accelerated tests to give answers that solve today's tooling problem today has long been a problem. Under the extremely overloaded conditions of high-speed tests, there is a great probability that the cutting edge will suffer abnormal breakdown due to minute chipping or cracking of the thin section of carbide near the point. This failure may be caused by variations in grinding or brazing techniques, variations within the carbide structure, hard particles or sections in the material cut, vibration or irregularity in the operation of the machine tool, and many other factors even more difficult to observe and control. Although the measurement of tool forces with a strain-gage dynamometer does not reduce the effect of these variables, it does enable the observer to determine that the introduction of abnormal wear has taken place and the resultant tool life has been affected.

Unfortunately, the length of cutting test possible with this equipment is somewhat limited, owing to temperature gradients set up in the strain gages, causing drift of the measured loads. These gradients are formed by the uneven flow of heat from the cutting zone into the dynamometer. This problem is partially reduced when machining short workpieces which enables the dynamometer to be rezeroed between passes.

The data presented in Fig. 18, giving the chip thickness versus the hardness of steel machined, appears to be contrary to past experience. The thickness of the fracture of broken chips sometimes has approached the thickness of the feed but not less than the feed. The authors' results may have been due to the use of a tool with a large side-cutting-edge angle.

In machining commercially pure titanium with a cutting tool having a 30-deg side-cutting-edge angle and a feed per revolution of 0.0052 in., the chip thickness was 0.014 at 25 fpm, 0.012 at 50 fpm, 0.011 at 100 fpm, 0.010 at 200 fpm, and 0.010 at 400 fpm. Speed did not seem to affect the chip thickness above 200 fpm where it was about twice the thickness of the feed per revolution.

[5] Chairman, Department of Production Engineering, University of Michigan, College of Engineering, Ann Arbor, Mich. Fellow ASME.

[6] Research Engineer, National Twist Drill and Tool Company, Rochester, Mich.

[7] Engineer, Design and Application, Carboloy Department, General Electric Company, Detroit, Mich.

The optimum grade of carbide tool is dependent upon the conditions of the machining operation. In the shop, under conditions of good rigidity and correct tool design, the extremely hard cast-iron grades of carbide give the best tool life as shown in Fig. 19. The majority of operations are not run under these conditions and it has been found necessary to use the tougher carbides such as grades 883 and 44A to eliminate excessive tool breakdown caused by minute chipping. The rigidity of the workpiece and machine tool is one of the main factors in determining tool life for machining titanium in the shop.

Authors' Closure

Prof. O. W. Boston points out very correctly some effect of cratering of a tool on the feed load. This effect can be seen in Fig. 35. Incidentally, edge wear on tools, Fig. 36, is slight compared to cratering. Therefore it would have been difficult to analyze machinability of titanium 150A without a yardstick for determining simultaneously the effect of both cratering and edge wear while a tool was progressing in a cut. As a crater becomes deeper, it also grows toward the cutting edge while a tool is cutting and eventually causes a sudden breakdown of a tool, thus making the wear land an uncertain guide. After an initial wearing-in period, cratering also has the effect of gradually increasing feed loads, see Fig. 35. Furthermore, the initial effect of cratering on the feed load is rarely noticeable at high cutting speeds, see Figs. 3, 4, 7, and 8.

The authors are in agreement with some points raised by Mr. Carl J. Oxford, Jr. The 50 per cent increase in feed load is an admittedly arbitrary value which theoretically should be modified with respect to tool geometry. Measurements of wear lands on test tools and subsequent life tests of tools, however, have proved, Figs. 28 and 35, that reliable trends in tool life can be established by using a constant percentage increase over the initial feed load rather than a prescribed final load. Furthermore, cutting speeds have a definite effect on tool loads. The general tendency when machining most steels with carbide tools is that tool loads go down with increase in cutting speeds until a speed of 400 to 500 fpm is reached, above which the loads tend to level off (1). A feed load may be reduced as much as 50 per cent by increasing speed sufficiently, thus upsetting the use of a prescribed final feed load. Twenty-five per cent increase in feed loads for free machining steels is generally sufficient to obtain valid information, whereas a 100 per cent increase in feed load may be required for hard steels.

One advantage in the use of the tool dynamometer is to avoid a "cascading" of tool wear. We wish to point out that the shape of the curves in Fig. 35 are foreshortened 35 times and therefore appear exaggerated. Blowholes, variation in hardness and structure in the titanium billets, were variables which influenced not only the feed loads but which we believe accounted for most of the inconsistency of some of the carbides.

Mr. H. J. Siekmann points out limitations of the strain-gage tool dynamometer due to temperature gradients causing drift of measured loads. This problem is actually not serious. When a cut is stopped and if the recording pen does not come back precisely to its original zero-line, the actual load can still be found by using the new no-load position of the pen as the zero-line, because the temperature gradients do not change the calibration. Furthermore, such difficulties can be practically eliminated by cooling and by a proper design of the dynamometer. Our experience has been that it is not temperature, but rather stresses set up by uneven temperatures, which should be avoided.

The data presented in Fig. 18 are not that of the chip thickness but of the height of the fracture of the chip. A chip as actually measured with a micrometer is always thicker than the feed which produced it. In this case the height of the fracture of the titanium chip was .017 whereas the thickness measured with a micrometer was .022. We agree fully with the findings of Mr. Siekmann regarding chip thickness versus feed (1). In one case the maximum thickness is used, whereas the fracture represents the minimum thickness.

Finally, it should also be pointed out that when conditions of good rigidity and tool design are not available, thus preventing the use of the harder cast-iron grades of carbides on the production lines, it becomes necessary to reduce cutting speeds, as a soft grade 44A will wear excessively when used at the highest economical speeds for hard carbides such as 999, 905, etc.

Testing Large Steam Turbines With Weighing Tanks

By W. A. POLLOCK,[1] MILWAUKEE, WIS.

Forty-three years of favorable experience with weighed water testing of steam turbines influenced a decision to install scale tanks at Wisconsin Electric Power Company's new Oak Creek Power Plant to permit testing the 120,000-kw cross-compound reheat turbines. At a total cost of less than ten cents per kilowatt installed capacity, the weighing tanks serve the dual purpose of providing a means for testing turbines and their auxiliaries accurately and a needed facility for storage of cold condensate. Manufacturer's guarantees of turbine heat rates can be checked more reliably and closely than with flowmeters, and with assurance of accurate reliable tests the manufacturer frequently can improve his guarantee. Once favorable guarantee commitments are made, experience shows that the manufacturer makes special efforts to provide the very best design. He also encourages operation at closer clearances to attain the better heat rates. Other advantages are the help in evaluating turbine internal condition which may or may not require overhaul, and in learning the effects of changes in clearance adjustments and in design changes. Routine tests are conducted with a minimum of preparation time and a relatively small test crew. Accurate measurement of all values of steam flow, electrical output, pressure, and temperature are required for reliable results, but the major emphasis on accuracy is placed on the input and output quantities which have the greatest effect on the result. The paper concludes that weighing tanks can well be considered a definite requirement whenever it is possible to fit them into the flow cycle.

Introduction

THE difficulty of making precise measurement of steam-flow rate is generally recognized as the biggest single obstacle of accurate determination of turbine efficiency. True data cannot be determined by inaccurate measuring devices and methods. Obviously, a test is no more reliable than its least accurate data.

Minimizing of testing errors is desirable to allow a much closer comparison of actual turbine performance with the manufacturer's guarantees. With complete confidence in the test results, a manufacturer finds less necessity to add a margin in his guarantees for the inaccuracies of the tests. The designer who can accept test results without reservation is in the position to evaluate the effect of minor modifications on turbine efficiencies and can predict more reliably the turbine heat rate and likewise the overall station performance.

The higher accuracy gives the operator greater confidence in the service tests and thus may eliminate the premature opening of a turbine where deposits are suspected. Stage-pressure changes are not sufficiently accurate to show blade deposits of relatively moderate magnitude which could reduce efficiency and cause excessive waste of fuel. With reliable tests there will be fewer unexplained "very good" or "very bad" indications of performance.

The quantities which must be determined most carefully in conducting a turbine test are steam flow to the turbine and the electrical output from the generator. An error in either of these determinations will be reflected directly in the final result.

Steam-Flow Measurement

Measuring the steam flow to a turbine with condensate weighing tanks always has been the preferred method from the time the original test codes were made up to and including the latest 1949 ASME Power Test Code for Steam Turbines. The limits of possible error allowable for several methods of measurement are stated briefly in the Test Code as follows:

(*a*) Actual weighing of the water by means of tanks on suitable scales, ±0.25 per cent.

(*b*) Measurement by means of volumetric tanks, ±0.50 per cent.

(*c*) Steam-flow measurement by a thin-plate orifice or nozzle, ±1.50 per cent.

(*d*) Condensate flow by a thin-plate orifice, nozzle, or venturi tube, ±1.25 per cent.

(*e*) Properly equipped gravity tanks with calibrated orifices in base of tank discharging freely and flow determined by head on orifices, ±0.50 per cent.

When comparing turbine performance and turbine guarantees, is it logical and reasonable to accept differences which are less than the tolerable error of the testing method?

The truth of such differences can be challenged. Questionable comparisons can be misleading. To gather doubtful data is a waste of time and expense when more positive methods can be used, and at low cost.

The concept of using weighing tanks to determine the steam flow to a steam turbine is not new. Some of the older editions of the ASME Power Test Codes mention only two methods for determining the total steam used by the turbine—weighing condensate or measuring it volumetrically in tanks. Owing to the increased size of turbine generators, the trend toward the use of flowmeters has become almost universal, even though the results are less satisfactory. The introduction of the many stages of extraction heating and of reheat has resulted in complex cycles that discourage nearly everyone in the consideration of weighing tanks for turbine tests.

Electrical output can be determined readily and to a high degree of accuracy with carefully calibrated commercial or special test instruments.

Temperature and pressure measurements are important and should be made reliably, but an error in their case affects the final result much less than an error of equal percentage in the determination of input or output. The effect of an error in determina-

[1] Technical Engineer of Power Plants, Wisconsin Electric Power Company. Mem. ASME.

Contributed by the Power Division and the Joint Research Committee on Boiler Feedwater Studies and presented at the Annual Meeting, New York, N. Y., November 29–December 4, 1953, of The American Society of Mechanical Engineers.

Note: Statements and opinions advanced in papers are to be understood as individual expressions of their authors and not those of the Society. Manuscript received at ASME Headquarters, July 24, 1953. Paper No. 53—A-66.

tion of pressure or temperature is shown by the average correction factors furnished by the manufacturer for the five Port Washington turbines. To cause an error of 1 per cent in the final result an error of 147 psi would need to occur in the determination of throttle pressure; or an error of 60 F in throttle temperature; or an error of 47 F in reheat-outlet temperature; or an error of 0.31 in. of mercury in the exhaust pressure.

Forty-Three Years of Experience

The first provision for weighing turbine condensate in the Wisconsin Electric Power Company power plants was in the form of an Avery dumping scale provided at Commerce Street Power Plant about 1910, when surface condensers were installed with two 14,000-kw vertical turbines. The scale was piped to serve both the boilers and the turbines. This scale was used as recently as a year ago to answer the question of how much steam was required to run these turbines at a very low load.

V-notch meters were provided initially at Lakeside Power Plant for boiler and turbine testing. Later, when 1300-psig boilers were put into operation, it became necessary to control the amount of oxygen introduced into the boiler feed, and one pair of weighing tanks was installed with proper pipe lines to permit testing any of the eight condensing turbines in this station.

Weighing tanks were installed with the first 80,000-kw unit at Port Washington Power Plant and the test lines to and from the tanks were extended to serve the other four turbines as they were added.

When the first 120,000-kw unit at the Oak Creek Power Plant was being planned, the question was raised whether a special flow nozzle in the suction of the boiler feed pumps would provide the desired accuracy for measuring water quantities. Accordingly, a flowmeter and flow nozzle were purchased and installed in the condensate line at Port Washington for calibration.

The error obtained in the meter tests was found to be 1.45 per cent despite the fact that the meter was cleaned and checked prior to the test and the flow nozzle carefully installed in a piping arrangement ideal for good metering accuracy. The error shown was in accord with that allowed by the 1937 Turbine Test Code which indicated that an error of ±1.5 per cent could be expected for a specially calibrated water flowmeter and ±2.5 per cent for a steam flowmeter.

Value of Accuracy

Value of the 1.0 per cent greater accuracy of weighing tanks than condensate flowmeters and 1.25 per cent better than steam flowmeters was brought to prominent attention during negotiations for the first turbine for the Oak Creek Power Plant. A representative of one of the turbine manufacturers stated that his company would agree to guarantee 1.0 per cent better turbine heat rate if weighing tanks were installed at Oak Creek for turbine testing instead of relying upon condensate flowmeters.

A 1.0 per cent gain in turbine efficiency justifies capital expenditure of $300,000 per 120,000-kw turbine, or $2.50 per kw. Savings equivalent to a capitalization of $1,200,000 are possible because the Oak Creek expenditure for scale tanks will not be recurring except for interconnections to other units and because the 1.0 per cent better turbine-efficiency guarantee may be realized on each of the four units planned. The actual cost of installing the Port Washington scale tanks and the estimated cost of the tanks for Oak Creek are derived (Tables 1 and 2) at less than 10 cents per installed kw.

It cannot be stated that a 1.0 per cent better turbine is assured simply by a better guarantee. However, one may be certain that if a manufacturer guarantees a better heat rate, he will endeavor to provide as good a machine as is economically possible in order to meet his guarantees. He will reduce clearances progressively, within safe limits, to meet such better guarantees.

TABLE 1 COST OF WEIGHING TANKS FOR TURBINE-EFFICIENCY TESTING, PORT WASHINGTON POWER PLANT

Two weighing tanks	$ 1,795.00
Supports	452.00
Insulation on tanks	591.00
Two scales	1,262.00
Transfer pump (2000 gpm, 10 in. × 10 in., 25 hp)	950.00
Pipe, valves, fittings, and insulation	1,729.00
Labor, overhead, sundries	2,620.00
(Port Washington No. 1, 1935 cost)	$ 9,399.00
Tie lines PW No. 2 to No. 1 (1943)	$ 3,820.00
Tie lines PW No. 3 to No. 2 (1948)	6,100.00
Tie lines PW No. 4 to No. 3 (1949)	6,360.00
Tie lines PW No. 5 to No. 4 (1950)	6,430.00
PW Nos. 1, 2, 3, 4, and 5 total actual costs	$32,109.00
Unit cost	8¢/kw

TABLE 2 COST OF WEIGHING TANKS FOR TURBINE-EFFICIENCY TESTING, OAK CREEK POWER PLANT

Two weighing tanks	$ 3,730.00[a]
Overflow tank (tell-tale tank)	484.00
Supports	900.00
Two scales	4,280.00
Transfer pump (2400 gpm, 8 in. × 8 in., 50 hp)	2,460.00
Expansion joints	251.00
Pipe, valves, and fittings (actual)	9,562.00[b]
Labor, overhead, sundries	8,200.00
Oak Creek No. 1 initial cost	$29,867.00
Tie lines OC No. 2 to No. 1 estimated	$ 3,880.00
Tie lines OC No. 3 to No. 2 estimated	6,540.00
Tie lines OC No. 4 to No. 3 estimated	4,270.00
OC Nos. 1, 2, 3, and 4 estimated	$44,560.00
Unit cost	9.3¢/kw

[a] Tanks will not be insulated.
[b] Piping will not be insulated.

Effect on Wage-Incentive Plan

Another important reason why the Wisconsin Electric Power Company requires accurate tests of its equipment is a gain-sharing bonus plan which is a part of the wage structure. Standards of operating efficiency are established on the basis of manufacturers' guarantees and test results. These conditions of operation can be attained if avoidable losses are reduced to a minimum. The turbine test is an important part of the "standard" calculation and a 1.0 per cent error in the test on one turbine would result in a 0.4 per cent overpayment or underpayment in the total plant payroll. The annual payroll for the plant being $1,464,000, the 0.4 per cent would amount to $5,856 in a year's time, the normal period between "standard" heat-rate determinations.

Cost Chargeable to Tests

The costs involved in conducting a weighed-water test are small. In the routine turbine tests, less than 100 manhours are required for preparing, conducting, and calculating a series of three runs of 2 hr each. This time does not include that spent by the operating crew in setting up and changing back to normal operation upon completion because the regular crew finds time to isolate the turbine from the rest of the plant along with its regular work.

A total of 10 man-hours is spent for special preparatory calibration. During the test period six men collect data, two at the weighing tanks, one at the turbine, and the others on the auxiliaries. One extra man is assigned as roving. He takes special leakage information, checks to be sure valve leakage is not occurring which would result in gain or loss of condensate, double checks the regular crew, and is available for relief as required.

Three runs of 2 hr each usually are conducted in a single day with a waiting period for stabilizing after a load change. Manhours chargeable are as follows:

Pretest calibration	10
Conducting test, 7 men at 8 hr	56
Calculations, 2 men 2 days at 8 hr	32
Total manhours	98
Estimated 100 hr at $3.50/hr	$350

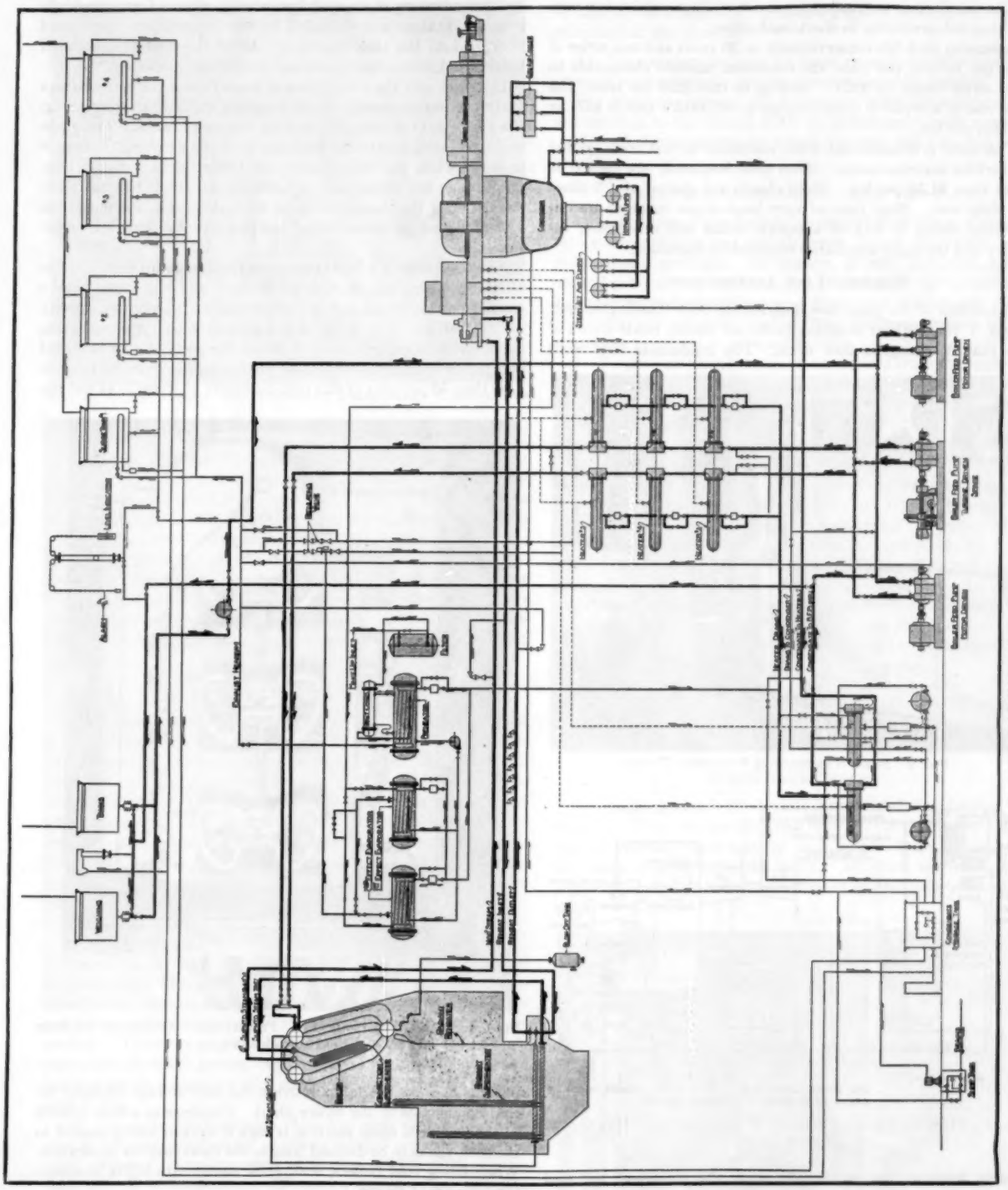

FIG. 1 FLOW DIAGRAM 80,000-KW INSTALLATION—PORT WASHINGTON POWER PLANT

The calculations are made on a standard form and by two men working independently to check each other.

Assuming tank life conservatively at 20 years and one series of tests per turbine per year, the maximum amount chargeable to each series would be $321. Adding to this $350 for labor, the total cost of a series of three runs on an 80,000-kw unit is $671 or $0.0084 per kw.

This total is insignificant when compared to test costs quoted by turbine manufacturers. Shop tests frequently are quoted at more than $1.50 per kw. Field checks are quoted at 1.5 times the shop cost. Shop tests of very large steam turbines are impractical owing to lack of adequate boiler and condensing capacity and the many auxiliaries required for operation.

Weighing-Tank Arrangement

Inspection of the basic flow diagram for Port Washington unit 1, Fig. 1, reveals that weighing tanks are readily made a part of the Port Washington flow cycle. The condensate (hot well)

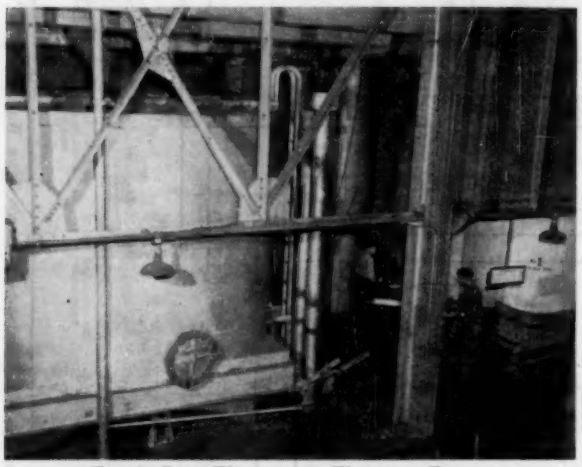

Fig. 2 Port Washington Weighing Tanks

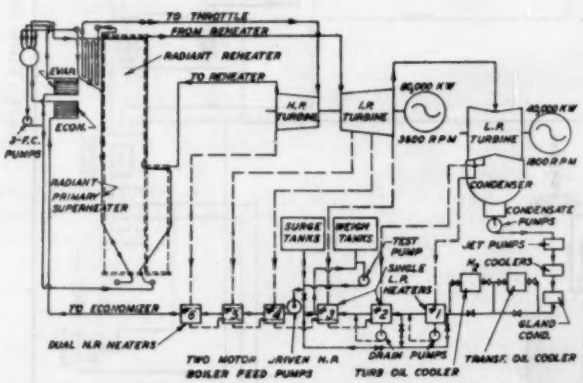

Fig. 3 Flow Diagram—120,000-KW Installation—Oak Creek Power Plant

pumps transfer the condensate from the condenser hot well through the steam-jet air pumps, the generator coolers, two stages of feedwater heating, and to the surge tanks which float on the suction of the boiler feed pump. The boiler feed pumps then pump through three stages of high-pressure heaters to the boiler. For units 2 to 5, inclusive, two 8-in. pipes were run the length of the plant, one to conduct condensate to the weighing tanks and the other back to the unit.

All condensate is weighed because the drains from the high-pressure heaters are cascaded to the lowest two stages and pumped into the tank-inlet line. All of the heaters are closed heaters and deaeration is accomplished in the condenser.

During a test the condensate is routed from the second-stage feedwater heater directly to the weighing tanks. After weighing, the condensate is pumped back to the surge tanks. The surge tanks permit intermittent discharge from the weighing tanks as is required when the tank weights are being struck. Water temperature in the surge tank is normally at 210 F but to insure against error the temperatures to the tanks and in and out of the boiler feed pumps are measured and compensations made if necessary.

The test pump is a 2000-gpm pump with a 25-hp motor. The weighing tanks, Fig. 2, each 17 ft diam and 9 ft high, have a capacity of 11,840 gal and are set on scales with a beam capacity of 100,000 lb. The scales are equipped with type-registering beams with ticket printers. A list of the costs of all equipment and piping specially installed for turbine test is given in Table 1. Less than 50 per cent of this cost is directly chargeable as test ap-

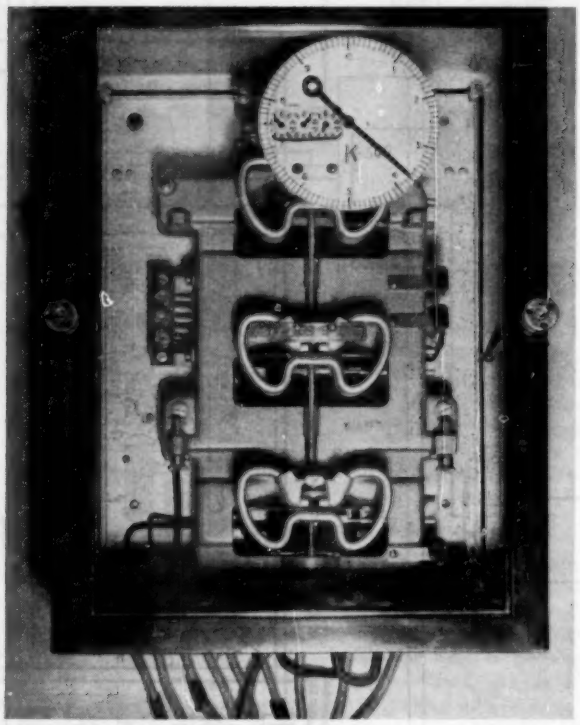

Fig. 4 Special Integrator Permitting Accurate Output Measurement

paratus because the tanks provide the only storage capacity for cold condensate in the entire plant. Condensate which collects in the hot wells upon starting is high in oxygen and is routed to the scale tanks to be drained later to the condenser for deaeration. When filling cold boilers, scale-tank condensate limits temperature stresses of drums.

The Oak Creek flow cycle, Fig. 3, is similar to the Port Washington cycle and the tanks at Oak Creek are similarly placed. Cost of the weighing system for Oak Creek is shown in Table 2.

Calibrating Weighing Tanks

The scale tanks were calibrated initially by accumulating a

FIG. 5 GAGE TESTER FOR ACCURATE INSTRUMENT CALIBRATION

known weight of water at known temperature in the tanks. To do this, several thousand pounds of test weights were placed onto the scale platform and the weigh beam balanced. Then the weights were removed and water was admitted to balance the weigh beam again. This procedure was repeated until the tanks were filled to a level which was within the range of an inclined water-gage glass and a reference mark was established permanently on this glass. This mark is used to check scale accuracy on future occasions. The tank level is measured accurately and a volumetric check is made periodically with water of known temperature as a further check of the weight obtained by original calibration.

MEASURING ELECTRICAL OUTPUT

The electric integrator, used to measure turbine output, Fig. 4, is a specially calibrated polyphase wattmeter with a 6-in-diam units-dial to permit an accurate hourly reading. All other indicators of electrical output are read frequently during the test to provide adequate checks. The current transformers for the polyphase meters are specially selected and must undergo rigid acceptance tests. The meters are not compensated for temperature but are calibrated at operating temperature, and error due to temperature is a minimum because the electrical control room experiences limited variation in temperature.

CALIBRATING ASSOCIATED INSTRUMENTS

Annual routine testing of each turbine is performed by the same procedure and with care equal to that used in the initial acceptance tests. Accurate measurements of steam pressures, steam and water temperatures, as well as water and electrical outputs are needed. Therefore gages and thermometers, as well as the scale tanks and electrical meters, require careful and exact calibration prior to test in accordance with accepted ASME Test Code practices.

(*a*) Gage standardization in place has been shown by experience to be most satisfactory to insure reliable pressure-measurement accuracy. Strain applied while reconnecting after calibration, as well as temperature differences, can cause errors under operating conditions of gages checked in the laboratory and thought to be accurate. Therefore turbine gages are calibrated in place shortly before the test by connecting a lever-operated Crosby tester into a tee connection as shown in Fig. 5. It is possible to measure the line pressure to the nearest pound and then to calibrate the gage over the range experienced in the test by shutting off the valve in the gage line and using the tester as it would be used in the laboratory. Pressure gages of less importance are calibrated in the laboratory.

(*b*) Manometers are used for most vacuum readings and low-pressure applications to provide greatest accuracy possible.

(*c*) Absolute-pressure gages equipped with micrometers permit readings to the nearest 0.001 in. of turbine-exhaust pressure.

(*d*) All thermometers are tested carefully and adjusted as required.

OTHER PRECAUTIONS FOR ACCURATE TEST DATA

1 Unit design of the station has simplified isolation of condensate systems during test periods, even though surge-tank interconnection is provided. Tie headers, in most instances, have a shutoff gate valve at each end, and all such gate valves have bonnet bleeders to check for leakage. Both seats of most gate valves are tight and a bonnet bleeder thus confirms absence of test errors due to inward or outward leakage.

2 To prevent loss of steam or condensate from the cycle and to prevent inflow, all extraneous uses of steam and condensate are halted. All valves are closed and all tank levels are measured accurately before and after each run.

3 To insure proper isolation, a check list of valve positions for test conditions for each unit has been prepared. Operating engineers of the first shift follow the list step by step, marking how valves were found, how left, and whether bonnet bleeders are opened. Several hours before the test begins a member of the testing staff and two assistants to the engineer-in-charge follow the list once more and then make final closing of several valves. Manipulating two valves to route condensate through the weighing cycle is the last operation. Men at the weighing tanks are alerted before change-over occurs. Thus simultaneous slow opening of one valve and closing of another at one location allows easy change-over to test routing of the condensate.

4 Condensate is weighed at test load for a period prior to starting time to insure stable conditions. Men at the weighing tanks can call by phone for change to normal routing if the test pump should fail.

WEIGH-TANK DETAILS

One weighing tank is filled while the other is being weighed and emptied. Two men are stationed between the two tanks. They operate various valves and, by push button, start and stop the test pump which empties the tanks. All valves are quick-opening, lever-operated, with levers located on the aisle between the tanks.

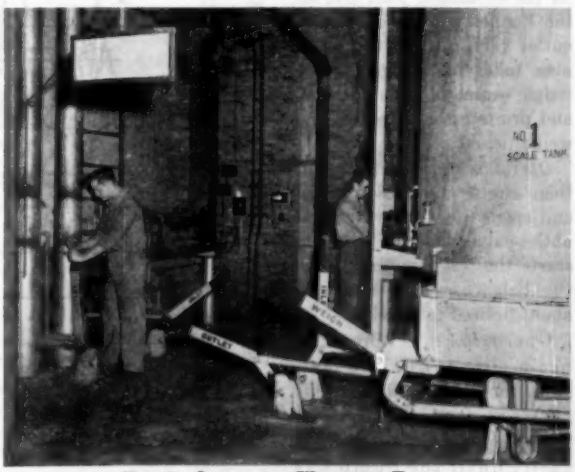

FIG. 6 OPERATING WEIGHING TANKS

Floating storage on the boiler feed-pump suction header is more than ample to supply boiler requirements during tare filling of the tanks at the test start and during the initial 6-min period of filling the first tank. During maximum load tests, gross weight for a 6-min period is about 80,000 lb. Tare weight of about 12,000 lb is maintained.

An overflow pipe leading to the No. 1 unit drain tank is provided in the main scale tank-inlet header ahead of the Y-connection to individual tanks. Protection against stoppage of flow if both tank-inlet valves were closed at any time is thus also provided, Fig. 1. A gage glass connected to it permits detection of approaching overflow if the tank is filled.

Floating covers are installed in the tanks to limit oxygen absorption, and float drains are open-ended to a funnel to permit detection of leakage. Oxygen content to the boiler is less than 0.05 cc per liter and this is taken care of by feeding an excess of sodium sulphite.

The tanks are vented to atmosphere through piping extending through a skylight. Maximum water temperature of 208 F at the tanks is desirable to prevent flashing in the test pump. This is accomplished by partial by-passing of No. 2 heater at higher loads to limit No. 2 heater-outlet temperature.

To permit accurate and rapid weighing, the following features were incorporated in tank design:

1 A single inlet and outlet opening with a Y-connection to the inlet and outlet valves.

2 A weigh valve in this line just below the tank.

3 An expansion-joint bellows below the weigh valve.

4 Expansion-joint bleed to eliminate hydraulic interference with beam balance.

5 Quick-opening bonnet bleed on weigh, inlet, and outlet valves to check for valve leakage.

Sequence of Operation

Operation 1. While tank No. 1 is being filled, its weigh and inlet valves are open. At the end of a weigh period, its inlet valve is closed at the same instant that the inlet valve of tank No. 2 is opened. Tank No. 2 weigh valve was already open. Two men perform this operation, Fig. 6.

Operation 2. One man closes tank No. 1 weigh valve and then opens the bleed valves on the expansion joint and on the bonnets of the inlet and outlet valves, while the other man takes his station at the weigh beam, obtains balance, and prints gross weight on the weigh ticket.

Operation 3. The first man then closes the bleed valves and opens the weigh valve and outlet valve while the first man starts the test pump and runs the balance weight down to about desired tare weight.

Operation 4. When the beam tips down, one man stops the pump and takes his station at the bleed valves. The other man waits momentarily until the pump has

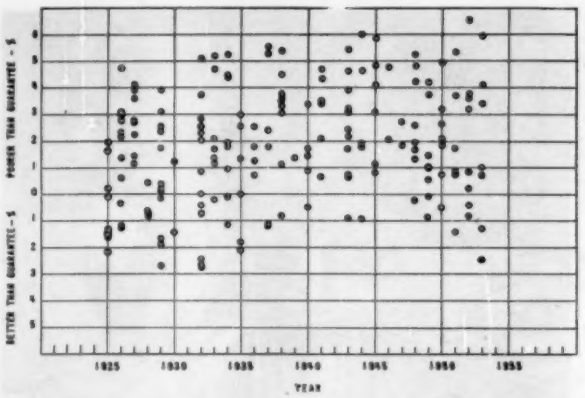

Fig. 7 Thirty Years of Test Results—Nonreheat Turbines

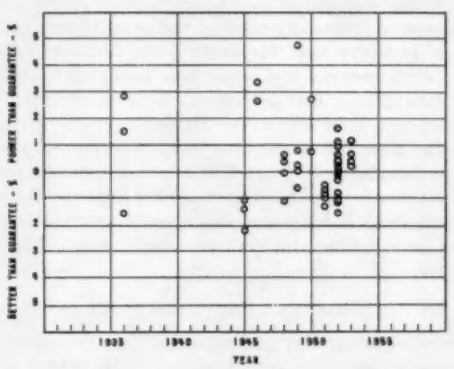

Fig. 8 Twenty Years of Test Results—Reheat Turbines

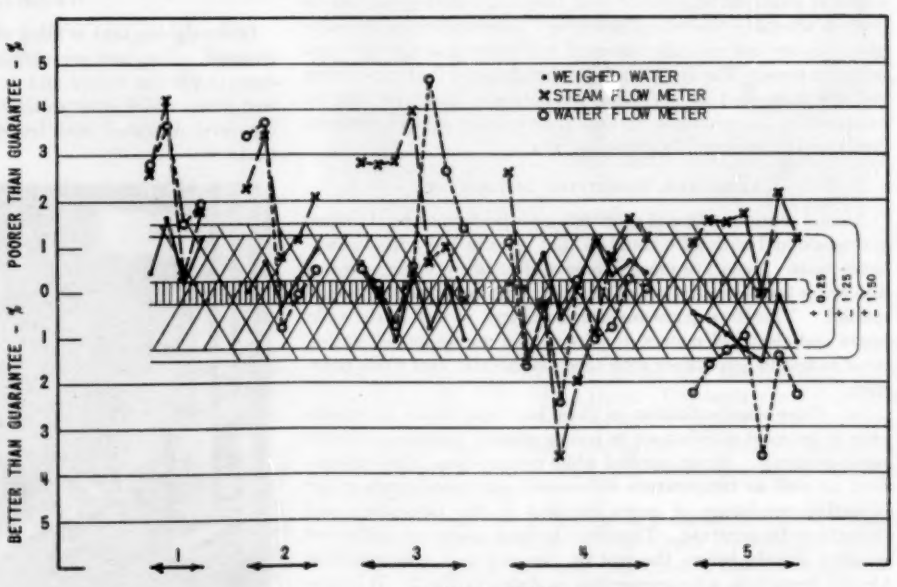

Fig. 9 Variations on Turbine-Test Results—Calculated on Basis of Weighed Water and Flowmeters

coasted to stop and then closes the outlet valve and the weigh valve. This momentary pause prevents slamming of the test-pump check valve.

Operation 5. The first man then opens the bleed valves and obtains tare weight. The bleed valves are then closed, and the weigh valve opened to prepare for the next weigh cycle. During maximum-load tests approximately 90 sec are left between printing of tare weight and opening of the inlet valve for the next weigh period.

Start and stop of weighing for each hour of a 2-hr test period is synchronized with reading of the integrating watthour meter.

Weighed condensate is compared with boiler steam and water-flowmeter in the test report.

Data are recorded 10 times each hour on printed forms and so arranged that each man covers one floor level.

Special observations are made during the progress of the test to determine if any unusual leakage occurs and also to determine leakages into and out of the cycle by watching tanks for unusual increase or decrease in levels.

Test calculations are made routine by standardization. Corrections for water leg on gages are tabulated so that the same corrections are applied to each test. Calculations for dummy leakages, end point, and so on, are also standardized as far as possible to avoid any errors.

Results

Figs. 7 and 8 show test results of a large number of tests conducted through the years. Acceptance and service test results are plotted chronologically. Some of the very poor results may be explained if conditions existing at the time of the test are known. Because this background information is historical in nature, it is not included in this paper. Data plotted in Fig. 9 are from weighed-water tests on the turbines at Port Washington.

A comparison of actual turbine performance with the guaranteed heat rates as determined by weighed water is shown, together with curves showing what the results would have been if the feedwater flowmeter and steam flowmeter had been used in the calculations. The tolerances allowed in the test code for steam flowmeters and feedwater flowmeters are indicated and it is interesting to notice that the results according to the weighed-water tests were more consistent than the results for the flowmeters.

In some cases the curves show the performance for weighed water poorer than calculated by flowmeter but the turbine manufacturer accepted the weighed-water result without question as being correct. Where there is no such reliable standard, the best result is the one usually accepted unless a calculated station heat rate shows that result to be impossible of realization. Fig. 10 shows meter errors on the 32 tests at Port Washington referred to in Fig. 9. Five turbines are involved and inspection shows that there is no correlation between the time a meter has been in service and the amount of error as caused by deposits on the flow nozzles.

Important decisions as to major expenditures and operating practices are frequently based on results of turbine tests. Two such decisions serve to illustrate this point. In one case there was a question whether spring-back packing should be installed in six 25-year-old impulse turbines. Favorable recommendation followed a turbine test which showed a gain of 0.81 per cent creditable to the installation of the packing, this gain being equivalent to a $4000 annual saving. In another case, the question of whether to run Port Washington turbine No. 4 regularly at 80,000 kw or 92,000 kw was easily decided when turbine tests showed the turbine heat rate only 9 Btu per kw hr higher at the maximum capability.

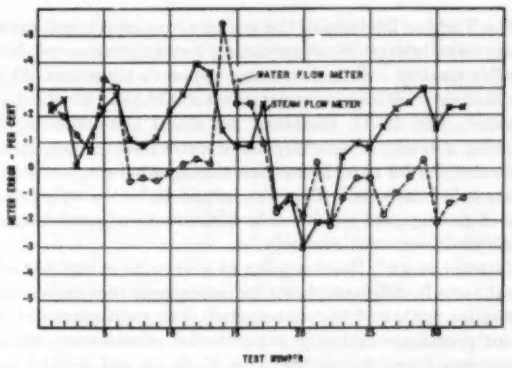

Fig. 10 Flowmeter Errors Determined by Weighed-Water Tests

Other Uses for Turbine-Test Data

Performance of nearly all of the equipment in the plant may be calculated with data observed during tests. Some of the equipment performances which may be calculated are as follows:

1 Condenser performance.
2 Condenser circulating-water-pump capacity and efficiency.
3 Condenser leakage.
4 Boiler-feed-pump capacity and efficiency.
5 Extraction heater performance.
6 Hot-well-pump capacity and efficiency.
7 Flowmeter calibrations are determined to be used later in boiler heat-balance calculations.

In cases of pumps, the motor data need to be obtained in order to calculate pump efficiencies.

Conclusion

Weighing tanks can well be considered a definite requirement whenever it is possible to fit them into the flow cycle. Minor modifications in some cycles would permit use of weighing tanks, and cycle selection can well be influenced by the ability to weigh the condensate.

Costs of weighing tanks and of conducting accurate tests derived herein are shown to be extremely low. If a turbine with a fraction of a per cent better heat rate can be assured, the total cost of weighing tanks is readily justified.

Manufacturers are not equipped to shop-test large reheat turbines with several extraction points. Because these turbines must be tested in the field, it is logical to provide facilities for obtaining the best possible results.

Acknowledgment

The author wishes to express his appreciation for the valuable suggestions and helpful conclusions received from his associates while preparing this paper.

Discussion

P. H. Knowlton.[3] The author has presented a very interesting paper on the design and use of a weighing-tank system for water-flow measurement in a large modern power plant. One can hardly take issue with any of his statements regarding the desirability of accurate measurements or the suitability of weighing tanks for such measurements of water flow.

[3] Thermodynamic Engineer, Turbine Division, General Electric Company, Schenectedy, N. Y. Mem. ASME.

The Turbine Division of the writer's company has always had a very keen interest in accumulating test information of the best possible quality. Since it became apparent more than 20 years ago that very few new power stations would have weighing tanks installed, Mr. B. O. Buckland set about the business of developing a family of carefully made water-flow nozzles, carefully calibrated, to be used in turbine testing wherever necessary as research instruments. This was judged to be the only practical way of getting good reliable data of the required precision, where weigh tanks were not available.

Experience with those nozzles in a very large number of different tests in different plants indicates to us that such a family of nozzles, with suitable manometers, can yield results of much better precision—certainly much better consistency—than the statements from the ASME Test Code quoted by the author would indicate. Experience also proves, however, that consistent results with this flow-nozzle equipment require the most careful installation and use.

It definitely appears to the writer that for the usual periodic power-plant testing, weigh tanks will be much less troublesome in achieving accurate results. It may be hoped that other power-plant designers can agree that the installed cost of such tanks is low and that their installation is justified.

F. H. Light.[3] This paper is most interesting since it represents the ultimate in accurate flow measurement. However, the use of weigh tanks requires a substantial increase in investment cost as well as increased personnel to conduct the test itself. In Fig. 9 of the paper the consistency of test results on any one unit using weighed water appears to be of the order of ±0.5 per cent.

It has been the experience of the writer's company that nearly the same degree of accuracy can be obtained using a well-designed and calibrated flowmeter. It is the general practice of our company to test all main turbines on a monthly schedule, using the regular station instruments. Flowmeters are calibrated several times per year. The test is conducted by station personnel; a maximum of three men is required. Fig. 11, herewith, is a chronological plot of 10 years of routine test results for a 165,000-kw tandem-compound condensing turbine. From this plot it can be seen that practically all tests fall within a band of 1.5 per cent width and that the trend due to increased turbine losses between inspections is well defined. The test results are based on condensate-flow measurement using a venturi-type primary metering element. Calibrations of the flowmeter before and after annual inspection showed practically no change in meter accuracy. Nearly all the tests plotted were run at the same control-valve opening with loads from 130 mw to 135 mw.

It is our opinion that consistent test results within ±0.7 per cent can be obtained using either condensate or boiler-feedwater flowmeters providing the primary metering element is calibrated initially by weighed water, and the flowmeter is carefully maintained and frequently checked during its service life.

J. W. Murdock.[4] The author is to be congratulated for making available the results of 43 years of test experience. That weighing of condensate is the most accurate means of measurement few will argue. However, comparisons between this method and inferential flowmetering as presented in this paper may be misconstrued.

It is suggested that the author include in his closing a complete description of inferential-type meters used for steam and water-flow measurement. It would be helpful if these were compared with the requirements of ASME Power Test Code for Steam Turbines (PTC6-1949). If, for example, a commercial meter with a 4½-in. chart span were read at part loads, the reading accuracy alone would cause serious errors. Since many tests are now conducted with differential flow measurement the full value of the author's experience could be utilized. Errors and variations shown in Figs. 9 and 10 are greater than those experienced by the writer.

C. A. Robertson.[5] This paper offers a practical approach to the solution of one of the most difficult problems encountered in the quantitative measurements required for the testing of large steam turbines. The precise determination of turbine efficiency requires a high degree of accuracy in steam or water-flow measurement.

From the turbine manufacturer's point of view the importance of accurate test results cannot be overemphasized. Facilities for the shop-testing of large turbine units under normal operating conditions are not practical; consequently, the turbine designer must rely on field-test data for the verification of his design calculations.

In earlier times, when steam turbines were smaller, weighing tanks were used exclusively for measuring steam, i.e., by weigh-

[3] Senior Engineer, Economy Division, Philadelphia Electric Company, Philadelphia, Pa.

[4] Superintendent, Instrument Division, U. S. Naval Boiler and Turbine Laboratory, Philadelphia Pa. Mem. ASME. The opinions or assertions contained in this discussion are the private ones of the writer and are not to be construed as official or reflecting the views of the Navy Department or the Naval Service at large.

[5] Steam Turbine Section, Power Department, Allis-Chalmers Manufacturing Company, Milwaukee, Wis. Mem. ASME.

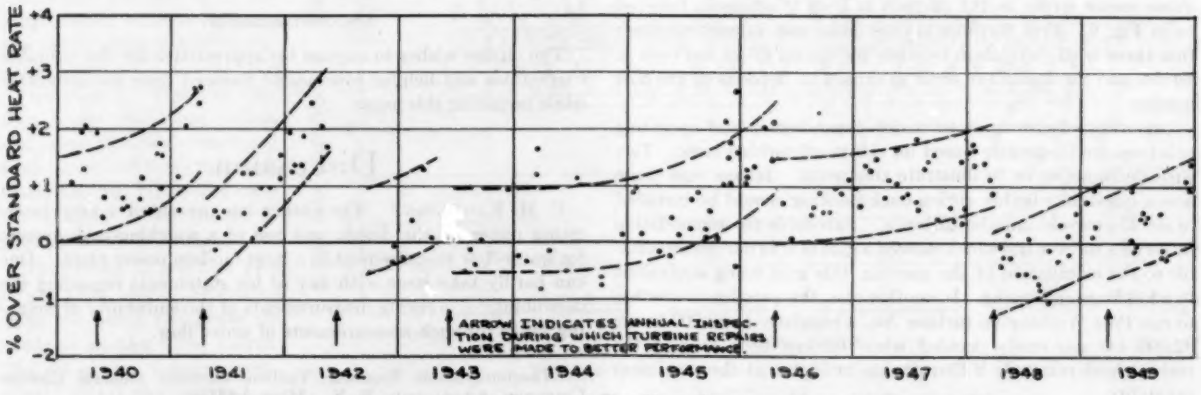

Fig. 11 Richmond Station, No. 12 Turbine; Ten-Year Trend of Monthly Turbine Tests

ing the condensed steam. But, as turbine size increased, this method was considered too cumbersome. In view of this, the ASME Test Code Committee was pressed for recommended means for measuring steam rate accurately.

After arduous debate, it finally was agreed to qualify flowmeters for steam-rate measurement. This was done by specifying accuracies to be obtained within certain tolerance limits.

The writer's experience has indicated that flowmeters for test purposes in power plants are not consistently accurate.

In his excellent paper the author makes a valuable contribution to the subject of steam-rate measurement by showing means for applying weighing tanks to large power-plant installations without adding greatly to the cost and without occupying valuable space. The weighing-tank method is still the basic and most accurate method of steam-flow measurement.

R. E. Sprenkle.[6] There can be no valid argument against the use of weigh tanks for testing turbines, except for the fact that it is a costly method of doing the job and many times not feasible.

Twenty years ago a system of using a specially calibrated flow nozzle of moderately low diameter ratio to measure the steam flow to a turbine in turbine acceptance tests was promulgated by Messrs. S. A. Moss and W. W. Johnson.[7] The following year a similar scheme, but measuring the turbine condensate, was proposed by Mr. B. O. Buckland.[8] This paper gave the results of a series of water-flow calibrations on seven highly machined nozzles ranging in size from 4 × 1¼ in. to 12 × 5 in. This paper also compared results of the hydraulic-laboratory calibrations of these nozzles with other nozzles, not only those which had previously been calibrated by Messrs. Moss and Johnson with steam flow, but others heretofore unreported which had been calibrated with water flow at the Bureau of Standards and at Hydraulic Laboratories of the writer's company.

The amazing thing about these calibrations was that despite the fact the nozzles in each of these four groups differed somewhat from each other and were calibrated by different experimenters, the results all checked each other within ¼ per cent through the normal working range of Reynolds number from 500,000 to 3,000,000.

Both of these systems are so simple to use as compared with the weigh-tank system that immediately after the publication of these papers, turbine manufacturers and users began to use them. In fact, Mr. Buckland stated he had made seven turbine-performance tests in which the flow was measured only by means of flow nozzles and that in every one of these tests the flow-nozzle readings checked the turbine water rate within ½ per cent. Each test consisted of 15 or more points for comparison. Since then dozens of similar tests have been made by the turbine manufacturers which have given equally close agreement.

There is no reason, therefore, to assume that just because the ASME Power Test Code for Steam Turbines has established a limit of ±1½ per cent for steam-flow measurement by means of an orifice or nozzle, and 1¼ per cent by water measurements with orifice, nozzle, or venturi tube, one cannot obtain better accuracy than that. Just recently, for example, a large eastern utility established a water rate in two of its large units within ½ per cent by measuring condensate, and a midwestern station established the water rate on its new unit within ¾ per cent by measuring the steam flow.

To obtain such accuracy does require that care be taken in a number of things. In addition to the hydraulic-laboratory calibration made before the nozzle is installed permanently, the actual installation must have an adequate length of straight pipe both preceding and following the nozzle. Preferably, hydraulic calibrations should be made with the immediately associated main line piping in place so as to reproduce in the laboratory the actual installed installation conditions. This detail of providing adequate lengths of straight pipe is too often overlooked or considered inconsequential, and the resulting errors blamed on the meter when more properly they should be placed upon the engineers responsible for the layout at the plant.

Another requirement is the inspection of the nozzle and immediate pipe sections for cleanliness before such acceptance tests are run. This can be accomplished most readily by placing the nozzle in a removable section of pipe, or by using a thin-plate orifice between pipe flanges from which it can be removed easily for inspection. Such inspection insures that the laboratory condition of the nozzle or orifice is being maintained or can be restored by cleaning if required.

Whether the foregoing precautions were followed in the case of the author's test is not clear. Mention was made of calibrating the first Oak Creek unit but nothing was said about the units for Port Washington Station. In no case were assurances given that the meter installations had the requisite lengths of straight pipe or, except for the Oak Creek installation, whether the installations had been inspected carefully before the test to insure their freedom from extraneous material. Without such precautions being taken, as well as without checking the calibration of the meters themselves, comparisons with weighed-water tests may be meaningless and certainly of questionable value, particularly so since the comparisons given in Fig. 9 show such wide variations from test to test.

A flowmeter simply does not read 4½ per cent high in one test and ¾ per cent low in another test as reported for unit No. 3 in the author's Fig. 9, unless there are marked disturbances being created by lack of suitable straight pipe, the accumulation of dirt, derangement of the meter calibration, or other irregularities resulting from insufficient attention being given to the meter before the test was made.

One also might question on what basis could it be assumed that the guaranteed heat rates on all five turbines, against which both the weighed tests and the flowmeter readings were compared in Fig. 9, were actually being met. Obviously, again these comparisons would not be correct if the turbines were not meeting their guarantees. It might explain, in part at least, why the average steam-flow and water-flowmeter readings on turbine No. 4 read about ½ per cent low whereas the average meter readings for the other turbine units were 1½ to 2½ per cent high.

Considerable emphasis was placed upon the low cost of the weigh-tank apparatus, as well as the cost of making the tests themselves. Suppose we compare these against the cost of providing a flowmetering system. Every self-respecting turbine of today's vintage has a steam flowmeter, or a condensate flowmeter, as standard equipment. It is only necessary, therefore, to provide special calibration for such meters to make them suitable for acceptance-test purposes. This can be done at a cost of from $300 to $1000, depending upon size and conditions. Even at the top rate this would total no more than $4000 for the four units per station, as compared with $32,000 and $44,000 for the Port Washington and Oak Creek Stations. Of course, if special by-pass or other arrangements were provided in the flowmeter system, the total cost would be somewhat higher, but in no case should it approach the cost of the weigh-tank system.

Thus it can be seen that with suitable precautions, the flow nozzle or orifice flow-measuring system can be made fully as ac-

[6] Hydraulic Engineer, Bailey Meter Company, Cleveland, Ohio. Mem. ASME.

[7] "A System for the Measurement of Steam With Flow Nozzles for Turbine Performance Tests," by S. A. Moss and W. W. Johnson, Trans. ASME, vol. 55, 1933, Paper No. FSP-55-10, pp. 145–170.

[8] "Fluid-Meter Nozzles," by B. O. Buckland, Trans. ASME, vol. 56, 1934, pp. 827–832.

curate and dependable as the weigh-tank system, and at a fraction of the cost. Further, it is applicable to any type of turbine and plant and involves no more cost, if as much, and needs no more skill in using it, than does the weigh-tank system. As an extra bonus, a continuous record can be made of each day's performance, thus helping maintain test conditions in day-by-day operation.

Author's Closure

It is indeed gratifying to learn that there is such general agreement by the several discussers in the ideas expressed in the paper.

Messrs. Knowlton and Sprenkle point out the invaluable work of B. O. Buckland in developing the family of high-accuracy water-flow nozzles. In the absence of weighing tanks, reliable turbine tests would have been impractical without the flowmeters. However, unless the nozzle is cleaned of deposit prior to test, a very thin film could readily produce large errors equal to or in excess of ASME test code tolerances.

Mr. Light presents an interesting family of curves for a large turbine. It is assumed that Mr. Light assumes periodic inspection of the primary element as well as the flowmeter. Current practice of welding nozzles into boiler feed lines and steam lines makes inspection impractical so only the condensate meter nozzle or orifice can be recalibrated throughout the years.

Mr. Robertson has had considerable experience with the test facilities described in the paper. Many tests conducted were at loads which permitted his company's design engineers to evaluate effects of design changes and minor adjustments.

That ASME tolerances for errors can be bettered in practice is properly pointed out by Mr. Sprenkle. However, to attain such high accuracy with flowmeters, lengths of straight pipe and other conditions not always practical with high-pressure, high-temperature piping are required. At Port Washington as well as at Oak Creek, many more lengths of straight pipe were always used than specified by the meter manufacturer on feedwater meters but not on steam flowmeters.

Use of weighing tanks for turbine tests will not obviate the necessity for flowmeters for control and regular operation. The paper shows that dependable tests of consistent high accuracy are practical using the same tanks that store cold condensate.

In answer to Mr. Murdock's request for a description of the meters compared in the test, these meters were standard commercial-design meters with uniformly divided charts with a 10-in. diameter chart. These meters are calibrated with a water column prior to turbine testing.

The author wishes to express his appreciation of the remarks by the several discussers and feels that the information they have contributed has resulted in a valuable addition to the paper.

Transient Gas-Flame Temperatures in a Spherical Bomb

By Y. M. MIAO,[1] T. W. PRICE,[2] and J. H. POTTER[3]

The transient-flame temperature in a gaseous mixture, burning in a constant-volume spherical vessel from a point of central ignition, has long been of interest. Flamm and Mache developed a theoretical analysis relating the adiabatic temperature distribution to measured values of the bomb pressure. In this investigation a modified sodium D-line method was used to determine temperatures at several radii on a spherical vessel. Pressure measurements also were taken. Comparison is offered between the measured transient-flame temperatures and those computed from the Flamm and Mache equations.

Introduction

THE measurement of flame temperature has enlisted the research efforts of many workers in the fields of thermodynamics and combustion. The importance of such information is that it serves to validate certain chemical theories of combustion, makes possible more accurate determinations of the thermodynamic properties of the burned gases, and aids in the calculations incident to heat transfer.

Some of the early workers measured flame temperatures with heated thermocouples (1)[4] or heated platinum wires (2). In these methods the wire or thermocouple was heated, electrically, usually in a vacuum, and the temperature determined by an optical pyrometer. A graph was prepared showing the relation between the heating current in the wire or thermocouple and the observed temperature. A second plot was made showing the heating current for various temperatures when the wire or thermocouple was held in a flame. The intersection of the two curves was considered to represent a point of energy balance between the measuring device and the flame, and was reported as the flame temperature. Although each of these methods permitted of considerable refinement, obviously they were limited to steady-state conditions.

Many attempts were made to establish methods which would not require the insertion of a measuring device into the flame. One of these was the infrared spectrograph (3) in which galvanometer deflections were recorded for the flame alone, for a blackbody alone, and for the two in combination. From these data the emissivity of the flame was determined, and the temperature could then be found from the laws of radiation.

Perhaps the most widely accepted technique is the sodium D-line reversal (4, 5, 6, 7, 8), originally proposed by Féry. In this method sodium salts are introduced into the flame and the yellow doublet at 5890 Å – 5896 Å (Angstrom units) is observed in a spectroscope. A tungsten-ribbon lamp, previously calibrated for brightness temperature over a range of heating currents, is then placed behind the flame. With the lamp temperature below that of the flame, the bright doublet will be seen against the continuous spectrum of the lamp. However, the lines turn black after the lamp temperature has exceeded that of the flame. The actual point of balance, where the lines apparently disappear, is taken as the equilibrium temperature. From the lamp calibration, duly corrected for the wave-length difference between the sodium doublet and the screen of the optical pyrometer, the flame temperature can be determined.

Agnew (8) developed an interesting extension of the line-reversal method, which he used to measure gun-flash temperatures in artillery pieces. The contaminants in the propellent charge of an artillery shell contain both sodium and potassium salts. Thus the flame was colored for line-reversal purposes in the prominent wave lengths associated with these elements. A calibrated lamp was beamed through the zone in which the flame was anticipated and onto the slit of a monochromator. The monochromator in turn was focused upon a photocell, the response of which could be observed on an oscilloscope. The lamp current was fixed, producing a base line on the oscilloscope. The cannon was then fired. The passage of the projectile caused a sharp spur on the oscillogram. Next the propelling gases emerged and expanded, undergoing a temperature drop which was observed as a dip on the oscillogram. The whole gas mass then burst into flame, causing a rise in the phototube response. This final peak on the oscillogram was compared to the base line produced by the lamp. When on the oscillogram the flame peak reached the same vertical displacement as that produced by the lamp, the flame and corrected lamp temperatures were taken as equal. Although the Agnew method was tedious, in that it required a number of lamp settings and firings, it did afford a technique for determining instantaneous flame temperatures by line reversal.

Objectives

The objectives of this investigation were as follows:

1 To construct a spherical bomb with pairs of windows at each of three radii, and, using the Agnew technique, to determine instantaneous flame-front temperatures at these radii.

2 To compare the measured temperatures with those calculated from pressure measurements using the analytical method of Flamm and Mache (9).

Experimental Procedure

The theory of the sodium-line-reversal method for measuring flame temperatures has been presented in many places and need not be repeated here. An excellent explanation was given by Hershey and Paton (6) in connection with flame-temperature determinations in an internal-combustion engine. The Agnew modification (8) has been detailed in the foregoing.

The principal apparatus is shown diagrammatically in Fig. 1. At the left, the tungsten-filament lamp is shown connected to a variable source of electrical energy. Light from a small section of the tungsten filament is focused by lens I to the parting plane

[1] Design Engineer, Channel Master Corporation, Ellenville, N. Y.
[2] Assistant Professor of Mechanical Engineering, University of Illinois, Urbana, Ill. Assoc. Mem. ASME.
[3] Professor of Mechanical Engineering, Stevens Institute of Technology, Hoboken, N. J. Mem. ASME.
[4] Numbers in parentheses refer to the Bibliography at the end of the paper.

Contributed by the Process Industries Division and presented at the Annual Meeting, New York, N. Y., November 29–December 4, 1953, of The American Society of Mechanical Engineers.
Note: Statements and opinions advanced in papers are to be understood as individual expressions of their authors and not those of the Society. Manuscript received at ASME Headquarters, December 22, 1953. This paper was not preprinted.

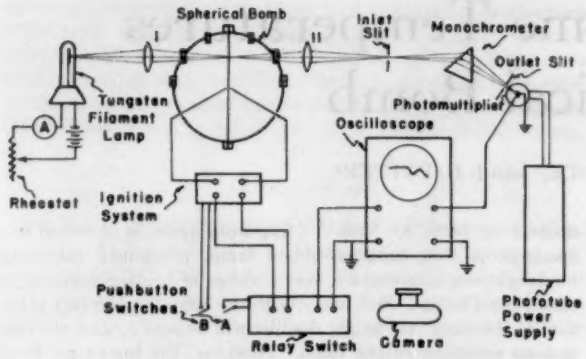

FIG. 1 SCHEMATIC DIAGRAM OF EQUIPMENT

The bomb is shown in cross section in Fig. 3. The heavy ribs furnished additional metal into which the window cartridges could be fastened. The windows were made from quartz plates $^1/_{16}$ in. thick. The quartz windows were held in mild-steel cartridges, with copper gaskets top and bottom. A mild-steel follower held the window in place. The bomb with the windows was tested hydrostatically to 300 psig.

Because the optical system was very sensitive to alignment, great care was taken to insure optimum adjustment. The left half of the bomb was replaced by a sheet of frosted glass upon which concentric circles had been drawn to correspond with the positions of the windows. The diameter of the largest circle was made to coincide with the internal diameter of the bomb. The ignition electrodes were adjusted to the center of the glass plate. The image of the tungsten filament was brought to a sharp focus on the glass plate at the appropriate radius. The lens I was used

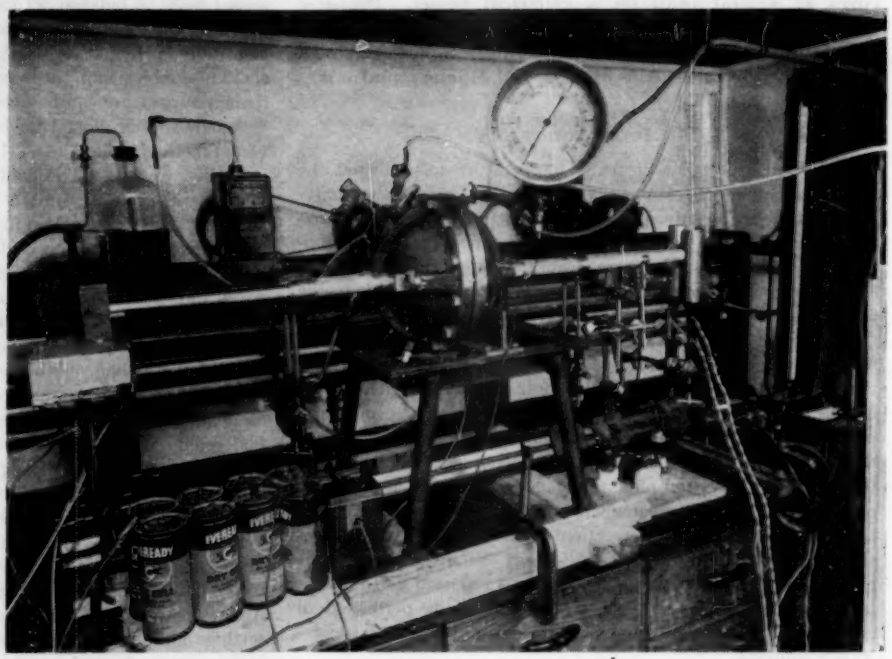

FIG. 2 (*right*) SPHERICAL BOMB AND AUXILIARY EQUIPMENT USED IN PRELIMINARY RUNS

of the spherical bomb. With the assistance of lens II, the light is focused upon the slit of the monochromator. This instrument then brings the light to the photomultiplier tube.

The ignition system and the oscilloscope sweep circuits were set to operate in the correct sequence while the camera shutter was open. The principal commercial items are identified in the Appendix (where the triggering circuit has been included as Fig. 14).

The spherical bomb was designed and built just for these experiments. The patterns were made at the foundry and the finishing was done at the machine shop of the Mechanical Engineering Department of the University of Illinois. The 18-8 stainless-steel casting was made at the Alloy Casting Company of Champaign, Ill.

The bomb on its supporting stand is shown in Fig. 2. This view was taken during some preliminary measurements, and the auxiliary equipment was not that used in the final runs. At the bottom of the bomb, on the left side, a standard automotive spark plug is shown. Two such spark plugs were installed 130 deg apart. The firing electrodes were made by adding appropriate lengths of stainless-steel rod to normal central electrodes of the spark plugs. The electrodes were sharpened and the tips brought to a gap of about $^1/_{32}$ in. at the center of the bomb.

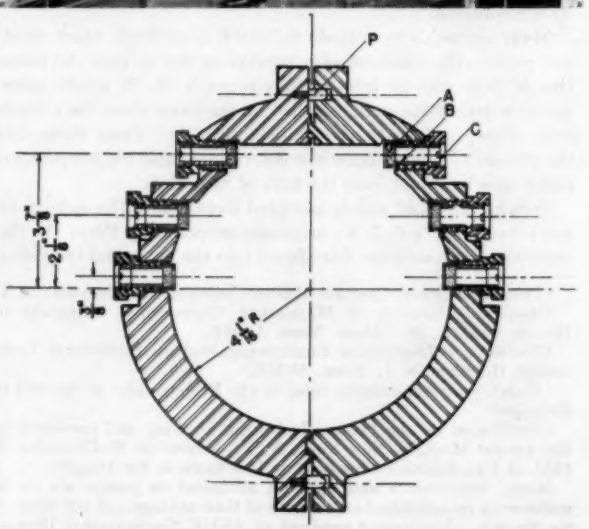

FIG. 3 CROSS SECTION OF BOMB SHOWING WINDOWS AT SEVERAL RADII

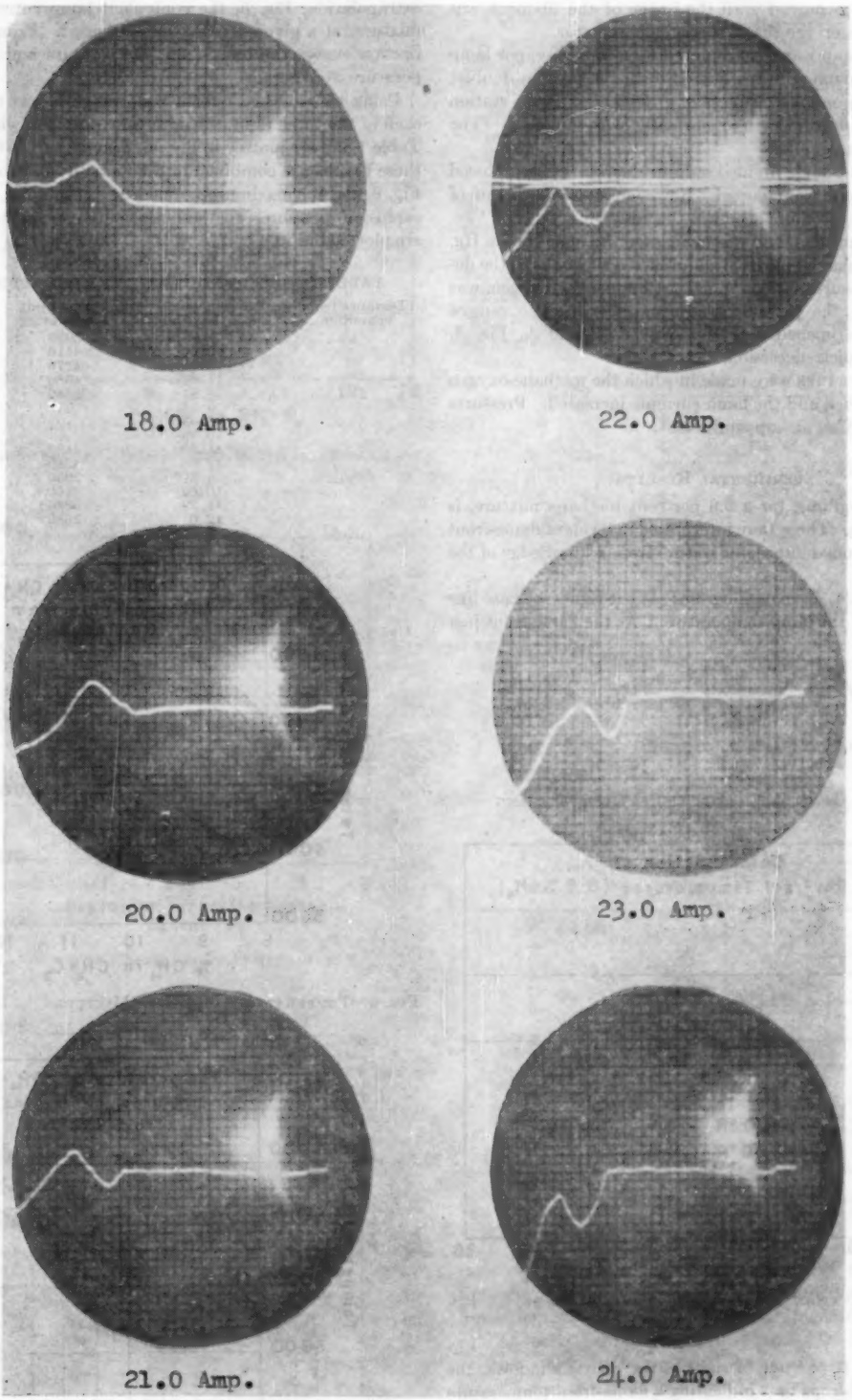

FIG. 4(a) TYPICAL OSCILLOGRAM MEASUREMENTS

to effect this adjustment. The frosted glass was then removed and the lens II was moved until the image of the filament was brought to a focus on the slit of the monochromator.

The tungsten lamp was then replaced by a sodium-vapor lamp and the monochromator was adjusted until the sodium doublet was in sharp focus on another piece of ground glass at the station where the photomultiplier tube normally was mounted. The system was then assembled.

In the early runs, finely divided sodium chloride was introduced at the time the bomb was charged. However, an accumulation of salt provided ample sodium atoms in the later runs.

Prior to each run the bomb was evacuated to about 20 mm Hg. Methane, of commercial purity, was admitted slowly until the desired partial pressure was obtained. Commercial oxygen was then added until the pressure was atmospheric. The camera shutter was then opened, and the switches B and A, Fig. 1, were thrown in quick succession.

Many successive runs were made in which the methane-oxygen mixtures were varied and the lamp currents increased. Pressures were recorded on Cox pickup equipment.

Experimental Results

A set of oscillograms, for a 9.6 per cent methane mixture, is shown in Fig. 4(*a*). These were interpreted in terms of flame-front temperature and maximum temperature from a knowledge of the lamp calibration.

Consider Fig. 4(*b*) as an oscillogram: At the right, the base line *A* is a measure of the lamp temperature. As the flame front just

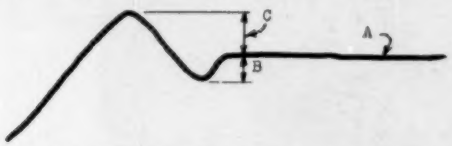

Fig. 4(*b*) Oscillograms for 9.6 Per Cent Methane

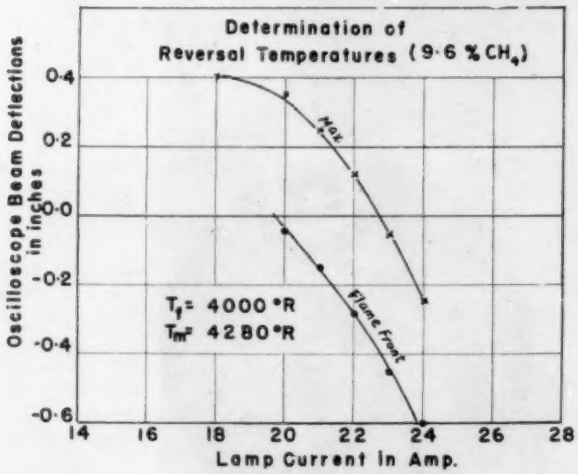

Fig. 5 Determination of Reversal Temperatures; 9.6 Per Cent CH_4

becomes tangent to the line of sight of the quartz windows, the oscilloscope trace drops to *B* indicating a flame-front temperature below the lamp temperature. As the flame continues to move radially a peak *C* is observed above the base line.

The oscillograms were measured for the flame-front-temperature displacement, and the maximum temperature displacement at each value of lamp current. By graphical interpolation and extrapolation, Fig. 5, the equivalent lamp currents for a given mixture, at a given radius, were obtained. From the lamp-calibration curve, the flame-front temperature and maximum temperature were found.

Using this method over a wide range of gas mixtures and at each of the three radii, the data were obtained which are listed in Table 1 and are plotted in Figs. 6, 7, and 8. The faired data from these graphs are combined in the flame-front-temperature graph, Fig. 9, and the maximum-temperature graph, Fig. 10. Maximum explosion pressures for various methane-oxygen combinations are plotted in Fig. 11.

TABLE 1 OBSERVED FLAME TEMPERATURES, DEG R

Distance from center, in.	Per cent methane in mixture	Flame-front temperature	Maximum temperature
3/8	8.88	3930	4050
	9.60	4116	4280
	10.9	4170	4420
	11.6	4360	4560
2 1/8	8.81	3850	3940
	9.31	..	3970
	9.98	..	4100
	10.79	..	4150
	11.30	4130	4180
	12.05	4260	4280
3 7/8	9.31	2930	3250
	10.62	3160	3340
	11.29	3380	3730
	12.0	3580	3900

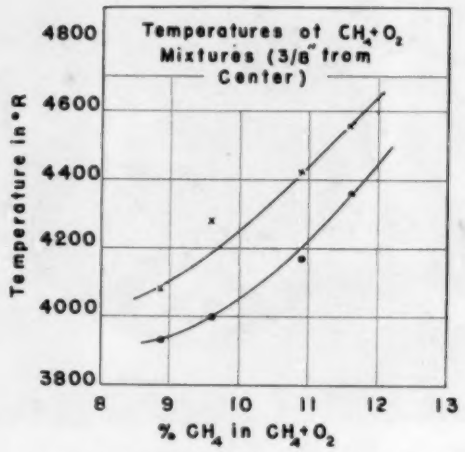

Fig. 6 Temperatures of CH_4-O_2 Mixtures, 3/8 In. From Center

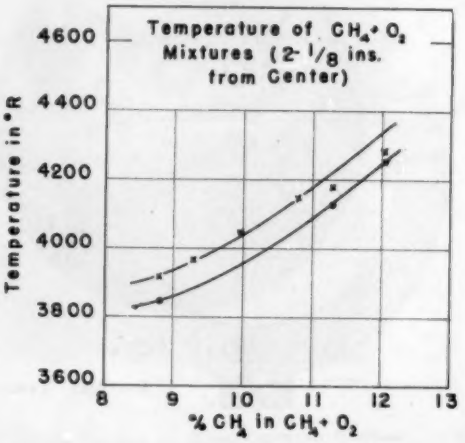

Fig. 7 Temperatures of CH_4-O_2 Mixtures, 2 1/8 In. From Center

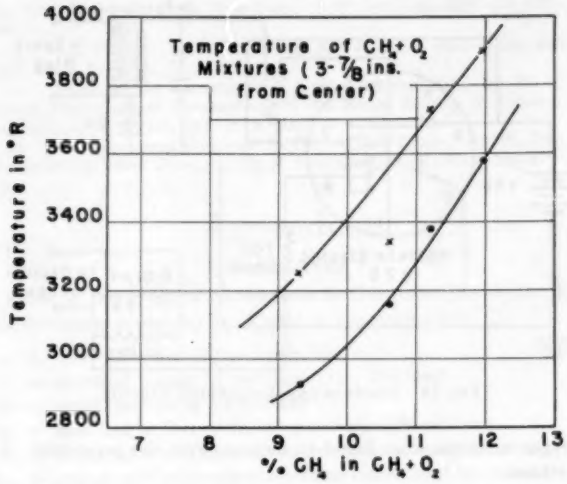

FIG. 8 TEMPERATURES OF CH_4-O_2 MIXTURES, 3 7/8 IN. FROM CENTER

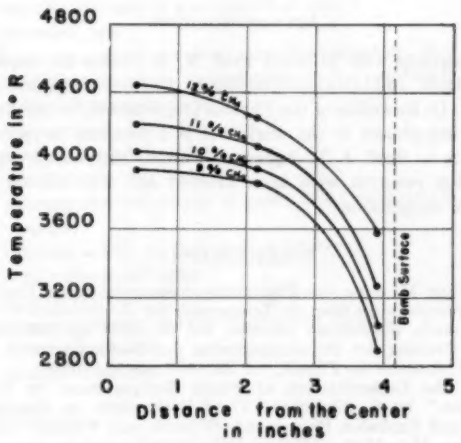

FIG. 9 OBSERVED FLAME-FRONT TEMPERATURES

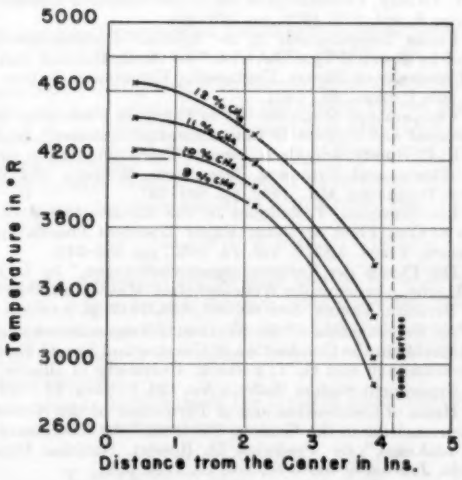

FIG. 10 MAXIMUM FLAME TEMPERATURES

DISCUSSION

The measured flame temperatures plotted in Figs. 9 and 10 give rise to some speculation. While it was not expected that the process would be adiabatic, the sharp falling off of temperature near the walls of the bomb was not quite anticipated.

The theoretical adiabatic combustion of the charge from point to point would indicate that the temperature would increase with radius. This would be due to progressive adiabatic compression of the unburned gas in the outer layers by the core of burned gas in the center. As each element of gas was burned, the compression temperature, and therefore the unignited enthalpy, of the next layer would rise. Combining the analytical method of Flamm and Mache (9) with the chemical and equilibrium method of Goodenough and Felbeck (10), values of theoretical adiabatic flame temperatures were computed.[5] These are plotted in Fig. 12 for four methane-oxygen mixtures.

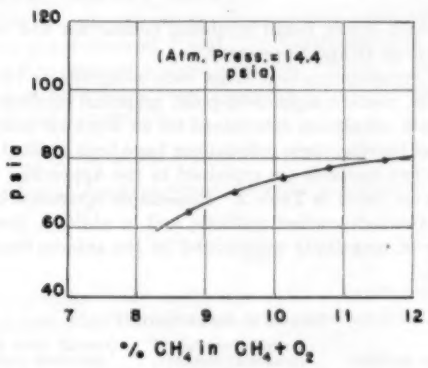

FIG. 11 MAXIMUM EXPLOSION PRESSURE

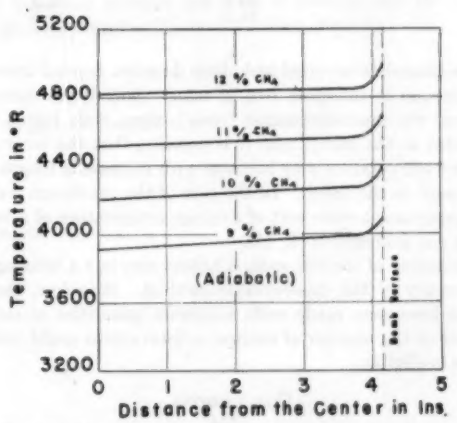

FIG. 12 THEORETICAL FLAME-FRONT TEMPERATURES

In Fig. 13 the observed and theoretical adiabatic flame temperatures have been compared for a 10 per cent methane mixture. It is interesting to note that the difference amounts to only 5 per cent at the smallest measured radius, increasing to 37 per cent at the maximum measured radius.

Other observers have found heat losses of the same order of magnitude. Hershey and Paton (6), using the sodium D-line technique in the combustion chamber of an internal-combustion engine, found over-all heat losses ranging from 11.1 to 26.3 per cent in an assumed isometric combustion. David (14), working

[5] This type of computation is outlined in the Appendix.

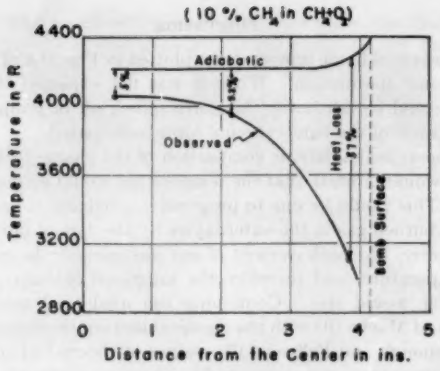

FIG. 13 COMPARISON OF OBSERVED AND THEORETICAL FLAME-FRONT TEMPERATURES

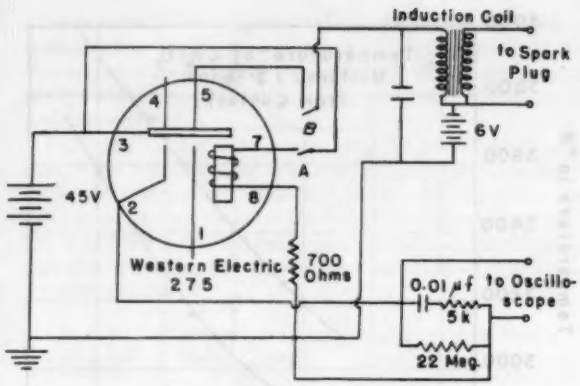

FIG. 14 IGNITION AND TRIGGERING CIRCUIT

with a closed bomb, found combined conduction and radiation losses between 10 and 18 per cent.

In this investigation heat losses were computed on two different bases, namely, a point-by-point graphical method, and an over-all loss calculation determined for an isometric bomb. For the sake of brevity, these calculations have been omitted. However, the two methods are explained in the Appendix. The results also are listed in Table 2. Reasonable agreement is shown for these two independent methods, and in addition, they are of the order of magnitude experienced by the authors cited in the foregoing.

TABLE 2 VALUES OF Y

Per cent methane in mixture	Average heat loss, Y (graphical method), per cent	Over-all heat loss z (isometric process) per cent
9	16.1	17.4
10	18.5	21.1
11	20.9	23.2
12	21.5	24.6

The sodium-line-reversal technique does not depend upon total radiation and is therefore free of many geometrical difficulties. However, the monochromator "sees" more than just a single focal point in the bomb, and it is possible that the error in the measured temperature may increase with increase in length of the optical path in the bomb. In the case of the maximum temperature measurement some sort of average temperature of a band of burning gas is observed (7, 15).

The number of excited sodium atoms also has a bearing upon the accuracy of the line-reversal method. However, the tests reported here were made with minimum quantities of salt, and the effect of the number of excited sodium atoms could safely be taken as negligible.

CONCLUSIONS

As the present investigation represented a first effort, both the equipment and technique could be improved greatly. Also, only the lean mixtures of methane and oxygen were used; further ranges of mixtures and other combustibles should be investigated. However, it is hoped that this paper may stimulate other workers in the field of combustion to undertake flame-temperature measurements of this type.

The present experiments appear to justify the following conclusions:

1 The sodium D-line reversal technique, as modified by Agnew, is adaptable to the measurement of transient-flame temperatures in a closed bomb.

2 The heat losses from the flame fronts of the lean methane-oxygen mixtures were found to increase with the percentage of methane.

3 The heat losses during the combustion of the lean methane-oxygen mixtures were found to more than offset compression effects in the unburned mixture.

ACKNOWLEDGMENT

The authors wish to thank Prof. N. A. Parker for encouragement, funds, and laboratory facilities. Particular thanks are due Prof. R. D. Rawcliffe of the Physics Department, for assistance in the optical phases of the work. It is a pleasure to record our gratitude to Prof. J. T. Agnew of Purdue University, who followed the research with keen interest and who offered many valuable suggestions.

BIBLIOGRAPHY

1 "Zur Messung von Flammentemperaturen durch Thermoelemente, insbesondere über die Temperatur der Bunsenflamme," by F. Berkenbusch, *Wiedemann Annalen*, vol. 67, 1899, pp. 649–667.

2 "Prüfung der Strahlungsgesetze der Bunsenflamme," by H. Schmidt. *Annalen der Physik*, vol. 29, 1909, pp. 971–1028.

3 "The Determination of Flame Temperatures by Infrared Radiation," by S. Silverman, Third Symposium on Combustion, Flame, and Explosion Phenomena, Williams and Wilkins Company, Baltimore, Md., 1949, p. 498.

4 "Sur la Temperature des Flammes," by Ch. Féry, Comptes Rendus, vol. 137, 1903, pp. 909–912.

5 "The Measurement of Flame Temperatures," by E. Griffiths and J. H. Awbery, Proceedings of the Royal Society of London, England, series A, vol. 123, 1929, pp. 401–421.

6 "Flame Temperatures in an Internal Combustion Engine Measured by Spectral Line Reversal," by A. E. Hershey and R. F. Paton, University of Illinois, Engineering Experiment Station Bulletin, No. 262, Urbana, Ill., 1933.

7 "Temperature Measurement in Complex Flames by Sodium Line Reversal and Sodium D Line Intensity Contours," by H. M. Strong, F. P. Bundy, and D. A. Larson, Third Symposium on Combustion, Flame, and Explosion Phenomena, Williams and Wilkins Company, Baltimore, Md., 1949, pp. 641–647.

8 "Line-Reversal Techniques in the Determination of Temperature of Gun Flash or Other Rapid Transient Phenomena," by J. T. Agnew, Trans. ASME, vol. 74, 1952, pp. 333–342.

9 "Die Physik der Verbrennungserscheinungen," by L. Flamm and H. Mache, Akademie der Wissenschaften Mathematischen Klasse Sitzung Berichte, Vienna, Austria, vol. 126, 1917, p. 9.

10 "An Investigation of the Maximum Temperatures and Pressure Attainable in the Combustion of Gaseous and Liquid Fuels," by G. A. Goodenough and G. T. Felbeck, University of Illinois, Engineering Experiment Station Bulletin No. 139, Urbana, Ill., 1924.

11 "Heats of Combustion and of Formation of the Normal Paraffin Hydrocarbons in the Gaseous State, and the Energies of Their Atomic Linkages," by Frederick D. Rossini, National Bureau of Standards, *Journal of Research*, vol. 13, 1934, p. 21.

12 "Combustions, Flames, and Explosions," by B. Lewis and G.

von Elbe, Academic Press, New York, N. Y., 1951, pp. 448–459, 653–656.

13 "Gas Tables," by J. H. Keenan and J. Kaye, John Wiley and Sons, New York, N. Y., 1948.

14 "Radiation in Explosions of Coal, Gas and Air," by W. T. David, Philosophical Transactions of the Royal Society of London, England, series A, vol. 211, 1912, pp. 375–410.

15 "Explosion and Combustion Processes in Gases," by W. Jost, McGraw-Hill Book Company, Inc., New York, N. Y., 1946, pp. 219–241.

Appendix

Nomenclature

Some of the types of calculations in this paper are outlined; the following nomenclature is used in the Appendix:

- a = internal radius of the bomb, in.
- C = chemical energy of methane (11), Btu/mol
- dn = small fraction of burned gas
- dQ_r = heat lost in Btu as dn is burned from flame front
- H_b = enthalpy of products at measured flame-front temperature
- H_{ad} = enthalpy of products at adiabatic flame-front temperature
- k = specific-heat ratio of unburned mixture
- M_u = mols of unburned gas originally in bomb
- M = mass of gas in bomb
- n = fraction of mass of gas burned at time t
- P = pressure, psia
- Q_r = heat loss from flame front during combustion, Btu
- Q_t = total heat loss from burned gases during combustion, Btu
- r = radius of flame front, in.
- R = gas constant, 1.986 Btu/mol R
- t = time, appropriate units
- T = temperature, deg Rankine
- U_e = average internal energy of gases after combustion, Btu/mol
- U_i = internal energy of gases before ignition
- V = total volume of bomb
- V_B = volume enclosed by flame front at time t
- y = apparent energy deficiency at flame front
- Y = average heat loss
- z = over-all heat loss

Subscripts:

- b = state of dn at instant after burning
- e = state of dn when flame reaches wall
- i = initial uniform state of gases before ignition
- u = state of dn at instant before burning

Calculation of Theoretical Temperature of Adiabatically Burned Gas at Flame Front

At any time t, the burning of an element dn is considered, where dn is a small mass of gas between the core of burned gases and unburned mixture. At this particular instant the bomb pressure is constant and equal to P, and this small element may be considered to undergo isobaric combustion. For purposes of analysis, this process also is considered to be adiabatic, and

$$H_{ad} = C + H_{T_u} \quad [1]$$

The required theoretical temperature can be found as soon as H_{ad} is known; however, this depends upon H_{T_u} which in turn is a function of the temperature at the end of adiabatic compression, T_u. This last term is determined from the Flamm and Mache analysis as follows:

At any time t, the volume of the bomb is divided between the burned and unburned gases as

$$V = V_B + \frac{M_u(1-n)RT_u}{P} = \frac{M_uRT_i}{P_i} \quad [2]$$

The fraction of the gas burned at time t can be closely approximated by (12)

$$n = \frac{P - P_i}{P_e - P_i} \quad [3]$$

Equations [2] and [3] may be combined to yield

$$\frac{V_B}{V} = \left(\frac{r}{a}\right)^3 = 1 - \frac{P_i\,T_u}{T_iP}\left[\frac{P_e - P}{P_e - P_i}\right] \quad [4]$$

Before combustion, the element dn is considered to be adiabatically compressed from T_i and T_u

$$T_u = T_i\left[\frac{P}{P_i}\right]^{\frac{k-1}{k}} \quad [5]$$

where k (13) is the average ratio of specific heats for the unburned mixture between T_i and T_u.

Equations [4] and [5] are two independent relationships involving the two unknowns, P and T_u. A trial-and-error method is then used to determine these variables. When T_u has been found H_{ad} is determined from Equation [1], and from it the adiabatic flame temperature.

Average Heat-Loss Calculation

Let us define an apparent energy deficiency at the flame front by

$$y = 1 - \frac{H_b}{H_{ad}} \quad [6]$$

where y is a fraction of the energy unaccounted for when dn burns. The loss of heat when the flame front traverses this small element is

$$dQ_r = MyC\,\mathrm{dn}$$

and the total loss between the time of ignition and the time at which the flame reaches the bomb wall is given by

$$Q_r = C\int_0^{'} My\mathrm{dn} \quad [7]$$

The average heat loss Y, may be defined as

$$Y = \frac{Q_r}{CM} \quad [8]$$

from which

$$Y = \left[\frac{\int_0^{'} My\mathrm{dn}}{M}\right] \quad [9]$$

But

$$M\mathrm{dn} = \frac{P}{RT_B}\,[4\pi r^2]dr$$

hence

$$Y = \frac{4\pi}{RM}\int_0^a \frac{Pyr^2dr}{T_B} \quad [10]$$

Equation [10] may be solved graphically. Values of T_B are found from experiment, and P, y are determined from Equations [5] and [6]. The values of Y are listed in Table 2.

Over-All Heat Loss

Consider the maximum indicated gas temperature for the position nearest the bomb center.

Assume (*a*) that this temperature is the average temperature of the gases in the bomb at the instant that the flame front reaches the wall; (*b*) that this average temperature is equal to the so-called constant-volume flame temperature.

The energy equation for constant-volume combustion is

$$U_i + C = U_e + Q_l$$

which may be written

$$C - Q_l = U_e - U_i \quad \ldots\ldots\ldots\ldots\ldots\ldots [11]$$

If z, the over-all heat loss, is defined as that proportion of the chemical energy which is lost as a constant-volume process

$$z = \frac{Q_l}{C} = \left[1 - \frac{U_e - U_i}{C}\right] \quad \ldots\ldots\ldots\ldots [12]$$

Assumptions (*a*) and (*b*) allow that U_e be identified with the maximum experimentally determined temperature for the position nearest the center. U_i and C are, of course, known. Calculated values of z are listed in Table 2.

It is noted that z compares favorably with Y, tending to substantiate the high energy deficiencies in burned gas at the flame front.

Commercial Equipment Used

1 Tungsten Filament Lamp, 6 volt 18 amp; General Electric Co.

2 Lenses, 15 cm focal length, 1.5 in. diam; Central Scientific Co., Chicago, Ill.

3 Monochromator; Adam Hilger Ltd., London, England (modified by Physics Department, University of Illinois).

4 Photomultiplier Tube, 931A; RCA.

5 Oscilloscope, Model 250H; Allen B. Du Mont Laboratories Inc., Passaic, N. J.

6 Cox pressure element; Commercial Research Laboratories, Inc., Detroit, Mich.

7 Direct-current ammeter, 0–25 amp; Weston Electric Instrument Company, Newark, N. J.

8 Vacuum pump; Central Scientific Company.

9 Sodium lamp; George W. Gate & Company, New York, N. Y.

10 Optical pyrometer; Leeds and Northrup Company, Philadelphia, Pa.

Engineers' Reference Books

Published by
The American Society of Mechanical Engineers

METALS ENGINEERING-DESIGN

Published 1953. $10.00—One of the four-volume ASME Handbook, this book discusses the essential properties which need to be evaluated by the design engineer in his selection of one material over another. Comprising 48 sections and written by 43 well-known authorities, it deals with the over-all problem of selection of material and takes up such specific items as high temperature considerations, plasticity, residual stresses, vibration, fatigue, shot peening, cold working, nitriding, flame strengthening, impact, corrosion, nondestructive testing, surface finish and mass production, and design theory and practice.

METALS PROPERTIES

Published 1954. $11.00—This second of the four-volume ASME Handbook provides, in convenient charts and tables, data on a broad range of metals in common industrial use—AISI steels, ASTM steels, cast copper alloys, aluminum alloys, tin, magnesium, etc. Tabulated under each of the more than 500 metals listed is such information as the chemical composition of the metal; its brittleness, heat-treatment, and other characteristics; its industrial uses; treatment temperatures for forging, annealing, quenching, etc.; such technological properties as recrystallization temperature and hot working temperature, and a great deal of other pertinent information to help the designer choose the proper metal for each part or product.

MANUAL ON CUTTING OF METALS WITH SINGLE POINT TOOLS

Published 1953. $10.00—This book contains shop-tested data on the machining of high nickel alloys, stainless steels, copper and brass alloys, magnesium, cast irons, and plastics. It offers valuable information on the structure of the metals to be machined, the correct tool material, size and shape of cut, and the proper cutting fluid. It shows how to predetermine the power requirements and best operating speed for all jobs. It helps time-study men to set standards of practice and cost of production, and it provides 322 tables of cutting speeds and horsepower for various feeds and depths of cut when turning commonly used steels and cast iron.

GENERAL DISCUSSION ON HEAT TRANSFER

Published 1951. $10.00—This is an authoritative reference on a decade's development in heat transfer and in the design of apparatus relating thereto. The 93 contributions and discussions in its 500 pages provide first-hand information on heat transfer with change of state; heat transfer between fluids and solids; conduction in solids and fluids; radiation, instrumentation, measurement techniques, and analogies; special problems such as heat transfer in turbine blade cooling, in liquid metals, in gas turbines, in piston engines, the mercury boiler, etc.

DESIGN DATA AND METHODS

Published 1953. $4.00—This 200-page compilation includes formulas and methods of calculating stresses in beams, bars, columns, plates, shafts, and crane hooks; stress component formulas; procedures for computing stresses and deformation in pressure vessels; design data on press, and shrink-filled assemblies and also for piping; factors of working stresses; numerical values of tangential stress in thick-walled cylinders; numerical solution of problems of gas flow when properties change continuously; graphical and numerical procedures for method of characteristics for two dimensional supersonic flow; chart for oblique shock waves under water; accurate bearing calculations; and methods of treating and solving problems of vibration and balancing of rotating apparatus.

DYNAMICS OF AUTOMATIC CONTROLS

Published 1948. $6.00—This complete and lucid treatment of the subject has been written for engineers who use or must eventually use automatic controllers. It examines the functional elements of a control, surveys and describes the mathematical methods of handling control problems, deals with the important components of the control loop, and specific control problems, considers the causes of nonlinearities in the control loop, and the on-off controller and its field of application. The theory of excursion-dependent periodic regulation is fully covered, formulas for the Laplace transformation are given, and the essential concepts concerning difference equations are presented.

AUTOMATIC CONTROL TERMINOLOGY

Published 1954. $1.00—This edition has been broadened to include automatic control combinations and the concepts common to the field of feedback control systems as they apply in industrial process control. Forty-six illustrative diagrams are presented to assist users to gain an understanding of the definitions. There is an index of nonstandard terms listing the standard terms which supersede them, and also an alphabetical list of standard terms showing the classification under which each definition will be found.

SMALL PLANT MANAGEMENT

Published 1950. $7.00—This is a well rounded management aid which will help you in setting up an internal organization that will function smoothly, in choosing the production process, in machine and equipment planning, and creating a good distribution system. Pertinent topics discussed are financing and banking, how to organize the plant, principles of scientific management, rating products, choosing the legal form of the organization, getting the best workers and labor relations, technical research, obtaining the best facilities and materials, and about everything else that would be likely to interest an individual or a group planning to start a small manufacturing business.

TEN YEARS' PROGRESS IN MANAGEMENT, 1942–1952

Published 1953. $1.50—Prepared in collaboration with fifteen nationally recognized authorities, this Report reviews and appraises the significant achievements made in such areas as statistical quality control; production planning and control; work simplification; wage incentive; industrial plant operation; purchasing, marketing, and distribution; personnel; public and labor relations; cost accounting; federal administrative management; and international co-operation.

REHEAT TURBINES AND BOILERS

Published 1952. $2.00—Aspects of reheating treated include advantages and disadvantages of the reheat cycle; normal start-up, quick start-up, and shutdown of modern reheat boilers; design factors relating to performance and operation of reheat boilers; performance of several new reheat boilers and special features of operation; starting schedules after shutdown of various durations; reheat economies; conversion to centralize control of auxiliaries; temperature control; turbine overspeed control as affected by reheat; and reheat development during the past twenty-five years.

VISCOSITY OF LUBRICANTS UNDER PRESSURE

Published 1954. $5.00—This publication reviews and co-ordinates twelve experimental investigations made in England, Germany, Japan, Russia, and the United States over a period of thirty-five years. The tests were made on 148 lubricants comprising of 25 fatty oils, 94 petroleum oils, 17 compounded oils, and 12 other lubricants. Data are co-ordinated by means of sixty tables in which the results originally appearing in diversified units are compared. The methods proposed for correlating viscosity-pressure characteristics of oils with properties determined at atmospheric pressures are reviewed and illustrated. Pertinent aspects such as experimental work on heavily loaded bearings, lubrication calculations, and additional techniques for viscosity are covered. Conclusions and recommendations are presented. The required computation of the temperature coefficients of viscosity, the method of computing pressure coefficients, a bibliography of 180 items, and symbols used are also given.

THERMAL BARRIER SYMPOSIUM

Published 1954. $4.50—This is a timely and useful contribution to the literature on the thermal barrier and its effects on propulsion systems, equipment and accessories, and aircraft structures. Of the articles in this book, one group is concerned with supersonic aircraft propulsion, the effect of supersonic aircraft flight on power plant installation systems, and the melting of bodies due to aerodynamic heating. Another group gives consideration to temperature problems of equipment in high-speed aircraft, personnel and equipment cooling in supersonic airplanes, and human problems associated with high-speed high-altitude flight. The concluding group deals with the thermal barrier, some structural aspects of thermal flight, and problems in the design of aircraft subjected to high temperature.

PROCEEDINGS OF THE 1954 OIL AND GAS POWER DIVISION CONFERENCE

Published 1954. $3.00—This publication provides a fund of information on a number of problems associated with oil and gas power. They include: Deterioration of Cooling Tower Lumber. Automatic Sulfur Burning Equipment for Treating Cooling Water. Foundations for Pipeline Compressors. New AIEE-ASME Speed Governing Specifications for Internal Combustion Engine-Generator Units. A New Method of Gas Engine Supervision. Turbocharging Two-Stroke Cycle Engines. Trends in Gas Compressor Cylinder Design. Gas Turbine Operating Experiences. Pictorial Description of Gas Turbine Installations. A Discussion of Aspects of Economical Production of Power With Internal Combustion Engine by Plant Supervisors. A Discussion of Mechanical, Electrical, and Hydraulic Drives as Applied to Auxiliary Equipment and Pipeline Pumping Stations. Influence of Fuels and High Engine Ratings on Diesel Plant Design.

1954 REPORT ON OIL AND GAS ENGINE POWER COSTS

Published 1954. $2.50—Statistics in this report are for 1953 and previous years. Data for 1953 come from 113 plants having 488 engines totalling 654,733.5 rated bhp. For each plant, the report gives details on fuels and lubricating costs, attendance and superintendence, maintenance and repair. Other pertinent facts given are type of engine, kind of fuel, installed capacity, type of load, data on major repairs and the number and duration of enforced shutdowns, and comparative costs figures for past years.

ELEVATED-TEMPERATURE PROPERTIES OF SELECTED SUPER-STRENGTH ALLOYS

Published 1954. $4.75. To ASME members $3.50—Here are graphically summarized the elevated temperature strength data for thirteen selected superstrength alloys and the summary curves for tensile strength; 0.2 per cent offset yield strength; per cent elongation and reduction of area; stresses for rupture in 100, 1000, 10,000, and 100,000 hr when available; and stresses for creep rates of 0.0001 and 0.00001 per cent per hr (1 per cent in 10,000 and 100,000 hr). In addition there are brief descriptions of each alloy giving chemical composition and recommended heat-treatments and processing; the primary data from which the summary curves were prepared; and an appendix containing some very-short-time rupture data for several of the alloys and a compilation of chemical compositions for approximately 100 superstrength alloys.

ELEVATED-TEMPERATURE PROPERTIES OF CHROMIUM-MOLYBDENUM STEELS

Published 1953. $4.75. To ASME members $3.50—This report of the ASTM-ASME Joint Committee on Effect of Temperature on the Properties of Metals is a graphical summary of the elevated-temperature strength data for the chromium-molybdenum steels. It includes summary curves for tensile strength; 0.2 per cent offset yield strength; per cent elongation and reduction of area; stresses for rupture in 100, 1000, 10,000, and 100,000 hr and stresses for creep rates of 0.0001 and 0.00001 per cent per hr. The appendix contains data sheets which include chemical composition, processing data, heat-treatment, and other pertinent information about steels in the survey; also primary data from which the survey curves were prepared.

Mail This COUPON Today

ASME ORDER DEPT.
29 W. 39th St., New York 18, N. Y. Date.....

Please send the following "circled" books:

A—$10.00	E—$4.00	I—$1.50	M—$3.00
B—$11.00	F—$6.00	J—$2.00	N—$2.50
C—$10.00	G—$1.00	K—$5.00	O—$4.75*
D—$10.00	H—$7.00	L—$4.50	P—$4.75*

☐ Payment herewith or ☐ Bill me

20% discount to ASME members
* Member's price, $3.50

NAME.....

ADDRESS.....

CITY.....ZONE NO.....STATE.....